Investigating rare earth elements and water stable isotopes dynamics in forest ecosystems

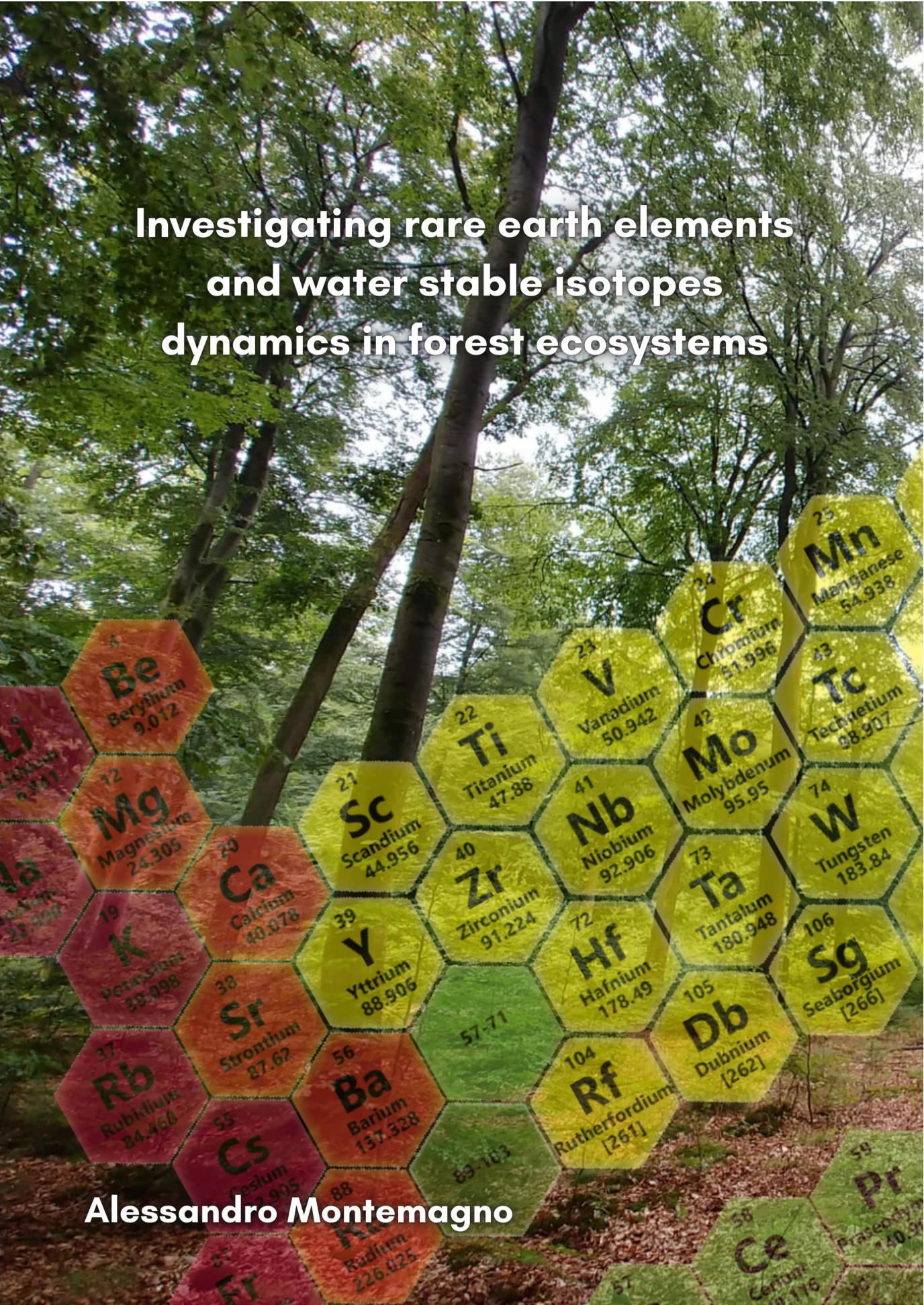

Alessandro Montemagno

Propositions

1. Water stable isotopes are inefficient tools for studying tree water uptake. (this thesis)

2. In order to make progress in eco-hydrology, more investments in the study of rare earth elements are needed. (this thesis)

3. Artificial Intelligence should be allowed for the actual writing of research articles so that researchers can focus on the more applicative aspects of science.

4. Universities should prioritize fostering scientific knowledge and technical skills over tending to students' wellbeing, which can be addressed outside the academic sphere.

5. The pressure to publish enhances rigor, reproducibility, and research quality.

6. Adopting cultivated meat as alternative to conventional animal farming is not a morally responsible solution.

7. Gender quotas represent discrimination against men and a disregard for women's intelligence.

Propositions belonging to the thesis, entitled

Investigating rare earth elements and water stable isotopes dynamics in forest ecosystems

Alessandro Montemagno
Wageningen, 06/11/2023

Investigating rare earth elements and water stable isotopes dynamics in forest ecosystems

Alessandro Montemagno

Thesis committee

Promotors

Dr Victor F. Bense
Associate Professor, Hydrology and Quantitative Water Management Group
Wageningen University & Research

Dr Christophe Hissler
Senior R&T Associate, Catchment and Eco-Hydrology
Luxembourg Institute of Science and Technology

Co-promotor

Dr Adriaan J. Teuling
Associate Professor, Hydrology and Quantitative Water Management Group
Wageningen University & Research

Other members:

Prof. Dr Pieter A. Zuidema, Wageningen University & Research

Prof. Dr Michael Bau, Constructor University, Germany

Dr Ilja van Meerveld, University of Zurich, Switzerland

Prof. Dr L.H. Erik Cammeraat, University of Amsterdam

This research was conducted under the auspices of the Graduate School for Socio-Economic and Natural Sciences of the Environment (SENSE)

Investigating Rare Earth Elements and water stable isotopes dynamics in forest ecosystems

Alessandro Montemagno

Thesis

submitted in fulfilment of the requirements for the degree of doctor
at Wageningen University
by the authority of the Rector Magnificus,
Prof. Dr A.P.J. Mol,
In the presence of the
Thesis Committee appointed by Academic Board
to be defended in public
on Monday 6 November 2023
at 11 a.m. in the Omnia Auditorium.

Alessandro Montemagno
Investigating rare earth elements and water stable isotopes dynamics in forest ecosystems, viii + 202 pages.

PhD thesis, Wageningen University, Wageningen, the Netherlands (2023)
With references, with summary in English

ISBN 978-94-6447-796-2
DOI https://doi.org/10.18174/634664

A mia Madre

CONTENTS

CHAPTER 1

Introduction

1.1 Project background: Hydro-CSI

The research presented in this PhD thesis resulted from Hydro-CSI, a larger project funded by the Luxembourg National Research Fund (FNR), which had the aim to uncover the complex water transformation processes across hydrological systems in the Critical Zone (CZ) through the development of new knowledge, technology and the use of new tools and tracers. In this project, particular attention was given to the understanding of the hydrological functioning of catchments through 3 pillars: interdisciplinary research; innovative and technological approaches; proposing new solutions for hydrological forecasting and prediction under changing conditions. Hydro-CSI was structured into four interdependent clusters:

Cluster 1 – Innovative field-deployable instruments for high-frequency monitoring

Cluster 2 – New tracers and approaches for investigating hydrological processes

Cluster 3 – Remote sensing applied to hydrology

Cluster 4 – Hydrological forecasts and projections under global change

This PhD research was part of Cluster 2, and represents a pioneering effort to investigate the application of novel hydrological tracers for the analysis of water movements in forested catchments. In particular, the use of rare earth elements (REEs) as complementary tracers to the most common water isotopes (^{2}H and ^{18}O) is proposed to uncover hydrological and bio-geochemical processes involving water in the regolith-plant continuum, whose knowledge can contribute to a more accurate recognition of the water resource(s) uptaken by trees.

1.2 Forests and the water cycle

Forests are complex ecosystems that provide for numerous benefits and represent one of the most important natural means for mitigating climate change at global scale (Rizvi *et al*.,

2015). They help regulate the Earth's climate by reducing carbon dioxide concentrations in the atmosphere through carbon storage and sequestration. They also absorb and release heat affecting temperature, precipitation, and atmospheric circulation. Finally, they preserve biodiversity, which maintains the resilience of natural systems reducing the impacts of climate change (Grantham *et al*., 2020; Heidari *et al*., 2021). However, due to anthropogenic impacts such as deforestation and land-use shift, forests are facing significant challenges in maintaining their ecological functions. Forests cover 31% of the Earth's land surface (FAO, 2022) and contribute significantly to water cycling, by storing and releasing vast amounts of water.

Above all major roles that forests play in the global assessment of the planet, the regulation of the water cycle is likely among the most important (Lachassagne and Lafforgue, 2016). Trees indeed help capture and store water reducing the risk of floods and droughts and, at the same time, keeping water sources available to life. Forests present also the capability of moving water from the regolith to the atmosphere via root water uptake and transpiration. The term “evapotranspiration” was first introduced by Wilm in 1944 – who described it as the total water loss to the atmosphere – and subsequently widely used after the first attempt of the author to calculate it in 1948 (Wilm, 1944). With the technological and hydrological advancements, the need to differentiate evapotranspiration into two of its main components, transpiration and evaporation, was gradually recognized. This differentiation arose from the need to distinguish the different processes that regulate the water flow towards the atmosphere due to the growing importance attributed to vegetation in the water cycle and its role in the mobilization of water from the regolith to the atmosphere. Such a differentiation would have eventually led to a more accurate quantification of the regolith-atmosphere water flux. The impact of transpiration in the water cycle was provided through a global assessment by Schlesinger and Jasechko in 2014, who estimated that transpiration accounts for 61 ± 15% of global evapotranspiration. Such an important role of the transpiration flux makes crucial the tracing of the water flow path for assessing the disturbance of climate change to forests equilibrium in order to develop effective management strategies to sustain the health and ecological services of these vital ecosystems in a world where change is becoming so fast that the environment is unable to adapt (Jandl *et al*., 2019).

Water dynamics in forests are influenced by various factors such as regolith properties, type of vegetation cover, topography, and climate (e.g. Carlier *et al*., 2018; Cai *et al*., 2022; Fujino *et al.,* 2023). Several techniques and tools have been developed to trace

water dynamics in the CZ (Fig. 1.1) from the groundwater to the canopy level, including water stable isotopes, chemical tracers, geologic and hydrometric measurements (e.g. Muir and Coplen, 1981; Gourdol *et al*., 2021; Kuglerovà *et al*., 2014; Hissler *et al*., 2014 and 2016; Galewsky *et al*., 2016; Pfister *et al.,* 2017; Carrión-Mero *et al*., 2022; Martínez-Carreras *et al*., 2016 and 2021; Bonanno *et al*., 2021; Douinot *et al*., 2022; Fabiani *et al*., 2022). These techniques have been extensively used to investigate water movement in various forest ecosystems, ranging from tropical rainforests to boreal forests. When it comes to understanding water dynamics in forest ecosystems for management purposes, one of the most pressing questions relates to the recognition of the water source uptaken by trees under different hydrological conditions. It is important to understand to what extent water resources as well as the associated nutrients are accessible, and for how long they are available to trees especially during dry periods. Knowing which water source(s) trees use during the different seasons is of crucial importance. Climate change indeed puts a strain on the survival of ecosystems, and specific measures of prevention might be necessary to ensure the sustainability of human activities by maintaining ecosystem services. A thorough understanding of the water absorption dynamics of trees can inform decision-making processes in forest management, such as selecting the most suitable tree species for reforestation based on climate forecasts. This knowledge is essential for effectively addressing the challenge of climate change, as it allows us to ensure the long-term resilience of forest ecosystems and their ability to sustain life. Therefore, tracing and modelling water flows in the CZ is of fundamental importance to assess water source(s) nourishing the plants especially during droughts, and it depends on the understanding of water origin, storage, mixing and release from the regolith to the trees.

Unfortunately, the use of tracers to track water movement in complex systems such as the CZ often exhibits non-conservative behaviour, presenting a significant challenge for accurately monitoring water movement in the regolith-plant continuum. This is where the current doctoral project fits in. As part of Cluster 2, this PhD aims to unveil the fractionation processes of some of the most common geochemical and hydrological tracers in the regolith-plant system, so that future studies can incorporate this information to calibrate hydrological models and gain more precise insight into water flows within the transpiration pathway.

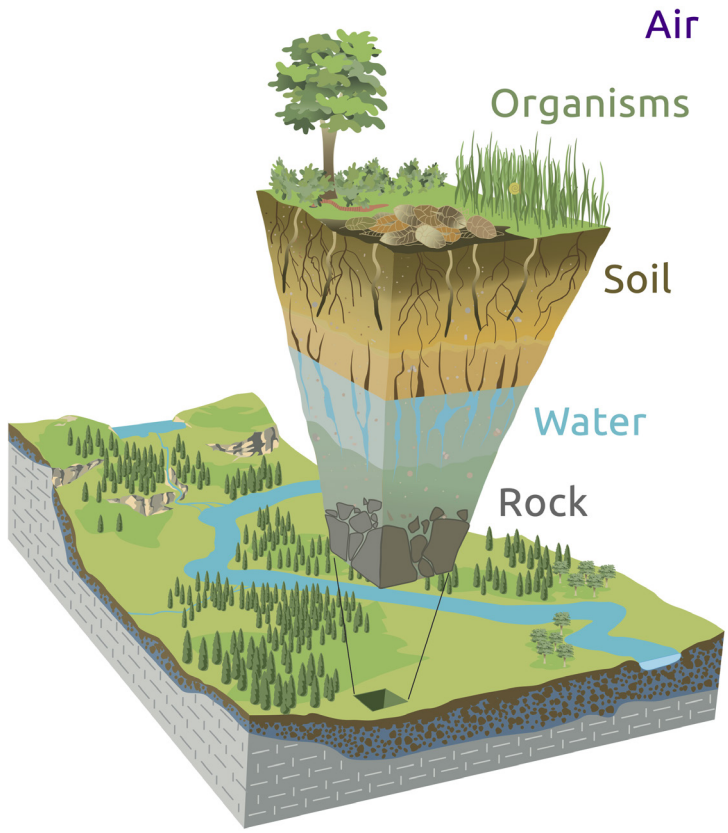

Figure 1.1: Critical Zone, the "heterogeneous, near surface environment in which complex interactions involving rock, soil, water, air, and living organisms regulate the natural habitat and determine the availability of life-sustaining resources" (National Research Council, 2001). Illustration modified from Chorover, J., R. Kretzschmar, F. Garcia-Pichel, and D. L. Sparks. 2007. Soil biogeochemical processes in the critical zone. Elements 3, 321-326. (Artwork by R. Kindlimann).

1.3 Stable isotopes as tracers for water exchanges in the CZ

Among the mentioned tools, water stable isotopes are the most common tracers to identify water sources, determine water residence time, track the movement of water through the hydrological cycle and understand how water is partitioned among different water pools across the system. Stable isotopes of water refer to the isotopes of hydrogen and oxygen composing the water molecule. These include hydrogen-1 (^{1}H), deuterium (^{2}H), oxygen-16 (^{16}O) and oxygen-18 (^{18}O). The isotopic composition of a given water – also referred to as "signature" – can be characterized from the ratios of these isotopes, and it can be influenced by various factors such as temperature, humidity, precipitation, pressure and the chemical

and physical properties of the material in contact with the water. The isotopic signature of water is determined by measuring its O and H isotope ratios and by comparing them to those of a standard reference, typically the Vienna Standard Mean Ocean Water (VSMOW) in the case of water samples. Water isotopic signature is usually reported with the notation "δ", which relates to the difference between the isotopic ratios of the sample and the one of the standard as per mil (‰) deviation from the standard. For O and H, the isotopic signature is calculated as follow:

$$\delta^{18}\mathrm{O}_{\mathrm{sample}} = \left(\frac{^{18}\mathrm{O}/^{16}\mathrm{O}_{\mathrm{sample}}}{^{18}\mathrm{O}/^{16}\mathrm{O}_{\mathrm{VSMOW}}} - 1\right) \times 1000\ ‰ \qquad \text{(Eq. 1.1)}$$

$$\delta^{2}\mathrm{H}_{\mathrm{sample}} = \left(\frac{^{2}\mathrm{H}/^{1}\mathrm{H}_{\mathrm{sample}}}{^{2}\mathrm{H}/^{1}\mathrm{H}_{\mathrm{VSMOW}}} - 1\right) \times 1000\ ‰ \qquad \text{(Eq. 1.2)}$$

Where $^{18}O/^{16}O$ and $^{2}H/^{1}H$ are the isotopic ratios of the water sample and the VSMOW certified standard. The principle behind the use of water stable isotope in hydrology is linked to the fact that the isotopic signature of water varies across the hydrological cycle due to fractionation processes. These refers to the physical or chemical processes that can cause the isotopic signature of the water – or more in general of a given element – to vary among different substances or phases. These fractionation processes depend on various factors, such as temperature, pressure, humidity, precipitation, but also on the physical and chemical processes in which the water is involved. Therefore, it is possible to differentiate water pools in forest ecosystems according to their unique isotopic signature. By measuring the isotopic composition of water at different stages along its flow path, it is possible to track its movement and transformation and to infer information about its origin, pathways, and residence times. For example, a known isotopic composition of precipitation can be used to estimate the contribution of different water sources (e.g., oceanic vs. continental) to the total water budget of a specific region. Similarly, the isotopic signature of soil water or streamflow can provide information about the origin, flow paths and mixing of groundwaters, as well as the processes of evaporation and transpiration that affect water availability to plants (Kendall & McDonnell, 2012; Wassenaar & Terzer-Wassmuth, 2018; West, 2019).

The first use of stable isotopes as tracers for water dynamics dates back to 1947, when Harold Urey and his colleagues published the first study (Urey *et al.,* 1947) on the isotopic composition of precipitation, showing that the O and H isotopic signatures of water varied together with temperature and latitude. Subsequently, researchers began to

increasingly use stable isotopes to study a variety of hydrological processes. Among the initial applications of these tracers were studies conducted to determine the variability of water dynamics in soils (Gascuel-Odoux and Mérot, 1986) and to identify water sources for groundwater recharge while estimating its age (Clark and Fritz, 1997). Since then, the use of stable isotopes of H and O has become a standard practice in hydrology and they are still widely used to study evaporation, transpiration, water vapor transport and mixing of water sources (Gat, 2010), as well as to study the effects of climate change on the hydrological cycle and to improve water management practices (Wassenaar *et al.,* 2018).

1.4 Water isotopes data interpretation

Water stable isotopes occur naturally in a watershed due to precipitation and snowmelt events. These isotopes are part of meteoric processes and can be used to trace and distinguish different water and air masses contributing to a watershed. The stable isotopic composition of water changes only through mixing and well-known fractionation processes that occur during evaporation and condensation. Initially, stable isotopes were thought to remain conservative in their mixing relationships after entering the subsurface as no longer affected by evaporation. This means that the isotopic composition of a mixture of two water sources will fall on a linear graph, and its position will be determined solely by the proportions of the mixed sources. A characteristic fingerprint of its origin is present in the water entering a watershed, aiding in identifying its source (McGuire and McDonnell, 2007). However, with the advancement of multidisciplinary studies, it has been shown that despite evaporation does not affect water isotopes composition below ground, other processes such as freezing and thawing, mineral-water interaction, diffusion and biological processes can (Jouzel and Souchez, 1982; Sousa Silva *et al*., 2018; Basov *et al*., 2019). Thermodynamic reactions fractionate atoms of different masses, resulting in a distinctive isotopic composition indicative of the water source and its formation process. Moreover, differences between masses of the same elements have an impact on the diffusion rates during phase changes due to differences in bond strength between lighter and heavier isotopes. The breaking of molecular bonds is indeed influenced by the mass of the isotopes involved. Specifically, the molecular bonds between lighter isotopes such as $H_2{}^{16}O$ are easier to break than those between heavier isotopes like $HD^{16}O$ and $H_2{}^{18}O$. This means that heavier water molecules need more energy to break their hydrogen bonds than their lighter counterparts, resulting in slower reaction kinetics. The mass-dependent fractionation of oxygen and hydrogen isotopes occurring during evaporation and condensation processes results in the

relationship between $\delta^{18}O$ and $\delta^{2}H$ in meteoric water. Such a relationship was first observed in 1961 by Craig, who expressed it as the "global meteoric water line" (GMWL - Craig, 1961) and described it with the following equation:

$$\delta^2 H = 8 \times \delta^{18} O + 10‰ \quad \text{(Eq. 1.3)}$$

Where the 10‰ refers to the deuterium-excess (*d-excess*), which represents a measure of the direct isotopic fractionation of the meteoric water.

When working on a local scale, it might be more convenient to use the Local Meteoric Water Line (LMWL), defined as the linear relationships between $\delta^{2}H$ and $\delta^{18}O$ based on local precipitation data (Kendall & McDonnell, 1998), which may result different from the GMWL. Figure 1.2 provides a comparison between the LMWL of the Weierbach experimental catchment in Luxembourg (Hissler *et al.*, 2021), and the GMWL.

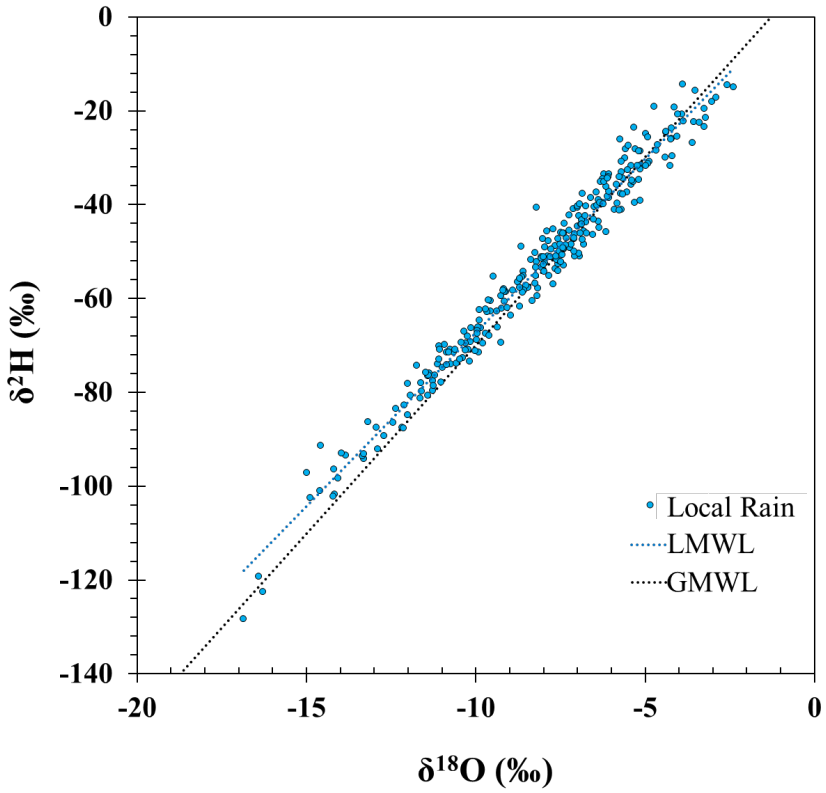

Figure 1.2: Comparison between the GMWL calculated according to the Graig equation (1961) and the LMWL derived from the historical database of the isotopic composition of the precipitation collected in the Weierbach experimental catchment in Luxembourg. Data from Hissler et al. (2021).

A deviation from the LMWL in the isotopic composition of another local water sample (e.g. soil water), indicates that the sample has undergone fractionation processes. Details of processes leading to isotopic fractionation in the regolith-plant continuum will be treated on a case-by-case basis in Chapters 2 and 3.

1.5 Limitations of the use of water isotopes in eco-hydrology

One of the pressing questions in eco-hydrology relates to the understanding of which water source(s) trees uptake under different hydrological conditions, with a focus on drought periods. Despite their historical extensive use in research, when applied to systems with complex interactions such as those of the soil-plant continuum, water stable isotopes lose their effectiveness and do not allow for a correct recognition of the water source absorbed by plants. This is due to a multitude of factors, ranging from the lack of standardized protocols for sampling and analysis to the numerous chemical and physical processes that may occur in the environment and inside trees and which may create isotopic fractionation. Many authors showed different isotopic signatures for the same samples when applying different sampling or analytical procedures (Orlowski *et al*., 2016), or discrepancies between the isotopic signature of xylem sap and of the available water source(s) (Brooks *et al*., 2010; Evaristo *et al*., 2016), suggesting that isotopic fractionation may occur during, before or even after the water uptake or the sample collection. The dissimilarities observed in the isotopic signatures between sap and the assumed water sources can be attributed to the differential water residence times in the plant's tissues. Plants possess a water storage system in addition to their transportation system, which usually differ in the periods of water retention within their tissues. Meinzer *et al.* (2006) investigated the sapwood capacitance in diverse tree species by employing $^{2}H_{2}{}^{16}O$ injections and found that the transit times of deuterated water to the upper crown varied from 2.5 to 21 days, while the residence times ranged from 36 to 79 days, depending on the diameter of the tree. Lehmann *et al.* (2018) conducted a simulation of a fog event to demonstrate that the assimilation of water vapor can modify the isotopic signature of leaf water. This results in heterogeneity of isotopic compositions between different plant water compartments, leading to difficulties in identifying the source of transpired water. Such a complexity, therefore, strongly affects the water stable isotopes dynamics in plants, limiting their use for eco-hydrological purposes.

The most common method used to collect water from trees is the cryogenic vacuum distillation or more simply cryogenic extraction (CE), which makes use of a heat trap to

extract water from tree cores and which will be treated more in detail in Chapter 3. This technique has been at the center of a debate among researchers concerning the interpretation of the obtained results and its accuracy and repeatability when used for eco-hydrological purposes. The unreliability of CE-derived isotopic results is mainly related to the very likely occurring of organic contaminations of the samples before and during the extraction and to the compartmentalization of the water within the different tissues of the tree. Compartmentalization, indeed, leads to differences in the isotopic signatures between the sap of the xylem – which represents the recently absorbed water – and the water collected from other tissues (Barbeta *et al*., 2022). As a result, the heterogeneity of the isotopic compositions among plant water compartments makes it difficult to assess the origin of water uptaken when using the CE for the collection.

Despite the utility of O-H stable isotopes in water tracing has been abundantly proven, the lack of knowledge about isotopic fractionation occurring inside trees and the lack of standard protocols for sampling and analysis represent strong limitations in the use of stable isotopes for tracing water sources in the transpiration pathway. What is needed is a better understanding of the effect that bio-geochemical processes may have on the isotopic signature of the water once it is taken up by trees, and new tracers to be used where water stable isotopes cannot deliver enough reliable information.

1.6 Rare earth elements as complement to stable isotopes

The CZ is a complex system characterized by a multitude of biological, chemical and physical processes that can affect the isotopic signatures of water and limit the use of O and H stable isotopes to trace water. To overcome these limitations, a multidisciplinary and multi-tracer approach is needed and hereby proposed. In this regard, REEs can be useful as additional tracers to understand the dynamics of water forests, thanks to the comprehensive knowledge of their biogeochemical behaviour accumulated over the past decades.

REEs are a group of elements composed of lanthanides (from ^{57}La to ^{71}Lu) and ^{39}Y. These elements have already proven to be among the best-suited tracers for investigating CZ processes such as: the origin of solid and dissolved load transported by stream (Aubert *et al*., 2001; Hissler *et al*., 2015a); metal adsorption in organic matter (Schijf and Zoll, 2011) and in bacterial cell walls (Takahashi *et al*., 2005 and 2010); characterization of water-rock interaction and regolith weathering processes (Bau, 1996; Aubert *et al*., 2001; Stille *et al*., 2006, Ma *et al*., 2011, Hissler *et al*, 2015b; Jin *et al*., 2017; Laveuf and Cornu, 2009; Moragues-Quiroga *et al*., 2017, Vázquez-Ortega *et al*., 2015 and 2016); as an indicator for

atmospheric dust composition in leaves (Censi *et al*., 2017); or wastewater spillage in freshwaters (Merschel *et al*. 2015; Hissler *et al*., 2016); and metal mobilization and fractionation in the soil-plant continuum (Liang *et al*., 2005 and 2008; Censi *et al*., 2014a; Cheng *et al*., 2014; Srmhi *et al*., 2009). By knowing the REEs composition of the different compartments of the studied system (e.g. water, roots, sap, leaves, etc.) and their fractionation processes, it is potentially possible to understand how water is exchanged between the aforementioned compartments, and therefore understand from which source the roots absorb water. The particular chemical-physical properties of REEs (lanthanide contraction, electron configuration, oxidation states – discussed in detail in the following paragraph), make them among the best tracers for bio-geochemical processes for understanding water interactions inside the CZ. Despite the evidence of their effectiveness as tracers, REEs are not yet widely used in hydrological research. This could be due to a lack of awareness among researchers of their potential applications, or the perception that they are too complex to work with. However, with the growing need for a multidisciplinary and multi-tracer approach to understand complex environmental systems, the importance of using new tracers is becoming increasingly evident. REEs have great potential to complement and improve existing knowledge at the interface between hydrology and geochemistry by providing valuable information on water movement and element transport within the CZ.

1.6.1 Introduction to rare earth elements geochemistry

REEs are found in various natural sources, including rocks, waters and vegetation. The distribution of REEs in the earth's crust is not uniform, and their concentrations can vary significantly depending on the geological setting. Regardless of geochemical considerations, the importance of REEs is linked to their use in technology for the production of superconductors, magnets, catalysts, components of the latest generation hybrid vehicles, optical fibres, medical equipment, and for welding (Zhou *et al*., 2018). The main sources of REEs are lateritic clays, where REEs are present in residual deposits within phosphates (xenotime and monazite). Alternatively, primary REEs deposits are associated with carbonatites where these elements are contained as bastnaesite and loparite. A widely accepted REEs classification – which does not consider Y – is based on their atomic weight, resulting in their categorization into three distinct groups: Light Rare Earth Elements (LREEs), Middle Rare Earth Elements (MREEs), and Heavy Rare Earth Elements (HREEs) (e.g. Censi *et al*., 2014 and 2015; Hissler *et al*., 2015). Another classification was provided

by the US Geological Survey (Schulz *et al*., 2017), which suggested the division of REEs into two groups according to their electron structure, with LREEs (from La to Gd) having unpaired electrons in the 4*f* orbital and HREEs (from Tb to Lu) having paired electrons in the same orbital. However, the REEs classification exhibits a lack of consistency among authors, presenting different combinations of elements within the groups, often reflecting the geochemical behaviour observed by the authors on a case-basis.

Like Y, the lanthanides generally exist as trivalent ions, except for Ce and Eu which may have respectively 4+ and 2+ charge, depending on the redox conditions of the system. The lanthanides are characterized by the progressive filling of the 4*f* orbital. This latter is not the outer orbital, therefore the electrons contained in it do not become part of the valence electrons, which are instead represented by the two electrons in the 6*s* orbital and the single electron in the 5*d* orbital. This is highlighted by the radial distribution function around the lanthanide nuclei for the various outermost orbitals (Fig. 1.3), which shows that the 4*f* orbital is closer to the nucleus in comparison to the 6*s* and 5*d* orbitals (Friedman *et al*., 1964).

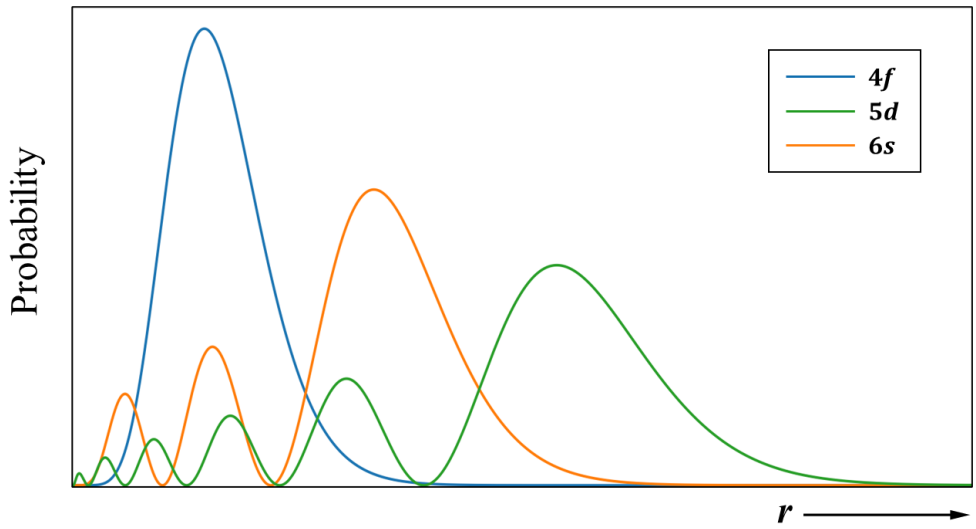

Figure 1.3: Radial distribution functions for the 4f, 5d, and 6s orbitals, representing the probability density of finding an electron at a distance **r** from the nucleus. Data from Friedman et al., 1964.

As a result, the outer electron configuration is the same for all the lanthanides, being $[Xe]4f^n6s^25d^1$ in neutral form and $[Xe]4f^n6s^05d^0$ in the ionic form Ln^{3+}. This results in a substantial identity in the chemical reactivity of these elements, which is traduced in a serial behaviour during geochemical processes rather than being characteristic of a single element of the series. This is not valid for the Y, which does not have electrons in the 4*f* orbitals and therefore has a different outer electron configuration.

An element of differentiation in the geochemical behaviour of the elements along the series is determined by the variation of the screening effect of the nuclear charge of the atom that the progressive filling of the 4*f* orbital has towards the 5*d* and 6*s* electrons. As a consequence, there is a higher-than-expected decrease in the size of the lanthanide atoms and ions known as *lanthanide contraction*. This has an immediate effect on the geochemical behaviour of the lanthanides during Charge and Radius Controlled (CHARAC) processes (Bau, 1996), but it also affects non-CHARAC processes by influencing the ionic potential (Z/r) along the series. As a result, the behaviour of these elements during the formation of coordination bonds changes progressively from La to Lu. Therefore, in CHARAC processes, such as in pure melt systems (Bau, 1996), REEs show similar behaviour, while in non-CHARAC systems, such as in aqueous solutions, their behaviour may differ as it is also affected by their electron configuration and the nature of the solutes in the solution. Finally, as a result of the lanthanide contraction, the ionic radius of Y^{3+} (0.9 Å) is almost identical to that of Ho^{3+} (0.901 Å), which supports the belonging of Y to the REEs group and establishes the Y-Ho geochemical pair.

In the geochemical investigation of REEs, the normalization of their concentrations is preferred over the consideration of absolute values. Normalization facilitates the study of REEs serial behaviour without the interference of the higher natural abundance of elements with even atomic numbers in comparison to elements with odd atomic numbers, in accordance with the Oddo-Harkins rule (Harkins, 1916) (Figure 4a). The normalization entails dividing the analytical concentrations of each element in the series by the concentration of the same element in a standard, as per the following equation:

$$[\mathrm{REE}_i]_n = \frac{[\mathrm{REE}_i]_{sample}}{[\mathrm{REE}_i]_{standard}} \qquad \text{(Eq. 1.4)}$$

Where *n* refers to the normalized concentration, the numerator represents the analytical concentration of a given element *i* of the series measured in the sample, and the denominator represents the analytical concentration of the same element in the reference material (Alibo & Nozaki, 1999). Typical standards used for the normalization are the Chondrite and the Post Archean Australian Shale (PAAS). The study of REEs is typically conducted by examining the patterns of the series obtained by plotting the normalized concentrations of each element against their respective atomic numbers (Figure 4b). From the patterns of normalized REEs concentrations, it is possible to extract information about

the geochemical processes occurring in the system under examination, depending on their shape and on the presence or absence of so-called "anomalies". Anomalies represent enrichments (positive anomalies) or depletions (negative anomalies) in certain elements of the REEs, in comparison with the elements immediately adjacent in the series.

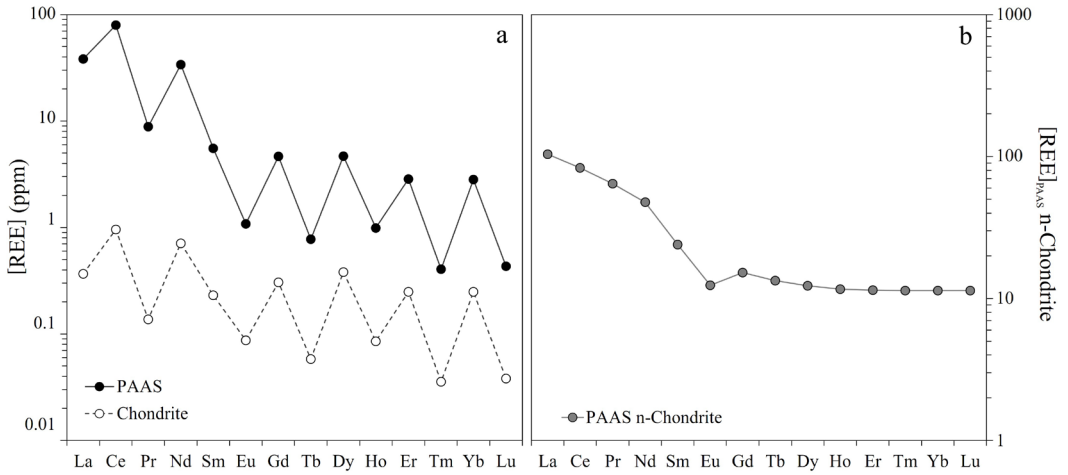

Figure 1.4: Effect of the normalization on the rare earth elements patterns. The “zig-zag” shape of the patterns of the REEs analytical concentrations plotted against the atomic number (3a) is avoided with the normalization (3b).

The anomalies are usually quantified as the ratio between the normalized concentration of an element and its presumed concentration based on the average normalized concentrations of the single REEs that precede and follow the element of interest, according to the following formula:

$$\mathrm{REE}_i^* = \frac{2\times[\mathrm{REE}_i]}{[\mathrm{REE}_{i-1}]+[\mathrm{REE}_{i+1}]} \qquad \text{(Eq. 1.4)}$$

where REE_i^* indicate the anomaly for the element i, $[\mathrm{REE}_{i-1}]$and $[\mathrm{REE}_{i+1}]$ the concentrations of the elements that respectively precede and follow i in the series. Anomalies are of great interest because they allow for the identification of specific geochemical processes. For example, positive Gd anomalies in rivers may indicate anthropogenic contributions from wastewater treatment plants (Bau and Dulski 1996; Hissler *et al*., 2015), positive Eu anomalies may indicate the occurrence of hydrothermal contributions in natural waters (Olivarez and Owen, 1991), while negative or positive anomalies of Ce may suggest respectively oxidizing or reducing conditions in the dissolved phase. However, a

comprehensive explanation of the geochemical significance of REEs anomalies and pattern shapes will be provided a case-by-case basis in chapters 4,5 and 6.

1.7 Thesis outline and research questions

The research questions, on which this study is based, aim both to fill some of the existing gaps in eco-hydrology regarding tree water extraction techniques and interpretation of the resulting isotopic data, and to explore REEs as new potential eco-hydrological tracers through the study of their dynamics in the regolith-tree continuum. A first introduction to the research questions addresses in this manuscript is given in the outline of the thesis' chapters reported below.

Chapter 3 focuses on understanding the potential influence of physical and biochemical processes on the O-H stable isotopes composition of the water across the soil-branch flow path of *Fagus sylvatica* trees. Innovative in-situ extraction techniques for sampling tree water are presented, specifically designed to examine the interplay between isotope chemistry and tree physiology in shaping the isotopic signature of diverse tree water pools, with an emphasis on xylem water. In this chapter, the following research questions are addressed:

i. How does the isotopic signature of water change as it flows through *Fagus sylvatica* trees, and what are the (bio)chemical and physical processes potentially responsible for such changes?
ii. How does this affect the accuracy in the identification of the water source absorbed by trees?
iii. Does water collected from roots represent a better tree water pool for identifying water source absorbed than samples collected from other parts of the tree, due to a shorter exposure time to the fractionation processes discussed in questions i and ii?

Chapter 4 is a short chapter that centers on the comparison of the tree water extraction techniques developed in this project, and presented in chapter 2, with the conventional method used in eco-hydrological studies. Both the advantages and drawbacks of these techniques are examined and new perspectives on the interpretation of isotopic data of tree waters are proposed. In this chapter, the following research question is addressed:

i. What are the (bio)chemical and physical processes that occur during tree water extraction via cryogenic vacuum distillation and during isotopic analysis that may potentially lead to bias in the resulting water isotopic signature?

Chapter 5 delves into the geochemical behaviour of Rare Earth Elements at the root/soil interface, as well as the mechanisms involved in their transportation along the root-shoot pathway of *Fagus sylvatica* trees. Special consideration is given to the processes of fractionation of these elements between the solid fraction of the root and the xylem during the water uptake. This investigation enables for the first-time the use of REEs as potential tracers for identifying the water source absorbed by trees. In this chapter, the following research questions are addressed:

i. What processes are involved in the fractionation of REEs between water, roots, and sap during water uptake in *Fagus sylvatica* (European beech) trees?
ii. Can the identification of the processes responsible for REEs fractionation during water uptake be used to determine the environmental source of the water absorbed by trees?
iii. To what extent could REEs be considered as conservative in the root-branch flow path?

Chapter 6 briefly explores the influence of European beech exudates on the REEs composition of throughfall. Particular attention is therefore given to the chemical composition of precipitation, throughfall and transpired water – which contains the exudates, also considering the potential impact of atmospheric dust in the resulting REEs patterns of the above-mentioned solutions. In this chapter, the following research questions are addressed:

i. How do leaves exudates influence the REEs composition of throughfall?
ii. How does the chemical interaction between transpired water and throughfall with the atmospheric dust, impact the resulting REEs signature of these solutions?

Chapter 7 continues on the notes of the previous chapter, examining the release of REEs back to the environment through the wet degradation of litter. Via laboratory leaching experiments, a thorough investigation of the potential mechanisms involved in the REEs fractionation between the solid matter and resulting solution was carried out. The tree species investigated are *Fagus sylvatica* and *Pseudotsuga menziesii*, with distinct REEs dynamics observed during the degradation. The outcomes of the leaching experiments also demonstrate how the degradation of litter from various tree species can affect the REEs

composition of soil solutions differently. In this chapter, the following research questions are addressed:

i. What processes are primarily responsible for the fractionation of REEs between leaf tissues and water during the wet degradation of *Fagus sylvatica and Pseudotsuga menziesii* (Douglas-fir) litter?
ii. Are REEs suitable indicators for the level of degradation of litter?
iii. To what extent can the degradation of litter impact regolith waters and influence their REEs composition?

Chapter 8, finally, presents a synthesis of, and reflection on, the results described in chapters 3-7. A conceptual model describing the REEs cycle at tree scale is also proposed, comprehending all processes highlighted in the present document from their uptake together with the water to the release back into the environment with the exudates and litter degradation.

CHAPTER 2

The Weierbach experimental catchment

2.1 Study site

All data provided in this thesis has been obtained from The Weierbach experimental catchment (WEC) (Hissler *et al*., 2021). This 0.45 km² headwater catchment is part of the Alzette River basin and is situated within the Luxembourg Ardennes Massif (latitude: 49.8273, longitude: 5.7956 – Figure 2.1). The catchment has an average altitude of 500 meters above sea level and experiences a semi-oceanic climate, with an annual average precipitation of 953 mm (Pfister *et al*., 2017).

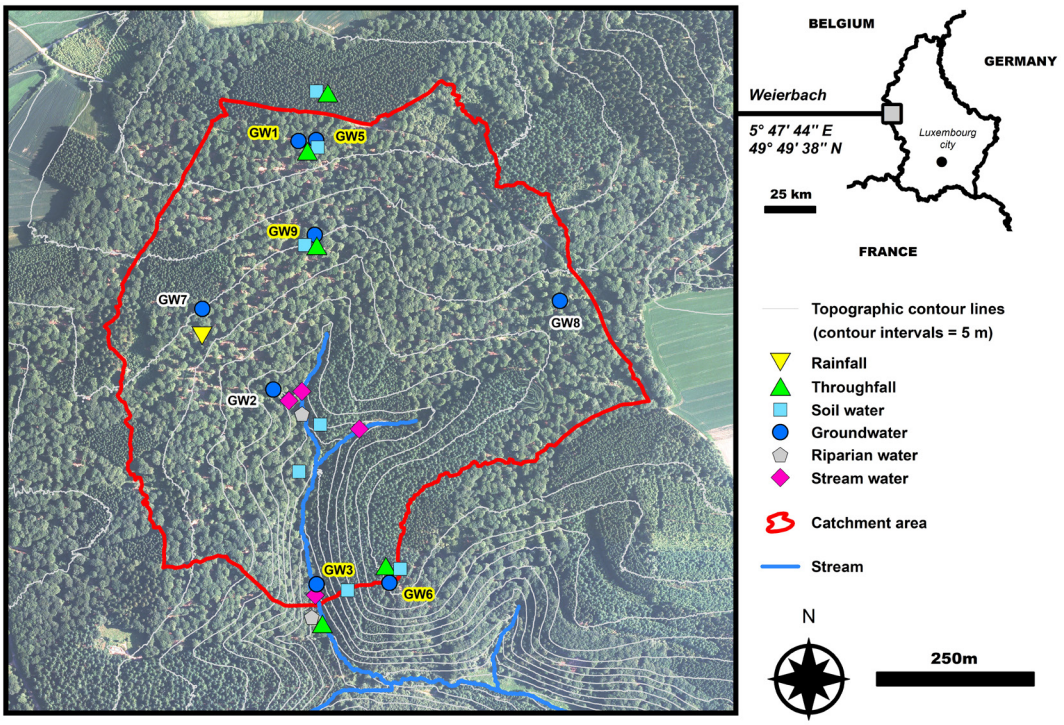

Figure 2.1: the Weierbach experimental catchment and the relative sampling locations. GW refers to groundwater wells. All locations but P9 were used to obtain the historical database (2009 – 2016). Yellow-highlighted sites refers to the sites chosen for this thesis and related newly acquired data.

The geological composition of the WEC consists of Devonian metamorphic slates overlain by Regolith Saprolite (Gleyic, Ruptic, Rootic, Siltic, Skeletic) (Juilleret *et al*., 2016). The soil is composed of Pleistocene Periglacial Slope Deposits and classified as Dystric Cambisol (Ruptic, Endoskeletic, Siltic, Protospodic) (Juilleret *et al.*, 2016; Moragues-Quiroga *et al.*, 2017). The catchment is predominantly forested, with 70% covered by European beech (*Fagus sylvatica* L.) and sessile oak (*Quercus petraea*), and the remaining 30% by Norway spruce (*Picea abies*) and Douglas fir (*Pseudotsuga menziesii*). Hydro-meteorological parameters have been monitored at the WEC since 2000 (Pfister *et al*., 2017), along with chemical data for regolith compartments and water pools from 2009 to 2016 including soil, bedrock, rainfall, throughfall, groundwaters, soil solutions, and streamwater.

2.2 REEs-based statistical separation of WEC waters

In order to provide a comprehensive understanding of the long-term chemical characteristics of various water pools within the WEC and to observe whether or not the difference water source can be distinguished for their REEs characteristics, the REEs data from the historical database was used. This data was employed to classify the waters into distinct groups based on their similarities in terms of REEs composition and patterns. To accomplish this, a Hierarchical Cluster Analysis (HCA – Figure 2.2a) (Hartigan, 1975) and a Principal Component Analysis (PCA – Figure 2.2.b) (Pearson, 1901) were performed. These analyses were conducted using a long-term monitoring dataset spanning from 2009 to 2015, which encompassed fortnightly assessments of water quality in various compartments of the WEC CZ. This included samples collected from above-ground sources, such as rainfall and throughfall, as well as samples obtained from different locations across the catchment, as illustrated in Figure 2.1, including soil solutions extracted at depths of 10 cm, 20 cm, 40 cm, 60 cm, and 100 cm, along with groundwaters, riparian water, and streamwater. The parameters chosen for the statistical analysis were: concentrations of LREEs, MREEs and HREEs, Ce anomalies, Pr anomalies, Gd anomalies, Eu anomalies, La_N/Yb_N, La_N/Eu_N and Gd_N/Yb_N ratios.

The objective of the HCA is to divide observations into clusters. This method may implement a bottom-up (agglomerative) or a top-down (divisive) grouping strategy, where observations are categorized in a way that those in the same cluster have minimal dissimilarities, unlike those from different clusters (Hastie, 2009). HCA is a prevalent clustering approach in Earth sciences and sees consistent application in hydro-chemical and geochemical studies (e.g. Güler *et al*., 2002; Reimann *et al*., 2002; Güler and Thyne, 2004;

Ayenew *et al.* 2009; Zhou *et al*., 2018). HCA requires a metrics for dissimilarity or linkage. For this instance, the chosen linkage rule applied was the Ward's method (Ward, 1963) with the Euclidean distance as the measure of dissimilarity between data points.

PCA is instead a statistical method used in multivariate analyses, with the primary objective to simplify the complexity of a multivariate dataset while retaining as much of its original variation as possible (Everitt and Hothorn, 2011). This is achieved by converting the dataset into a new set of variables, referred to as principal components (PCs). These latter represent linear combinations of the initial variables and are mutually uncorrelated. Furthermore, these PCs are ranked so that they account for the variance in the original dataset in decreasing order of significance, with PC 1 explaining the highest variance and so on. The total variance in the initial dataset can be accurately represented only by the complete set of PCs, but not all PCs are beneficial in comprehending the inherent structure of the data. PCA is usually applied together with the HCA in order to have a better understanding of the correlation (or uncorrelation) between variables, as other studies suggest (Melloul and Collin, 1992; Winter *et al*., 2000; Guler et al., 2002; Guler and Thyne, 2004; Thyne *et al*., 2004; Cloutier *et al*., 2008). While HCA is typically employed to initially group the samples in most workflows observed in multivariate statistical studies, the PCA simplifies the dimensionality of a complex dataset and reveal hidden data patterns (Davis and Sampson, 1986).

It is worth noting that both HCA and PCA were not performed on the raw data but applied on log transformed and z-standardized values (Reimann *et al*., 2011). While the prior log transformation is used to reduce the skewness of the variables (i.e., to reduce the influence of extreme values or outliers), the standardization is important to solve problems related to scale differences as data variables often have different scales or units of measurement. Without standardization, the variable with the larger scale would disproportionately influence the result, simply due to its larger values. The Z-standardization, or z-scaling, involves transforming the data such that it has a mean of 0 and a standard deviation of 1.

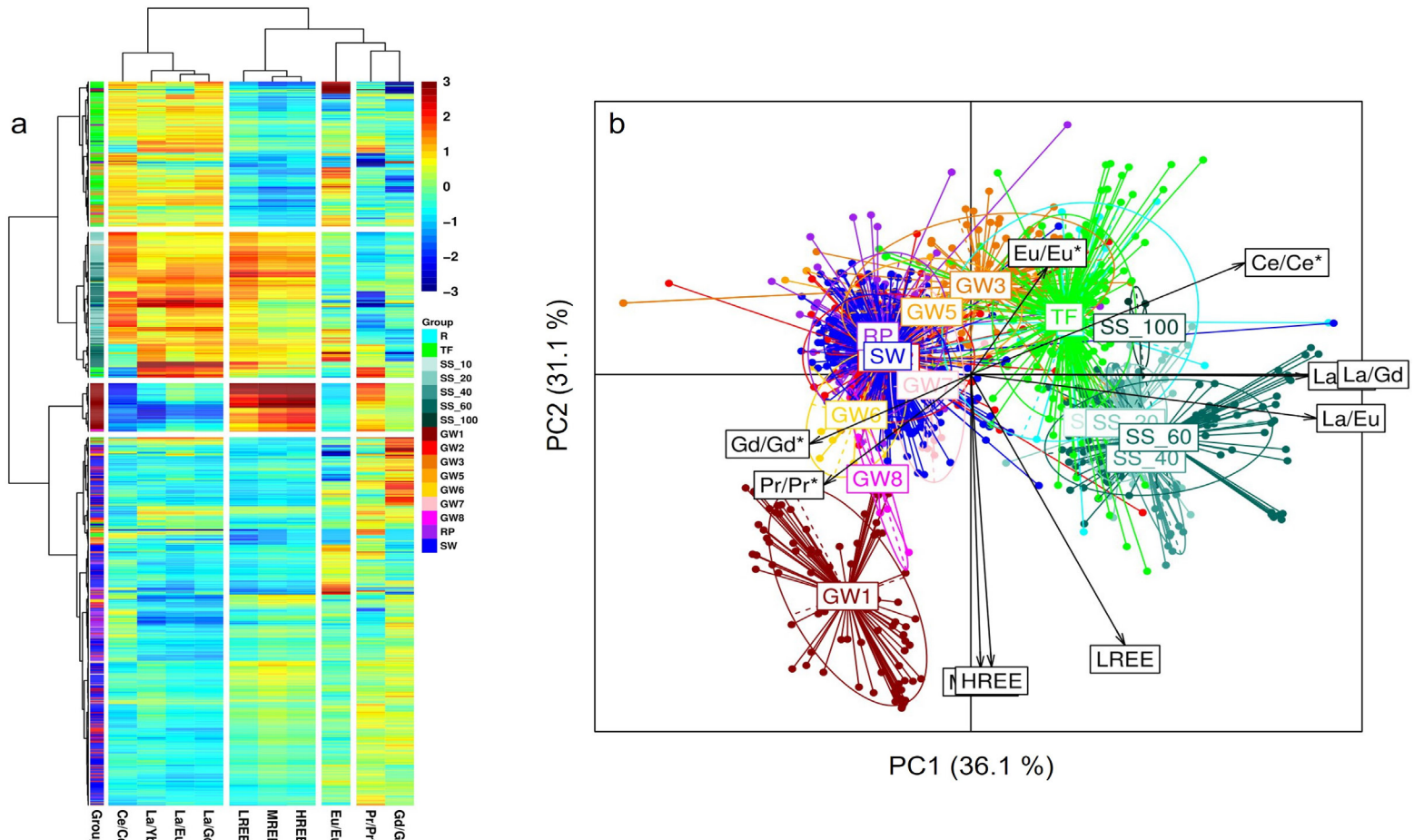

Figure 2.2: Hierarchical Cluster Analisis (a) and Principal Component Anaylisis (b) of REEs concentrations and pattern parameters for the regolith water sources from the Weierbach experimental catchment database (2009-2015). Both the HCA and the PCA were performed on Log-transformed and scaled data. For the HCA, Euclidean distance was used for the grouping and the Ward's method for the linkage rule. The color scale of the heat map refers to the values of the scaled data.

The main outcomes of the HCA and PCA based on REEs concentrations and patterns' features calculated from the historical database comprehending groundwaters (GW), soil solutions at different depths (SS) riparian water (RP), throughfall (TF), rainfall (R) and streamwater (SW) are illustrated in Figure 2.2. The classification of the samples was determined through visual observation of the dendrograms in Figure 2.2a and the choice to create four clusters was arbitrary but dictated by the trends of the different components in the PCA reported in Figure 2.2b. The horizontal dendrogram subdivides the water pools used for the HAC in groups according to the trend of the variables.

Cluster 1 is mainly associated to the throughfall, GW3 and GW5. This cluster is characterised by particularly low concentrations of REEs (LREEs, MREEs and HREEs), as well as low Ce/Ce*, Pr/Pr*, Gd/Gd* and LREEs.

Cluster 2 is composed of soil solutions at all depths (10, 20, 40, 60, 100 cm) and rainfall, which suggests a direct connection between these water pools, probably linked to percolation processes following rain events. This cluster is associated to higher Ce/Ce* values, LREEs and MREEs enrichment, as well as low values of Gd/Gd* and Pr/Pr*.

Cluster 3 comprehends GW1, which is the only shallow groundwater sampled. This cluster is characterized by the lowest Ce/Ce* amongst the water pools, low Eu/Eu*, high Pr/Pr* and by a depletion in LREEs in comparison to MREEs and HREEs. On the other hand, REEs concentrations appear to be the highest among the sampled water types.

Cluster 4 is associated to GW2, GW6, GW7, GW8, RP and SW. This cluster shows Low Ce/Ce* values, as well as depletion in LREEs. Together with Cluster 1, Cluster 4 is characterized by the lowest REEs concentrations, as well as high variability in the Eu/Eu* values.

The PCA (Fig. 2.2b) show the groups from another perspective. The principal component 1 (PC1) accounts for 36.1% of the total variance. This indicates that PC1 captures a significant portion of the variability in the dataset and it appears to be driven by Ce/Ce* and LREEs enrichment parameters (La/Gd, La/Eu, La/Yb). It is possible indeed to notice the positive correlation between all soil solutions, which usually show a positive Ce anomaly and an LREEs enrichment as already observed in the dendrograms of the HCA. On the other hand, all GWs result instead negatively correlated to the soil solutions, due to LREEs depletion and negative Ce anomalies. The PC2 explains the 31.1% of the variance and is mainly driven by the REEs concentration in the waters. GW1 indeed presents the highest correlation together with GW8, GW6 and soil solutions. All the other GWs, as well

as rainfall, throughfall, riparian water and streamwater are negatively correlated, due to their lower REEs content.

Collectively, PC1 and PC2 explain a cumulative variance of 67.2%, highlighting their significant role in capturing the majority of the variability in the REEs concentrations and patterns characteristics. This underscores the importance of these principal components in summarizing and understanding the underlying structure of the dataset, particularly in relation to grouping water sources based on the given parameters. PC1 and PC2 effectively represent the primary patterns in the hydro-chemical parameters, allowing for meaningful differentiation and classification of the water sources based on their REEs patterns and similarities. Furthermore, the clustering analysis highlights the potential for classifying the various water sources stored in the regolith of the catchment area and their relative temporal stability during the recording period (2009-2016). This can aid in the understanding of water exchange dynamics between different compartments of the CZ, with a particular focus on investigating processes at the interface between compartments, such as the regolith-plant continuum.

CHAPTER 3

Progressive enrichment in ^{18}O and ^{2}H in xylem sap of *Fagus sylvatica* trees

Abstract

Isotopic signatures of xylem water in different tree compartments such as roots, boles, and branches, differ due to physiological and physical processes occurring inside trees. Accordingly, we hypothesized that the extent of such differences among the isotopic signatures of tree compartments is coherent with the distance travelled by the water inside trees and to its residence time. To test, we compared the O-H isotopic composition of xylem water collected using an in-situ water extraction method from roots, boles, and branches of Fagus sylvatica trees growing on 3 geomorphological units of the Weierbach experimental catchment, Luxembourg. There was progressive ^{18}O and ^{2}H enrichment in xylem waters along the root-branch flow path for all the studied trees. There are three potential explanations – or a combination of these – for the progressive enrichment: internal fractionation by xylem-phloem water exchange; chemical reactions of metabolic pathways; variable ages of water retained in the xylem, reflecting historical variation in isotopic composition of uptake water. Support for the hypothesis of isotopic fractionation linked to xylem-phloem water exchange and chemical reactions, is that enrichment was generally consistent with the distance travelled by the water and to its residence time inside the trees. However, the relative enrichment of ^{2}H and ^{18}O was not consistent along the flow path, with $\Delta^{2}H/\Delta^{18}O \approx 7.5$ from the soil into the roots and bole, and ≈ 4.7-6.5 for pathways that included smaller branches. This contrast suggests different processes controlled above-ground isotopic enrichment. In particular, the slope of ~7.5 in the lower tree is also consistent with variation in tree water uptake varying along the local meteoric water line, with water in the roots being closer to the composition of rainfall close to the time of sampling and water in the bole being closer to the composition of rainfall the previous summer.

The timing of root and bole sampling in early spring, just before leaf-out, means sap flow was very slow and makes it plausible that varying-age water was present in the tree at that time. We also compared the O-H isotopic composition of those samples with the ones of the potential water sources to identify the origin of the water uptaken. The latter varied during the three years of sampling, with a preferential uptake from near-surface waters. Our results suggest multiple biochemical, physiological, and physical processes may play fundamental roles in the isotopic composition of xylem water within trees.

3.1 Introduction

Water availability in forest ecosystems controls tree physiological processes such as transpiration, photosynthesis, and growth (Breda et al., 2006). Brinkmann et al. (2019) showed that the water uptake depth of deciduous temperate trees varies according to soil water availability and that species differ in root system plasticity in response to water accessibility in the subsurface. When water availability is reduced during the growing season – as is common in temperate forests, and intensified during droughts, it affects water transfer along the soil-tree-atmosphere continuum, restricting growth and transpiration and thus affecting tree adaptation strategies and survival. Despite the number of research projects focusing on this topic, a full understanding of where trees uptake water remains elusive.

Most ecohydrological studies to determine tree water sources rely on water stable isotopes, which have been used since the 1960s. The principle behind their hydrological application is that different water pools are often characterized by distinctive H and O isotopic composition. These so-called “isotopic signatures” allow tracing water through various hydrological processes such as groundwater recharge (Muir and Tyler, 1981; Joshi et al., 2018; Liu and Yamanaka, 2012; Adomako et al., 2015), water dynamics in the vadose zone (Gascuel-Odoux and Mérot, 1986; Barnes and Allison, 1988; Dawson, 1993; Barbecot et al., 2018; Rodriguez et al., 2018) and in urban environments (Wilcox et al., 2004; Houhou et al., 2010; Ehleringer et al., 2016). They can also be used to reconstruct past environmental conditions (Dawson and Ehleringer, 1993; Yakir 1992), both in terrestrial and aquatic environments (DeNiro and Epstein, 1981), relying on the isotopic composition of wood cellulose, since this derives from the source water at the time of biosynthesis.

Despite the extensive use of water stable isotopes to study tree-water interactions, such as transpiration and tree water uptake (Wilm, 1944; Wang and Yakir, 2000; Brooks *et al*., 2010; Schlesinger and Jasechko, 2014; Ehleringer & Dawson, 1992; Farrington *et al*., 1996; Burgess *et al.*, 2000; Fabiani *et al*., 2021), the effect that tree physiology and the related biochemical processes have on O-H isotopic composition of xylem water is still poorly understood because most studies have focused on the isotopic composition of bulk water in trees rather than specifically on the most mobile xylem sap in the young sapwood. Water in trees consists of several pools, each of which is characterized by a distinct isotopic signature (Barbeta *et al*., 2022 – and reference therein). This phenomenon, known as water compartmentation (Yakir, 1992b), can be linked to a multitude of factors including differences in the residence times of the water distributed among the tree tissues, biochemical interactions along metabolic pathways, and physical processes involving water. Water

participates in several chemical reactions in trees, modifying its isotopic composition via O and H isotopic exchange processes. Cormier et al. (2018), for instance, showed H isotopic exchange between water and organic molecules during plant carbohydrate and lipid biosynthesis, resulting in ^{2}H-enrichment for the water and depletion for the organic compounds. Photosynthetic and post-photosynthetic metabolism, indeed, play a role on the O-H isotopic modification of water and organic molecules. Organic matter produced during photosynthesis exhibits a lighter isotopic signature than the available water (Estep & Hoering 1980) and, when transported through the tree, exchanges isotopes with water (Yakir & DeNiro, 1990; Yakir, 1992a). A typical example is cellulose biosynthesis, which involves isotopic exchange between water and organic precursors influencing $\delta^{2}H$ mutually (Yakir, 1992a; Sternberg, 2009; Hill *et al*., 1995). More recently, Nehemy et al. (2022) reported that light water molecules are more prone to flow from xylem to phloem vessels, leading to an enrichment in heavy water isotopes in the xylem and a depletion in the phloem, supporting what was already assumed in previous studies (Ziegler, 1989). Most ecohydrological studies that used water isotopes have not considered that these multiple isotopic exchanges processes – both biochemical and physical – inside trees make isotopic signatures in the root-branch pathway non-conservative. The impact that tree physiology and the different chemical dynamics associated to the diverse isotopes have on the isotopic signature of xylem water along the root-branch flow path needs to be investigated in more detail. A better understanding of the net effect of multiple isotopic fractionations is needed to improve the utility of isotopic tracers for evaluation of plant-water interactions.

In this study, we hypothesized that isotopic signatures of xylem water extracted from different tree compartments such as roots, boles, and branches, differ due to continuous changes of the originally uptaken source, due to physical and physiological processes occurring inside trees. Moreover, the intensity of such changes is coherent with the distance travelled by the water and to its residence time inside trees. Assuming that no isotopic fractionation occurs during the water uptake (White *et al*., 1985; Dawson and Ehleringer, 1991; Ehleringer and Dawson, 1992), the hypothesis entails that the O-H isotopic composition of root sap is the closest to that of water sources and the longer the distance travelled by the water and/or the longer the residence time inside trees, the longer the sap is exposed to physical and metabolic processes and the greater is the change in its O-H isotopic composition. We base the investigation on liquid water extracted at low vacuum and ambient temperature from xylem, avoiding methodological biases associated with the typical cryogenic distillation technique (Allen and Kirchner, 2022). We focused our study on Fagus

sylvatica trees during the beginning of the growing season, when trees start photosynthesis. The latter is an important phase for the recovery of the hydraulic conductivity of trees after winter embolism, during which biochemical processes – such as the ones promoting the formation of a new xylem ring (e.g. cellulose biosynthesis) – may alter the isotopic composition of xylem water (Cochard *et al*., 2001; Améglio *et al*., 2002). The choice of Fagus sylvatica as candidate for this study is linked to the fact that this species is one of the most widespread in Europe, and one of the most sensitive to droughts (Lindner *et al*., 2014). Furthermore, its importance resides in its dominance in regional ecosystems and in its economic utility (Durrant *et al*., 2016). Therefore, understanding water uptake and storage dynamics of F. sylvatica is crucial for preventing climate change from threatening its geographical and ecological distribution (Fang and Lechowicz, 2006; Martinez del Castillo *et al*., 2022). The study aims to provide evidence that the isotopic signature of xylem water changes during longitudinal flow from roots to branches and to emphasize potential physical and biochemical processes that may act in this way and that should be considered when studying the isotopic composition of tree waters for hydrological purposes.

3.2 Materials and methods

3.2.1 Study site

The study was conducted in the Weierbach experimental catchment (Hissler *et al*., 2021), which is a 0.45 km2 forested headwater catchment of the Attert River Basin, in the Luxembourg Ardennes Massif at 512 m a.s.l. The Attert River Basin has been a focus area for eco-hydrological research since 2009 (e.g. Glaser *et al*., 2016; Antonelli *et al*., 2017; Hoek van Dijke *et al*., 2019). The most abundant tree species are European beech (Fagus sylvatica L.) and oak (Quercus petraea), together covering 75% of the catchment, while Norway spruce (Picea abies) and Douglas-fir (Pseudotsuga menziesii) cover the remaining 25%. As geomorphology and hydrological processes vary within the catchment (Martinez-Carreras *et al.,* 2016), three sites were chosen to identify the potential variation of water sources available to tree uptake across the different morphological units: a plateau, a hillslope, and a riparian area (Figure 3.1).

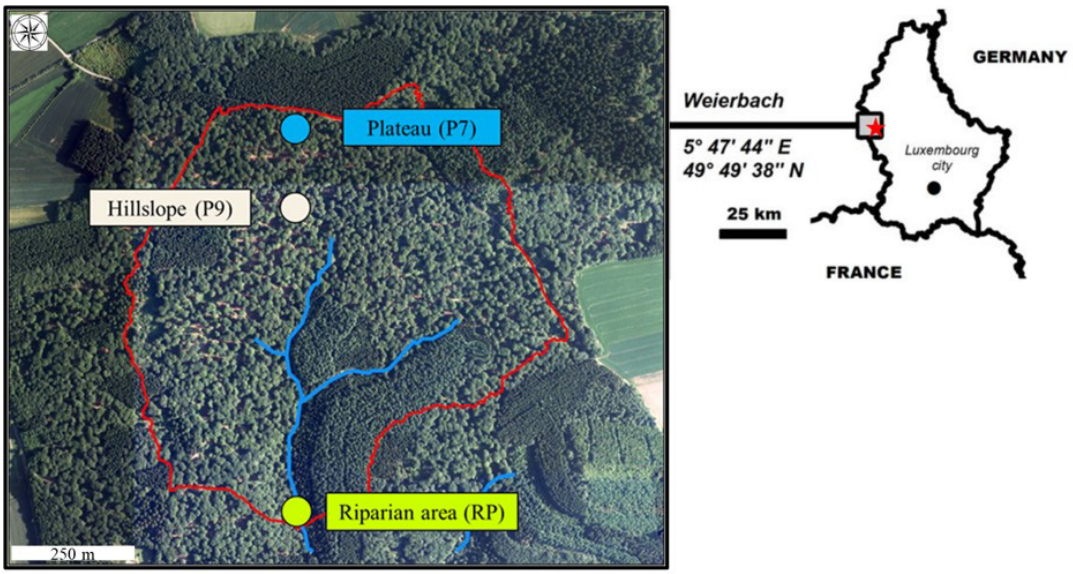

Figure 3.1: Aerial map of the Weierbach experimental catchment and its relative position in Luxembourg.

3.2.2 Sampling campaigns

Three sampling campaigns were carried out in three years with varying methods and hydro-climatic conditions (Fig. 3.2) over the beginning of the growing season. The sample campaigns included sap collection from different structural parts of the trees (roots, bole, branches) and different potential water sources (streamwater, soil solutions, shallow and deep groundwaters). From March to May 2017, we collected sap samples only from roots and branches of the plateau trees, soil solution at 20 and 60 cm depths, shallow groundwater (220 cm depth), and deep groundwater (720 cm depth). In March 2020, a one-day sampling campaign was carried out on the three sites to collect root sap, branch sap, soil solutions at 20, 40, and 60 cm depths, groundwaters, and streamwater. In July and August of the same year, we collected branch sap, groundwaters, and streamwater, but no soil solutions or shallow groundwater because the soil and well were dry in summer. In March 2021, sampling was carried out at the three morphological units to collect branch sap, root sap, bole sap, soil solutions, groundwaters, and streamwater.

For all sampling campaigns, 3 beech trees in each experimental site were sampled. All sampled trees in the plateau and hillslope were large-diameter individuals (50-75 cm diameter), while in the riparian area only trees with smaller diameters (25-50 cm) were available. The hydro-climatological conditions and the sap velocity at the time of the

sampling were recorded for a better understanding of water stable isotopes dynamics in trees (Figure 3.2).

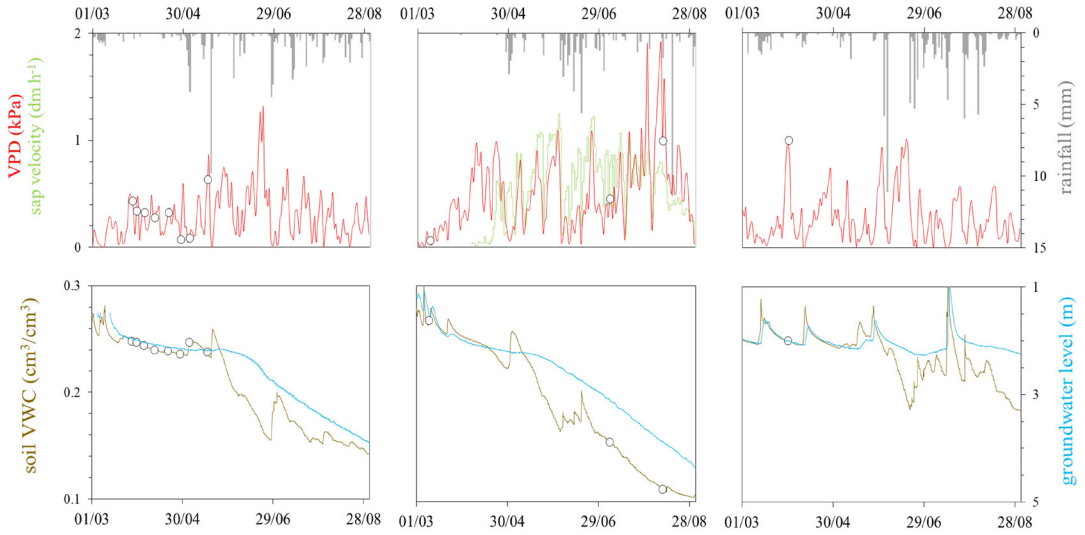

Figure 3.2: Hydro-climatological parameters (Hissler *et al.* 2021) and sap velocity (Fabiani *et al.,* 2021) measured at the Weierbach experimental catchment during the tree sampling campaigns in 2017, 2020 and 2021. White dots indicate the specific dates of sampling. Groundwater level relates to the depth below the surface; sap velocity and temperature are the daily means derived by hourly measurements.

3.2.3 Waters sampling, tree sap extraction techniques and sample analyses

Precipitation was collected using a 3-L Palmex rain sampler (M.Gröning *et al*., 2012), which minimizes gas transfer between the bottle headspace and the open atmosphere to reduce evaporation. The average isotopic composition of the summer and winter precipitations was computed using the online database of the Weierbach experimental catchment (Hissler et al., 2021). The soil solution was collected at 20, 40 and 60 cm depth using Teflon/quartz suction cups (SDEC, Reignac-sur-Indre, France) connected to 2-L Nalgene bottles under a vacuum of 80 kPa. Shallow and deep groundwaters were collected from wells using a peristaltic pump, while the streamwater was directly gathered into polyethylene bottles.

Sap from upper tap roots, boles, and from 2nd and 3rd order branches was directly extracted as liquid in the field using in-situ extraction techniques. Two in-situ vacuum extraction (*I*SVE) and one overpressure techniques were applied to collect sap according to the targeted tree compartment and to the season, as sap accessibility greatly differs between the beginning of the growing season in spring (March to May) and the transpiration period

in summer (July to August). These extraction techniques were all designed to collect sap flowing in the xylem at the moment of sampling, so we considered all sap samples as equal.

The first *IS*VE technique was used in spring for roots and boles. Cores from roots and boles were removed (data not shown in this study) with an increment borer, and the sap was collected by connecting the resulting cavity in the tree to a modified version of the portable device developed by Regulski and Peterson (1982) and applying vacuum. The apparatus consists of a vacuum system (Fig. 3.3a, b) composed of a Duran® 100 ml glass bottle capped by a 2-hole KIMBLE® filtration adapter cap and a metal-free 50 ml centrifuge tube for sap conveyance. A vacuum of 0.80 kPa was applied using a field vacuum pump (SDEC, model PAV 2000). This system allows for the collection of 10 to15 ml/min of sap. The second *IS*VE technique was applied in spring for sap collection from non-suberized, 2nd and 3rd order branches. After cutting away the extremity (~1 cm), a 60 ml polypropylene syringe (BD Plastipak™) was connected via a rubber tube to the end of the branch and the sap was extracted by pulling and blocking the syringe piston (Fig. 3.3c). To obtain representative samples, 10 syringes were installed on each tree in all radial directions and at branch heights from 2 to 5 meters. All sampling replicates were pooled into one liquid sample per tree. The overpressure technique was used to obtain the sap during the growing season, from July to August. During this period, the highly negative water pressure in the xylem did not allow the extraction of sap with the low vacuum techniques used in spring, so extraction of water was performed on 2nd order branch chunks of 10-15 cm length (Fig. 3d) by extrusion using a peristaltic pump (Solist, peristaltic pump model 410).

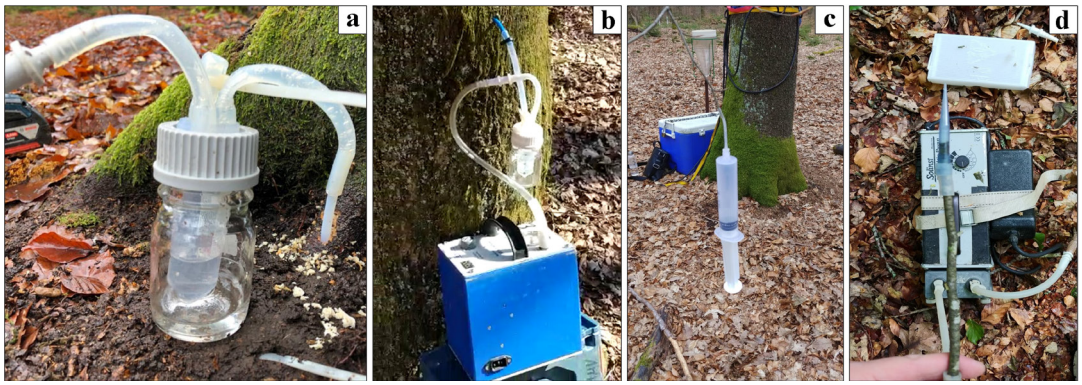

Figure 3.3: Apparatus for in-situ vacuum extraction of sap from (a) roots and (b) boles prior to leaf out; (c) syringe system for branch sap collection prior to leaf-out; and (d) branch sap extraction system used during transpiration.

Once a chunk of branch was cut, the bark at each chunk extremity was removed to avoid contamination from phloem. A rubber tube was then used to connect one end of the chunk and the peristaltic pump. The peristaltic pump was then activated to push air into the chunk, forcing the sap out from the other extremity directly into a 5 ml syringe equipped with a 0.45 µm filtering membrane. To avoid isotopic fractionation due to the contact with the atmosphere, sap samples collected in this way were immediately expressed into 2 ml vials and sealed. With this technique, the volume of water extracted over time was lower than that of *IS*VE methods and 10 to 15 chunks were needed to collect 1 ml of sap in ca. 5 minutes. We applied the minimum pressure necessary to push the water out of the branch (pressure applied was not measured).

All sap and water samples were filtered at 0.45 µm, transferred to 2-ml glass vials, and stored at 4 °C before analysis. Precipitation, soil solutions, groundwater, and streamwater were analysed using a Los Gatos Research Triple Isotopic Water Analyzer (LGR TIWA-45-EP) coupled with an automatic sampler (PAL System). The analytical precision of the instrument is ± 0.50 ‰ for $\delta^{2}H$ and ± 0.15 ‰ for $\delta^{18}O$. The data obtained were processed with LWIA Post Analysis software. All sap samples were analysed via Picarro Cavity Ring Down Spectrometer (CRDS) (L2140-i, Picarro Inc., USA) coupled with an automatic sampler and a Micro-Combustion Module™ to eliminate organic compounds within the water samples. The presence of remaining organic contaminants was monitored with ChemCorrectTM software (Picarro Inc., USA). The analytical precision of the instrument is ± 0.7 ‰ for $\delta^{2}H$ and ± 0.05 ‰ for $\delta^{18}O$. The potential memory effects during the analyses with LGR and Picarro was minimized by measuring the isotopic composition 9 and 10 times for each sample and, among those, using only the last five values as the results (Penna et al., 2012).

3.3 Results

Table 3.1: Average δ^2H and $\delta^{18}O$ and standard deviation values for all the samples collected in this study. Legend: GW=groundwater; SS=soil solution; SW=streamwater; RS=root sap; TS=bole sap; BS=branch sap; *IS*VE=*In-situ* vacuum extraction from trees; *IS*VE PP=*in-situ* vacuum extraction from branch chunks; P7=plateau; P9=hillslope; RP=riparian area. Full dataset reported il Table A3.1.

Method	Sample	Site	2017		2020		2021	
			δ^2H (‰)	$\delta^{18}O$ (‰)	δ^2H (‰)	$\delta^{18}O$ (‰)	δ^2H (‰)	$\delta^{18}O$ (‰)
Peristaltic pump from wells	GW	P7	-52.35 ± 0.33	-8.21 ± 0.07	-55.17 ± 0.21	-8.61 ± 0.12	-56.30 ± 0.29	-8.80 ± 0.03
		P9	-	-	-54.72	-8.61	-56.10	-8.83
		RP	-	-	-53.99	-8.40	-55.05	-8.70
Teflon/quartz suction cups	SS	P7	-56.53 ± 5.15	-8.75 ± 0.75	-53.11 ± 3.12	-8.39 ± 0.39	-65.58 ± 7.63	-9.85 ± 0.97
		P9	-	-	-52.59 ± 6.82	-8.21 ± 1.00	-62.95 ± 7.09	-9.39 ± 0.83
		RP	-	-	-53.43 ± 0.18	-8.34 ± 0.06	-55.87 ± 0.45	-8.74 ± 0.06
Hand-collection with Polyethylene bottles	SW	RP	-	-	-54.02	-8.51	-55.39	-8.67
IS VE with syringes or vacuum pump	RS	P7	-47.77 ± 2.15	-7.51 ± 0.28	-49.47 ± 2.18	-7.91 ± 0.29	-59.99 ± 2.77	-9.06 ± 0.38
		P9	-	-	-47.39 ± 1.47	-7.62 ± 0.16	-55.97 ± 2.67	-8.67 ± 0.35
		RP	-	-	-51.30 ± 0.05	-8.15 ± 0.00	-52.70 ± 3.30	-8.07 ± 0.47
	BS	P7	-36.83 ± 1.37	-5.20 ± 0.36	-34.97 ± 0.74	-5.70 ± 0.16	-28.20 ± 8.89	-2.86 ± 1.75
		P9	-	-	-34.97 ± 0.41	-5.84 ± 0.13	-32.16 ± 3.62	-3.69 ± 0.73
		RP	-	-	-34.71 ± 1.19	-5.73 ± 0.06	-26.80 ± 6.46	-3.13 ± 0.98
	TS	P7	-	-	-	-	-53.13 ± 4.83	-8-27 ± 0.74
		P9	-	-	-	-	-49.81 ± 3.93	-7.85 ± 0.53
		RP	-	-	-	-	-48.86 ± 3.91	-7.61 ± 0.38
Overpressure with peristaltic pump (PP) on branch chunks	BS PP	P7	-	-	-45.66 ± 2.03	-6.73 ± 0.51		
		P9	-	-	-46.87 ± 1.20	-6.88 ± 0.15		
		RP	-	-	-42.55 ± 3.66	-6.41 ± 0.78		

3.3.1 O-H isotope composition of rainfall, regolith waters and sap

The historical database of the O and H isotopic composition of the rainfall (Hissler *et al.*, 2021 – and subsequent isotopic measurements) collected in the Weierbach Experimental Catchment revealed δ^2H ranging between -128.36 ‰ and -14.37 ‰, and $\delta^{18}O$ between -16.86 ‰ and -2.38 ‰ yielding the following Local Meteoric Water Line (LMWL):

$$\delta^2H = 7.4 * \delta^{18}O + 6.8 \quad \text{(Eq. 3.1)}$$

The rain collected during the summer and the winter before the sampling was enriched and depleted, respectively, in heavy isotopes in comparison with rain collected during the sampling campaigns (Fig. 3.4). Despite the different locations, spatial and temporal variations of the O and H isotopic composition of the groundwaters was low, while the variation of soil solution was the highest among all potential tree water sources (Table 3.1). Based on the depth and sampling dates, the isotopic composition of water sources collected at the plateau and hillslope sites varied spatially and temporally, whereas isotopic composition of all water types collected in the riparian area was quite consistent. Such

homogeneity is probably linked to the fact that groundwater, streamwater, and riparian soil solution mix in this location (Bonanno *et al*. 2021). Spatial variability of isotopic composition of root sap was lower in 2017 and 2020 than in 2021. The variability of the branch sap collected by *IS*VE in summer 2020 was low and its isotopic composition was lighter than that of samples collected in March of the same year. The isotopic signatures of *IS*VE-extracted sap by fell onto the LMWL (Fig. 3.4) for all sampling sites regardless of their geological morphology, hydrological conditions, sampling date, or tree size.

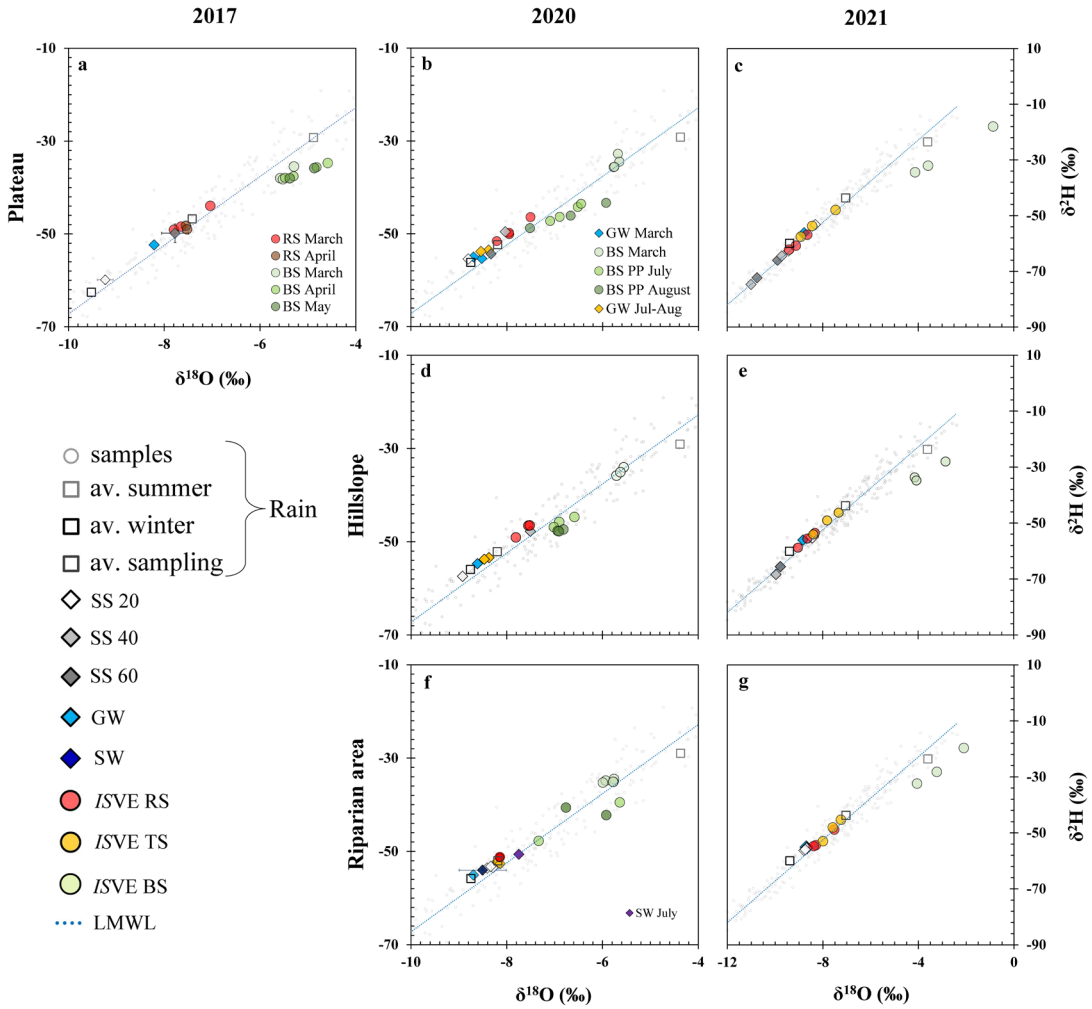

Figure 3.4: Dual isotope diagrams for all the collected waters in this study, sorted by year of sampling and morphological units. Legend: SS20,40,60 = soil solutions at 20, 40 and 60 cm depth; GW = groundwater; SW = streamwater, RS = root sap; TS = bole sap; BS = branch sap.

To measure the offsets from the LMWL, the line-conditioned excess (lc-excess) (Landwehr and Coplen 2006) was calculated for all collected samples as:

$$\text{lc-excess} = \delta^{2}H - 7.4\ \delta^{18}O - 6.7 \qquad \text{(Eq. 3.2)}$$

where 7.4 and 6.7 are the coefficients from the LMWL. The lc-excess values for all samples are reported in Figure 3.5.

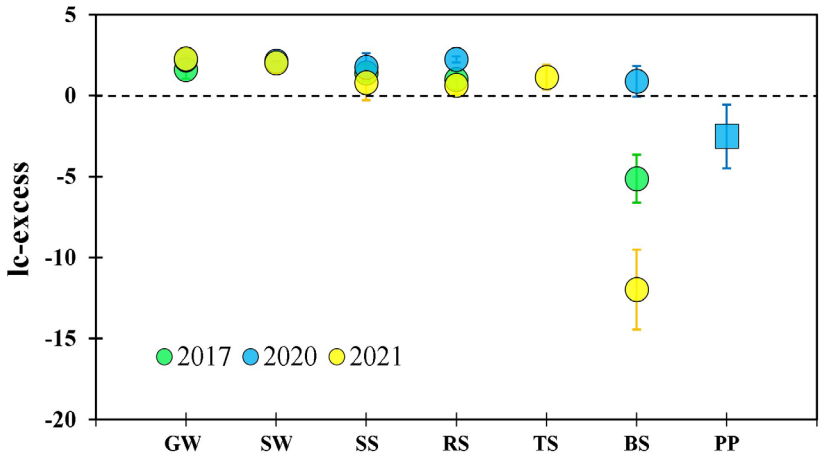

Figure 3.5: Lc-excess means and standard deviations for all types of samples collected in this study. GW=groundwater; SW=streamwater; SS=soil solutions; RS=ISVE root sap; TS=ISVE bole sap; BS=ISVE spring branch sap; PP=ISVE summer branch sap.

Among all the trees and sampling campaigns, lc-excess (deviation in observed $\delta^{2}H$ from the LMWL; Landwehr and Coplen 2006) was stable for *IS*VE root sap and bole sap (lc-excess$_{RS}$ = 1.34 ± 0.91 and lc-excess$_{TS}$ = 1.14 ± 0.83, respectively) and close to that of the groundwaters, streamwater, and soil solutions (lc-excess$_{GW}$ = 1.78 ± 0.61, lc-excess$_{SW}$ = 2.08 ± 0.08 and lc-excess$_{SS}$ = 1.24 ± 0.93, respectively) (Fig. 5). On the other hand, branch sap collected with syringes and peristaltic pump showed the highest variability and deviation from the LMWL and from the potential water sources (lc-excess$_{BS}$ = -5.12 ± 1.56 in 2017, lc-excess$_{PP}$ = -2.52 ± 2.03 in 2020 and lc-excess$_{BS}$ = -11.97 ± 2.77 in 2021), with the only exception of March 2020 (lc-excess$_{BS}$ = 0.89 ± 0.99).

3.3.2 Root-to-branch progressive ^{18}O and ^{2}H enrichment in xylem water

For all trees and all sampling dates at all locations, the trend of the O-H isotope signature of the sap collected by *IS*VE was a systematic enrichment in heavy isotopes from the roots,

through the bole, to the branches (Fig. 3.6). The sap collected from the branches plotted below the meteoric water line (Fig. 3.4), so the lc-excess of these samples was negative (Fig. 3.5).

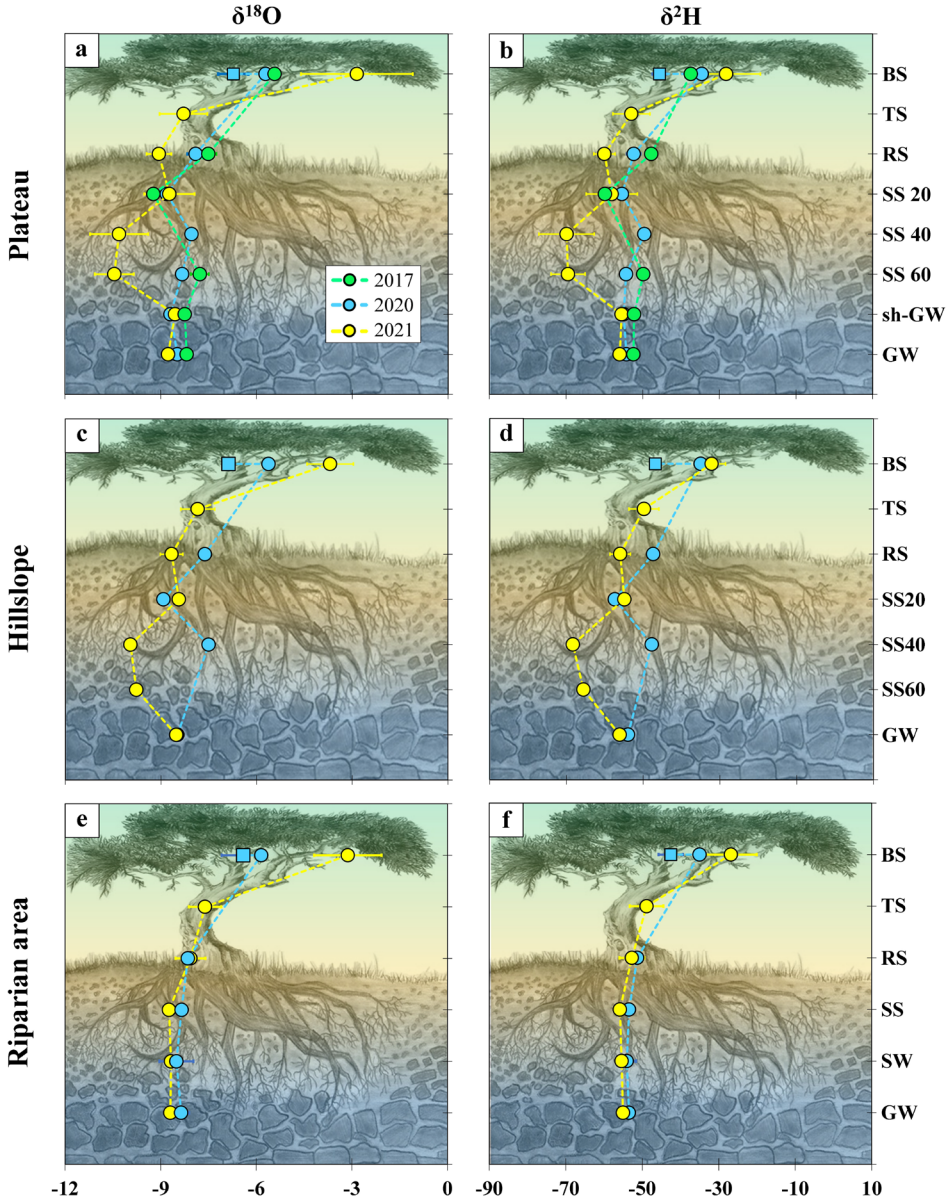

Figure 3.6: Progressive enrichment of the isotope ratios from the groundwater to the branches in the three experimental plots. For tree waters, circles indicate ISVE (syringe – vacuum pump) samples collected in spring, while squares indicate summer samples collected with the peristaltic pump. sh-GW=shallow groundwater; GW=deep groundwater; SW=streamwater; SS=soil solution; RS=root sap; TS=bole sap, BS=branch sap.

The gradual enrichment has been quantified for both elements as increments (Δ):

$$\Delta^{18}O = \delta^{18}O_b - \delta^{18}O_a \quad \text{(Eq. 3.3)}$$

$$\Delta^{2}H = \delta^{2}H_b - \delta^{2}H_a \quad \text{(Eq. 3.4)}$$

where specific tree compartments are denoted *b* and *a* (e.g. bole and roots). $\Delta^{2}H$ and $\Delta^{18}O$ for root-bole, bole-branch and root-branch were significantly correlated across all trees, sites, and dates (Fig. 3.7). The slope of this relationship is the ratio of the net fractionation of ^{2}H to ^{18}O along the sap flow path. Generally tight fits of data to sampling-event lines indicates that the ratio was consistent in time and space. The morphological characteristics of the sampling locations did not play a role in the slope of the relationship in the for soil-root or root-bole comparisons, whereas the $\Delta^{2}H$ and $\Delta^{18}O$ relationship from root to branch was specific for each year, varying from 6.5 to 5.0 among the three sampling campaigns (Fig. 3.7). The slope of $\Delta^{2}H/\Delta^{18}O$ for the root-bole segment was 7.5, which matched the slope of the LMWL, but the lower slopes in branch samples are consistent with an evaporation-like trend.

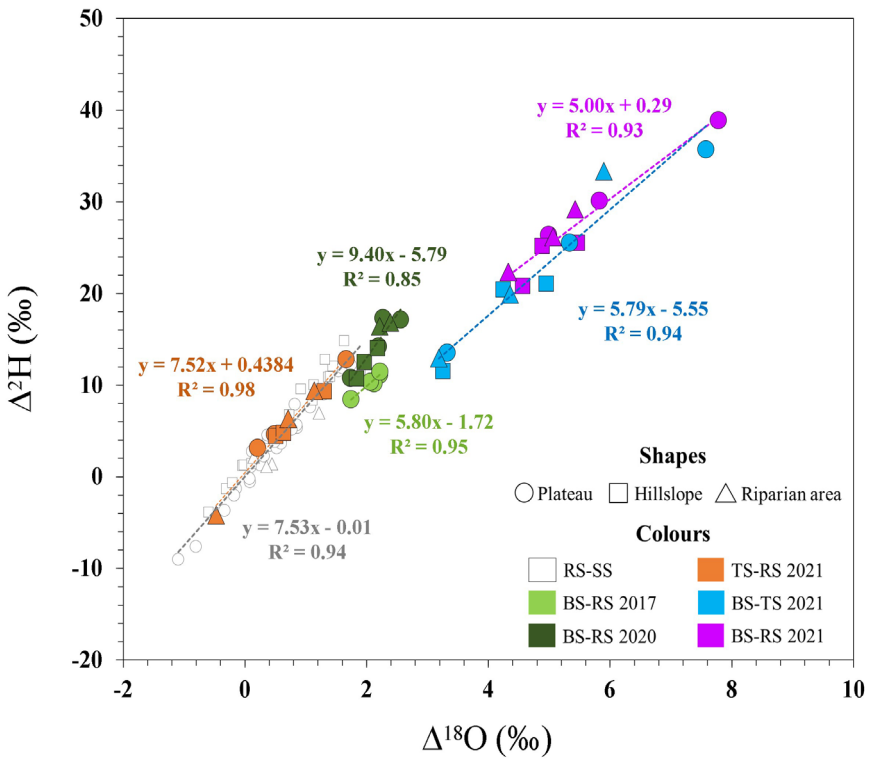

Figure 3.7: $\Delta^{2}H_{b\text{-}a}$ vs $\Delta^{18}O_{b\text{-}a}$ for all sap sampled collected in this study.

3.4 Discussion

3.4.1 Progressive ^{2}H and ^{18}O enrichment in xylem water

Our results show progressive heavy isotopes enrichment in xylem water, which appears to be consistent with the distance travelled from roots towards the upper tree compartments. However, the results also indicate that this progressive enrichment seems to be controlled by different mechanisms according to the tree compartment where it occurs. The enrichment observed from the soil to the bole stayed coherent between both O and H elements and is located along the meteoric water line, whereas the enrichment that appears between the bole and the branch presents a more evaporation-like trend.

The easiest way to explain the enrichment between the roots and the bole is to consider the mixing of water of different ages. It is likely that the sap collected from the above-ground parts of the trees is characterized by a mixing between the recently uptaken water and water stored in the tree. This mixing mechanism is consistent with the evolution of the root-to-bole isotopic signature of the xylem water along the LMWL: the farther the water flows upward, the closer its isotopic composition was close to that of the rain collected the previous summer. Low transpiration and evaporation of *F. sylvatica* during winter might have kept the isotopic signature of this storage water unchanged until spring, when the mixing likely began due to the uptake of fresh water for embolism recovery and for the development of new twigs and buds. This is corroborated by the isotopic composition of xylem sap collected in this study, which is always located on the LMWL between the summer and the winter rainwater (Fig. 3.4). Unfortunately, the water in this soil type was not sampled in summer, making a direct comparison between the soil water and the root sap in winter and summer impossible.

Another mechanism that should be considered in the sap isotopic composition enrichment between the roots and the bole in regard to a recent publication by Nehemy *et al*. (2022) is xylem-phloem water exchange. They reported a lighter isotopic signature of phloem water in comparison to xylem water, attributing it to fractionation during water flow from xylem to phloem through aquaporins. If the extent of water exchange between xylem and phloem increases with the distance and/or time of exposure of the xylem sap to such a process, it would result in the progressive enrichment we observed (Fig. 3.6). Moreover, water participates in biochemical reactions linked to the biosynthesis of many molecules, undergoing biochemical isotope fractionation (Sternberg, 1988; Yakir and DeNiro, 1990). Some of these metabolic pathways involving xylem water may be responsible for the gradual enrichment observed, due to difference in chemical reaction rates between light and heavy

water molecules. Indeed, lighter isotopes preferentially participate in chemical reactions due to the kinetic isotope effect, according to which the reaction rate of lighter isotopes is greater than that of heavier isotopes since the former are characterized by a lower bond dissociation energy (Ouellette & Rawn, 2018; Costa *et al*., 2013). This kinetic isotope effect might have an important role in the isotopic exchange between metabolic intermediates and water during post-photosynthetic metabolism, creating fractionation. This type of isotope exchange during plant biosynthetic pathways involves a preferential fractionation of light O-H isotopes into organic molecules and the consequent enrichment of heavy isotopes in the water, as shown for several biochemical processes such as lipid and carbohydrates biosynthesis (Cormier *et al*., 2018), including cellulose (Sternberg *et al*., 1986; Hermoso de Mendoza *et al*., 2021; Kagawa and Battipaglia, 2022). Post-photosynthetic O-H isotopic exchange mainly occurs via carbonyl hydration which is a good candidate reaction to explain xylem transformations, as it involves isotopic exchange between xylem water and metabolites during cellulose biosynthesis (Samuel and Silver, 1965; Sternberg *et al*., 1983; Hill *et al*. 1995; Cheesman and Cernusak, 2016). Considering the kinetic isotope effect, it is likely that light water isotopologues preferentially participate in this reaction, systematically “depriving” xylem water of the lighter isotopes and leading to a progressive enrichment of xylem water due to the exposure of sap water to the biochemical interactions.

Sap velocity might play a role in the seasonal variation of enrichment. In summer, when flow is faster due to transpiration, the residence time of xylem water within the tree is reduced. If water exchanges and chemical reactions drive the isotopic enrichment of xylem water, the degree of contact (i.e. distance travelled and residence time) likely drives the extent of isotopic modification along the flow path within the tree. This hypothesis is supported by observations of less-enriched branch sap in July and August compared to March (Fig. 4 b, d, f), when sap flux is near zero (Fabiani *et al*., 2021; Fig. 3.2). However, the extent of isotopic enrichment linked to the aforementioned mechanisms remains highly uncertain, and further investigations are needed to elucidate the impact of the relationship between water masses, sap velocity, and isotope exchange reactions. Further studies are also needed to elucidate, for example, whether the isotopic enrichment along the sap flow-path is a species-specific pattern or is recurrent also in other tree species, or if an isotopic gradient in the cellulose along the tree exists, since the composition of this latter is affected by the isotopic signature of the xylem water at the time of biosynthesis.

The branch xylem water, in 2017 and 2021, plotted below the LMWL (Fig. 3.5) and to the right of the other xylem waters (Fig. 3.4), in a characteristic pattern of evaporation.

This pattern is consistent with bark evaporative enrichment, Martín-Gómez *et al*. (2017). The authors studied the effect that the reduction in the sap flow rate has on the isotopic composition of twigs water by a series of experiments based on the simulation hydraulic failure and reduced leaf transpiration. They showed that O and H isotope composition of the tree water resulted enriched in heavy isotopes following the typical evaporation line. This led to the conclusion that, in reduced sap flow conditions, the bark evaporative enrichment plays a key role in the isotopic signature of sap water, even in short time lapses (<1h). Moreover, considering that root sap and bole sap showed regolith source-like lc-excess values, the marked changes observed in branch sap samples can be attributed to processes occurring at the branch level and not below. The total absence of evaporative enrichment in the sap of roots and bole, even in low sap flow condition, is likely linked to the presence of hydrophobic suberized bark, and by a higher volume of water in those compartments in comparison with finer twigs. The absence of suberized tissues in twigs likely enhances this evaporative effect, due to the lack of hydrophobic properties of non-suberized bark (Franceschi *et al*. 2005; Krokene, 2015). The apparent evaporative effect was indeed stronger in water extracted from young non-suberized twigs than in that collected from suberized branches. The fact that the sap extracted from the branches in summer had a lower evaporative effect than that of the water collected from the finer twigs in spring, is consistent with this reasoning (Fig. 3.4). Moreover, higher temperatures contribute to reduce the difference in evaporation rate between heavy and light water isotopologues (Mook, 2006), potentially reducing the evaporative enrichment at the branch level in summer. But why was the evaporative enrichment in branch sap not observed in March 2020? The most likely answer is that varied local meteorological conditions, such as air temperature variations, among the sampling campaigns might have affected the bark evaporation process. In spring 2020, when the evaporative-like enrichment was smaller, the temperature was around 4 °C, while in 2017, summer 2020, and in spring 2021, the temperature was near or above 10 °C (Fig. 3.2). The $\Delta^{2}H$ and $\Delta^{18}O$ relationship slope evolved accordingly (Fig. 3.7). In the case of our sampling dates, the air temperature was different, which might matter for a range of eco-physiological and physical processes governing isotopic fractionation in twigs. However, further investigations on branch sap under different meteorological and environmental conditions are needed to elucidate and quantify their effect on the isotopic composition of the branch sap and therefore the lc-excess values.

3.4.2 *IS*VE vs overpressure

A question arises for *IS*VE techniques: what water pool are we collecting? Our experimental design did not allow us to answer this question directly, but previous works aid in the interpretation. Zhao *et al*. (2016) extracted xylem sap by exudation through a needle, taking advantage of positive xylem pressure during the absence of transpiration, and successfully matched the isotopic composition of the water source to that of the exuded sap. Barbeta *et al*. (2022) extracted water from cut twigs by centrifugation and found the water so obtained plotted close to the expected water sources, while parallel samples obtained by cryogenic vacuum distillation showed the typical offset in ^{2}H. Root sap extracted by *IS*VE gave similar results to extraction by needle or centrifuge: isotopic composition coherent with the potential water sources. Indeed, *IS*VE waters did not result in the bias in ^{2}H that is typical of cryogenic extraction and, more specifically, isotopic signatures of *IS*VE root and bole sap samples fell onto the LMWL along with potential water sources (Fig. 3.4). However, the fact that the three extraction techniques reported in this manuscript were not compared to determine whether or not they extract the same sap fraction (i.e. sap with the same isotopic composition) represents a limitation of this study and further investigations are needed to shed light on the matter.

The apparent success of the *IS*VE sampling technique is an unusually good clarity in the sources of water used by trees. The isotopic signature of root sap collected in plateau and hillslope was close to that of the soil solutions in 2017 and 2020, suggesting a preferential uptake of shallow soil waters (Fig. 4), which is in line with what already suggested by Fabiani *et al*. (2021) for the same site. In 2021 instead, sap isotopic signature seems to be resulting from a mixing of soil solutions and groundwater. Results from the cryogenic extraction presented by the above-mentioned authors – who made also use of sap flow and groundwater table measurements, showed that groundwater does not significantly contribute to the tree water uptake. However, capillary processes and the resulting capillary fringe were not considered in both studies, leaving an open question regarding the origin of the water uptaken in summer. Concerning the riparian area, it was not possible to identify the origin of the water uptaken, due to the similar isotopic signature shown by the available water sources in the experimental plot. However, our data suggest that, of all sampled tree waters, root sap is the most directly related to the recently uptaken source, and that it had not encountered isotopic modification by metabolic processes, transpiration, mixing, or other transformations that were more important in the above-ground parts of the tree.

Apart from the large volume of water extracted, which represents a great advantage for hydrological and geochemical studies, *IS*VE methods illustrated are cheap and easy-to-apply. Pumps are the only expensive instruments, but we assume that any lab working on field experiments already owns. All the used *IS*VE equipment (vacuum chamber, syringes and tubings) can be clean and re-used indefinitely, lowering even more the cost of these techniques in the long term. Moreover, tree waters extracted with *IS*VE resulted clean and transparent and the post-processing showed low or absence of organic interferences during the analysis of these samples (data not shown). This suggests that methodological biases linked to organic interferences, usually resulting from more common methods (Millar *et al.*, 2018; Wen *et al*., 2022) were avoided. Thus, *IS*VE appears to be a simple and viable alternative to extraction by needle, centrifugation or cryogenic techniques.

The main limitation of the *IS*VE techniques is that they can be applied only until the early stage of leaf development. After leaf out, transpiration reduces the pressure inside the xylem so that extraction with weak vacuum techniques is more difficult. In this sense, an *IS*VE extraction with a more powerful vacuum pump can be tested in order to overcome the negative water pressure in the tree. However, such a high pressure may disrupt or alter the hydro-connectivity of the water compartments inside trees – by, for example, destroying vessels and creating internal water mixing – delivering a sample of water that is a mix of different pools and potentially harming the tree. A viable solution to the transpiration problem, is offered by the overpressure technique that allows to collect water, albeit in a much smaller volume, even during the growing season. The principle behind the overpressure technique is the same of the Scholander pressure chamber (SPC - Scholander *et al*., 1965), where a leafy twig is sealed inside a vacuum chamber with an end exposed in the outside and pressure is applied through a gas tank, pressurizing the chamber and pushing the water out from the twig's outside-end. The volume of water collected from each chunk with the overpressure method was low (not measured) but probably higher, in the unit of time, in comparison with the SPC. Zuecco *et al*. (2022), for instance, collected less than 200 µL of water from a single twig in less than 10 minutes with SPC, while with the overpressure method, 10 to 15 chunks were used to collect about 1 mL of water in 5 minutes ca. Therefore, in comparison with the SPC, the overpressure appears as a more efficient technique to extract water from branches. However, a comparative approach applying both techniques on the same species and under the same environmental conditions are needed to avoid potential biases in the comparison as the volume of water collectible with these techniques may varies seasonally (Rennenberg *et al*., 1996). Finally, the overpressure method does not

require any other specific equipment (such as gas tank or vacuum chamber) making this technique a viable alternative to the SPC, also in terms of costs and field user comfortability. The main limitation of the overpressure is related to concerns that may arise with its application on roots. The significant number of roots needed to collect a sufficient volume of water and the destructiveness of the method, make the overpressure technique potentially harmful not only for the tree but also for the soil, whose stratification and hydraulic properties would be altered following its mobilization. This is why the overpressure technique was not applied on roots in this study.

3.5 Conclusions

We focused on understanding how physical and biochemical processes may lead to changes in the isotopic composition of xylem sap along the root-branch flow path of *Fagus sylvatica* at the beginning of the growing season. We used an *in-situ* water extraction method on beech trees to obtain xylem water from roots, boles, and branches. We then were able to directly compare the isotopic composition of sap liquid samples with potential water sources.

Our results showed that there was a vertical gradient in the isotopic composition of xylem water, characterised by a progressive ^{18}O and ^{2}H enrichment along the root-branch flow path and an evaporation-like trend in the branch sap. The extent of the enrichment of heavy isotopes in xylem water appeared to be consistent with the distance travelled by the water and to its residence time inside the trees. Thus, water extracted by *IS*VE from roots appears to represent the recently uptaken water, while water extracted above the stems is progressively affected by various fractionating processes. The fractionation is likely attributable to a combination of the following:

- mixing of water of different ages inside the trees
- xylem-phloem water exchange,
- bark evaporative enrichment
- kinetic isotope effect on carbonyl-hydration reactions involving xylem water during cellulose biosynthesis

with dominant processes varying by location within the tree. Some of these processes are likely more apparent in our experiment because of the early-spring bias to our sampling, but the results clearly indicate that isotopic transformations within trees are multiple and complex.

CHAPTER 4

Comparative analysis of cryogenic extraction and *IS*VE methods

Abstract

Cryogenic extraction (CE) is a widely used method for obtaining water from trees for eco-hydrological studies. However, its accuracy in identifying the source of absorbed water has been questioned due to high temperatures and vacuum applied during extraction, as well as tree water compartmentalization, which may bias the final isotopic composition of the sample. This study compares the CE method with the *IS*VE method for determining oxygen and hydrogen isotopic composition in root and boles, aiming to assess potential discrepancies attributable to physiological/biochemical processes within tree tissues. Our results reveal significant differences in the isotopic signatures between CE and *IS*VE extracted water, with CE samples resulting enriched in ^{2}H and representing more a bulk representation of various water pools – rather than an accurate depiction of the absorbed water source. These findings highlight the importance of selecting an appropriate extraction method for understanding plant-water interactions in eco-hydrological studies. The application of the *IS*VE method is recommended for a more accurate determination of the water source absorbed, as it better accounts for the isotopic heterogeneity within tree tissues and provides a more reliable representation of the plant's water uptake dynamics. This improved understanding of plant-water interactions is essential for informing sustainable water management practices and enhancing our knowledge of eco-hydrological processes.

This Chapter is based on: Montemagno, A., et al., Comparative analysis of cryogenic extraction and in-situ vacuum extraction methods for determining water stable isotopes composition of tree waters. – in preparation

4.1 Introduction

Cryogenic vacuum distillation, also known as cryogenic extraction (CE), is a widely used method for collecting water from trees for eco-hydrological studies. However, it has significant limitations in accurately identifying the source of absorbed water due to high temperatures and vacuum applied during extraction, as well as tree water compartmentalization. CE, indeed, involves extracting water from tree cores typically collected from the trunk at breast height, by using a heating system to evaporate the water from the wood core and a cold trap to condense it. The water extracted in this way does not accurately represent the actual absorbed water, as it contains a mixture of xylem sap and other water fractions, including symplastic water (from living parenchyma and phloem), capillary water (from intercellular spaces between xylem cells), and fiber water (from within cell walls) (Barbeta *et al*., 2022). Moreover, trees can store water in their heartwood for a longer duration compared to sapwood (Holbrook, 1995; Matheny *et al*., 2015, Hu *et al*., 2018), resulting in the extraction of a mix of waters with varying ages and isotopic compositions when applying CE. Isotopic non-homogeneity among plant tissues has been documented by other researchers (Yakir *et al*., 1989; Zhao *et al.,* 2016), who have also estimated the distribution of total water volume across different plant tissues (Yakir *et al.,* 1989; Tyree and Jarvis, 1982; Boyer, 1967). They discovered that only a small portion of this water volume is contained within the veins (Yakir, 1992), which suggest a potential high impact of the other tree water pools on the final isotopic signatures of the water when extracted via CE. Differences in isotopic signatures between sap and potential water sources may also result from varying water residence times in plant tissues (Meinzer *et al*., 2006) or water vapor absorption from bark and leaves (Earles *et al*., 2016; Lehmann *et al*., 2018). As a consequence, when applying CE to tree cores, the extracted water serves more as a bulk representation of various water pools located within and between different tree tissues, rather than an accurate depiction of the absorbed source at the moment of the sampling. The analysis of CE water often produces unexpected isotopic signatures that can significantly differ from ambient sources at the time of sampling, usually resulting depleted in ^{2}H. This leads to misunderstandings regarding water origin and renders it impossible to accurately identify the water sources plants uptake.

For this study, it was hypothesized that O and H isotopic compositions of water extracted from tree tissues using the CE method will result depleted in ^{2}H in comparison to those obtained using the *IS*VE method, as a result of CE's inherent limitations in accounting for tree water compartmentalization and the influence of physiological and biochemical

processes within tree tissues. For verifying this hypothesis, CE was applied on root and bole cores from which holes were subsequently used to directly extract the flowing sap through the *IS*VE method. O and H isotopic composition of the two types of samples were then compared to observe differences attributable to the techniques and, eventually, to physiological and biochemical processes occurring within the tree tissues.

4.2 Materials and methods

4.2.1 Study site and sampling campaigns

For the study site and the sampling campaigns, please refer to Chapter 3.

4.2.2 Core sampling, water extraction and isotope analysis

CE was applied to root and bole cores collected by using an increment borer at breast height and in the tap roots below the humus layer. The cores were then put inside 30-ml glass tubes, sealed with caps and Parafilm® and frozen at −20 °C before the cryogenic extraction of the water content. The same holes left after the core drilling were used for the sap extraction with the *IS*VE technique, therefore it is assumed that the two types of samples can be compared. Water was extracted from the cores with a similar cryogenic vacuum distillation setup described in Orlowski *et al.* (2016) and illustrated in figure 4.1.

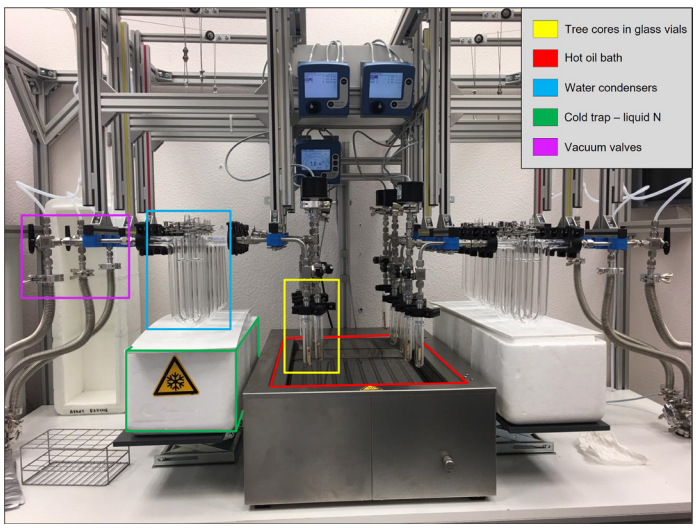

Figure 4.1: Cryogenic extraction ramp used in this study.

Samples were immersed into 100 °C oil bath for 3 h under a vacuum of 0.03 hPa to evaporate water. This latter was then condensed through a cold trap composed of glass

tubes immersed in liquid nitrogen. The samples so obtained were then collected with glass pipettes, poured into 2 ml glass vials and stored at 4 °C for subsequent isotope analyses. For the isotope analyses, please refer to Chapter 3.

4.3 Results

Results are reported in Table A4.1 and in Figure 4.2, adapted from Chapter 3.

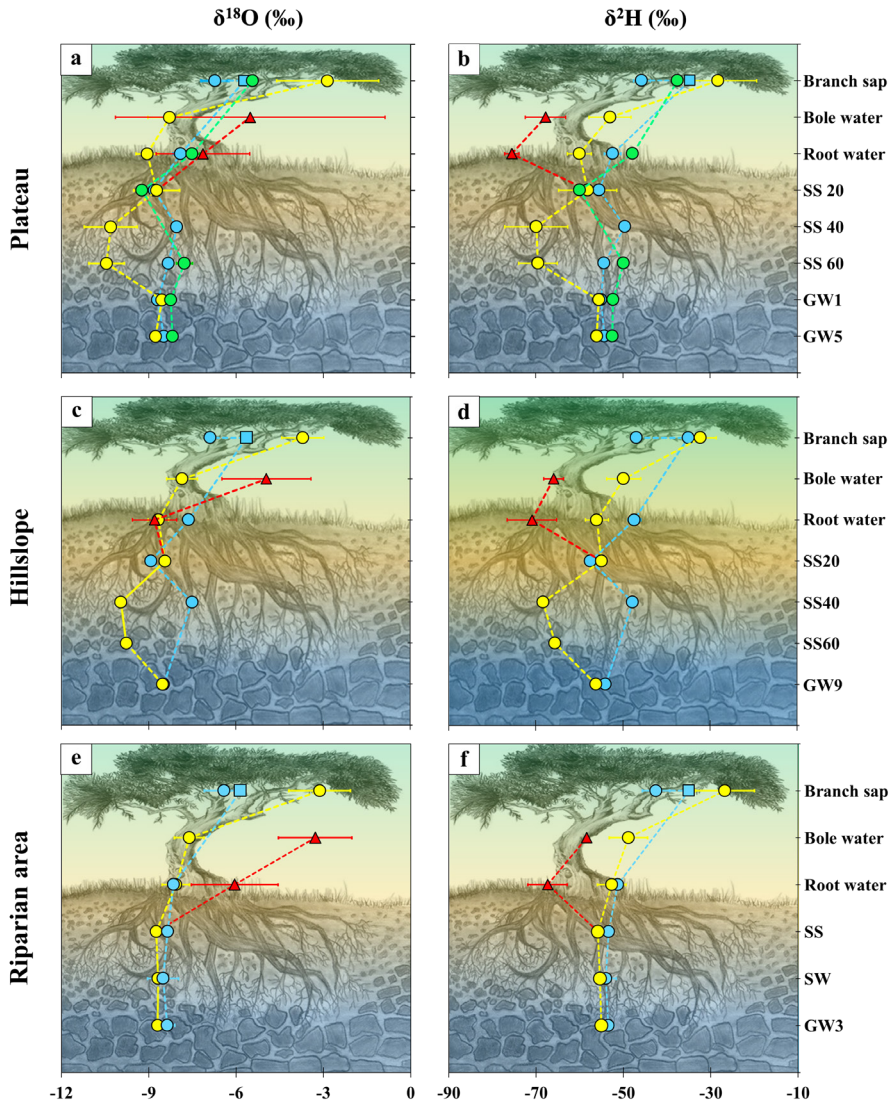

Figure 4.2. Evolution of the isotope ratios, in the three experimental plots, from the groundwater to the branches. Triangles relate to the cryogenically extracted water (2021); round dots relate ISVE collected sap (green – 2017, blue – 2020, yellow – 2021) and squares indicate summer samples collected with the peristaltic pump.

CE root samples (RC) showed values of $\delta^{18}O$ = −7.33 ‰ ± 2.28 and $\delta^{2}H$ = −71.26 ‰ ± 5.09, whereas CE bole samples (TC) of $\delta^{18}O$ = −5.92 ‰ ± 0.84 and $\delta^{2}H$ = −54.85 ‰ ± 4.34 in 2020, $\delta^{18}O$ = −4.58 ‰ ± 1.76 and $\delta^{2}H$ = −64.03 ‰ ± 5.20 in 2021. Among all tree water samples collected during the sampling campaigns, CE waters showed the highest variability as suggested by Figure 4.2, adapted from Chapter 3.

Interesting to notice also how the enrichment in ^{18}O mainly occurs in all bole CE samples, while instead is a more rare phenomenon for the roots samples as suggested by Figure 4.3 illustrating the isotopic shift observed between *IS*VE and CE samples collected in the same spot of the trees and in the same timeframe.

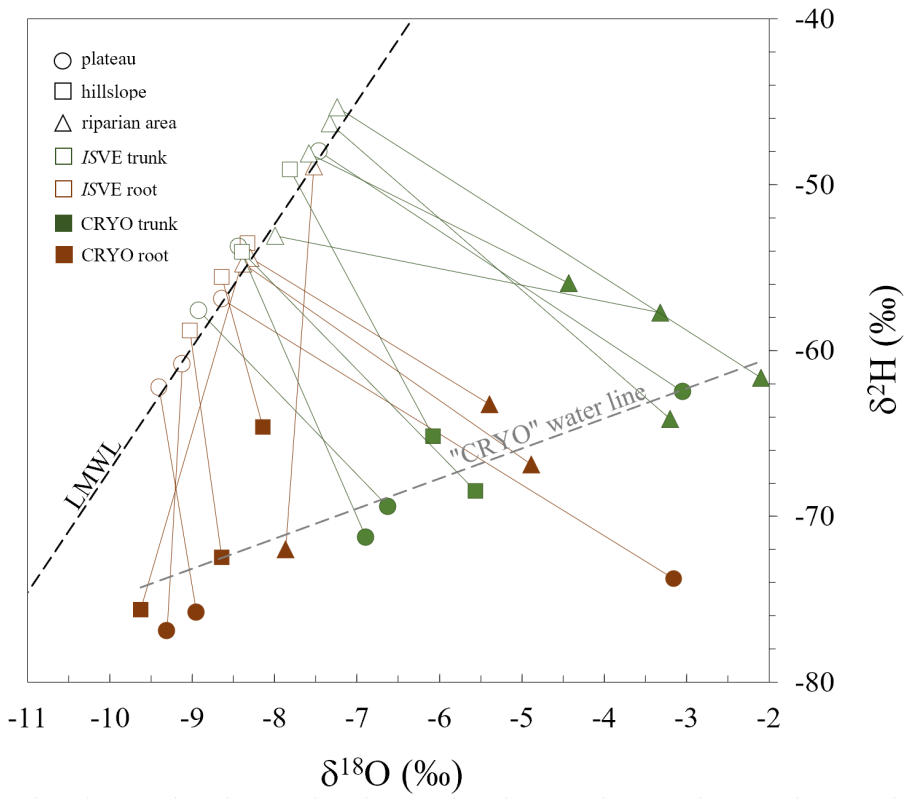

Figure 4.3: Isotopic shift between *IS*VE and CE tree water samples collected in 2020. Noticeable that the enrichment in ^{18}O mainly occurs in the bole.

Moreover, such ^{18}O enrichment in CE waters is stronger in boles than in roots, as suggested by the difference $\Delta^{18}O$ between the $\delta^{18}O$ values of the *IS*VE sap and those of CE, which show average $\Delta^{18}O$ = −1.27 ± 2.20 ‰ for root samples and $\Delta^{18}O$ = −3.33 ± 1.32 ‰ for bole samples. The two water extraction techniques showed discrepancies in the isotopic composition even in samples obtained from the same spots in the trees. Indeed, while the

isotopic signature of waters extracted applying the *IS*VE method fell onto the LMWL (Fig. 4.3), CE waters showed an offset characterised by an enrichment in ^{18}O and a depletion in ^{2}H. This trend is observable in all sampling sites regardless of the morphology, hydrological conditions, sampling dates and tree ages. Moreover, during the analysis, CE waters showed a high interference from organic compounds. Interference that was not observed for the *IS*VE samples (Chapter 3 – Montemagno *et al.*, 2023).

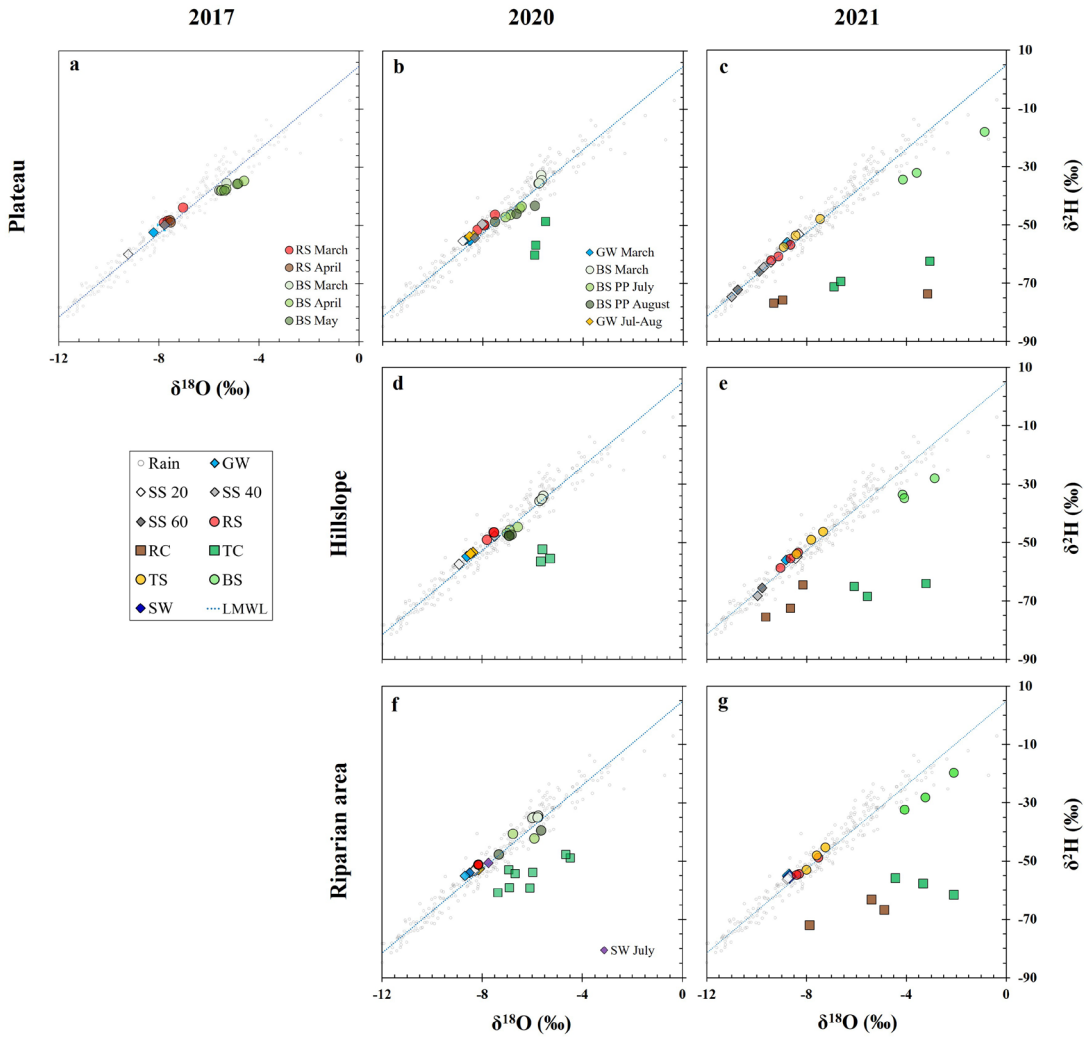

Figure 4.3: Dual isotope diagrams related to the 2017, 2020 and 2021 sampling campaigns for the three experimental plots. Legend: GW = Groundwater; SS 20/40/60 = Soil Solution 20, 40 and 60 cm depth; RS = Root Sap; RC = Root CE; TC = Trunk CE; TS = Trunk Sap; BS = Branch Sap; SW = Stream Water; LMWL = Local Meteoric Water Line. If not otherwise specified, all samples relate to March.

4.4 Discussion

The CE samples demonstrated a marked off-set from LMWL, characterized by a depletion in ^{2}H and an enrichment in ^{18}O (Figs. 4.2 and 4.3), which can be recognized as a standard regarding all literature available in this field. These isotopic alterations have not been fully explained in the current literature, necessitating further examination of potential factors that may influence such discrepancies. In the following discussion, we will explore potential physiological and biochemical processes and methodological considerations that may contribute to the observed differences in isotopic signatures between CE and *IS*VE-obtained waters. Through a comprehensive analysis, the aim is to advance our understanding of these phenomena and their implications for eco-hydrological studies.

4.4.1 Physiologically-driven ^{2}H-depletion in CE waters

The ^{2}H-depletion in CE waters observed in this study is in line with previous studies reporting not only an offset from the LMWL linked to methodological bias in the CE technique, but also the discrepancies between xylem sap and CE extracted water (Zhao *et al.* 2016; Chen *et al.* 2020; Barbeta *et al*. 2019, 2020 and 2022). Barbeta *et al*. (2022) argued that the CE water obtained from tree cores contains also other fractions of water (such as symplastic, capillary and fiber waters) in addition to xylem sap and that those fractions may contribute to the final isotopic signatures.

A possible explanation for the changes in the water isotope composition of the different pools in trees, may be given by the numerous H-exchange processes occurring between water and organic molecules during biochemical pathways in trees and which can result in a H-depletion in the sap water. Cormier *et al*. (2018) explained that three main factors affect the H isotopic ratios in trees' organic compounds during photosynthetic (e.g. reduction of NADPH in the light reaction of photosynthesis, primary assimilation of triose phosphates) and post-photosynthetic pathways (e.g. glycolysis, TCA cycle): the plant's water source, the leaf evaporative ^{2}H-enrichment and the biosynthetic fractionation. Of course, post-photosynthetic processes are of major interest in our case, due to the fact that we focused our attention on roots and boles – and during non-photosynthetic period, rather than on leaves in which we would expect photosynthetic and transpiration processes dominating the H isotopic exchange and fractionation. It is important to mention that $\delta^{2}H$ of organic post-photosynthetic molecules is not only linked to the H composition of the organic precursors and redox factors in a biosynthetic pathway, but also to the cellular water which is used as a source of H during specific enzymes activity (e.g. Phosphoglucose isomerase

in the glycolysis/gluconeogenesis), and which is generally ^{2}H-enriched in comparison to the precursors (Rieder and Rose, 1959; Albery and Knowles, 1977; Rambeck and Bassham, 1973; Cormier *et al*., 2018).

The aforementioned authors devised a conceptual model (Fig. 4.4) that portrays the hydrogen exchange processes between water and organic compounds during both photosynthetic and post-photosynthetic stages, which result in the formation of n-alkanes and α-cellulose. The authors proposed that these processes contribute to the overall ^{2}H-enrichment of plant metabolites when there is limited photosynthetic carbohydrate supply.

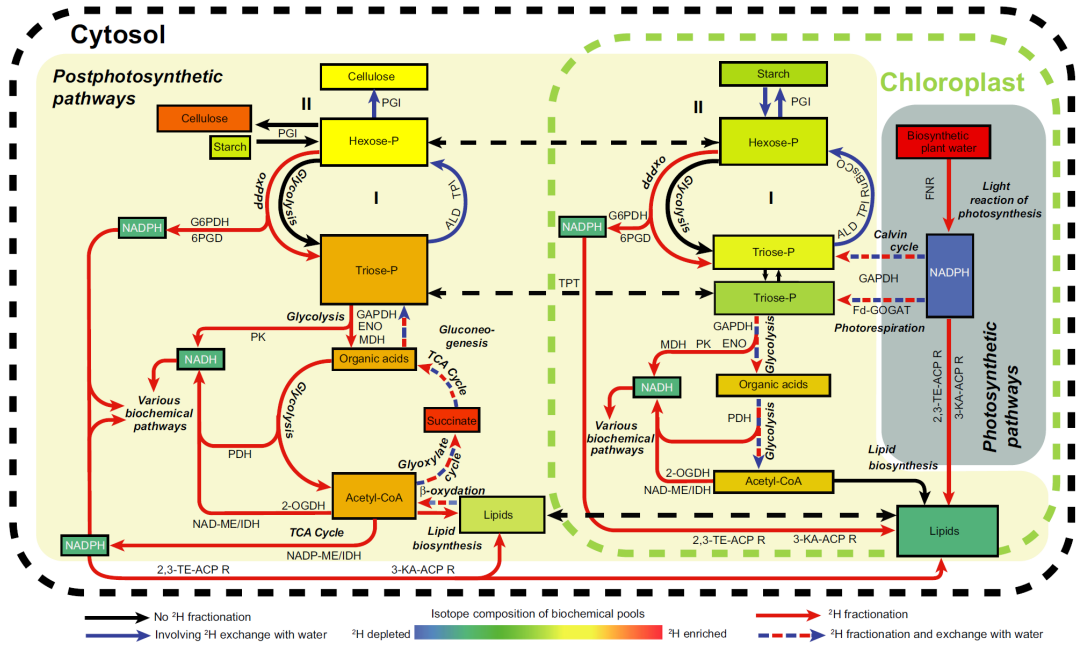

Figure 4.4: Perceptual model illustrating H-exchange steps during photosynthetic and post-photosynthetic pathways of n-alkanes and α-cellulose biosynthesis. The model and the illustration are taken from Cormier et al., (2018).

The model clearly illustrates numerous biochemical reactions where water and organic molecules exchange H atoms, demonstrating the complexity that could lead to the observed fractionation. Since the samples for this study were collected during non-photosynthetic periods before and after budbreak, this model is particularly relevant as it highlights H-exchange processes occurring under limited photosynthetic carbohydrate supply. Furthermore, it encompasses pathways involved in cellulose formation, a critical aspect to consider during this period when plants begin constructing new functional lignocellulose vessels (Cochard *et al*., 2001; Ameglio *et al*., 2002). Other several studies

attributed water and organic molecules isotopic modifications to H-exchanges occurring during these biochemical processes. Yakir and DeNiro (1990), for example, argued that post-photosynthetic metabolism influences the $^{2}H/^{1}H$ ratio of plants' photosynthesis products. They showed that up to 50% of carbon-bound hydrogen in leaf cellulose was exchanged with the hydrogen of water during growth of Lemma and maize plants in the darkness, concluding that photosynthesis produced carbohydrates with carbon-bound hydrogen depleted in ^{2}H relatively to the water medium and that this trend is opposite in the post-photosynthetic metabolism, which instead revealed ^{2}H-enriched carbohydrates and ^{2}H-depleted water. This happens because the biosynthetic material, which is transported from leaves across the plant, undergoes further $\delta^{2}H$ modifications while being exposed to waters characterised by different $\delta^{2}H$ values (Yakir, 1992; Ziegler, 1989; Luo and Sternberg, 1991). Augusti *et al*. (2006) reported the occurrence of specific enzyme-catalysed H isotopes exchanges between photosynthates (glucose) and water during cellulose biosynthesis. Also, the authors showed that glucose in leaves was characterised by a lower ^{2}H content when compared to the same molecule at the tree-ring level, which instead resulted enriched. These findings strengthen the fact that the continuous exchange of H between the water and the organic molecules leads to a ^{2}H enrichment in the organic compounds and to a relative depletion in the surrounding water, finally justifying the resulting ^{2}H-depletion in the CE-extracted waters.

According to what reported above, this set of biochemical exchanges leads to the overall ^{2}H-enrichment in organic molecules and the consequent depletion in the surrounding water. It follows, therefore, that the capability of plants of modifying the $\delta^{2}H$ of water during the different biosynthetic pathways of organic compounds has a direct impact on the isotopic signature of CE water. The latter, indeed, will be reflecting all the H-exchange processes that water has undergone, showing a ^{2}H-depleted signature with respect to the potential water sources and/or to the water extracted with non-conventional methods (such as *IS*VE), which presumably collect "fresher" and/or less metabolically impacted water, as it refers to the water flowing in the xylem vessels. This is clearly shown in Figures 4.2 and 4.3, where all CE samples show a depletion in ^{2}H when compared to the *IS*VE extracted waters and, more in general, to the LMWL.

4.4.2 Organic-induced isotopic modification of CE water samples

Considering that some aspects of the hydrological dynamics of water stable isotopes in trees are still unclear and that pioneering studies in that sense are quite recent (Chen *et al*., 2020; Barbeta *et al*., 2019, 2020 and 2022; Fabiani *et al*., 2022), another question arises when applying the CE to tree cores: are we collecting only water?

Plants are complex organisms which are able to produce a plethora of different molecules for the most diverse reasons. Among all, biogenic volatile organic compounds (BVOCs) caught our attention due to their characteristic high volatility, which is linked to high vapour pressure and low boiling points. Many studies have been conducted regarding production and release of BVOCs from plants (Guenther *et al*., 1995; Graus *et al*., 2004 and references therein; Peñuelas and Llusià, 2001; Dudareva *et al*. 2006) and different types of molecules have been identified. Among those, the most representative are isoprenoids, terpenoids, terpenes, alkenes, phenylpropanoids/benzenoids, alcohols, aldehydes, ketones and carboxyl acids in general.

Plants are responsible for the 90% of BVOCs emissions to the atmosphere (Guenther *et al.,* 1995) and produce them to interact with biotic and abiotic elements in both above- and below-ground environments. For example, BVOCs can be used to interact with other organisms for defense (e.g. against pathogens or herbivores), for reproduction (e.g. by attracting pollinators), for intra- and inter-specific competition, and to alert neighbours of incoming danger (Effah *et al*. 2019; Dudareva *et al.* 2006). During the CE, these highly volatile substances can be extracted from the tree cores due to the high temperatures and low pressure reached in the extraction chamber, and subsequently collected together with the water in the liquid nitrogen heat trap. BVOCs would be then introduced in the analytical instrumentation along with the water sample, having a potential impact on the isotopic signature of these latter, which result lighter-than-expected in H. In this perspective, interpreting the isotopic values of the liquid extracted via CE as referring to the sole water may be a simplification. Lopez Dias *et al*. (2022) developed a device which is able to trap and isolate the organic compounds released during the heating step of the cryogenic extraction, avoiding their collection further on. The authors were also able to analyse the above-mentioned trapped molecules and they revealed that almost the totality was represented by BVOCs (data not published yet).

Unfortunately, this new technique was not applied during the cryogenic extraction performed for this study, as it has been developed later. Nonetheless, already existing literature in the matter of H isotope composition of BVOCs is available and can be used as

reference for the discussion. The average δ^2H values and the relative standard deviations for some of the plant-produced BVOCs reported in previous studies (Liu *et al*., 2006, Chikaraishi and Naraoka 2003 and Nhu-Trang *et al*., 2006) are illustrated in Figure 4.5, together with the values of the samples observed in this study. All δ^2H values of the organic molecules reported by the authors are lower than those of CE waters observed in our samples and worldwide (Dawson and Ehleringer, 1991; Song *et al*., 2014; Evaristo *et al*., 2016; Zhao *et al*., 2016; Yong-Qin *et al*. 2017; Zhao and Wang, 2018 and references therein; Tezlaff *et al*., 2020; Fabiani *et al*., 2021; Duvert *et al*., 2021; Barbeta *et al*., 2018 and 2022; Sohel *et al*., 2021).

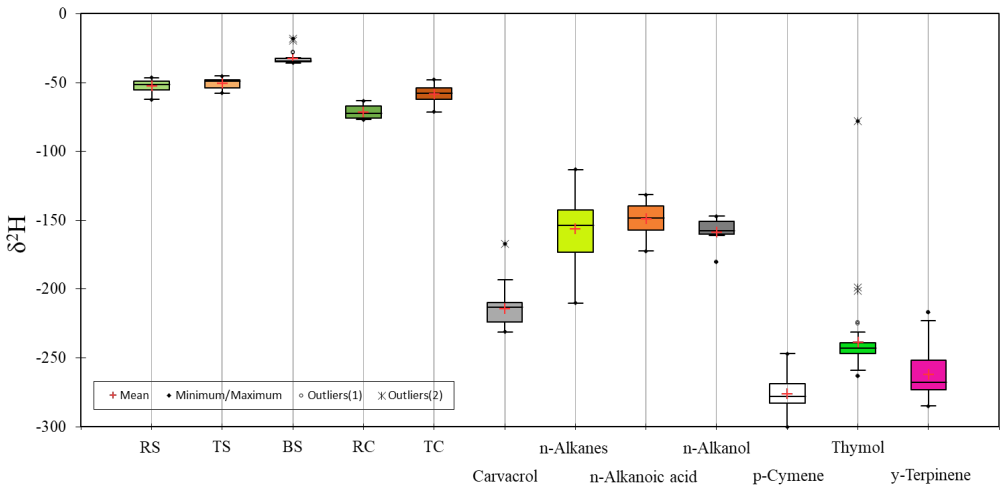

Figure 4.5: δ^2H Average values and standard deviations for the samples collected for this study and for some BVOCs reported in the literature. Legend: RS = Root Sap; TS = Bole Sap, BS = Branch Sap; RC = Root CE; TC = Trunk CE. Data from: Liu *et al*., 2006; Chikaraishi and Naraoka 2003; Nhu-Trang *et al*., 2006.

The high difference in the δ^2H values between the *IS*VE waters and the BVOCs, suggests that, even at low concentrations, BVOCs can potentially affect H isotopes analysis of the CE water samples by lowering their δ^2H. It we consider a simplified system where δ^2H of CE waters results from the mixing between *IS*VE sap – considered as the original water signature for the tree waters – and the BVOCs, it is possible to calculate what % in volume of analysed sample of these latter is necessary to obtain the CE δ^2H. For this purpose, the IsoSource model (Phillips and Gregg, 2003; Phillips *et al*., 2005) was applied. IsoSource is a numerical mixing model that estimates the proportion of each endmember contributing to a mixture based on stable isotope data. The model works through an iterative process that

explores the solution space for all possible combinations of source proportions that satisfy the isotopic constraints of the mixture. To simulate the mixing process that results in the observed δ^2H values for CE bole waters, we utilized the average δ^2H values of *IS*VE bole sap from the present study, as well as Carvacrol, p-Cymene, Thymol, y-Terpinene, n-Alkanoic acid and n-alkanes from Liu *et a*l. (2006), Chikaraishi and Naraoka (2003) and Nhu-Trang *et al*. (2006) as endmembers. The choice of these specific compounds lies on the greater availability of data for these molecules in comparison to others reported by the above-mentioned authors. The average δ^2H values of CE bole waters from this study were then used to represent the resulting mixture. For the modelling, the "Increment" – which represents the distance between the tested proportions of each source in the search for feasible solutions – was set to 1%, while the "Tolerance" – the acceptable deviation between the estimated isotopic values generated by the model and the observed isotopic value in the mixture – was set to 0.05 (Fig. 4.6). After running the model, IsoSource produces a "feasible output" (Fig. 4.6) which shows all the possible combination between endmembers, as % in volume, that can result in the isotopic composition of the mixture. According to the feasible outputs obtained, the model suggests that in an ipothetic mixing of these 7 potential endmembers, there are many possible solutions for the proportions that can satisfy the isotopic constraints of the CE water. However, all suggest a predominant contribution of the *IS*VE bole sap between 92% and 96%, and a total contribution from all organic endmembers between 4% and 8%, which varies between the different compounds (Fig. 4.6). These results, although referred to a simplified estimation of the mixing sources which may occur inside the plants, clearly illustrates that these organics can have a significant impact on the final isotopic composition of the CE waters, especially when highly depleted in ^2H.

Nonetheless, it is important to consider that many other water pools within the tree – such as symplastic water, capillary water and fiber water (Barbeta *et al*., 2022) – and which can be extracted from tree cores were not considered for this simulation. To gain a more accurate understanding of the contribution of the different water pools as well as of the organic compounds to the δ^2H of CE waters, further experiments are needed to identify the specific molecules extracted during the CE and assess their potential impact on the resulting isotopic composition. Additionally, since there is no available data regarding the O isotopic composition of BVOCs for comparison, it is necessary to conduct further investigations to acquire the O isotopic signature of the mentioned molecules. This would allow modelling the mixing between all potential contributions to the isotopic signature of the CE waters.

IsoSource - View Statistical Output

File Print Help Exit

Title:	BVOCs and					
Increment:	1%					
Tolerance:	.05					
Isotopes:	Hygrogen					
Mixtures:	-58.44					
Sources:						
ISVE bole sap	-50.60					
n-alkanes	-155.33					
Thymol	-238.27					
Carvacrol	-214.34					
n-alkanoic acid	-145.25					
p-Cymene	-276.12					
y-Terpirene	-261.81					
	**********					
FEASIBLE OUTPUT:						
ISVE bole sap	n-alkanes	Thymol	Carvacrol	n-alkanoic a	p-Cymene	y-Terpirene
---	---	---	---	---	---	---
0.92	0.03	0	0	0.05	0	0
0.93	0	0	0	0.06	0	0.01
0.93	0.03	0.01	0	0.03	0	0
0.93	0.05	0	0.01	0.01	0	0
0.94	0.01	0	0.03	0.02	0	0
0.94	0.01	0.01	0	0.03	0	0.01
0.94	0.02	0	0.01	0.02	0.01	0
0.94	0.03	0	0.01	0.01	0	0.01
0.94	0.03	0.02	0	0.01	0	0
0.95	0.01	0	0.01	0.01	0	0.02
0.95	0.01	0.01	0.03	0	0	0
0.95	0.01	0.02	0	0.01	0	0.01
0.95	0.02	0.01	0.01	0	0.01	0
0.96	0	0.01	0.01	0	0.01	0.01
0.96	0	0.03	0	0	0.01	0
0.96	0.01	0	0	0	0.03	0

Figure 4.6: IsoSource mixing simulation between *IS*VE bole sap collected in this study and BVOCs from Liu *et al*. (2006), Chikaraishi and Naraoka (2003) and Nhu-Trang *et al.* (2006). Full dataset reported in Table A4.2.

According to what discussed above, it appears that H stable isotopes signature of tree CE waters could results from the mixing of 4 different hydrogen-source endmembers simultaneously extracted: *i*) xylem sap, which represents the water flowing in the xylem vessels; *ii*) intra- and extra-cellular water which is depleted in ^{2}H due to the exchange of H with organic molecules; *iii*) biogenic volatile organic compounds; and *iv*) other types of water that do not necessarily exchanged H with organic molecules but that may have different $\delta^{2}H$ due, for example, to different residence times in tree tissues (e.g. storage water).

4.4.3 Combustion-driven $\delta^{18}O$ modification in CE waters

For the identification of the factors causing the ^{18}O enrichment of CE waters in comparison to xylem sap and to regolith waters, an additional process should be considered: the oxidation of organic molecules during the combustion. During the analysis of the tree waters,

a Micro-Combustion Module (Picarro) was used to eliminate spectral interferences caused by plant organic molecules such as alcohols, terpenes and volatiles, to process samples directly and enhance the quality of results. However, the combustion module works best when total organic concentrations is lower than 0.5%, as it generates new water which is after analysed together with the sample.

The combustion of organic matter requires the addiction of $O_2(g)$ from an external source (e.g. compressed air bottles) as reactant. As an example, we report below the combustion reaction of ethanol:

$$C_2H_5OH(l)+3O_2(g) \rightarrow 2CO_2(g)+3H_2O(g) \qquad \text{(Eq. 4.1)}$$

During the combustion, the oxygens of the organic compounds inside the water sample together with the external $(O_2)_g$ are transformed into carbon dioxide and water. During the subsequent analysis, the water released during this reaction would be analysed together with the rest of the sample leading to potential bias in the results. As a matter of fact, not only the organic-bound oxygen of the samples would be analysed – which could already represent a bias in the resulting isotopic ratio supposedly referring to water only – but also the oxygen acquired from the external source during the combustion. The combination of these two sources of O in the water sample may affect the $\delta^{18}O$ to a certain extent, depending on the isotopic composition of the added oxygen and of organic contaminants, as well as the volume of combustion-derived water produced.

Previously mentioned authors (Zhao *et al*., 2016, Barbeta *et al.,* 2022, Chen *et al.,* 2020) did not make the use of combustion modules for their analysis and their results did not show ^{18}O-enrichment in their CE samples when compared to water sources and/or xylem sap. This is strengthening our assumption regarding the potential role that the addition of O during the combustion reaction may play on the analysis of O stable isotopes of water samples.

The observation that *IS*VE extracted samples did not exhibit an enrichment in ^{18}O is probably related to the lack of organic contamination (Chapter 3) that was not detected during the analysis. This suggests that there were not enough organic molecules present to act as fuel for the combustion process, which would have otherwise caused a significant bias in the analysis. In contrast, all CE samples showed interferences from organic contaminants of which combustion may have led to the observed ^{18}O enrichment. However, the volume of the organic contaminants in the CE water samples was not measured and

further experiments are then needed in order to elucidate the potential impact that the use of combustion reactions can have on the analysis of the isotopic signatures of CE waters.

4.5 Conclusions

In this study, we conducted cryogenic extraction on root and bole cores to compare the isotopic composition of the resulting water with that of *IS*VE-collected samples. The initial hypothesis that the isotopic signature of cryogenically extracted waters is depleted in comparison to those extracted using the *IS*VE technique has been validated. Our findings revealed that CE waters display a lighter hydrogen and heavier oxygen isotopic composition in comparison to *IS*VE waters. These phenomena were attributed to:

I. Biochemical modifications that occur within trees during biosynthetic pathways, altering the isotopic composition of water through hydrogen exchange processes with organic precursors. This exchange results in the enrichment of deuterium in organic precursors and depletion in the water.
II. The simultaneous extraction of organic compounds during the cryogenic extraction procedure, leading to potential interferences during the analysis. These organic compounds, generally more depleted than water, may contribute to a deuterium depletion in CE samples compared to *IS*VE-extracted waters, which are not subject to organic interferences.
III. The enrichment of oxygen-18 may be associated with the utilization of oxygen during the analysis of water samples for organic compound combustion. The combustion process generates water, which subsequently mixes and is analyzed together with the rest of the sample.

These insights underscore the significance of choosing a suitable extraction method for accurately examining plant-water interactions in eco-hydrological research. Enhanced understanding of these interactions is crucial for informing sustainable water management practices and advancing our knowledge of eco-hydrological processes.

CHAPTER 5

Rare earth elements dynamics during root absorption and transportation to the shoots of *Fagus sylvatica*

5.1 Introduction

Transpiration – i.e. the water movement from the regolith to the atmosphere through plants and its evaporation from the aerial parts – is a crucial process to consider when studying water and nutrient balances, especially in forest ecosystems. Globally, transpiration accounts for 35–80% of the total water returned to the atmosphere (Coenders-Gerrits *et al*., 2014) and contributes to the elements' mobilization from the regolith (from the surface of the soil to the fresh bedrock). During vegetative periods in temperate climate, when the water is scarce, water storage compartmentalization in the regolith controls the water accessibility to plants. Considering the rapid climate change and the increasing severe droughts that may affect the resilience and sustainability of a given tree species in a certain environment, predicting the origin of the water and related nutrients uptaken by trees is important for forest management strategies.

The understanding from what regolith layer tree uptake water , and therefore the recognition of the water source uptaken, is a recurrent question mark for eco-hydrologists, who usually make use of water stable isotopes as tracers (Beyer and Dubbert, 2019; Fabiani *et al*., 2021; Barbeta *et al.,* 2022). The use of O and H stable isotopes for eco-hydrological studies relies on the assumption that no isotopic fractionation occurs during the water flows across the regolith-tree continuum so that the simple comparison of the isotopic composition of tree water with the available water sources (or their mixing) allows the identification of the one(s) uptaken. Even assuming the absence of significant isotopic fractionation across the different regolith layers, these tracers still show limitations in their use for the identification of the water source uptaken by trees. Such limitations mainly relate to the lack of understanding of fractionation processes occurring at the soil-tree interface, to the techniques that are usually applied for sampling and analysis of the different water pools

(Penna *et al*., 2018) and to the lack of knowledge regarding the effect of tree metabolism on O-H isotopic signature of tree waters (Chapter 3).

To overcome those limitations, the use of additional tools could be of interest to complement the information given by water stable isotopes. In this sense, as the diverse regolith waters (soil water, groundwater, and streamwater) may show different trace elements composition (Moragues-Quiroga *et al*., 2017), these latter can be seen as promising tools for the recognition of the water source uptaken by trees. Into specific, rare earth elements (REEs – i.e. the lanthanides and the Y) could be among the best candidates for understanding water absorption dynamics at the regolith-plant interface. Despite being non-conservative elements, their potential as tracers relies on their peculiar physical-chemical properties – such as outer electron configuration, oxidation state and lanthanide contraction, which make REEs a valuable tool for understanding biogeochemical processes at the interface between diverse CZ compartments, as well as in the rhizosphere. Additionally, the extensive REEs literature represents another valuable resource for the understanding of the functioning of natural environments. REEs have been and are currently used as tracers for studying a multitude of CZ processes including the ones occurring in the regolith-plant system. For example, they have been used to study: the effects of fertilizers on plants growth (Ding *et al*., 2006), metal accumulation and fractionation in plants organs (Zhang *et al*., 2002; Censi *et al*., 2014; Yuan *et al*., 2018, Zhenggui *et al*., 2001), plant physiological responses to high metal concentrations (Liu *et al*., 2022), effect of vegetation on soil chemical and mineralogical composition (Stille *et al*., 2006; Brioschi *et al*., 2013), and specific plant physiological and biochemical patterns (Burda *et al*.,1995; Lewis and Spalding, 1998; Zhu *et al*., 2002).

To better comprehend the tree-water uptake by using REEs, it is important to consider the biogeochemical processes occurring at the soil-root interface that dominate the REEs dynamics, during the water uptake by trees. The understanding of such processes could be accomplished by considering the chemistry of the different water sources, of tree roots in contact with the water sources, and of xylem sap. At the best of our knowledge, no research has been carried out on such a topic and no studies have been conducted considering the REEs composition of the available environmental water sources and of xylem water for a direct comparison to recognise the uptaken water source. Most of the studies that considered REEs transfer from soil to plants, focused on their fractionation across the tree organs, and their effect on plants metabolism (Brioschi *et al*., 2013;

Kovaříková *et al*., 2019; Cheng *et al*., 2015; Saatz *et al.,* 2015; Liu *et al*., 2021; Ding *et al.,* 2007). In this study, we put forth the hypotheses that:

I. The differential behaviour of REEs results in certain elements being preferentially taken up and mobilized in the root-branch flow path, while others are kept in solution or trapped in tree tissues.
II. A comprehensive understanding of the REEs fractionation at the rhizosphere level, combined with the distinct REEs composition of the waters, may aid in identifying the water sources taken up by trees.

To test hypothesis I, we compared the REEs composition of available water sources in three experimental sites of the WEC with that of bulk roots and xylem sap of European beech (*Fagus Sylvatica* L.*)* in order to understand REEs dynamics and fractionation during the water uptake. If the hypothesis is verified, we will be able to recognize the uptaken water source based on REEs pattern characteristics.
Hypothesis II was tested by comparing the REEs patterns of the root sap with those of the branch sap in the same trees, together with those of the bulk composition of wood collected from boles and big branches, whole branch, external and internal bole bark. If the hypothesis is verified, we will observe a preferential mobilization of certain elements of the REEs series towards the upper parts of the tree and their depletion in roots, and a preferential fractionation of some REEs in tree tissues in the root-branch flow path.

5.2 Materials and methods

5.2.1 Study site

The study has been conducted in the Weierbach experimental catchment (WEC), located in western Luxembourg. This site has been monitored for its hydro-climatic conditions since 2000 and for a range of eco-hydrological purposes since 2009 (Hissler *et al.,* 2021). The catchment has an area of 0.45 km^2 and its altitude ranges from 422 to 512 m above the sea level. It is a forested catchment, where 75% of the total coverage is represented by a mixture of European beech and sessile oak (*Quercus petraea*) and 25% of Norway spruce (*Picea abies*) and Douglas-fir (*Pseudotsuga menziesii*). Trees from other species, as alder (*Alnus glutinosa*) are sparse in the riparian areas close to the stream. The first 50 cm of soil of the catchment's plateau and hillslopes developed from a loamy material originated from periglacial slope deposits and lie on a fresh Devonian slate bedrock (Moragues-Quiroga *et al.,* 2017). The soil is classified as a Dystric Endoskeletic Cambisol Colluvic, Bathyruptic,

Siltic according to the WRB (Juilleret *et al.,* 2016) and is divided in an upper thin organic-rich A horizon (0–8 cm depth) and a cambic B horizon (8–50 cm depth). The C horizon, which extends from 50 to 120 cm, is composed of loamy periglacial deposits dominated by slate rock fragments (>50% v/v). At about 110 cm a lithic discontinuity occurs, separating the upper periglacial cover bed from the fractured and weathered slate rock substratum below (Gourdol *et al*., 2021). The nearly vertical fractures, which are gradually closing with depth (Martinez-Carreras *et al*., 2016), permit rooting and water infiltration in the non-saturated zone of the regolith, despite the impervious properties of the slate lithology (Scaini *et al*., 2016). The riparian zone is characterised by a 30 cm muddy layer composed of loamy material coming from the soil erosion and organic matter degradation, lying on fresh fractured slate bedrock. The tree species that dominate these areas are mainly European beech and alder.

5.2.2 Sampling campaigns and samples treatment

Two sampling campaigns were conducted for this study, one in 2017 and another in 2020. The 2017 campaign focused on the plateau site, where water pools from various compartments of the CZ were collected. This included soil solutions at depths of 20 cm, 40 cm, and 60 cm, as well as deep (~7m) and shallow (~2m) groundwaters. In addition, sap samples from roots and branches, whole roots, internal and external bark of boles, whole small branches, bark from big branches, and wood from boles and big branches, were collected from 1 to 3 selected trees. In 2020, the sampling campaign was expanded to include two additional morphological units: the hillslope and the riparian area. In these areas, samples collected included soil solutions at depths of 20 cm, 40 cm, and 60 cm, as well as groundwaters, streamwater, and sap from roots and branches from 3 trees in each experimental plot. In 2017, the sampling campaigns matched with the full water saturation of the catchment in spring, which represents the beginning of the growing season for European beech trees in the WEC, while in 2020 the sampling campaign was extended to August (Fig. 5.1). At the plateau and hillslope, deep (7 m depth) and shallow (2m depth – only from plateau) groundwaters were gathered into acid clean PP bottles from two distinct wells by using a peristaltic pump (Solist, peristaltic pump model 410) equipped with Teflon tubing. Soil solutions at 20, 40 and 60 cm depths were collected using Teflon/quartz suction cups connected to acid-clean 2-L Nalgene flasks (SDEC, Reignac-Sur-Indre, France) under a pressure of −0.8 bar applied with a field vacuum pump (SDEC, model PAV 2000).

In the riparian area, groundwater (3 m depth) and riparian soil solutions (20 cm depth) were collected using the same procedures, while streamwater was hand-collected at the outlet of the catchment with acid clean PP bottles.

To sample the xylem sap, 1 to 3 beech trees were selected at each experimental plot. Acid clean 60 ml polypropylene syringes (BD Plastipak™) were attached through a Teflon tube to thin roots (diameter <5mm) within 10 and 30 cm soil depth, and to young twigs after bark removal (Chapter 4). Vacuum was then applied by pulling and blocking the piston. All water and sap samples were filtered through 0.2µm cellulose acetate filters (Sartorius Stedim Biotech) and the resulting filtrates were acidified with purified HNO_3 1% v/v before storage at 4°C for the subsequent analysis. In order to destroy organic complexes that could create analytical interferences, sap samples were first chemically digested. After being totally evaporated in a clean room at 40 °C, sap samples were mineralized using concentrated purified HF, HCl and HNO_3. After total digestion of the samples, the acid mixtures were evaporated and the resulting residues dissolved in HNO_3 1% v/v before storage at 4°C.

Previously, fine roots were gathered from the plateau and sorted based on the soil layer they originated from at 0-10 cm, which corresponds to the organo-mineral soil horizon (Ah), and 10-30 cm, which corresponds to the upper part of the cambic horizon (Bw). In addition to roots, various other plant materials were also collected, including wood from boles and large branches, whole small branches, inner and outer bark from boles, and bark from big branches. All solid tree samples were gathered into clean paper bags and brought back to the lab where they were washed with ultra-pure water (MilliQ), dried at 40 °C and accurately brushed to remove remaining soil particles and/or dust as best as possible. The samples were then ground below 2mm using a bead grinder (Retsch© MM400). An aliquot was taken from each sample for the analysis of the bulk chemical composition. For the roots, a second aliquot was taken to observe the presence of surface-bound minerals which may affect the REEs behaviour during the water absorption by trees.

Root samples were digested in aqua regia in microwave-assisted oven (Anton Paar Multiwave PRO), using the same protocol described by Montemagno *et al.* (2022).
All the solutions resulting from the mineralization were clean and transparent and did not present any precipitate nor suspended solid.

5.2.3 Sample analysis and anomalies calculation

REEs concentrations were measured via Inductively Coupled Plasma - Mass Spectrometry (ICP-MS) with an Agilent© Quadrupole 7900 associated to an Agilent© ISIS 3 injection system. In order to minimize polyatomic interferences, analyses were conducted in He mode. ^{103}Rh and ^{185}Re were used as internal standards. Analytical blanks contribution was less than 1% for all elements. Detection and Quantification limits are given in Table 1. Calibration standards were prepared with Multi elements ICP standard solutions from CHEM-LAB Analytical© diluted in HNO_3 1% v/v. The SLRS-6 natural River Water Certified Reference Material (NRC-CNRC) was measured to validate the ICP-MS procedure for REEs concentrations in natural samples. REEs concentrations are not certified in the SLRS-6 but were compared to Yeghicheyan *et al*. (2019).

The prepared 2 mm powder samples were submitted to X-Ray Diffraction analysis on a X'Pert Pro diffractometer (Malvern-PANalytical, Eindhoven, The Netherlands) using Cu-Kα radiation, Wide Angle X-ray Scattering (WAXS), theta/2theta, configurations. For the analysis in transmission, the powders put into a thin-walled mica pouch which was mounted onto a specific holder perpendicular to the incident x-ray beam. Here, a first batch of samples was analyzed within the range 5–70° 2-theta in transmission with the following setup: A 0.026° 2-theta step, a counting time of 297 seconds per step, X-ray generator was operated at 45 kV and 40 mA. Because no peak was detected beyond 40° 2-theta, the remaining samples were analyzed within the range 5–40° 2-theta with the same setup. For the analysis in reflection, the powders were deposited onto a zero-background holder which was placed directly onto a flat stage in the diffractometer. Here, a second batch of samples was analyzed within the range 5–75° 2-theta with the following setup. A 0.026° 2-theta step, a counting time of 497 seconds per step, X-ray generator was operated at 45 kV and 40 mA. Because no peak was detected beyond 40° 2-theta, the remaining samples were analyzed within the range 5–40° 2-theta with the same setup. X-ray powder diffractograms were numerically recorded using the Data Collector provided by PANalytical (Eindhoven, Netherlands) and analysed using the Highscore Plus 5.1b software. The deconvolution of the WAXS diffractograms was performed using the Fityk software [M. Wojdyr, J. Appl. Cryst. 43, 1126-1128 (2010)]. The mineralogical composition of each sample was determined by comparing diffraction patterns of the samples with reference patterns of the ICDD 2023 database.

Cross sections of roots were mounted on aluminium stubs using double-coated carbon conductive tabs and covered with carbon. Samples were examined at LIST using a Hitachi S-4800 scanning electron microscope equipped with an energy-dispersive X-ray

spectroscopy (EDX) containing a lithium-drifted silicon detector. SEM analyses were carried out using an acceleration voltage of 10 or 15 kV with a working distance of 15 mm and with an average dead time of 100 seconds. For this study, Ce, Eu, Gd, Pr and La anomalies were calculated with the following Equations:

$$Ce/Ce^* = \frac{Ce_N}{(0.5 \bullet Pr_N + 0.5 \bullet La_N)}; \quad \text{(Eq. 5.1)}$$

$$Eu/Eu^* = \frac{Eu_N}{(0.5 \bullet Gd_N + 0.5 \bullet Sm_N)}; \quad \text{(Eq. 5.2)}$$

$$Gd/Gd^* = \frac{Gd_N}{(0.33 \bullet Sm_N + 0.67 \bullet Tb_N)}; \quad \text{(Eq. 5.3)}$$

$$Pr/Pr^* = \frac{Pr_N}{(0.5 \bullet Ce_N + 0.5 \bullet Nd_N)}; \quad \text{(Eq. 5.4)}$$

$$La/La^* = \frac{La_N}{(3 \bullet Pr_N - 2 \bullet Nd_N)}; \quad \text{(Eq. 5.5)}$$

where the subscript "$_N$" indicates the normalized concentrations.

5.3 Results

5.3.1 EDS, SEM and XRD analyses of rhizosphere soil and roots

The results derived from the Energy Dispersive X-ray Spectroscopy analysis of the rhizosphere soil are presented in Table 1, while Figure 5.3 illustrates the corresponding image and spectrum. The obtained spectrum reveals the predominant presence of oxygen O, C, and Si, accounting for weight percentages of 40, 29, and 18, respectively. Additionally, the soil sample exhibits trace amounts of aluminium Al, Fe, K, Ti, and Mg, constituting respectively 7, 4, 2, 1, and ≤1, of the Wt%.

Table 5.1: results of the EDS analysis of rhizosphere soil samples.

	C	O	Mg	Al	Si	K	Ti	Fe
Wt%	28.7	39.9	0.4	6.5	18.1	1.5	0.6	4.4
At%	40.4	42.2	0.2	4.1	10.9	0.7	0.2	1.4

SEM images of root and soil reported in Figure 5.2, illustrate the distribution of the predominant elements detected with the EDS analysis of roots and soil. The images show

the presence of Si, Fe, Al preferentially concentrated in the soil, whereas almost the totality of C was found in the roots. O is well distributed between soil and organic tissues. The spectra from XRD analysis of the root powder, reported in Figure 5.4, ascertained the presence of crystalline materials, mainly represented by Quartz and Opal, as well as non-crystalline phase consisting of cellulose, which accounts for the majority of the material and which explains the preferential higher distribution of C in the root material (Fig. 5.2).

Additional non-cellulose phases may be present as well, including $(Na_2O)0.33\ NaAlSiO_4$ (Sodium Aluminium Silicate), $Na_2MnSi_2O_6$ (Sodium Manganese Silicon Oxid), $Mg(SO_4)$ (Magnesium Sulphate), $Na_{1.45}Al_{1.45}Si_{0.55}O_4$ (Sodium Aluminium Silicate), $Na_{1.65}Al_{1.65}Si_{0.35}O_4$ (Sodium Aluminium Silicate) and $AlPO_4$ (Aluminium Phosphate). Among these mineral phases, phosphates are of particular interest as they have been shown to be able to fractionate Eu in the roots, leading to positive Eu anomalies in these organs (Ding *et al*., 2007).

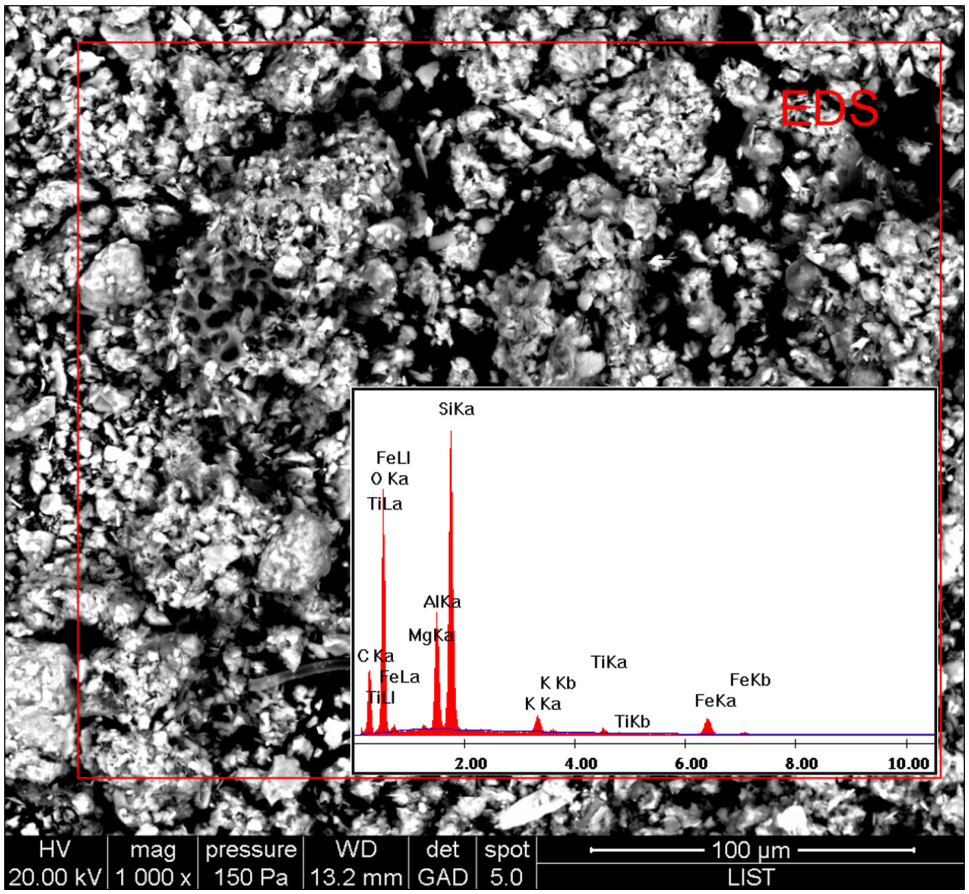

Figure 5.2: Image and spectrum resulting from the EDS analysis of rhizosphere soil.

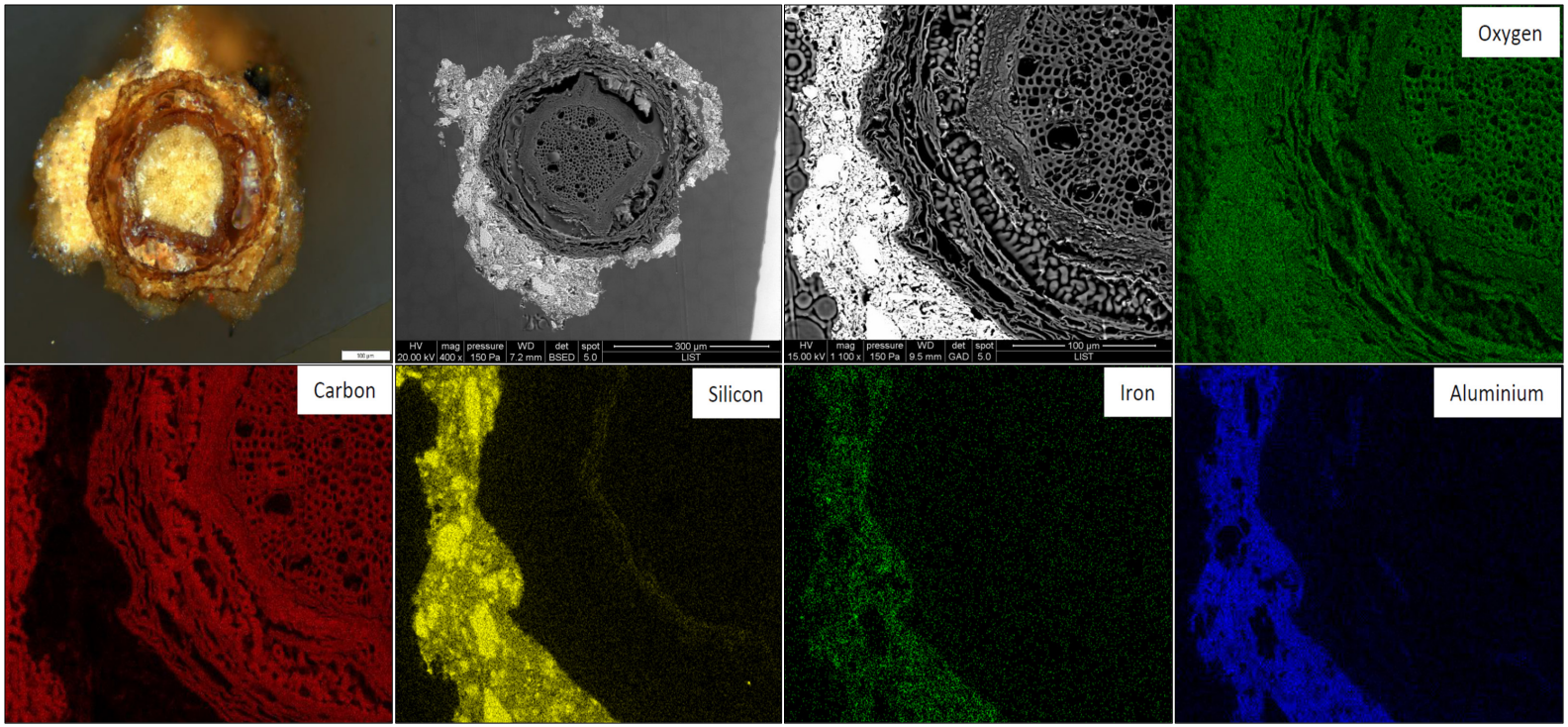

Figure 5.3: SEM images (chemical contrast) and X-ray mapping on root samples collected at 20 cm depth and associated soil particles.

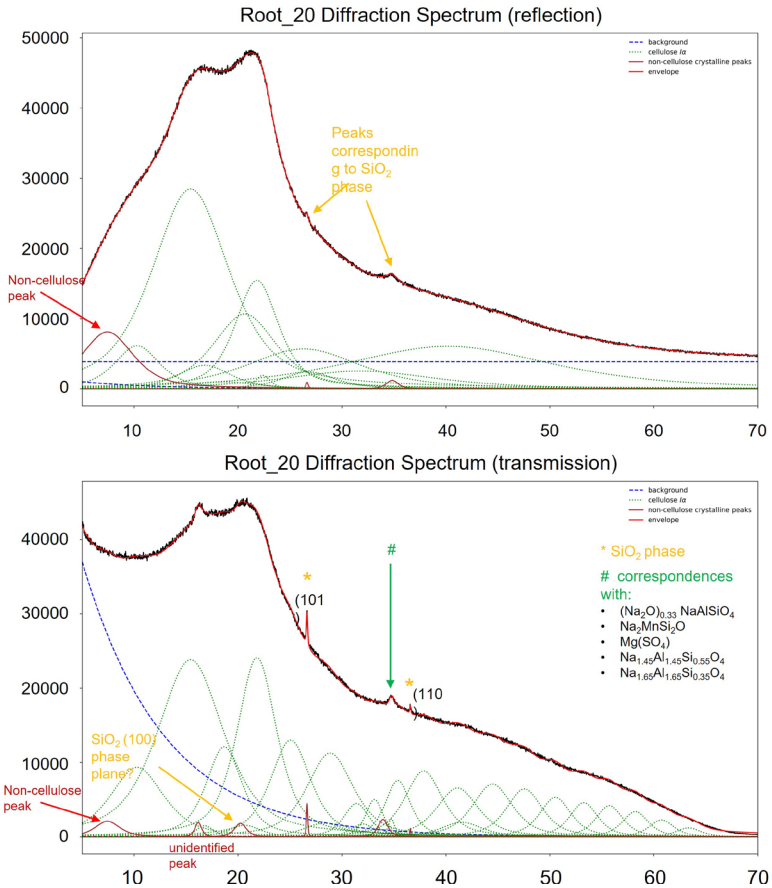

Figure 5.4: Reflection (above) and transmission (below) spectra resulting from the XRD analysis of roots powder. In the reflection spectrum, the intensity of the peaks provides insights into the crystallinity and preferred orientation of the material. The position, shape, and relative intensities of the peaks enable the determination of crystal structure and lattice parameters of the sample. The background signal, scattering signal as well as the cellulose and non-cellulose peaks are shown. The peak at approximately 7.5° could correspond to the highest intensity peak of Aluminium Phosphate. The peaks in the transmission spectrum provide information about the electronic and atomic properties of the sample. Variations in peak intensities and positions indicate variations in the material's composition, density, and absorption characteristics. The background signal, scattering signal as well as the crystalline and amorphous peaks are shown. The peak at approx. 16.5°could not be attributed to any phase in the selection. The peak at approx. 7.5° could correspond to the highest intensity peak of Aluminium Phosphate. The cellulose crystalline peak at approximately 21.7°could be a convolution of high intensity peaks from cellulose and Opal-A phases. The cellulose crystalline peak at approximately 21.7°could be a convolution of high intensity peaks from Sodium Aluminium Silicate, Sodium Aluminium Silicate phases with the highest peak at 21.15°.

5.3.3 REEs in water sources

Lanthanides (Ln) concentration varies among water types and across the catchment for both sampling campaigns. The highest average concentration and variability were observed in the shallow groundwater at the plateau site ($[Ln]_{GW1}$ = 8.21 ± 5.26 µg/L), while soil solutions and deep groundwaters showed quite stable concentrations in the same site with the latter showing the lowest [Ln] ($[Ln]_{P7SS}$ = 1.40 ± 0.32 µg/L, $[Ln]_{GW5}$ = 0.04 ± 0.05 µg/L). Same observations can be made for the hillslope site, where soil solutions were the water sources the most enriched in Ln ($[Ln]_{P9SS}$ = 2.32 ± 0.38 µg/L), while deep groundwater showed lower concentrations ($[Ln]_{GW9}$ = 0.11 ± 0.10 µg/L), but resulting higher in comparison to the deep groundwaters of the other experimental sites for the sampling date of March 2020 (Table A5.1). In the riparian zone, soil solutions presented the highest [Ln] among the available water sources ($[Ln]_{RPSS}$ = 0.53 ± 0.27 µg/L), while deep groundwater showed the lowest concentration, close to that of the plateau ($[Ln]_{GW3}$ = 0.03 ± 0.03 µg/L). Streamwater was found to have an average [Ln] comprised between the groundwater and the soil solution ($[Ln]_{SW}$ = 0.10 µg/L), probably due to mixing between these two water compartments at the sampling location (Bonanno *et al*., 2021).

Post Archean Australian Shale (PAAS – Taylor & McLennan, 2009) normalized REEs values plotted against the atomic number reveal that all groundwaters show almost identical patterns (Fig. 5.4a) characterized by negative Ce anomalies (Ce/Ce*= 0.36 ± 0.19) and a depletion in LREEs in comparison with MREEs and HREEs and a general MREEs enrichment (La_N/Gd_N = 0.13 ± 0.04, La_N/Yb_N = 0.20 ± 0.07, Gd_N/Yb_N = 1.44 ± 0.36). Plateau and riparian groundwaters are characterized by a general Y enrichment in regards of PAAS ($Y/Ho_{GW1,3,5}$ = 37.00 ± 5.68 and Y/Ho_{PAAS} = 27.5, respectively), whereas hillslope groundwater showed variations in the Y/Ho ratios between spring and summer above and below PAAS values (Y/Ho_{GW9} = 27.69 ± 4.92). Streamwater was characterized by almost identical REEs patterns as the groundwaters, with a difference in the Y/Ho ratio, which resulted below-PAAS values (Y/Ho_{SW} = 22.90).

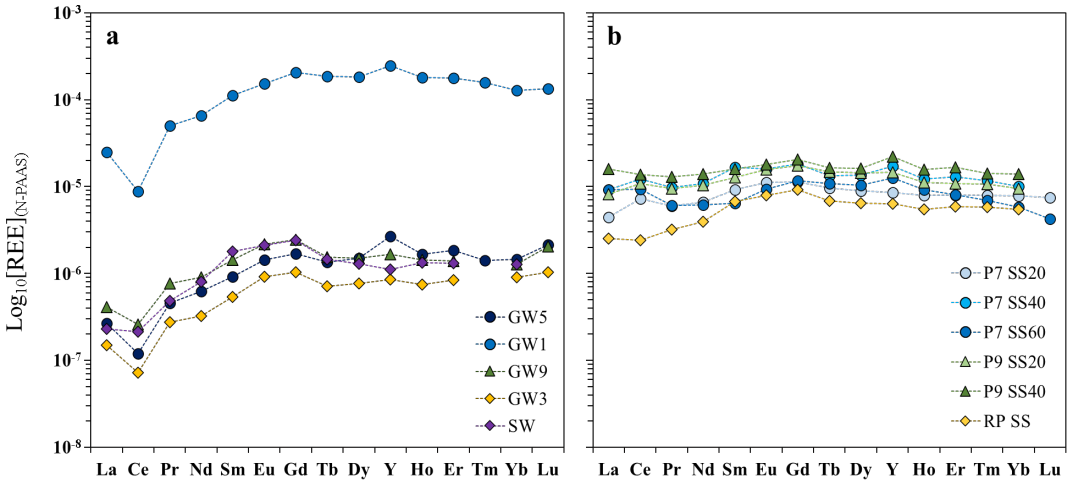

Figure 5.4: PAAS-normalized patterns of average REY values in (a) groundwaters and streamwater and (b) soil solutions collected in 2017 and 2020 from the 3 experimental plots of the Weierbach experimental catchment. Plateau (P7); hillslope (P9); riparian area (RP); SS20-40-60= soil solution at 20-40-60 cm depth; GW3-5-9 = deep groundwaters (~ 7 m) at RP, P7 and P9 respectively; GW1 = shallow groundwater at the P7 site (~ 2.5 m).

PAAS-normalized REEs patterns of plateau soil solutions (Fig. 5.4b) reveal similar patterns with slight differences depending on the depth of sampling. All depths are characterized by positive Ce anomalies (Ce/Ce* = 1.35 ± 0.10) and Y enrichment, which becomes generally higher with depth (Y/Ho_{SS20} = 29.49 ± 0.84 and $Y/Ho_{SS40,60}$ = 38.14 ± 3.43). An element of distinction in the REEs patterns of plateau soil solutions is represented by a depletion in LREEs in comparison with HREEs in the first 20 cm ($La_N/Yb_{N\text{-}SS20}$ = 0.54 ± 0.04), which disappears in the solution at 40 cm depth ($La_N/Yb_{N\text{-}SS40}$ = 0.91), whereas at 60 depth the trend is reversed resulting in an LREEs depletion and HREEs enrichment ($La_N/Yb_{N\text{-}SS60}$ = 1.65 ± 0.33). The inversion observed in the La_N/Yb_N ratios in the soil solutions is likely resulting from a combination between HREEs depletion and La positive anomaly (La/La^*_{SS20} = 0.95 ± 0.06, La/La^*_{SS40} = 1.18 and La/La^*_{SS60} = 1.57 ± 0.11).

At the hillslope site, REEs patterns of soil solution were similar to those of the plateau with a slight Ce enrichment only at 20 cm depth (Ce/Ce* = 1.23), which disappears at 40 cm probably due to the appearance of a La positive anomaly (La/La* = 1.44). Hillslope soil solutions are also characterized by Y enrichment (35.32 ≥ Y/Ho ≥ 38.75).

Riparian soil solutions patterns are different from the ones of the other experimental sites and similar to those of the stream. They are characterized by an evident LREEs depletion,

in comparison to HREEs (La_N/Yb_N = 0.43 ± 0.19), and a marked MREEs enrichment (La_N/Gd_N = 0.27 ± 0.18 and Gd_N/Yb_N = 1.78 ± 0.37).

5.3.4 REEs in tree tissues and sap

Ln in 10-30 cm deep roots were generally more concentrated than in 0-10 cm deep roots ($[Ln]_{R0-10}$ = 10451 ± 4282 ng/g and $[Ln]_{R10-30}$ = 2727 ± 677 ng/g), together showing the highest REE concentration among the sampled tree parts (Table A5.2). Following the roots, the highest concentrations of Ln were presented by the external bark of the boles ($[Ln]_{BT-ex}$ = 464 ± 200 ng/g), the whole big branch bark ($[Ln]_{B-BB}$ = 348 ± 22 ng/g) and the whole small branches ($[Ln]_{SB-tot}$ = 291 ± 49 ng/g). Much lower concentrations were detected in the internal bark of boles ($[Ln]_{BT-in}$= 98 ± 30 ng/g) and in the wood of big branches ($[Ln]_{W-BB}$= 22 ± 4 ng/g) and boles ($[Ln]_{W-T}$ = 16 ± 7 ng/g).

PAAS-normalized REEs patterns of roots (Fig. 5.5) have all similar shapes regardless of depth and are characterized by a positive Ce anomaly (Ce/Ce^* = 1.31 ± 0.14), an MREEs enrichment (La_N/Gd_N = 0.70 ± 0.12 and Gd_N/Yb_N = 2.86 ± 0.70) and a slight Y depletion (Y/Ho = 26.30 ± 2.59) in comparison to PAAS (Y/Ho_{PAAS} = 27.22). PAAS-normalized REEs patterns of the other trees' parts exhibit consistent shapes, which differ from those of the roots. These patterns are characterized by negative Ce anomalies (Ce/Ce^* = 0.80 ± 0.12), Y enrichment (Y/Ho = 34.48 ± 5.25), and positive Eu anomalies (Eu/Eu^* = 1.99 ± 0.88). Notably, the wood samples and internal bole bark display higher Eu anomalies compared to the external bole bark, bark of larger branches, and total small branches (Fig. 5.6). All tree samples present a general declining trend along the series (La_N/Yb_N = 2.82 ± 1.66) which is more explicit for wood samples and internal bark (Figure 5.5).

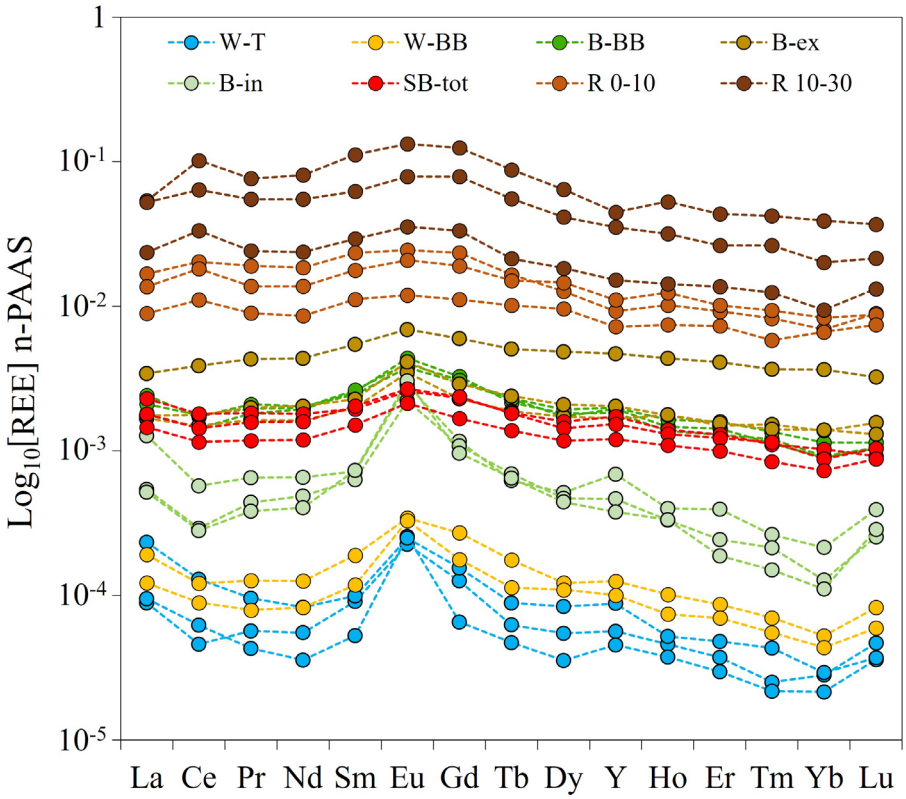

Figure 5.5: PAAS-normalized REEs patterns of all sampled solid tree compartments. Legend: W-T = bole wood; W-BB = big branch wood; B-BB = big branch bark; B-ex = bole external bark; B-in = bole internal bark; SB-tot = total small branch; R 0-10 and R 10-30 = roots at 0-10 and 10-30 cm depth respectively.

Root sap collected at the plateau and riparian area showed close [Ln] ($[Ln]_{RS}$= 2.85 ± 0.88 ng/g), whereas the ones collected at the hillslope site presented higher concentrations and variability in comparison to the others ($[Ln]_{RS}$= 13.17 ± 9.18 ng/g) (Table 1). Branch sap concentrations were in the same range of those of the root sap, with the same range of magnitude for all the sampling dates and sites ($[Ln]_{BS}$= 2.30 ± 1.41 ng/g) in spring. In summer, Ln concentrations in branch sap decreased ($[Ln]_{BSPP}$= 0.34 ± 0.08 ng/g).

When normalized to PAAS and despite the different locations, REEs patterns of root sap (Fig. 5.6a) show a general MREEs enrichment in comparison with HREEs and LREEs (La_N/Gd_N = 0.62 ± 0.18 and Gd_N/Yb_N = 4.36 ± 1.40) and a depletion in HREEs (La_N/Yb_N = 2.70 ± 1.09). Negative Ce anomalies (Ce/Ce* = 0.61 ± 0.07), positive Gd anomalies (Gd/Gd* = 1.50 ± 0.09), and Y enrichments (Y/Ho = 48.10 ± 5.19) were observed in all root sap samples.

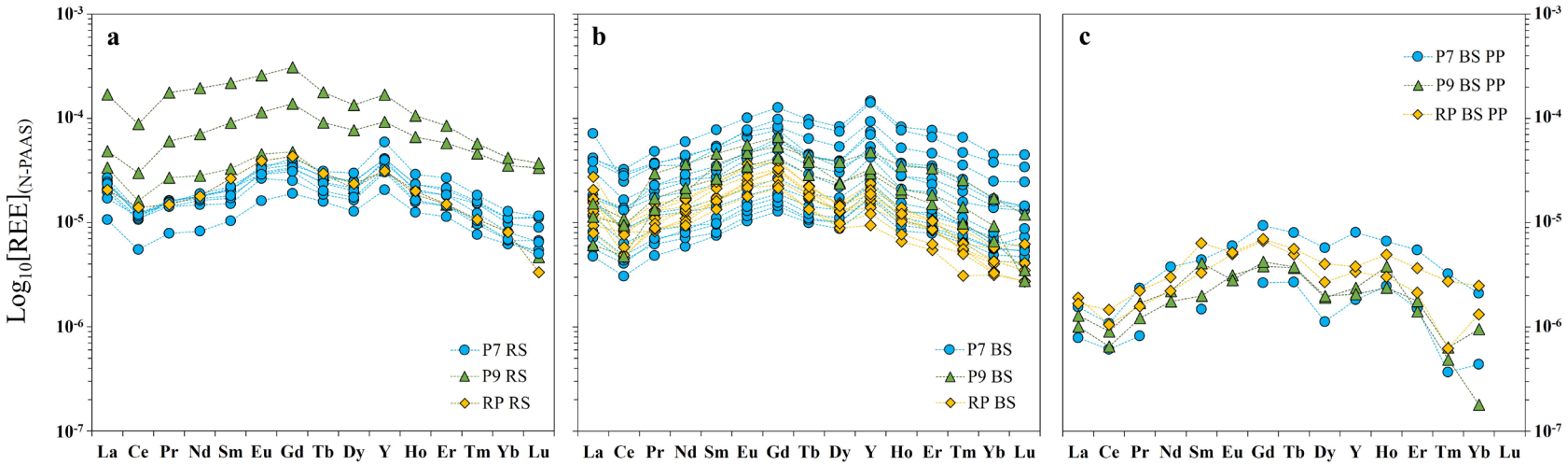

Figure 5.6: PAAS-normalized REEs patterns of (a) spring root sap, (b) spring branch sap, and (c) summer branch sap collected from beech trees at the plateau (P7), hillslope (P9) and riparian (RP) study sites.

The shape of branch sap REEs patterns (Fig. 5.6b) appears to be homogeneous among trees, with similar characteristics and anomalies (La_N/Gd_N = 0.47 ± 0.21, Gd_N/Yb_N = 5.34 ± 2.15, La_N/Yb_N = 2.48 ± 1.42, Ce/Ce* = 0.63 ± 0.13 and Gd/Gd* = 1.55 ± 0.11). REEs patterns of summer branch sap samples (Fig. 5.6c) remind the ones in spring, presenting negative Ce anomalies (Ce/Ce* = 0.64 ± 0.08), a weaker positive Gd anomaly (Gd/Gd* = 1.26 ± 0.14), a stronger average MREEs enrichment (La_N/Gd_N = 0.26 ± 0.05 and Gd_N/Yb_N = 7.34 ± 6.31) and a general HREEs depletion (La_N/Yb_N = 1.93 ± 1.69).

5.4 Discussion

5.4.1 REEs fractionation in rhizosphere and transfer to the sap

In previous studies focusing on REEs uptake and fractionation in plants, REEs content in tree organs were directly compared to those of the bulk soil. Such an approach limits the study of REEs uptake by plants, due to the different REEs composition characterizing the diverse mineral phases in a soil (e.g., Chang *et al*., 2016). Indeed, not all mineral phases present the same dissolution rate during the soil-root-water interactions, and soil water may inherit the REEs signature of specific soil mineralogic compartments after their dissolution, which will be different from the residual fractions as suggested by soil leaching experiments done in the past (Hissler *et al*., 2015; Stille *et al*., 2009; Aubert *et al*., 2002; Steinmann and Stille, 1997). Therefore, the best way to study REEs dynamics during the water uptake and the subsequent fractionation in trees, is given by the comparison of the REEs patterns observed in the water fraction of the considered CZ compartments, roots and xylem sap.

PAAS-normalized REEs patterns of roots (Fig. 5.5a) are characterized by a shape similar to that of shallower soil solutions with a positive Ce anomaly and an enrichment in MREEs. This is likely due to the fact that these roots have been collected from the shallower soil and suggests that roots acquire a REEs signature close to that of the water source absorbed. MREEs enrichment in roots has been previously proposed to be caused by preferential fractionation of these elements in the membrane system of plant cells (Gao *et al*., 2003), phosphates and oxalates precipitation (Ding *et al*., 2007; Wang and Liu., 2017) and binding with carboxyl groups of cell walls (Ding *et al*., 2005). However, in our case it is likely instead that roots just inherit the MREEs shape from the solution they are absorbing. Indeed, by comparing the REEs patterns of soil solutions (Fig. 5.4b) with those of the related root sap samples (Fig. 5.5b), it is possible to observe that also the latter are characterized by a MREEs “bulge”, suggesting that no preferential fractionation of MREEs in the root sap is occurring during the transportation across the root's tissues. By normalizing to the soil

solution at a 20 cm depth, the root patterns (Fig. 5.7) exhibit a continuous decline from La to Lu, without any distinct MREEs enrichment. This indicates that the binding to root tissues decreases along the series during water uptake, rather than being specific of any of the groups and suggesting that the lanthanide contraction plays a key role in REEs fractionation during water absorption.

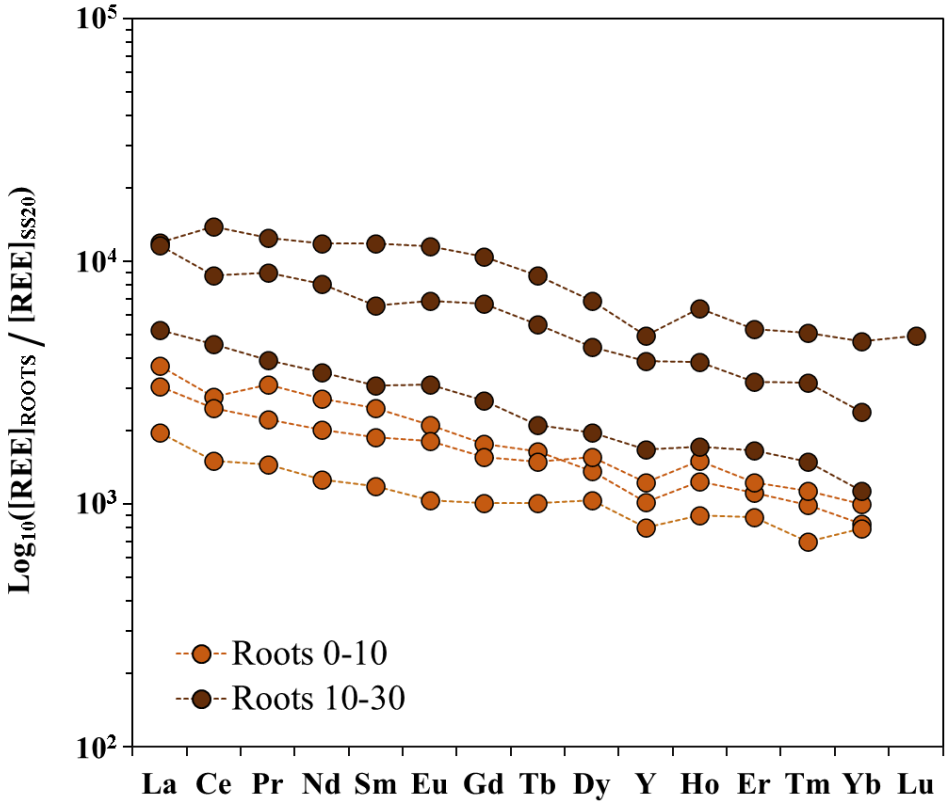

Figure 5.7: Rare earth elements patterns of root bulk normalized by the average REE concentrations in 20 cm deep soil solutions.

Being that HREEs are depleted in the roots, one may that an HREEs enrichment should be expected in the root sap due to the reduced impact of the “filtering” process of the root in their regards and which should enhance the passage of these elements directly to the xylem sap in comparison to the other REEs. Such an HREEs enrichment was not found in the root sap, where instead a depletion is observed (Fig. 5.5b). The very likely answer is that HREEs in soil solutions are already bound to some specific organic molecules, which prevent their absorption and passage through the root membranes. The sampled soil solutions are characterized by DOC = 10.94 ± 5.30 mg/L (Table A5.3) but no other types of

data are available to confirm this hypothesis. Further studies may elucidate the REEs complexation in the soil solutions at the rhizosphere level and unveil the potential molecules that act in this sense.

By studying the Ce behaviour with the related anomalies, it is possible to gather information regarding changing in redox conditions of the system or the presence of specific compounds which may affect its behaviour in the system, helping to uncover occurring geochemical processes. However, before making any consideration on the Ce anomalies for this study, it is important to verify whether or not these anomalies are legitimate. Since the normalized concentration of La is used for the calculation of the Ce anomalies, in the presence of an enrichment or depletion of La there is a risk of underestimating or overestimating the real value of Ce/Ce*. An adaptation of the diagram proposed by Bau and Dulski (1996), reported in Figure 5.8, helps to confirm whether or not the calculation of the Ce anomalies can be legitimate.

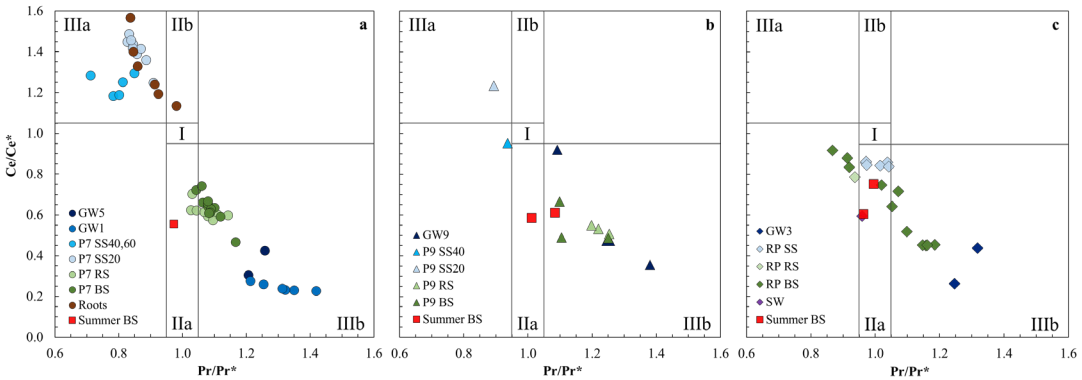

Figure 5.8: Ce/Ce* vs Pr/Pr* diagram reporting the values for all samples collected for this study for plateau site (a), hillslope (b) and riparian area (c). Field I: no Ce nor La anomalies; Field IIa: positive La anomaly; Field IIb: negative La anomaly; Field IIIa: positive Ce anomaly; Field IIIb: negative Ce anomaly.

Ce positive anomalies in the soil solutions at 20, 40 and 60 cm depth at the plateau and 20 cm depth at the hillslope are actual anomalies. Concerning the water sources at the riparian area (streamwater and soil solutions), they confirm the presence of a La positive anomaly rather than of a Ce negative anomaly. All groundwaters present legitimate negative Ce/Ce*. Most of the sap samples that present a La positive anomaly (field IIa – Fig. 5.8) were collected in summer at the plateau and riparian sites. The presence of a negative Ce anomaly in xylem sap can be attributed to the oxidizing conditions in the rhizosphere. Ce is the only Ln^{3+} capable of being oxidized under soil conditions (Laveuf & Cornu, 2009),

transitioning from its CeIII form to the more unstable CeIV, which precipitates as CeO_2 (cerianite) from the solution leading to a depletion of Ce in the water (Braun *et al*., 1998). However, soil solutions collected in this study display positive Ce anomalies, potentially discouraging this hypothesis. Nevertheless, a recent study of ours has demonstrated the ability of litter to induce Ce enrichments in soil solutions (Chapter 6), which would explain the presence of positive Ce anomalies in the soil water despite the oxidizing conditions. The very likely explanation for the negative Ce anomalies in root sap samples linked to changes in the redox conditions at the rhizosphere level, which are typically more oxidative due to the ability of roots to release oxygen. This characteristic is often employed by plants as a protective mechanism against the absorption of potentially phytotoxic metals through precipitation, particularly in wet conditions, and it causes the formation of Fe-Mn oxide plaques onto root surfaces (Levan and Riha, 1986; Xu and Yu, 2013; Suda and Makino, 2016; Khan *et al.,* 2016). The oxidative environment established at the rhizosphere linked to such release of oxygen may promote the precipitation of Ce as an oxide, thereby enriching the roots' composition. Moreover, the additional presence of Mn-Fe oxides plaques may further promote the oxidation of Ce and its precipitation through an oxidative scavenging mechanism (Bau, 1999; Bau and Koschinsky, 2009; Pourret and Davranche, 2013), acting as a barrier for Ce during the water absorption. This hypothesis is supported by the results of SEM analysis of roots (Figs. 5.2 and 5.3), which revealed the presence of Fe oxides in the rhizosphere soil and by REEs patterns of root sap normalized to soil solutions (Fig. 5.9) showing a depletion in Ce, confirming the impossibility for this element to pass across the roots and reach the sap.

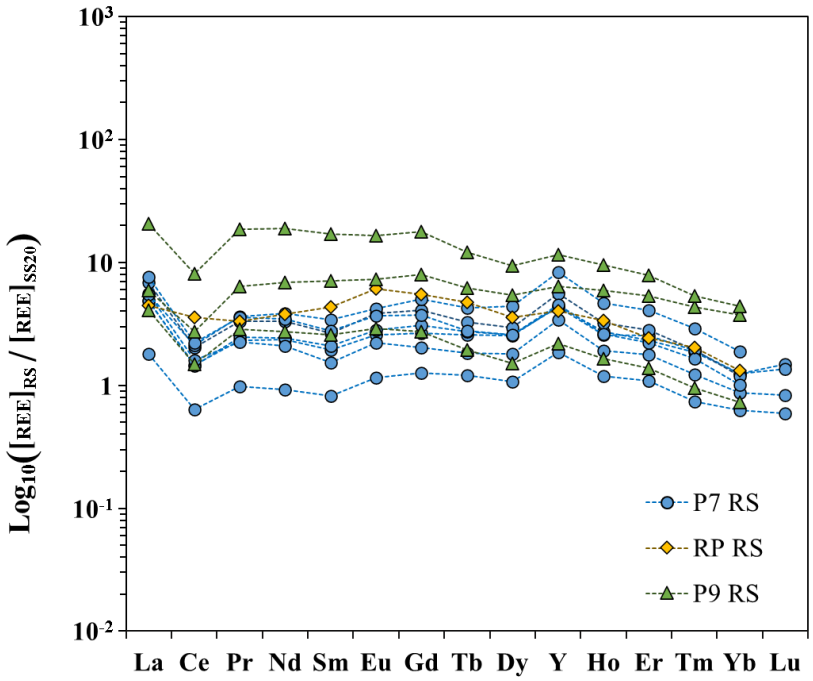

Figure 5.9: REEs patterns of root sap normalized by the REE concentrations in soil solutions at 20 cm depth collected during the same dates of sampling.

An element of distinction between REEs patterns of roots and soil solutions, is the presence of an Y depletion in the former (Fig. 5.5a), whereas the latter show a slight enrichment (Fig. 5.4b). Such difference is likely linked to the different behaviour of Y during the tree water uptake, indicating a higher mobility of this element in comparison with the other REEs (Möller *et al*., 2021) and, therefore, its preferential presence in the xylem sap. This evidence is supported by REEs patterns of root sap samples reported in Figure 5.5, which are characterized by an Y enrichment and by the patterns of the roots normalized to the soil solutions, being depleted (Fig. 5.7). While Y and Ho have same charge and close ionic radius (1.019 and 1.015 Å, respectively), justifying their CHARAC (Charge and Radius Controlled – Bau, 1996) behaviour during primary processes (such as the condensation of a pure silicate melt, during processes occurring in aqueous solutions these elements present a non-CHARAC behaviour and decouple), in non-CHARAC systems, REEs dynamics are not dominated only by their charge and radius but also by their electron configuration and by the nature of the complexing ligands present in the system (Byrne, 1995; Bau, 1996). The different dynamics of Y in such a system, and thus its separation from the twin element Ho, is then linked to its different electron configuration. Physico-chemical features of Y have a direct effect in its absorption during the water uptake operated by roots, which sees this

element less scavenged by Fe oxides in comparison to the other REEs (Bau, 1997; Quinn *et al*., 2004; Möller *et al.,* 2021), and less absorbed by organic barriers in the roots. This is corroborated by the increased Y/Ho ratios in plateau root sap (Y/Ho = 50.80 ± 3.68) in comparison with those of all available soil solutions in the stand (Y/Ho = 32.58 ± 4.67). The enhanced mobility of the Y is also illustrated by the soil solution-normalized REEs patterns of root sap (Fig. 5.9), showing an enrichment for this element in all sap samples.

The presence of positive Gd anomalies in soil solutions (Fig. 5.4b), which disappears in roots (Fig. 5.5) and reappears in root sap samples (Fig. 5.6) can also be highlighted here. The similar anomalous behaviour of Gd and Y was already reported during the interaction of a solution with different mineralogical phases (e.g. Terakado and Masuda, 1988; Toyama and Terakado, 2019; Coppin *et al*., 2002; Bau, 1999; Hannigan and Sholkovitz, 2001; Kage *et al*., 1993), where these metals show a lesser participation – in comparison with the other neighbouring REEs – to the formation of (or adsorption onto) mineralogical phases. The anomalous behaviour of the Gd at the rhizosphere level is likely linked to different processes than those dominating the Y. Like Y, Gd has been shown to be more hydrophilic and less scavenged in comparison to the neighbouring REEs (Möller *et al*., 2021) and tend to stay in solution as truly dissolved element rather than being incorporated in the colloidal fractions or adsorbed onto particles. While it was assessed that the anomalous behaviour of Y relates to its different outer electron configuration that affects the chemical reactivity of this element, for Gd it should not be the case as it shows the same outer electron configuration as the other lanthanides. The anomalous behaviour of Gd can be instead explained by the half filling of its 4*f* orbital, which leads to a higher stability of this element in solution in comparison to its neighbours (McLennan, 1994). Third ionization energy of Gd is indeed lower than those of Tb and Eu (Land and Smith, 2003) and it explains its preferential fractionation in the dissolved phase. Moreover, it has been shown that Gd is characterized by lower complexation constants in comparison to its neighbours (Byrne *et al*., 1995) and lower stability constants with some organic compounds (Smith and Martell, 1989), suggesting a reduced interaction with organic ligands during the water uptake operated by roots. This is clearly observed in the REE patterns of root sap normalized to soil solutions (Fig. 5.9), which generally show a slight positive Gd anomaly (Gd/Gd* = 1.23 ± 0.06). The enhanced mobility of Y and Gd during the water uptake is also supported by Figure 5.10, which shows the increasing values of Gd/Gd* and Y/Ho across the regolith-plant system in spring.

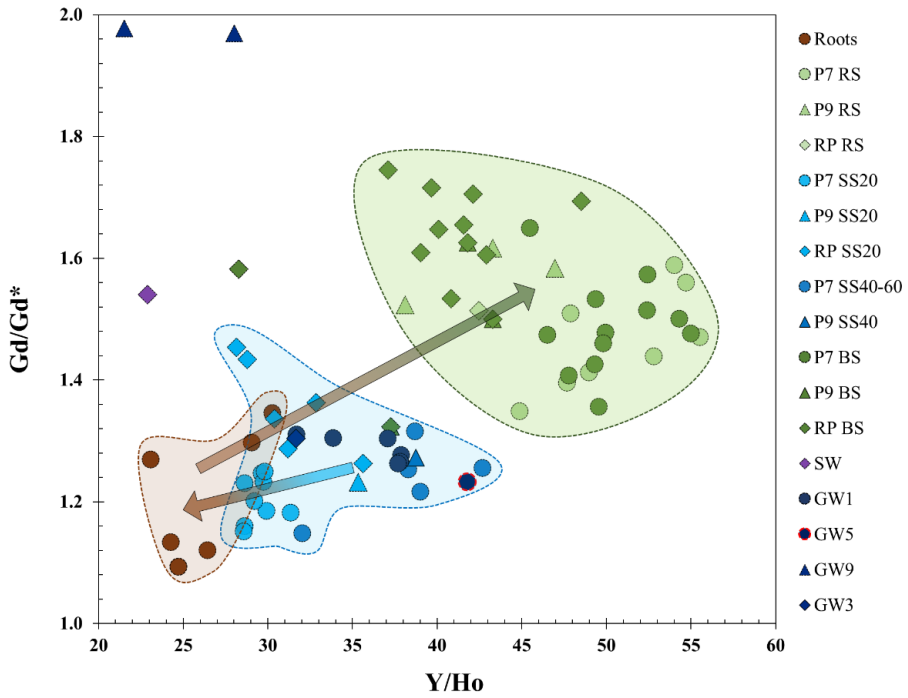

Figure 5.10: Gd/Gd* vs Y/Ho ratios of the spring samples collected for this study, highlighting the enhanced mobility of Gd and Y in comparison to the other REEs. Arrows display the water absorption dynamics from the waters (light blue area) through the roots (brown area) and then to the sap (green area). Noticeable are the decrease of the Gd/Gd* and Y/Ho values in the roots, and their increase in the sap, indicating the enhanced uptake of Y and Gd by trees.

Despite root samples being collected only on the plateau, there is evidence of enrichment in Gd and Y in the root sap across all sampling sites. This is supported by Figure 5.10, as well as by the values of δGd/Gd* and δY/Ho calculated as the difference between Gd/Gd* and Y/Ho values in the root sap and those in the soil solutions at a depth of 20 cm (δGd/Gd* = 0.29 ± 0.08 and δY/Ho = 16.00 ± 7.21). These findings indicate that Gd and Y enrichment occurs during water uptake in all sampled trees and across all morphological units. The tendency of Gd and Y to preferentially distribute into solution during water-organic tissues interaction was also reported during water leaching experiments carried out on litter material in a previous work on the same species and on the same experimental site (Montemagno *et al*., 2022), confirming a higher mobility of these elements during water-tree interaction processes, as well as within the trees – at least for *Fagus sylvatica*.

Although phosphates were potentially found in roots, as indicated by the SEM analysis of roots powder, no positive Eu anomalies were observed in these organs. This

implies that these mineral phases do not significantly contribute to the Eu fractionation during the water uptake process as previously suggested (Ding *et al*., 2007).

5.4.2 REEs translocation from roots to branches

REE patterns of branch sap normalized by the root sap samples collected during the same sampling dates are reported in Figure 5.11. Here, two main features can be highlighted: the general enrichment trend in relation to REEs atomic number, which is therefore observed as an increasing trend from La to Lu, and the negative Eu anomalies characterising most of the patterns. The increasing trend along the series, illustrated by the La_N/Yb_N ratios (La_N/Yb_N = 0.53 ± 0.20), is congruent with the mobilization of the REEs along the root-branch flow path through the complexation with organic acids present in the sap, as previously suggested by other studies (Brioschi *et al*., 2012; Censi *et al*., 2014; Yuan *et al*., 2017; Yuan *et al*., 2018), and with the shape of the patterns of the REEs stability constants with some organic acids (e.g. Pourret *et al*., 2007; Marsac *et al.*, 2010; Sonke and Salters,2006).

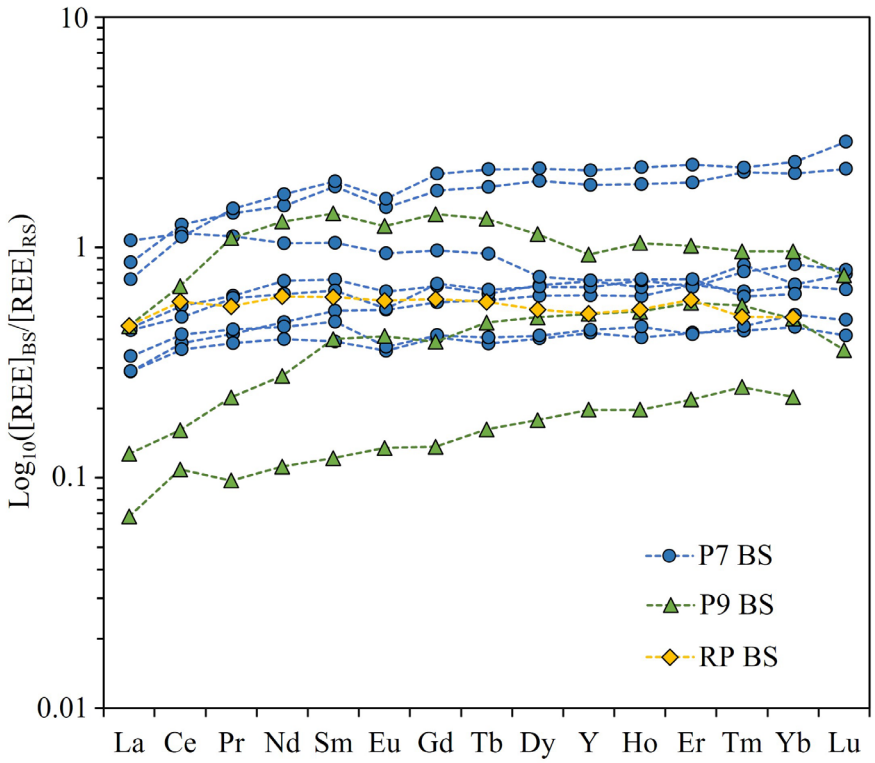

Figure 5.11: REEs patterns of branch sap normalized by the concentrations in the root sap collected in the same dates.

This assumption is corroborated by the higher DOC concentrations in the branch sap in comparison to the root sap (Fig. 5.12a, Table A5.3) and by the linear relationship between DOC and HREEs concentrations in the branch sap (Fig. 5.12b), which shows that [HREEs] increases with increasing DOC.

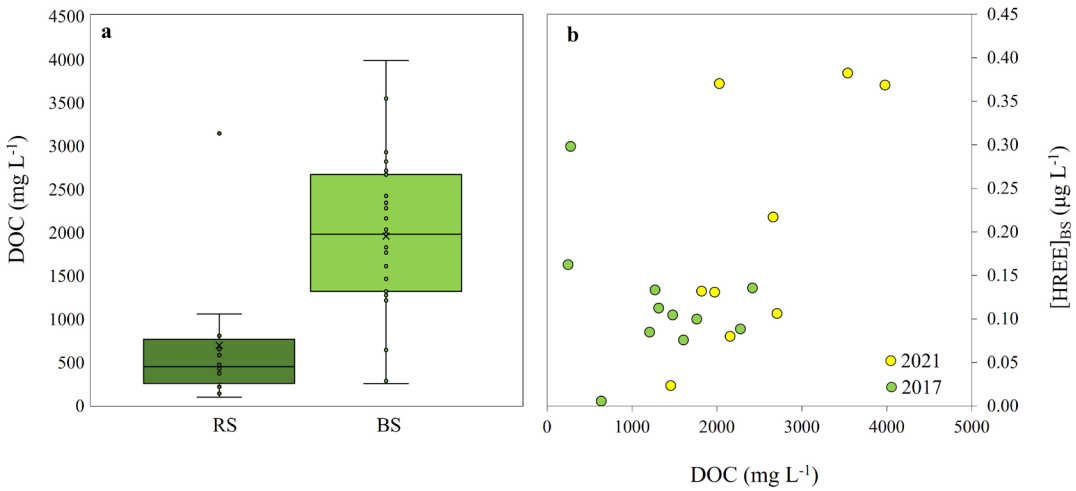

Figure 5.12: On the left, DOC concentrations in root sap (RS) and branch sap (BS); on the right, linear relationship between DOC and HREEs concentrations in branch sap samples.

However, this trend is observed only in 2021 samples, and the difference between the two years of sampling is not explained. Nonetheless it is noteworthy that the correlation between the DOC and HREEs content in branch sap appears to occur once a certain threshold of DOC concentration is exceeded, approximately 1500 mg/L.

To highlight the role of sap transportation in REEs fractionation across the regolith-tree system, it is convenient to study the mutual behaviour of the REEs groups in the different water pools considered in this study. By reporting the LREEs vs MREEs vs HREEs concentrations in water sources and sap, it is worthy to notice that all REE show a coherent behaviour in the water sources (Figure 5.13a, b) analysed. The situation in the sap is instead different. While, indeed, LREEs and MREEs demonstrate similar dynamics along the root-to-branch flow path (Fig. 5.13a), LREEs and HREEs exhibit a higher degree of fractionation in branch sap (Fig. 5.13b), indicating a more pronounced separation of HREEs from the other two groups during the flow to the upper parts of the trees. This plant-driven REEs fractionation was also observed in our previous study (Chapter 7), where we highlighted the potential role of the competitive binding processes of organic acids in regards of REEs during the litter degradation. It was shown a preferential fractionation of the LREEs and MREEs into the solid litter fraction, and HREEs in the leaching solution due to the presence of organic

acids for which HREEs have more affinity. It is noteworthy that 1 sample from the plateau, as well as the sample from the riparian area, show, respectively, a downward trend and a flat pattern shape (Fig. 5.11). This appears to be consistent with the lowest DOC concentrations found in the root sap samples (P7 RS2 and RP RS1 – Table A5.3), suggesting that these latter were insufficient to produce the HREEs enrichment observed in the other samples. However, LREEs-MREEs enrichment, as well as LREEs depletion were observed for 2 branch sap samples from the hillslope. The reason for such differences cannot be identified with the data collected. Potential explanation can be linked to the different nature of organics present in the sap, towards which LREEs and MREEs may show higher affinity in comparison to the HREEs.

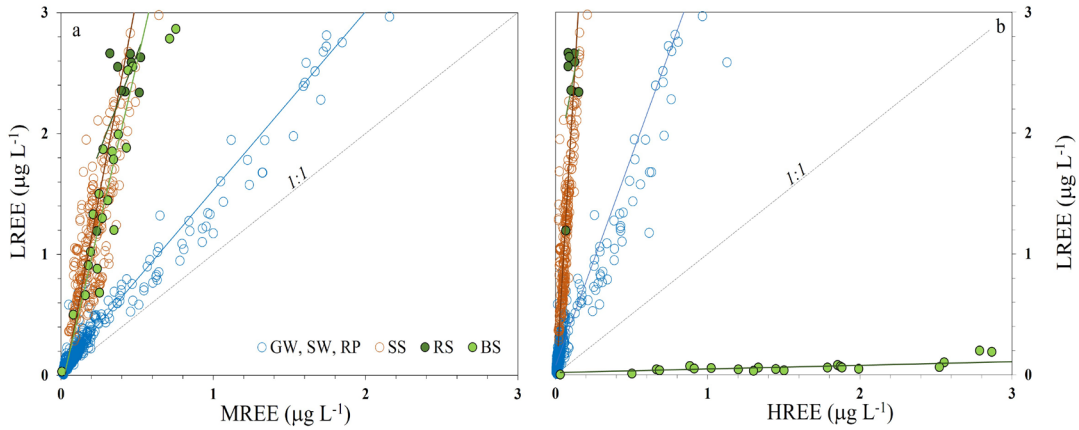

Figure 5.13: LREEs vs MREEs (a) and LREEs vs HREEs (b) for the historical database of the water sources and root sap and branch sap collected in this study.

Another interesting feature of the root sap-normalized REEs patterns of branch sap, is the slightly negative Eu anomaly shown for some of the samples (Eu/Eu* = 0.92 ± 0.08), which suggests the fractionation of Eu in the tree tissues during the root-branch sap flow. This hypothesis is corroborated by the REEs patterns of tree tissues in Figure 5.5 where a positive Eu anomaly is observed in all above-ground parts of the trees, indicating a preferential distribution of Eu into tree tissues – with a preference of lignin-rich material (e.g. wood – Sarkanen and Ludwig, 1971), and by the REEs patterns of above-ground tree compartments normalized to sap, reported below in Figure 5.14.

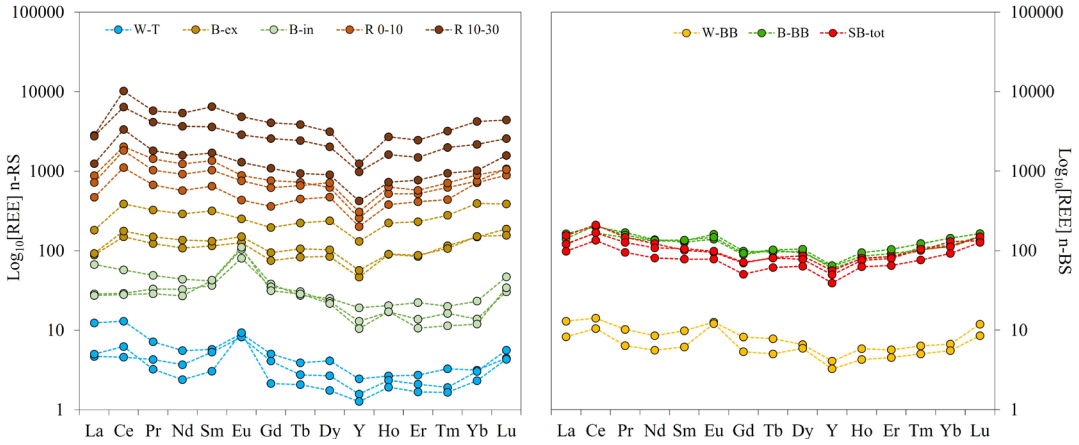

Figure 5.14: REEs patterns of above-ground tree compartments normalized to the composition of the sap. Samples collected from the bole are normalized to root sap (left), while samples collected from branches are normalized to branch sap (right). Legend: W-T refers to bole wood; B-ex and B-in to external and internal bark, respectively; W-BB to big branch wood; B-BB to big branch bark; SB-tot to bulk composition of small branches; R 0-10 and R 10-30 to roots at 0-10 and 10-30 cm depth.

An explanation to this phenomenon is given by the capability of Eu^{3+} to replace Ca^{2+} in some physiological processes and/or in specific molecules due to their similar ionic radii (Shannon 1976). Ca-replacement by Eu has been suggested to occur in plants grown on low Ca-content substrates (Brioschi *et al*., 2013; Shtangeeva and Ayrault 2007), in some physiological processes (Zeng *et al*., 2003) and in structural units of cell walls (Montemagno *et al.,* 2022). Here it is important to recall that the sampling campaigns were carried out in spring, which represents the stage of development of new xylem conduits to cope with embolisms following the winter freezing for deciduous trees in temperate forests (Cochard *et al*., 2001; Améglio *et al*., 2002). In this process, Eu may fractionate from the xylem sap during the synthesis of new building blocks for the formation of the afore-mentioned conduits, by replacing Ca in Ca-pectate molecules used by plants to link cell walls and give stability to the resulting structure (Proseus and Boyer, 2012). Such process, occurring all along the root-branch flow path, would lead to an impoverishment of Eu in the xylem sap due to its fractionation in the solid plant tissues. Such preferential fractionation of Eu in cell walls is also corroborated by the higher positive Eu anomalies observed in the wood and internal bark in comparison to the other samples (Figure 5.5 and 5.14).

Finally, another interesting features of the REEs patterns of branch sap, is the slightly different behaviour of Gd and Y during the root-branch sap flow. The enhanced mobility of Gd and Y that was observed during the water absorption, in the root-branch flow

path is confirmed only for the Y. Indeed, while the Gd/Gd* values of the root sap-normalized REE patterns of branch sap are close to 1 (Gd/Gd* = 1.00 ± 0.05) (Fig. 5.11), Y/Ho ratios in branch sap are higher than those of root sap (respectively Y/Ho_{BS} = 48.74 ± 5.4 and Y/Ho_{RS} = 45.43 ± 6.2). This indicate that, while the mobility of both elements is enhanced during the water absorption operated by roots, during the flow across the tree they show different dynamics, with the Y being the most mobile REEs in the system. This is corroborated by the REEs patterns of above-ground tree parts normalized to the sap (Fig. 5.14), showing no significant Gd anomalies overall (Gd/Gd* = 0.92 ± 0.5), while Y/Ho ratios appears to be depleted in comparison to sap samples (Y/Ho = 34.48 ± 5.25), suggesting the preferential fractionation of Y in the solution.

5.4.3 Identification of the water source absorbed

As already discussed previously, REEs patterns of roots appear to be mirroring the one of the water sources uptaken. This was shown for the PAAS-normalized REEs patterns of roots collected at the plateau, which show very similar shapes to those of the soil solutions at 20 cm depth. While it is true that REEs are not conservative tracers at the interface between compartments, it is possible to use our understanding of their fractionation across the soil-root system to recognize the uptaken water source by comparing the REEs shapes of the root sap with the ones of the potential water sources.

By looking at the various REEs patterns of root sap and of the related water sources reported in this manuscript, it appears that soil solutions are the most representative water sources nourishing the trees at the time of sampling. To understand the reasoning behind, few aspects must be considered, especially considering the 2017 sampling campaign during which root sap was directly extracted from the 20 cm deep roots:

I. All deep ground waters and streamwater (GW3, GW5, GW9, SW) have REEs concentrations that are 2 or 3 orders of magnitude lower than in root sap. Only shallower groundwater (GW1) showed REEs concentrations comparable to those of the root sap (Tab. A5.1). Plants can create an osmotic gradient in their roots by increasing the solute concentration in the sap. This mechanism allows them to attract and absorb water even in the absence of transpiration (McElrone *et al*., 2013). Consequently, it is plausible that the REEs concentrations in the root sap can be slightly higher than those in the water source. Nevertheless, the large difference in concentrations between the root sap and the deep groundwaters is such to suggest that these are not the potential resources for

the sampled plants, especially knowing that metals are preferentially trapped into root tissues to prevent potentially toxicity events (Yan *et al*., 2020), as previously discussed.

II. PAAS-normalized REEs patterns of all groundwaters (Fig. 5.4a) show to be highly depleted in LREEs. By considering that LREEs and MREEs are preferentially immobilized by roots – as suggested by REEs patterns of bulk roots normalized to soil solution at 20 cm (Fig. 5.7) – we should expect an even stronger depletion in LREEs in the root sap in comparison to the groundwaters due to the filtering process of the roots during the water uptake. Such a depletion is not shown in xylem sap, on the contrary, an increase in LREEs is observed with respect to groundwaters.

III. Soil solutions show more coherent REEs concentrations to those of the root sap (Table A5.1), and only a smaller LREEs depletion in comparison to the groundwaters, especially at 40 cm depth (Figs. 5.4a, b). Accordingly, the possibility of groundwaters to be the main water sources for trees during the sampling campaigns can be excluded.

Therefore, soil solutions appear to be the best candidates for nourishing the trees in the sampling period. By comparing the root sap collected in 2020 from the tap root at the trees' base with the root sap collected in 2017 from 20 cm deep fine roots, it is possible to notice that patterns are almost identical. As REEs patterns of the different water sources don't change over time (Chapter 7), we can assume that most of the water uptaken by trees during the sampling periods comes from the soil solutions and not from the groundwaters. The same reasoning can be done for the 2020 sampling campaign, despite the fact that the xylem water was collected from the tap root rather than from small roots. Indeed, the same REEs patterns shape of 2017 were found in 2020, suggesting the same water uptake regime in the two years of sampling. These findings are in line with the results obtained from a previous study based on water stable isotopes analyses carried out on the same site and tree species (Fabiani *et al*., 2021), and in the same samples used for this study (Chapter 3), reporting a preferential uptake of soil solutions by *Fagus s*. in the Weierbach catchment.

Concerning the summer, we did not find significant similarities between the branch sap and the available water sources at the time of sampling (groundwaters), potentially excluding a direct uptake of the deep groundwaters. Nonetheless, it is important to report that the Y anomalies observed in branch sap in March at the hillslope site (Fig. 5.6a and 5.6b), which were connected to the uptake of the Y-enriched soil solutions, disappeared in summer. This may suggest a shift in the water uptake regime of the trees – at least at the hillslope site – which in summer may absorb water from the groundwater that indeed does

not show Y enrichment. However, the fact that summer branch sap has similar shapes to those of spring suggests that a groundwater uprising and its consequential change in the REEs composition during the interaction with soil may occur before being uptaken by trees. It is also important to consider that branch sap is not as accurate as root sap to identify the potential water source uptaken, due to the REEs fractionation occurring within the root-branch pathway. The lower REEs concentrations observed in summer branch sap might be linked to the already depleted concentration – in the regards of soil solutions – in the uprising water and/or to the increased tree transpiration rate, which negatively impacts the sap osmotic pressure, reducing solutes concentration (Munns and Passioura, 1984). However, greater precision in understanding the extensive REEs fractionation at water-root-sap interfaces is crucial for identifying water sources absorbed by trees. Experiments using potted plants under controlled conditions could refine our understanding of these dynamics and enable an accurate modelling. This, in turn, would enhance the interpretation of REEs patterns in the root sap and improve the identification of assimilated water sources. Moreover, further experiments are needed to study the evolution of the REEs concentrations and patterns along the full vegetative period, considering changes in seasonal water availability and by coupling the study of groundwater uprising during dry periods.

5.5 Conclusions

In this study, the potential application of REEs as tracers for water movement across the regolith-plant continuum was investigated. This involved examining REEs fractionation at the root level and within the xylem sap flow pathway. We considered groundwater, streamwater, soil solutions at various depths, root bulk, root sap, and branch sap in our analysis. Additionally, REEs fractionation processes at the rhizosphere level and during their transport in the xylem sap was explored.

The results revealed that the roots exhibit PAAS-normalized REEs patterns comparable to those of the solutions they interact with. It was observed a preferential fractionation of Ce on the root surface during water uptake, which mightbe associated with a more oxidative environment. This environment is created by oxygen release from the roots and the presence of iron oxide plaques on their surface. These conditions promote the oxidation of CeIII to CeIV, causing it to precipitate as cerianite (CeO_2) and leading to a negative Ce anomaly in the root sap.

The roots displayed a depletion of HREEs when compared to the soil solutions they interacted with. This HREEs depletion was also evident in the root sap, ruling out the

possibility of preferential fractionation of these elements in this fluid. Instead, the data suggest that HREEs have a higher affinity for the organic compounds in soil solutions compared to other REEs, leading to their preferential distribution within these molecules.

Y and Gd demonstrated increased mobility during water absorption by roots and during the REEs transportation throughout the tree. Y unique behaviour is attributed to its distinct outer electron configuration, whereas Gd preferential fractionation in the solution appears to be related to the half-filled 4f orbital, lower third ionization energy, reduced stability constant with organic compounds, and lower complexation constants with organics compared to neighbouring REEs. Due to their enhanced mobility in the regolith-plant system, Y and Gd also become enriched along the root-branch pathway.

REEs mobility in the root-branch flow path was found to increase with increasing atomic number. This is associated with a growing affinity, along the REEs series, for organic acids present in the xylem sap. Simultaneously, Eu exhibited slight depletion during its flow to the branches, which reinforces its ability to substitute Ca in certain physiological processes and/or specific molecules due to their similar ionic radii. In particular, we propose that Eu replaces Ca in the Ca-pectate molecules found in cell walls.

Finally, the analysis of REEs patterns in root sap and various water sources indicates that soil solutions are the primary water sources nourishing the trees during the sampling period. This conclusion is supported by the significant concentration differences between root sap and deep groundwaters, the comparison of PAAS-normalized REEs patterns, and the consistency of these findings with previous studies on water stable isotopes at the same site. Further research is needed to explore seasonal water availability and groundwater uprising during dry periods.

According to these findings, the first hypothesis is verified, as certain REEs were preferentially taken up during the water absorption (Gd and Y), while others were mobilized in the tree tissues (Eu, LREEs) or kept staying in the soil solutions (HREEs).

The second hypothesis appears to be verified as well, as the understanding of the REE dynamics during the water uptake gave a clue regarding the potential water source uptaken. However, additional studies should be conducted in order to confirm these findings.

CHAPTER 6

Rare earth elements in *Fagus sylvatica* exudates

6.1. Introduction

Rainfall passing through the canopy, known as throughfall, plays an important role in the water balance, soil erosion, biogeochemical cycle of elements, therefore regulating the chemical composition of soil and water in forest ecosystems (Levia *et al*., 2017). The process of throughfall involves the interception of rainwater by leaves and stem, which leads to the leaching of various substances from their surface. These substances are collectively referred to as exudates or mucilage, and they are composed of a wide range of organic and inorganic compounds with different functions for plants (Galloway *et al*., 2019). They are used by plants for protection, acting as a physical barrier that can deter herbivores and protect from pathogens and insects; for mantaining moisture balance within the plant; for reducing water loss by decreasing the transpiration; and as response to physical damage to seal wounds and limit the spread of pathogens (Constabel and Barbehenn, 2008; Evert, 2006; Nobel, 1999; Patten *et al*., 2010; Raffa *et al*., 2013).

One of the aims of this thesis was to study the biogeochemical cycle of REEs at tree scale in terms of fractionation and dynamics across the regolith-tree continuum. To better comprehend the biogeochemical cycle of REEs in such a system, one cannot abstain from considering mucilage as one of the crucial stages to which REEs are linked in their environmental dynamics. The presence of REEs in throughfall can have significant implications for soil and water chemistry in forest ecosystems but the extent to which leaf exudates influence the REEs composition of throughfall, in complement to atmospheric deposition, has not been studied yet. Investigating the REEs at a tree level could contribute significantly to our understanding of the cycling and turnover of these elements within forest ecosystems and help to discern between atmospheric and plant-derived inputs on throughfall, and therefore on REEs chemistry of soil and soil waters. Throughfall chemistry is determined by the leaching process of rainfaill on atmospheric dust and leaves exudates. These two factors contribute to the chemical composition of the throughfall, as well as spatio-temporal variability of its REEs signature. This chapter briefly investigates the contribution

of leaf exudates on the REEs composition of throughfall in a forested catchment, considering also the interaction with the atmospheric dust deposited on leaves and stem. To achieve this, REEs composition of atmospheric dust, transpired water, throughfall and rainfall collected at three different European beech (*Fagus sylvatica* L.) stands of the Weierbach experimental catchment was studied in order to understand the REEs behaviour during their release from leaves, the subsequent impact on the chemical composition of meteoric water, and to discern the plants-derived impact from that of the atmospheric dust on throughfall chemistry.

6.2. Materials and methods

For analytical methods and study site, please refer to Chapter 5.

Rainfall and throughfall were collected from March to September 2020, while transpired water became available after the bud break on April, allowing its collection in May. Plastic bags were used to collect the transpired water by covering beech shoots at different height (1 to 5 meters) and radial directions and sealed (Fig. 6.1).

Figure 6.1: Plastic bags installed on European beech branches for the collection of transpired water and mucilage.

To monitor whether the exposure to environmental conditions would induce the release of any chemical from the bags capable of altering the composition of the resultant solution, one bag per tree was filled with 1 L of ultrapure water (MilliQ), sealed and attached to the tree. All bags were collected after 3 weeks from the installation. Throughfall and rainfall were collected in the same dates as the transpired water, by using 3-L Palmex rain sampler. All water samples were gathered into clean 1-L polypropylene bottles, sealed and brought to the lab as soon as possible where they were filtered at 0.20 µm with cellulose acetate membrane filters. The resulting solutions were then acidified with HNO_3 1% (v/v) and stored at 4 °C until analysis. Some samples of throughfall and transpired water were dark and turbid at the time of the collection and after filtration. These samples were first evaporated at 40 °C and then digested in aqua regia in Teflon tubes. Subsequently, the acids were evaporated and the residue dissolved in a solution 1% v/v HNO_3.

A modified polypropylene version of the passive SIGMA-2 collectors (German Meteorological Service in Freiburg - VDI 3787, 2010) was utilized to collect atmospheric particles larger than 2.5 µm (Grobéty *et al*., 2010) at a height of 1.5 m above the ground. The collected atmospheric dust represents a comprehensive sample that was exposed to atmospheric deposition from September 2018 to May 2019. Throughout the entire exposure period, the particles were gathered and stored in acid-clean Teflon vessel. Subsequently, they were kept in desiccator until digestion. Following the weighing of the collected atmospheric dust (2.3 mg), the sample was completely digested using a concentrated ultrapure acid mixture of HNO_3, HF, and $HClO_4$. The acids were then evaporated, and the resulting residue was dissolved in a solution of HNO_3 (1% v/v) and stored at 4 °C before analysis.

It is crucial to consider that during the ICP-MS analysis numerous samples, particularly transpired waters, exhibited concentrations of REEs below the limit of quantification (LoQ) but above the detection limit (DL). These measurements have a higher level of uncertainty due to their limited precision. However, given the fascinating nature of the topic and the substantial efforts invested in conducting the comprehensive sampling campaign and related sample analyses, the obtained data was included in this chapter. To provide a detailed perspective on this data, the values used are presented in Table A6.1, which highlights those falling below the LoQ.

6.3. Results and discussion

All bag blank samples appeared to be totally clean, suggesting that no chemical release from the bags occurred, despite their exposure to the environment (Table A6.1).

REE concentrations showed high variability in all the liquid samples collected with the lowest concentration in the Rainfall with [REEs] = 14.66 ± 9.83 ng/L, whereas the highest were found in the Throughfall with [REEs] = 174.10 ± 202.47 ng/L. Transpired waters presented REEs concentrations in between the two previous sample types, with [REEs] = 76.88 ± 56.24 ng/L. Atmospheric dust showed a [REEs] equal to 80.46 µg/g (Table A6.2). It is interesting to notice that REEs concentrations in transpired water increased progressively along the sampling campaign.

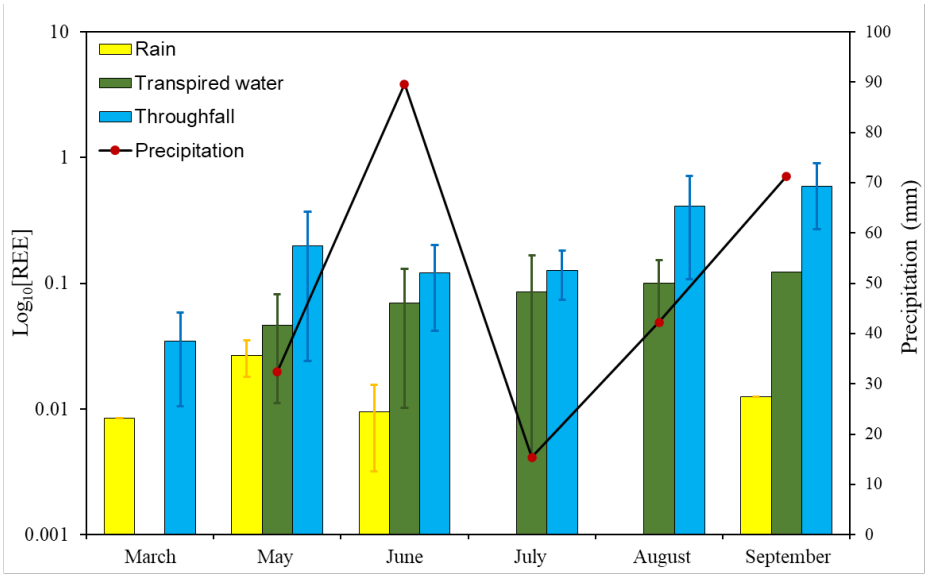

Figure 6.2: Logarithm of the concentrations of REEs in the different liquid samples collected for this study, and precipitation (in mm) during the sampling campaign..

While rain summer samples (June and September) show similar [REEs], in throughfall and transpired waters REEs concentrations increased with the former showing a stronger enrichment in comparison to the latter. Unfortunately, no rainfall REEs data was available for July and August. However, despite the increased precipitation occurred in August (in comparison to July) where one would expect a lower concentration due to increased dilution, REEs concentrations in throughfall increased too, suggesting a higher participation of the exudates to its total REEs content. This may be linked to the enhanced exudates release from leaves to reduce water loss (Lusa *et al.*, 2014), which is also corroborated by the increasing vapor pressure deficit observed during the sampling

campaign and to a reduced sap velocity in the late summer (Chapter 3, Fig. 3.2). However, it is important to consider that only leaf and small branches exudates were considered for this study. Other mucilage sources such as bark, as well as organisms like mosses and lichens which may be present in the tree bark were not considered and therefore their contribution could not be assessed. These latter could indeed explain the higher increase in REEs concentration in throughfall in comparison to the transpired water observed in the same period.

The normalized patterns of average REEs concentrations, as shown in Figure 6.3, indicate a gradual and slight increase in concentration with increasing atomic number Z.

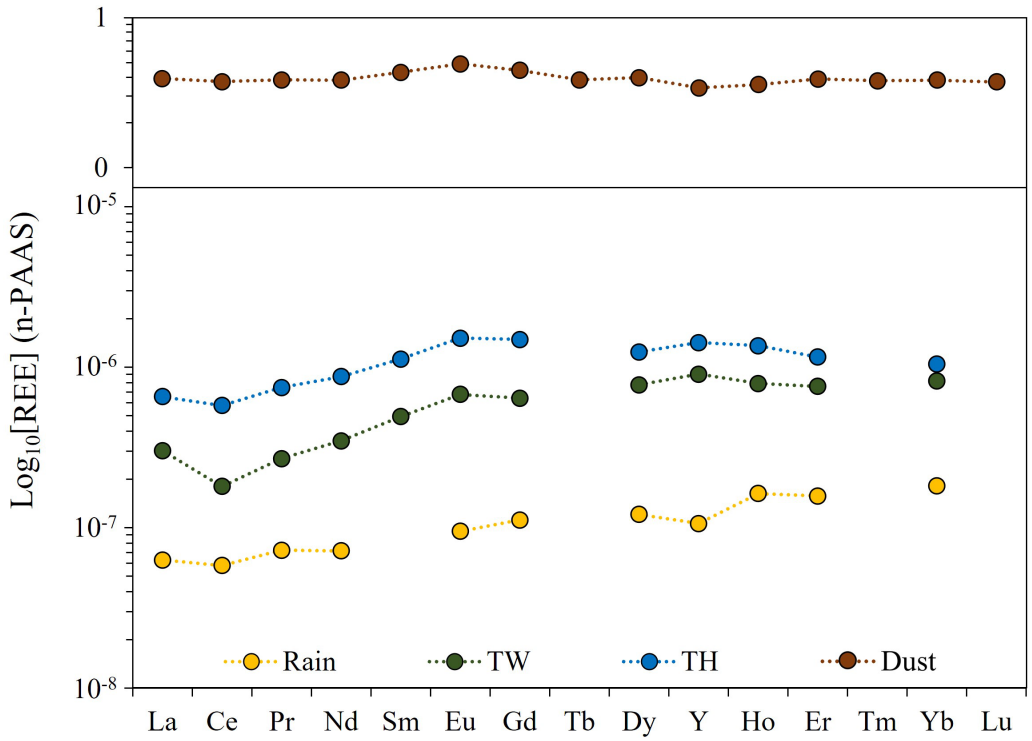

Figure 6.3: PAAS-normalized patterns of average REE concentrations in atmospheric dust, rainfall, transpired water (TW) and throughfall (TH) samples collected for this study.

This trend is more prominent in rainfall and transpired water, while being less evident in throughfall, as evidenced by the LaN/YbN ratios of 0.34, 0.37, and 0.64, respectively. All patterns show a negative Ce anomaly, which is stronger in the transpired water (Ce/Ce*= 0.63) and slighter for the other sample types (Ce/Ce*= 0.82 rainfall and Ce/Ce*= 0.86 in throughfall). The stronger negative Ce anomaly in the transpired water is justified by the preferential fractionation of this element – during the water uptake, in the lignified tissues of

the tree and in iron plaques present onto the root's surface as reported in Chapters 5 and 7, respectively. Such fractionation at the root/water interface produces a Ce-depleted REEs patterns in the root sap, which appears to be conserved in the root-shoot pathway (Chapter 5). Therefore, the resulting Ce-depleted REEs pattern of the transpired water may be due to an already depleted REEs composition of the sap and to the preferential fractionation of Ce in the tree tissues, which does not allow this element to freely move in the solution. This is also corroborated by previous findings showing a negative Ce anomaly in fresh leaves of *Fagus sylvatica* (Chapter 7) collected from the same trees used for this study, indicating a reduced transportation of Ce towards the upper parts of the tree.

One distinguishing feature between the patterns is a slight Y enrichment in transpired water and throughfall, which also show very similar values (Y/Ho_{TW} = 36.07 ± 13.83 and Y/Ho_{TH} = 37.47 ± 11.20), in comparison to rainfall (Y/Ho = 12.45 ± 7.49) and atmospheric dust (Y/Ho = 25.93) (Figure 6.4). The enhanced mobility of Y in the regards of the other REEs, explains its preferential release from leaves together with the exudates, and justifies the Y enrichment found in the throughfall. This is linked to its hydrophilic nature (Möller *et al*., 2021), which makes Y remain in the liquid phase rather than being absorbed in the solid plant material. Such Y behaviour is also supported by its enhanced intake observed during *Fagus sylvatica* water uptake (Chapter 5), which resulted in a preferential distribution of this element in the sap (in comparison to the other REEs) and a consequential enrichment that is conserved towards transpired water and exudates released from leaves and branches. However, the atmospheric dust contribution to the Y enrichment in throughfall and transpired water was not excluded. Previous studies (e.g. Möller, 2002) demonstrated that water/rock interactions can deliver enhanced Y/Ho ratios in the solutions in comparison to the source rock, highlighting the higher mobility of the Y during these processes. The slight Y depletion in the atmospheric dust (Figure 6.3) may indeed indicate a preferential release of this element during the interaction with waters. In our case, the atmospheric dust could interact with the transpired water inside the bags or with throughfall in the gauges, enhancing their Y content. REEs concentrations in the dust is indeed much higher than those of the liquid samples (Fig. 6.3) and such disequilibrium may enhance the release of Y from the dust particles during the interaction with the liquid samples. If this were the case, one would expect to observe an enrichment of Y in rain samples due to its interaction with dust particles in the rain gauges. However, such enrichment is not observed (Fig. 6.3). In Chapters 4 and 5, Y was shown to be highly mobile in the regards of the other REEs,

particularly at the interfaces between different compartments. Therefore, there is no reason to believe that the leaf/atmosphere interface represents an exception.

These results suggest that exudates from trees may be the primary source of Y in throughfall and transpired waters. They also underscore the significant impact of tree exudates on the REEs composition of throughfall and their potential contribution to soil water chemistry.

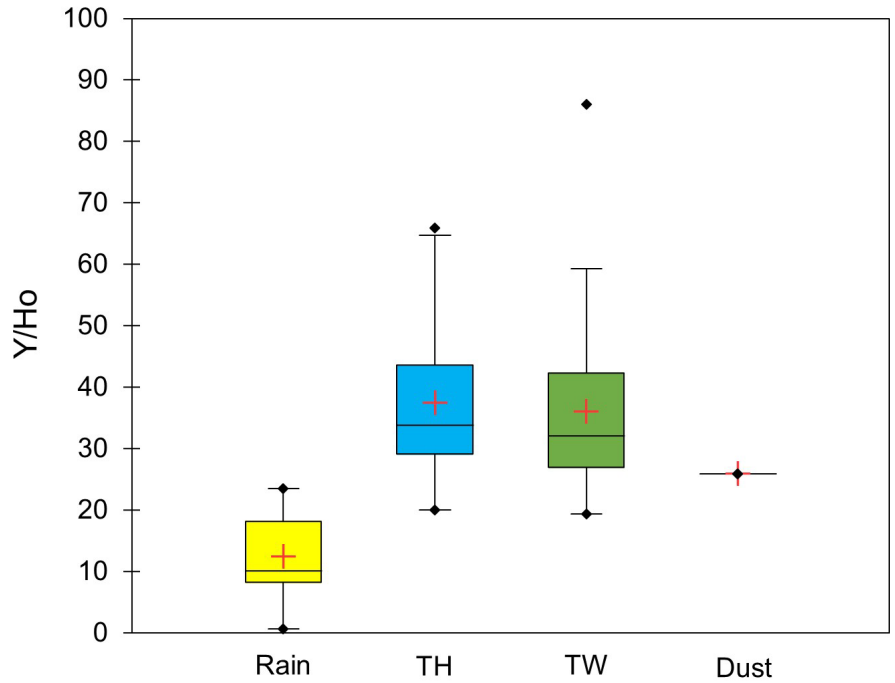

Figure 6.4: Y/Ho values for the Rain, throughfall (TH), transpired water (TW) and atmospheric dust collected for this study.

Both throughfall and transpired water are characterised by a positive Eu anomaly when normalized to the PAAS with, respectively, Eu/Eu* = 1.19 and 1.16. Such an anomaly cannot be explained by the enhanced mobility of Eu^{2+} as there is no reason to justify the existence of Eu under its divalent form in such a system. Indeed, as discussed in Chapter 5, Eu tends to preferentially fractionate in the tree tissues during the root-branch flow path rather than staying in the solution. An explanation to such positive Eu anomaly is given by the interaction of the transpired water with an atmospheric dust rich in plagioclase (Bau, 1991). By looking at the patterns of the average REEs concentrations of the different solutions normalized to the atmospheric dust (Fig. 6.5), it is possible to notice that the Eu

anomaly disappears, showing Eu/Eu* values of 1.04 and 1.07 for throughfall and transpired water, respectively.

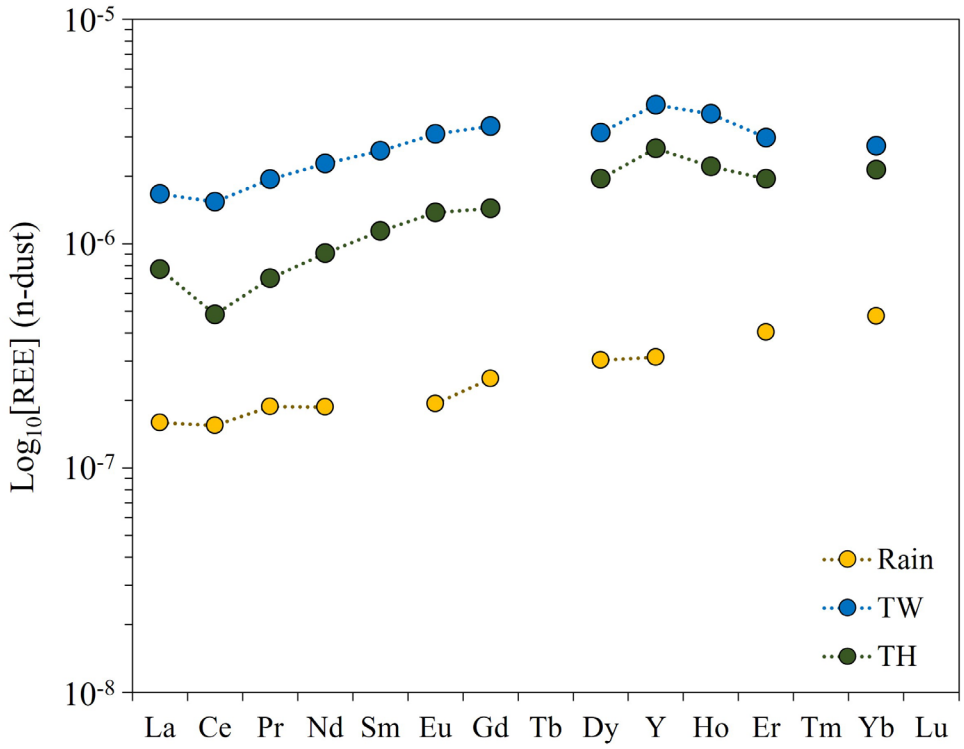

Figure 6.5: dust-normalized patterns of average REEs concentrations in rainfall, transpired water (TW) and throughfall (TH) samples collected for this study.

The disappearance of the Eu/Eu* suggests a contribution of the atmospheric dust on the chemical composition of the transpired water, due to the prolonged interaction occurring in between the bag installation and the sampling dates (3 weeks ca.). However, future investigations focusing on the chemical speciation in the transpired water, along with the study of the mineralogical composition of atmospheric dust, may help identify the primary processes at work in this context.

Gd enhanced mobility, observed in Chapters 4 and 5, could not be assessed due to the lower reliability of the data and the presence of Eu anomaly that did not allowed for the graphical observation of Gd enrichments in transpired water and throughfall samples. Additional experiments considering preconcentrations methods for REEs are then needed to to obtain more reliable data to accurately depict their dynamics during the release from trees, and their impact on the chemistry of incident waters.

6.4 Conclusion

The REEs concentrations in rainfall, throughfall and transpired water of *Fagus sylvatica* were studied to better understand the impact of the leaf exudates on the REEs composition of the throughfall. The REEs composition of these solutions was compared with that of the atmospheric dust to discern the contribution of this latter on the resulting transpired water and throughfall chemistry. All transpired water and throughfall solutions showed a negative Ce anomaly, suggesting the preferential fractionation of Ce into the tree tissues and its limited release into the environment with the leaf exudates.

The Y enrichment in the throughfall and transpired water samples appears to be linked to the higher mobility of this elements in the regards of the other REEs.

Transpired water and throughfall samples showed a slightly positive Eu anomaly, which can be attributed to the preferential release of Eu with the organic acids in the leaf exudates or to the interaction with an atmospheric dust rich in plagioclase or a combination of both.

The typical enhanced mobility of Gd at the interfaces could not be ruled out in this study, due to the lower reliability of the data and the presence of Eu anomalies.

Our findings contribute to a better understanding of the biogeochemical processes that regulate the distribution of REEs in forest ecosystems but further experiments are needed to clarify the origin of the Eu anomaly in transpired waters and throughfall.

CHAPTER 7

Rare earth elements dynamics during litter degradation

Abstract

Given the diverse physico-chemical properties of elements, we hypothesize that their incoherent distribution across the leaf tissues, combined with the distinct resistance to degradation that each tissue exhibits, leads to distinct turnover rates among elements. Moreover, litter layers of different ages produce diverse chemical signatures in solution during the wet degradation. To verify our hypothesis, Na, K, Mg, Mn, Ca, Pb, Al and Fe were analysed together with the Rare Earth Elements (REEs) in the solid fractions and in the respective leachates of fresh leaves and different litter layers of two forested soils developed under *Pseudotsuga menziesii* and *Fagus sylvatica* L. trees. The results from the leaching experiment were also compared to the in situ REEs composition of the soil solutions to clarify the impact that the litter degradation processes may have on soil solution chemical compositions.

Both tree species showed similar biogeochemical processes dominating the element dynamics during the degradation of the litter. REEs, Al, Fe and Pb were preferentially retained in the solid litter material, in comparison to the other cations, and that their concentrations increased over time during the degradation. Accordingly, different litter fractions produced different yields of elements and REEs patterns in the leachates, indicating that the tree species and the age of the litter play a role in the chemical release during the degradation. In particular, the evolution of the REEs patterns, relatively to the age of the litter layers, allowed us to deliver new findings on REEs fractionation and mobilization during litter decay. Into specific, the degradation of the litter was characterised by a decrease in the Y/Ho ratio and an increase in the La_N/Yb_N ratio.

This Chapter is based on: Montemagno, A., Hissler, C., Bense, V., Teuling, A. J., Ziebel, J., and Pfister, L.: Dynamics of rare earth elements and associated major and trace elements during Douglas-fir (Pseudotsuga menziesii) and European beech (Fagus sylvatica L.) litter degradation, Biogeosciences, 19, 3111–3129, https://doi.org/10.5194/bg-19-3111-2022, 2022.

The relationship between these ratios delivered information on the litter species-specific resistance to degradation, with Douglas-fir litter material showing a lower resistance.

During the degradation of the litter of the two tree species, two main differences were highlighted with the help of the REEs: i) in *Pseudotsuga menziesii* the Eu behaviour appeared to be linked to the Ca during leaves senescence and ii) species-specific release of organic acids during the litter degradation leads to a more pronounced MREEs enrichment in the *Fagus sylvatica* leachates.

Finally, we showed the primary control effect that white fungi may have in the Ce enrichment of soil solutions, which appears to be associated with the dissolution and/or direct transport of Ce-enriched MnO2 particles accumulated on the surface of the old litter due to the metabolic functioning of these microorganisms. Similar MREEs and HREEs enrichments were also found in the leachates and the soil solutions, probably due to the higher affinity of these elements for the organic acids, which represent the primary products of the organic matter degradation.

7.1 Introduction

Nutrient cycling is key to forest ecosystem sustainability and productivity, especially in sites characterized by low fertility or degraded soils. There are three types of nutrient cycles, which relate to geochemical, biochemical or biogeochemical processes (Morris, 2004). The geochemical cycle encompasses all processes inherent to the introduction or removal of nutrients – excluding any kind of biological activity (e.g., input from aerosols, leaching of nutrients from rocks and their removal from the system through runoff). The biochemical cycle refers to processes involved in the transport and retention of nutrients inside the trees (such as the withdrawal of specific nutrients from leaves before senescence). The biogeochemical cycle encompasses the processes that occur outside of the trees and lead to the degradation of the organic waste material (such as exudates of leaves and stems, dead leaves and branches or even a whole tree) into its primary components and therefore to the release of nutrients in a form that is reusable by trees (Morris, 2004). Organic matter degradation, which represents part of the biogeochemical cycle, is a major contributor to the nutrient stock available to trees in forest ecosystems (Staaf, 1980; Guo and Sims, 1999; Chadwick *et al*., 1999; J.M. Pacyna, 2008; M. P. Krishna and M. Mohan, 2017) and in this context, litter degradation is known to play a key role in the replenishment of the nutritional pools of forests (Tagliavini *et al*, 2007). Nutrient release from litter is possibly regulated by various biotic and abiotic factors. Temperature, abundance of precipitation, species of decomposers (including the microfauna and microorganism communities), litter composition and chemical structure of its components are all factors that regulate the degradation rate and therefore the recirculation of the elements in a forest (Krishna and Mohan, 2017).

Trees absorb many nutrients to supply metabolic demands for growth, the immune system and reproduction but at the same time unnecessary elements, such as toxic metals, can also be absorbed and "trapped" in specific tree's compartments (Gomez *et al*., 2018). Indeed, once absorbed, the elements are distributed within different tissues depending on their metabolic role or on their affinities with various compounds (Shan *et al*., 2003; Ding *et al*., 2005; Brioschi *et al*, 2013; Page and Feller, 2015; Ming Yuan *et al*., 2017). This distribution could play a key role in processes involved in element turnovers in forest ecosystems especially during litter degradation, which potentially leads to a preferential release into the environment of some elements rather than others, depending on the substances to which they are bound. Litter degradation, indeed, would preferably promote the release of elements from more labile fractions making them available for tree uptake during the first stages of the degradation (Swift *et al*., 1979), while pools of elements that

are trapped inside the most refractory tissues would remain unavailable for longer time spans.

The study of the biogeochemical processes involved in the distribution of the different classes of elements (toxic and nutrients) among the various leaf's tissues during the growth period, and their fractionation during the degradation of the litter is of crucial importance for a better understanding (and forecast) of the dynamics of the aforementioned classes of elements in forest ecosystems. To investigate such processes, REEs are interesting candidates due to their recognized use as tracers of geochemical processes, existing knowledge of their partitioning in plant tissues and recent studies related to their ecotoxicology as emerging pollutants (Liang *et al*. 2008; Li *et al*., 2013; Kyung Taek Rim *et al*., 2013). Indeed, knowledge of the processes involved in REEs dynamics during litter degradation is of importance to environmental and social matters due to the increase in their environmental concentrations linked to their extraction in mining areas and exploitation in modern technologies. Despite the large number of REEs studies on plant tissues (e.g. Fu *et al*., 1998; Wyttenbach *et al*., 1998; Wei *et al*., 2001; Han *et al*., 2005; Ding *et al*., 2005; Brioschi *et al*., 2013; Censi *et al*., 2014; Zaharescu *et al*., 2017), their dynamics during litter degradation is still scarcely known, since research has mainly focused on changes in the concentrations of elements according to the total mass loss of litter material during the duration of the experiment (Tyler, 2004; Brun *et al*., 2008; Gautam *et al*., 2020). To the best of our knowledge, no studies regarding the processes involved in the regulation of such dynamics have been carried out. Our aim is to elucidate which processes may control the release and retention of REEs in relation to major cations and other trace elements during the wet litter degradation – with a secondary focus on the qualitative impact of litter degradation on the REEs patterns of soil solutions. We believe that REEs environmental behaviour and its capacity to accurately trace biogeochemical processes add value to our understanding of nutrient cycles and in particular, could more precisely inform us about the processes that control the litter degradation stages and the release of nutrients in forest ecosystems. Since the different leaf tissues (across which leaves distribute the uptaken elements during the living period) exhibit distinct resistance to degradation, we hypothesize that during litter decay the combination of such a distribution process with the different levels of degradation resistance of the tissues will lead to distinct turnover rates among the elements. Consequently, this leads to a specific chemical release into the environment depending on the degradation stage of litter and the different tissues among which the elements are distributed. To test our hypothesis, we designed a field experiment in the

forested Weierbach Experimental Catchment (Hissler *et al*., 2021), relying on a series of biogeochemical tracers – including concentrations of Na, Mg, K, Ca, Mn, Fe, Pb, Al and REEs measured in fresh leaves and different litter fractions of Douglas-fir (*Pseudotsuga menziesii)* and European beech (*Fagus Sylvatica* L.) grown on the same soil. Moreover, we carried out leaching experiments on these samples with ultrapure water (MilliQ) in order to observe how the different fractions of litter can contribute to element release and sequestration and how this release may affect soil solution chemistry. Finally, we compared the leaching experiment results to the chemical composition of soil solutions collected from the two tree stands. If our hypothesis is confirmed, we expect the older litter fractions to show an enrichment in specific elements, which would be linked to their distribution in the most refractory tissues, limiting their release into the environment during the degradation. Subsequently, we expect that the solutions obtained through the leaching experiment (hereafter called “leachates”) will exhibit different chemical signatures according to the degree of degradation of the samples. On the contrary, if different litter fractions showed similar chemical compositions and similar chemical release during the leaching experiment, it would imply that the distribution of the elements among the tissues is coherent and, therefore, the degradation stage of the litter does not affect the chemical release during the litter decay.

7.2 Materials and methods

7.2.1 Study site

We selected two experimental plots in the Weierbach Experimental Catchment located in the Luxembourg Ardennes Massif, which have been monitored for ecohydrological purposes since 2012 (Hissler *et al.*, 2021). The “Be” profile (BeP) shows a deciduous cover of European beech (*Fagus sylvatica L.*), while the “Do” profile (DoP) is covered with Douglas-fir (*Pseudotsuga menziesii*). The altitude ranges from 450 to 500 m a.s.l. and the geological substratum consists of Devonian metamorphic slates covered by 70 to 100 cm of Pleistocene Periglacial Slope Deposit (PPSD) composed of past loamy aeolian deposition (Moragues-Quiroga *et al.*, 2017). The soil, which is developing below a Hemimoder type of humus (Jabiol *et al*., 2013) in the first 50 cm of the PPSD, presents homogenous properties all over the catchment. It is at an early formation stage and classified as dystric cambisol according to the World Reference Base for soil resources (Juilleret *et al*, 2016).

7.2.2 Sampling and preparation

The different plant materials (i.e. fresh leaves and needles, as well as new and old litter) were collected on the same sampling day in May 2019 at both beech and Douglas-fir stands. Fresh leaves (beech) and needles (Douglas-fir) (hereafter referred to as FL) were collected from 10 adult trees randomly selected per plot. The leaves were taken from different branches, accessible from the ground, at various heights and radial directions. All leaves were aggregated together in one sample per plot and stored in clean polypropylene bags. The litter material was collected from five different locations within an area of 500 m^2 of each experimental plot using a 25x25cm metallic frame and avoiding contamination by soil particles. During the collection, the different fractions of litter were sorted according to their degradation degree (Fig. 7.1) and stored in polypropylene bags.

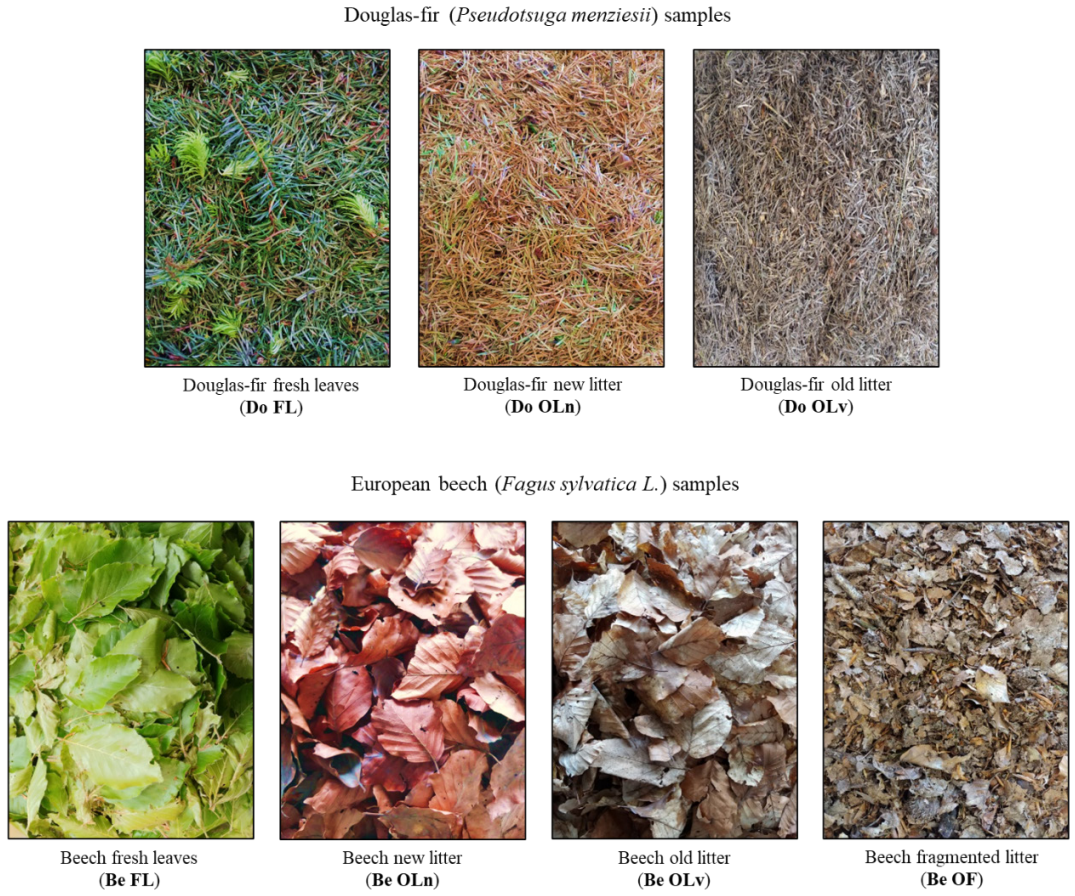

Figure 7.1: Fresh leaves and litter of European beech and Douglas-fir collected in the Weierbach Experimental Catchment and sorted by degradation degree.

In BeP, three litter fractions were identified: the new litter (OLn - unprocessed, unfragmented, light-brownish coloured), the old litter (OLv - slightly altered, bleached and softened, discoloured or dark-brownish coloured) and the fragmented litter (OF - partially decomposed and fragmented, grey-black coloured). For DoP only two fractions stood out: the new litter (OLn - unprocessed, unfragmented, light-brownish coloured) and the old litter (OLv - slightly altered, bleached and softened, grey-black coloured), whereas the fragmented litter layer was not sufficiently developed and was not considered in this study.

The atmospheric dust was collected in the Weierbach Experimental Catchment using a modified polypropylene version of the passive SIGMA-2 collectors produced by the German Meteorological Service in Freiburg, Germany (VDI 3787, 2010) installed at 1.5m above the ground. The SIGMA-2 passive sampler allows the sampling of atmospheric particles above 2.5 µm size (Grobéty *et al*., 2010). The atmospheric dust represents an integrated sample exposed to the atmospheric deposition from September 2018 to May 2019. The particles were collected and stored in an acid-cleaned Teflon vessel during the whole exposure period and stored in a clean desiccator in the laboratory until its preparation before the analysis. After precise weighing of the atmospheric dust collected (2.3 mg), the sample was totally digested using concentrate ultrapure HNO_3, HF and $HClO_4$ acid mixture. The acids were then evaporated, and the residue was dissolved in a solution of HNO_3 (1% in volume) and stored at 4°C before the analysis.

Fresh leaves and litter materials were cleaned with a strong air flux and with a brush avoiding the use of water in order not to disturb the chemical signature and the biotic communities existing on the samples' surfaces. The samples were then dried in the oven at 40 °C and homogenized. Two aliquots were taken to perform the total chemical composition and the leaching experiment. The leaves and litter aliquots for the total chemical composition were preliminarily reduced to a fine powder and incinerated in closed ceramic cups at 550 °C before mineralization in order to destroy organic matter and to pre-concentrate the trace elements. We opted for a more convenient digestion protocol for the organic-derived samples by using Aqua Regia in a microwave-assisted oven (Anton Paar Multiwave PRO), which allows using higher amount of sample (250mg) and reaching high temperature (212°C) and pressure (25bars) conditions. Although Aqua Regia is not a total digestion method, among the different method tested, it delivered the best results without any precipitates nor suspended particles in the digestates not only at the moment of the digestion but also long time after. The samples were then stored at 4°C before the analysis.

For the leaching experiment, 2L high-density polyethylene bottles were filled with the aliquots of leaves and litter fractions. 1L of ultrapure water was then added. There were two reasons for putting as much material as possible into the bottles: first, part of the samples had to be above the water level in order to enhance the aerobic degradation; and second, we wanted to be sure that the release of elements during the experiment period was abundant enough to be detectable with the instrumentations. The bottles were left with the cup partially open in order to allow gas exchanges to encourage bacterial and fungi activity. Samples were agitated for 1 hour/day for 7 days in an automatic vertical agitator (GFL type 3040) set at minimum speed to enhance the leaching process from all samples while avoiding further fragmentation. After one week, the leachates were separated from the solid material with a nylon sieve, filtered at 0.2 µm and acidified using HNO_3 (1% in volume). 50 ml aliquot from each leachate was evaporated in Savillex PFA vessels placed on a hot plate allowing the precipitation of the content. The residue was then sequentially mineralized with HF, HCl and HNO_3. After evaporation, the residue was then dissolved in HNO_3 (1% in volume) and samples were stored at 4°C before the analysis. All the chemicals used for the different digestion procedures were of ultrapure quality. Aliquots were also taken for DOC and pH measurement.

Thanks to the bi-weekly monitoring in place at the Weierbach catchment since 2009 (Hissler *et al*., 2021), we can rely on the chemical composition of soil solutions collected between 2012 and 2014 at the two sampling locations at 20, 40 and 60 cm depths. The sampling was performed using Teflon/quartz suction cups (SDEC, Reignac-sur-Indre, France) connected to acid-clean 2L-Nalgene flasks under a vacuum of 0.8 bar.

7.2.3 Sample analysis

The concentrations of major cations and trace elements in all samples were analysed via Inductively Coupled Plasma - Mass Spectrometry (Agilent 7900). The measured isotopes were chosen with no isobaric interferences, and the polyatomic interferences were minimized by using the collision cell in Helium mode. Calibration standards and Quality Controls (QCs) were prepared with certified solutions (Chem-lab, Belgium and Merck, Belgium). QCs at low, medium and high levels of concentration of the calibration range were analysed each after ten samples to control the validity of the measurements. Internal standards were prepared with Chem-lab (Belgium) Rhenium and Rhodium certified solutions. To ensure the quality of the mineralization procedure, mineralization blanks were prepared following the same steps as for the samples and analysed. The limit of

quantification (LoQ) for the different analyzed elements are reported in Table A7.1. DOC was measured via a Teledyne Tekmar® Torch Combustion Analyser and pH with SenTix® 940 WTW.

7.2.4 REEs normalization and anomaly calculations

All data presented in the following sections were normalized to the local atmospheric deposition (Table A7.2). This allowed us to compare our samples to a local reference for REEs. As atmospheric dust is an important input of cations and nutrients (Reynolds *et al*., 2006; Lequy *et al*., 2012) we also expected it to be important in terms of REEs input in forest ecosystems. Moreover, with this normalization, we could directly differentiate the vegetation contribution to the REEs patterns observed for the litter samples.

Gadolinium (Gd), Europium (Eu) and Cerium (Ce) anomalies were calculated from equations 1 to 3, respectively:

$$Gd/Gd^* = Gd_N/(0.33 \times Sm_N + 0.67 \times Tb_N) \quad \text{(Eq. 7.1)}$$

$$Eu/Eu^* = Eu_N/(0.5 \times Gd_N + 0.5 \times Sm_N) \quad \text{(Eq. 7.2)}$$

$$Ce/Ce^* = Ce_N/(0.5 \times La_N + 0.5 \times Pr_N) \quad \text{(Eq. 7.3)}$$

with La_N, Ce_N, Pr_N, Sm_N, Eu_N, Gd_N and Tb_N indicating the REEs normalized concentrations.

7.3 Results

7.3.1 Chemical composition of atmospheric dust and leaf material

REEs concentrations in atmospheric dust, fresh leaves and litter fractions are reported are reported in Table A7.2. When normalized to the local atmospheric deposition (hereafter referred to as “dust”), the REEs patterns of bulk fresh leaves and litter material show some similarities between the two tree species. The REEs concentrations increase with the age of the litter, with the lowest concentration in fresh leaves and the highest in the most degraded litter layers (Fig. 7.2a-b and Table A7.2).

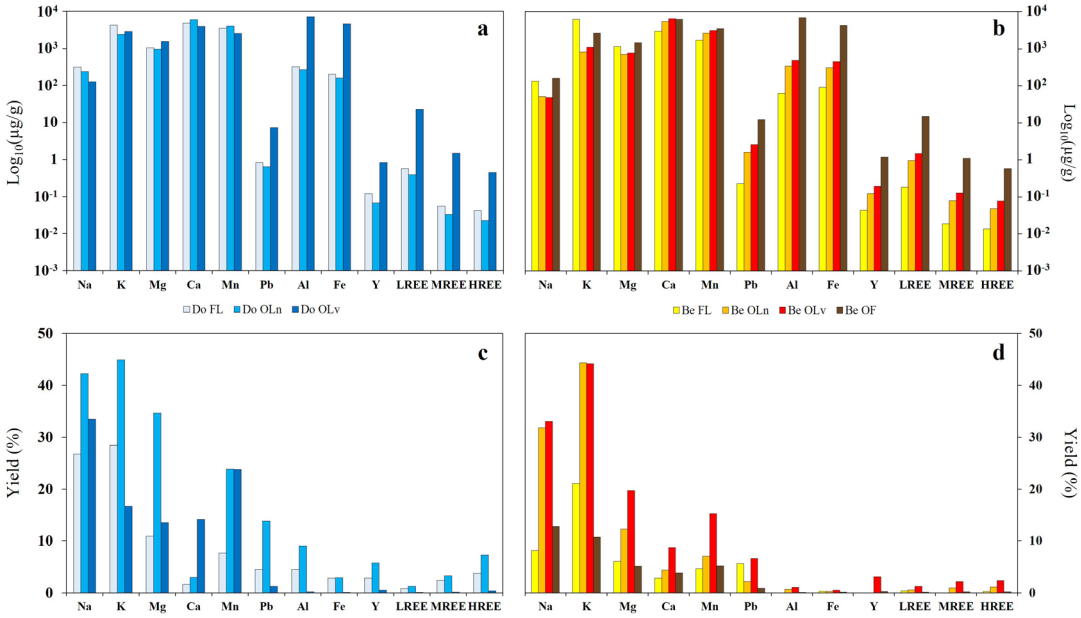

Figure 7.2: Log_{10} of the concentrations of the studied elements in fresh leaves and different litter fractions of (a) Douglas-fir and (b) European beech and elements yields (% of the total mass) for the leaching experiment of (a) Douglas-fir and (b) European beech fresh leaves and litter samples.

Additionally, both tree species present a depletion in HREEs according to LREEs and MREEs (Fig. 7.3a-b). Y appears to behave coherently for both tree species during the litter degradation, as illustrated by the evolution of the Y/Ho ratios. Indeed, the samples show a Y enrichment according to the dust (Y/Ho = 25.93) that is higher in the fresh leaves with Y/Ho ratios equal to 34.34 and 34.3 for Do FL and Be FL respectively, and decreases progressively with the age of the litter showing the lowest values in the oldest litter fractions (23.58 and 25.43 in Do OLv and Be OF, respectively).

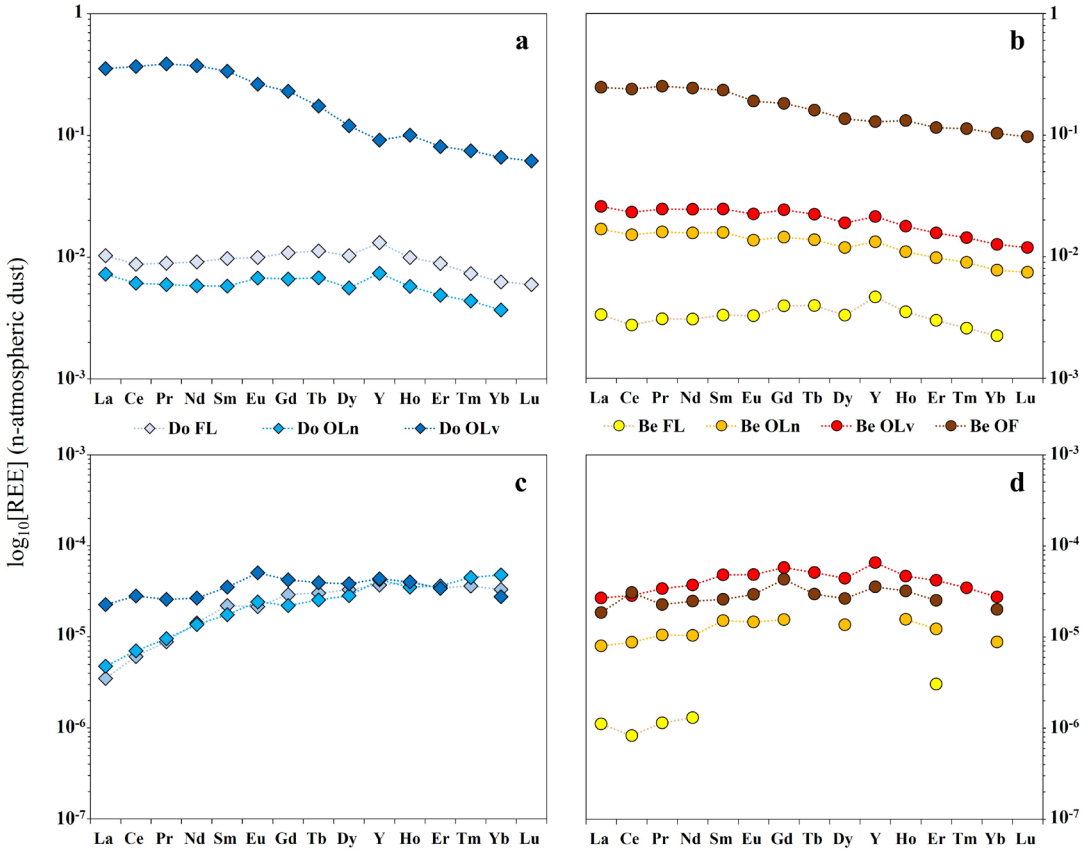

Figure 7.3: REEs concentration patterns in samples of fresh leaves and litter of Douglas-fir (**a**) and beech (**b**); REEs concentration patterns in leachates of fresh leaves and litter of Douglas-fir (**c**) and beech (**d**). Concentrations were normalized by the values in the local atmospheric dust.

In the bulk material, the REEs concentration and the LREEs enrichment also increase in line with the litter degradation stages but with differences between the Douglas-fir and the European beech. For the Douglas-fir samples, the REEs total concentrations decrease from the fresh material to the Do OLn litter layer before drastically increasing at the Do OLv sample. The total REEs concentrations are 0.78, 0.51 and 25.25 µg g^{-1} in Do FL, Do OLn and Do OLv, respectively. Here, the fractionations between the REEs groups are not visible between the fresh leaves and the Do OLn litter layer. However, the fractionation between LREEs, MREEs and HREEs in Do OLv are the highest for all the samples considered in this study, having La_N/Yb_N and La_N/Gd_N and Gd_N/Yb_N ratios of 5.35 and 1.53 and 3.5, respectively. For the European beech, the REEs total concentration in the fresh leaves is the lowest for all leaves and litter samples (Fig. 7.3b) and increases

progressively at each degradation stage to reach its maximum value of 17.7 µg g^{-1} for the Be OF litter layer. The LREEs enrichment increases during the degradation as illustrated by the La_N/Yb_N ratios, which progressively evolve from 1.49 in the fresh leaves to 2.40 in the Be OF. The degradation of the beech litter also leads to an MREEs enrichment as shown by the La_N/Gd_N ratio evolving from 0.84 in Be FL to 1.16 in Be OLn and finally 1.36 in the Be OF.

Major elements and metals can be sorted into three different groups according to the evolution of their concentrations in the bulk samples of the different litter layers (Fig. 7.2a-b). This classification stays coherent for the two tree species. Na, K and Mg have their highest concentrations in the fresh leaves and the older litter layers. Ca and Mn present a progressive increase of their concentration for the European beech, whereas they are less concentrated in the oldest litter layer of Douglas-fir in comparison to Do FL and Do OLn. The concentrations of the other trivalent metals (Fe, Al) evolve similarly to the REEs with a progressive increase from the fresh leaves to the OL litters and an enrichment in the oldest litter layer for both species (Do OLV and Be OF). In contrast to the European beech, Douglas-fir fresh leaves present metals concentrations as high as in the Do OLn litter sample.

7.3.2 Chemical composition, pH and DOC content of leachates

The leaching experiment led to similar REEs concentration ranges between the two tree species, except for the beech fresh leaves, which are one order of magnitude less concentrated (Table A7.3). The leachate patterns present strong differences to the REEs characteristics of the bulk leaves and litter material and in between the two tree species.

The total REEs concentrations of the Douglas-fir leachates are similar in Do FL and Do OLn samples and higher in the leachate of the Do OLv sample. As the HREEs show very similar concentrations in the three leachates, the difference is mainly related to the concentration of LREEs, as shown by the dust-normalized REEs patterns (Fig. 7.3-c). Indeed, LREEs are similarly depleted in the leachates of the two younger samples, showing La_N/Yb_N ratios of 0.10, while Do OLv presents a La_N/Yb_N ratio equal to 0.82. Noticeable are the Eu positive anomalies (Eu/Eu*) of 1.23 and 1.31 observed in the leachates of Do OLn and Do OLv, respectively. In Do OLv a slight positive Ce anomaly (Ce/Ce*) of 1.16 is also observed. The REEs concentrations in the leachates of beech samples increase from the fresh leaves to the highest stages of litter degradation but are higher for the Be OLv material. The dust-

normalized REEs patterns of beech leachates have an MREEs enrichment in comparison to LREEs and HREEs where Gd shows the highest peak.

The patterns of Be OLn and Be OLv leachates present very similar characteristics as indicated by their La_N/Gd_N ratios (0.46 and 0.43, respectively), Gd_N/Yb_N ratios (2.10 and 2.14, respectively) and the absence of any anomaly, whereas the Be OF leachate presents Ce and Gd positive anomalies (Ce/Ce* = 1.49 and Gd/Gd* = 1.52). In contrast, the leachate of the fresh beech leaves presents a Ce negative anomaly (Ce/Ce* = 0.74).

Similar trends in the percentage of elements leached from the material of both tree species were observed. The percentage of leaching of the studied elements can be classified according to their valence Na, K > Mg, Mn > Ca, Pb > Al, Fe, REEs, with the trivalent elements being less leached. However, some differences can be highlighted between Douglas-fir and beech.

The Douglas-fir material released a higher quantity of Na, Mg, Mn, Pb, Al, Fe, MREEs and HREEs compared to the beech. Major elements and Mn are preferentially released compared to trivalent metals and Pb, as shown in Figure 7.2c. The highest percentage of element release is observed from the Do OLn sample with Mn having similar values in Do OLn-L and Do OLv-L. An exception is made for Ca, which presents similar release percentages as those of the trivalent metals during the first stages of degradation and which shows the highest release from the Do OLv fraction.

In beech leachates, the elements show similar release trends as for Douglas-fir but the highest percentages of release for all elements are shown in Be OLv (Figure 7.2d) with Na and K having analogous values in Be OLn. In Be FL and Be OLn leachates, all the elements show lower release values than in Douglas-fir samples. Trivalent metals and Pb, similarly to those of Douglas-fir, show a low release from the solid material during the experiment (in the case of Al, the release from fresh leaves is below the limit of quantification, as well as for many REEs as shown in Table A7.3).

The Y/Ho ratios of the leachates of Douglas-fir litter can explain the appearance of a small Y depletion in the oldest litter sample. The leachate of Do OLn, which represents the stage of degradation that brings about the formation of the OLv fraction, indeed shows a Y/Ho ratio equal to 31.29 indicating a preferential release of Y (when compared to the neighbour) that leads to a lower-than-atmospheric dust value in the Do OLv sample (Y/Ho = 23.58 in Do OLv and Y/Ho = 25.93 in atmospheric dust).

In beech samples, we can observe a similar behaviour with values that are slightly higher. The Y/Ho ratio in the Be OLv leachate (Y/Ho = 36.59) justifies the absence of Y enrichment in the Be OF fraction, which instead shows a dust-like ratio (Y/Ho = 25.43).

The highest DOC concentrations (Table A7.3) were measured in the Douglas-fir leachates with values ranging from 89.42 mg L^{-1} in Do OLv to 252.83 mg L^{-1} in Do OLn, while beech leachates showed concentrations from 50.87 mg L^{-1} in Be OLn to 126.4 mg L^{-1} in Be OLv. Note that for both species, the highest DOC concentrations were measured in leachates of the second-to-last degradation stages with a decrease in the oldest fractions. The pH is inversely proportional to the DOC concentrations (Table A7.3). Indeed, for the Douglas-fir leachates, the most acidic pH was found in Do OLn, which showed a pH = 4.05, while the pH of Do OLv was the highest with a value equal to 5.02. In beech leachates, the lowest pH was measured in Be OLv (pH = 4.61) and the highest in Be OLn (pH = 5.97).

7.3.3 Average REEs in soil solutions

The average REEs concentrations in soil solutions collected between 2012 and 2014 are reported in Table A7.4. The REEs total concentrations differed by one order of magnitude and were lower under the Douglas-fir stand at 20 and 40 cm depth (∑REEs = 0.88 µg L^{-1} and 0.92 µg L^{-1} in Do SS20 and Do SS40, respectively), whereas the highest concentration was observed in beech samples at 40 cm depth (∑REEs = 6.70 µg L^{-1} in Be SS40).

Dust-normalized REEs patterns show an MREEs enrichment for all soil solutions and Ce positive anomalies at 20 and 40 cm depth (Fig. 7.4).

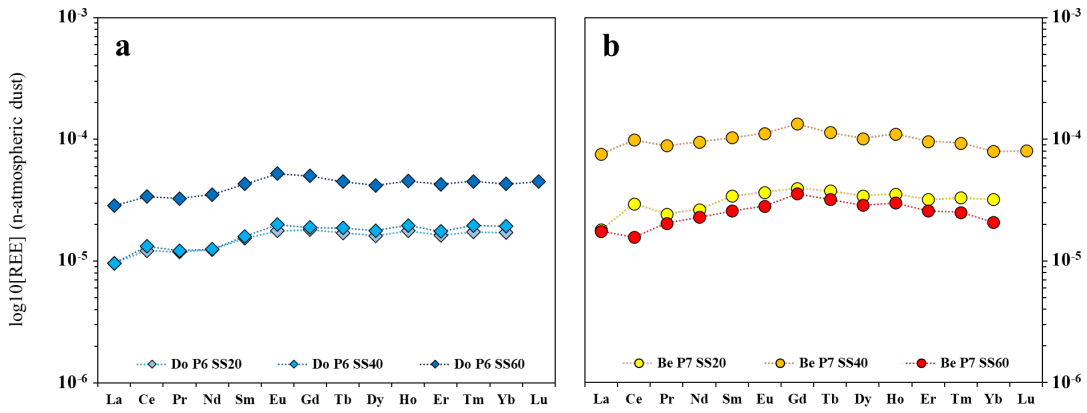

Figure 7.4 Patterns of the average REEs concentrations in soil solutions of DoP (**a**) and BeP (**b**). Concentrations have been normalized by the values in the local atmospheric dust.

Among the MREEs, Eu shows a peak in the soil solutions under the Douglas-fir, whereas Gd is more enriched in beech soil solutions. Do SS at 20 and 40 cm depth exhibit positive Ce anomalies (Ce/Ce* = 1.14 and 1.21, respectively) that disappear at 60 cm. Moreover, Douglas-fir samples also show an LREEs depletion as indicated by the La_N/Yb_N ratios, which range from 0.50 to 0.66 in Do SS40 and Do SS60, respectively.

Under the beech, the Ce positive anomaly is higher at 20 cm and decreases with depth until it becomes negative in soil solutions at 60 cm depth (Ce/Ce* = 1.39, 1.20 and 0.82 in Be SS20, Be SS40 and Be SS60, respectively), whereas the LREEs show a consistent depletion at 20 cm depth (La_N/Yb_N = 0.56) and a slight one at 60 cm depth (La_N/Yb_N = 0.85).

7.4 Discussion

7.4.1 REEs fractionation during litter degradation

The leaching yields clearly illustrate that during the leaching experiment, REEs are preferentially leached following the HREEs>MREEs>LREEs order (Fig. 7.2c-d). This justifies the decreasing trends (from La to Lu) observed in the REEs patterns of litter fractions for both tree species and demonstrates the tendency of the litter to retain LREEs rather than the other elements of the lanthanide series. This progressive LREEs enrichment in the litter (Fig. 7.3a-b) proceeding towards degradation is more evident for the Douglas-fir samples as suggested by the La_N/Yb_N ratios in the Do OLv and Be OF samples (La_N/Yb_N=5.35 and La_N/Yb_N=2.40, respectively). The leaching experiment also showed that REE, together with the other trivalent metals (Fe and Al) and Pb, are preferentially held inside the solid material, while the other major elements and Mn are more easily released during litter degradation. This behaviour suggests a preferential fractionation of the studied nutrients (Na, K, Mg and Mn) into more labile tissues, probably due to their role in the metabolic functioning of the tissues of living leaves (Alejandro *et al.*, 2020; Sardans and Peñuelas, 2021; Shaul, 2002; Maathuis, 2013). This partitioning results in a concentration decrease of these elements during litter degradation, while Fe, Al, Pb and REEs tend to remain embedded inside the most refractory tissues - increasing their concentration over time in the remnant litter material. In our experiment, all elements behave coherently according to their oxidation number (Fig. 7.2c-d). Monovalent elements (Na, K) are more likely to be released than the divalent elements (Mg, Mn), while trivalent metals (Al, Fe, REEs) tend to stay more tightly bound to the solid residual fraction. Exceptions can be seen for Ca in the Douglas-fir samples and for Pb in the oldest litter fractions of both tree species.

Given that REEs are preferentially retained in the recalcitrant tissues together with the other trivalent metals and Pb, the higher yields for these elements obtained from Douglas-fir samples during the leaching experiment might suggest a faster degradation process for the Douglas-fir litter when compared to the beech litter. The fact that LREEs are preferentially retained in the litter of both tree species can be explained by referring to existing literature and by normalising the REEs concentrations in the leachates to the ones of the respective litter material (Fig. 7.5).

The patterns of REEs in Douglas-fir samples show an HREEs enrichment when compared to the other elements of the series ($0.05 \leq La_N/Yb_N \leq 0.15$ and $0.25 \leq Gd_N/Yb_N \leq 0.51$), indicating a preferential release of the heavy REEs to the solution. In the European beech samples, the patterns are smoother between MREEs and HREEs ($0.94 \leq Gd_N/Yb_N \leq 1.21$), while they conserve the depletion in LREEs when compared to the other groups ($0.32 \leq La_N/Gd_N \leq 0.44$ and $0.38 \leq La_N/Yb_N \leq 0.48$). In general, these patterns show a progressive increase from La to Lu that mirrors the trend of the stability constants of REEs complexes with malate, EDTA, humic and fulvic acids (Suzuki *et al.*, 1980; Pourret *et al.*, 2007; Marsac *et al.*, 2010; Sonke and Salters, 2005).

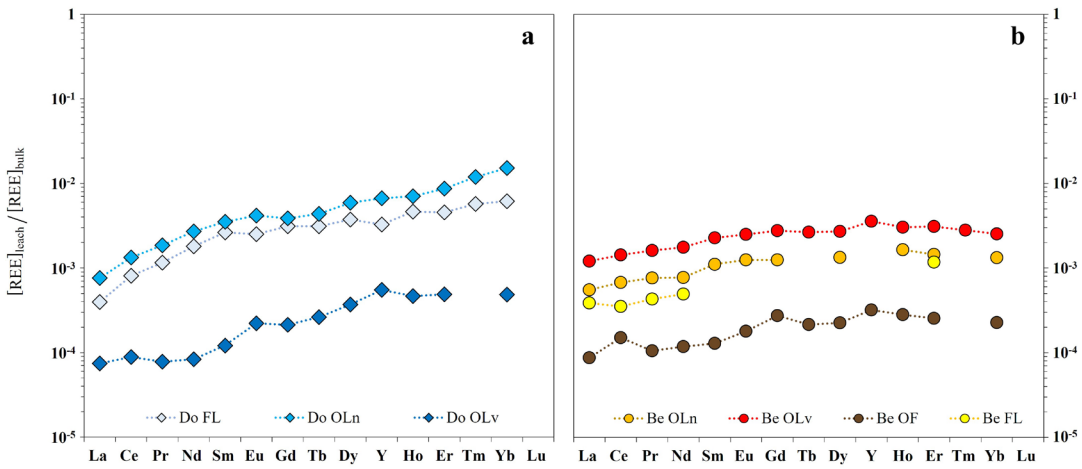

Figure 7.5: Patterns of the REEs in leachates normalized to the REEs concentrations in leaves and litter for Douglas-fir (**a**) and Beech (**b**) samples.

Humic acids, fulvic acids and malic acid are indeed primary products of organic matter degradation (Adeleke *et al.*, 2017 and reference therein) and they have been reported to have metal chelating properties. The increasing release of REEs from La to Lu in our leachates is likely due to an increase in the specific affinity - proceeding along the lanthanide series - of these elements towards the degradation products present in the aqueous solution

(Schijf and Zoll, 2011). This suggests that the nephelauxetic effect (Juranic, 1988; Tchougréeff and Dronskowski, 2009) plays a key role in the mechanism of REEs complexation with the dissolved organic ligands during the wet degradation of litter and is in line with the results shown by Sonke and Salters (2006), which experimentally demonstrated that the lanthanide contraction is responsible for a gradual increase in the complexation strength with humic substances when decreasing the ionic radius. The bond strength, indeed, increases with increasing ionic potential Z/r.

Differences in the atmospheric dust-normalized REEs patterns of leachates between the two tree species can be explained by the nature of the ligands present in the solutions. Tang and Johannesson (2010) showed that the REEs complexation with organic ligands in natural waters would produce patterns enriched in HREEs when the majority of the ligands in solutions are represented by low molecular weight-dissolved organic compounds (such for instance citric, oxalic, malic, succinic, malonic and maleic acids) while a preponderant presence of heavy molecular weight-dissolved organic compounds (such as humic acid and fulvic acids) would produce an enrichment in MREEs. Therefore, the results obtained indicate that the differences between the patterns of Douglas-fir and European beech leachates are likely due to the production of different classes of organic acids during the degradation of the samples.

Al, Fe, Pb and REEs behaviours are coherent during litter degradation for both tree species, as their concentrations progressively increase towards the oldest litter fractions (Table 7.3 and Fig. 7.2a-b). We can explain such an accumulation in the oldest litter fractions by the binding with lignins. Lignins constitute the most degradation-resistant compounds in leaves. Their resilience lets these metals persist longer in the organic material than carbohydrates, lipids, proteins, hemicellulose and cellulose, which can degrade at a faster rate (Rahman *et al*., 2013). Lignins are a class of organic polymers that have many functions in vascular plants. They provide structural support, improve cellular adhesion, enhance water transport and defence towards pathogens and are mainly situated in the cell walls of vascular and support tissues (Weng and Chapple, 2010; Leisola *et al.,* 2012; Labeeuw *et al.,* 2015). Moreover, the chemical structure of these molecules exerts a strong control on litter decay rates (Talbot *et al*., 2012). Increased lignin concentrations inhibit biological activity and linearly increase photo-degradation due to its wide spectrum of absorbance (Austin and Ballaré, 2010; Cogulet *et al*., 2016).

While Fe, Al and Pb toxicity in plants is well-known (Imadi *et al*., 2016; Bienfait, 1989; Woolhouse, 1983, Rout *et al*., 2001; Sharma and Dubey, 2005; Pourrut *et al*., 2011;

Singh *et al*., 2017; Miroslav Nikolic and Jelena Pavlovic, 2018), the toxicity of REEs is not yet widely studied as their micropollutant nature has only recently emerged (Gwenzi *et al*., 2018). However, the toxicity of REEs in plants is far beyond the scope of this work, we limit ourselves to mentioning that researchers observed REEs displaying redox-related toxicity mechanisms (Hassan Ragab El-Ramady, 2010; Pagano *et al*., 2015; Tommasi *et al*., 2021) and we assume that plants can trap REEs in lignified tissues as a defence to avoid the toxicity-related events with the same mechanism adopted for other potentially toxic metals, such as Pb and Al. Therefore, we propose that lignins constrain the REEs in the oldest litter fractions during the degradation of the leaves. Given the high affinity of such metals for oxygen, the absorption operated by lignins through the binding with the oxygen-bearing functional groups (such as phenolic, hydroxyl) may be the mechanism involved and would explain the accumulation of these metals in the oldest litter fractions. Therefore, during the living cycle of leaves, lignins are able to sequestrate the elements that show higher affinity for the exposed functional groups. As lignins are the most resistant tree components in forests, they would prevent the release of the absorbed elements for longer during the litter degradation. The chemical elements that are more important for tree nutrition and metabolism would then be preferentially released to the soil solutions.

As shown by the evolution of the chemical composition of leaves and litter fractions along the different degradation stages, our hypothesis on the distribution of different elements among the different tissues is confirmed. This finding is further corroborated by the result of the leaching experiment, which clearly confirms our hypothesis that during litter decay, the release of elements is linked to the degradation stage of the litter itself. As conjectured, elements partitioned in the most labile tissues are more easily released during the degradation process than those bound to more refractory tissues, which are instead accumulated over time. According to our findings, two main REEs fractionation processes are specific to a leaf's life-span:

I. An inter-tissue fractionation occurring during the leave's "living period", through which recalcitrant tissues would preferentially absorb REEs as a result of binding with lignins, developing a particular signature;
II. A degradation-driven fractionation, which has the different affinities of REE towards the products of the decay as the main factor for their partitioning between the remaining solid fraction of litter and the resulting solution.

7.4.2 Cerium anomalies in leachates

Another interesting aspect of our results is the presence of positive Ce anomalies in the leachates of the oldest litter fractions (Ce/Ce* = 1.16 and Ce/Ce* = 1.49 in Do OLv and Be OF leachates, respectively) and a slight W-type tetrad effect in the Be OF leachate. The tetrad effect can be defined as a graphical effect that divides the REEs patterns into 4 segments so-called “tetrads” (T1 from La to Nd; T2 from Pm to Gd; T3 from Gd to Ho; T4 from Er to Lu), resulting from the increased stability at a quarter, half, three-quarter and complete filling of the 4f orbital (McLennan, 1994). The tetrad effect is usually classified according to the shape of the patterns into the “W” type and “M” type.

Davranche et al. (2005) demonstrated that the REEs complexation by organic acids inhibits the development of the tetrad effect and of Ce anomalies in the REEs patterns of aqueous solutions. This is because the complexation operated by organic acids is not selective towards any specific lanthanide and therefore also Ce. The REEs complexation with the organic acids can therefore explain the absence of Ce anomalies and of the tetrad effect in the REEs patterns of the leachates of the younger litter fractions (Do FL, Do OLn, Be FL, Be OLn, Be OLv), but it does not justify the positive Ce anomalies found in the patterns of the leachates of the oldest fractions (Do OLv and Be OF) and the W-type tetrad effect observed in the pattern of the Be OF leachate. The presence of both positive Ce anomalies and the tetrad effect can be explained by a biological-driven accumulation of manganese oxides (MnO_2) particles on the surface of the components of the oldest litter layers and their subsequent transport into solution. Keiluweit et al. (2015) demonstrated how litter decomposition is controlled by the manganese redox cycle. The authors explained that, during the first three years of the litter degradation, specific microorganisms (in particular fungi) are able to transform the Mn^{2+} supplied by the decomposing organic material into the more reactive Mn^{3+} form. This latter would be subsequently used by other microorganisms for the degradation of the aromatic compounds (such as lignin and tannins) through redox reactions with the litter components, which would give the Mn back under its reduced Mn^{2+} form. After the first few years, the excess of Mn^{3+} produced by the biological activity precipitates under the form of Mn^{3+} / Mn^{4+} oxides accumulating on the surface of the litter during more advanced stages of degradation (Keiluweit *et al.,* 2015). Unlike organic acids, manganese oxides are capable of a selective adsorption of Ce, along the other REEs, with a mechanism of oxidative scavenging through which Ce is preferentially trapped onto the surface of the above-mentioned oxides (Bau, 1999; Bau and Koschinsky, 2009, Pourret and Davranche, 2013). The Ce enrichment linked to Mn oxides could be the reason for the

formation of positive Ce anomalies in the waters that leached the litter material. We conjecture that after a rainfall event, residual water that is deposited onto the surface of the oldest litter fraction has inherited a specific REEs signature after passing through the younger litter layers above. We can assume that such a signature is similar to that of the leachates of the younger litter fractions recovered during our experiment (with the related MREEs-HREEs enrichment). Once the MnO_2 deposited onto the surface of the old litter interacts with this solution, it would preferentially adsorb Ce with the scavenging mechanism previously mentioned. A question mark here is related to the form (complexed or free ions) of the REEs when they enter in contact with the MnO_2. We assume that their main form during such an interaction occurs mainly as free ions as their complexation with organic acids could inhibit the preferential adsorption of Ce onto MnO_2 as observed by Davranche *et al*. (2005 and 2008). Moreover, they also highlighted a process of REEs-organic acids complexes dissociating with time and with decreasing HA/MnO_2 ratios. The reduced DOC concentrations (Table A7.3) and the presence of the MnO_2 in Do OLv and Be OF would then lead to the dissociation of the OA-REEs complexes and to the re-adsorption of the REEs onto the MnO_2 with a preferential intake of Ce. Note that when compared to the Do OLv leachate, the Be OF leachate shows lower DOC, a higher Ce anomaly and the presence of TE, which may be a direct effect of the decrease of the OA/MnO_2 ratios on the development of these specific REEs features in the solutions during the litter degradation. Interestingly, for both species the leachates of younger litter fractions (Do FL, Do OLn, Be FL, Be OLn and Be OLv) show higher DOC concentrations and lower pH than those of the oldest litter fractions (Do OLv and Be OF), as shown in Table A7.3. This strengthens the assumption that the REE patterns in leachates of fresh leaves and young litter fractions are shaped by the presence of organic acids, which confers the typical increasing trend from La to Lu and the absence of positive Ce/Ce* and of TE (Fig. 7.4). On the contrary, leachates of the oldest litter fractions show higher pH, lower DOC, positive Ce anomalies and TE (in Be OF leachate), indicating that the shapes of the REEs patterns in the leachates of the oldest litter fractions are mainly resulting from the OA-REEs dissociation accompanied by Ce-enriched MnO_2. This would explain both the increasing trend from La to Lu and the development of positive Ce anomalies (with a TE in the Be OF sample) in the leachates of the oldest litter fractions. We propose that the process leading to Ce enrichment in waters that are in contact with the oldest litter fractions occurs in three steps, as reported below (and more accurately in Figure 7.6):

I. Biologically-driven accumulation of MnO_2 particles onto the surface of the old litter components;
II. Dissociation of OA-REEs complexes and subsequent oxidative scavenging of Ce onto the MnO_2 particles' surface in the presence of stationary water in the litter surface during the degradation;
III. Dissolution of Ce-enriched MnO_2 particles and/or their direct transport as MnO_2 nanoparticles into solution operated by incident waters characterized by higher water volume and higher turbulence, which may then "wash" the surface of the oldest litter layers. One or the combination of these two processes would lead to Ce enrichment in the solutions, thus developing a positive anomaly.

One may argue that the yields of Mn during the leaching experiment are higher in the Do OLn and Be OLv leachates where the Ce anomalies do not appear. Here it is important to consider not the overall concentration of Mn in the leachates, but rather the chemical form in which this element is present in the litter layers. We recall, in fact, that the formation of Mn oxides (which lead to the development of Ce enrichment) only occurs during the last stages of the litter decay, in our case Do OLv and Be OF.

For completeness of information, it is worth mentioning two other factors, which may play a role in the development of Ce positive anomalies in solution: the presence of siderophores and Fe oxides. Siderophores are a group of small molecules characterised by a strong affinity towards Fe^{3+} and that are among the strongest iron-chelating agents in nature. Plants (*Poaceae*), fungi and bacteria are able to synthetize and release these compounds to enhance the Fe assimilation in iron-deficiency conditions (Chennappa *et al.*, 2019). Accordingly, one would expect siderophores to be released by the above-mentioned organisms to enhance the Fe assimilation especially during the first stages of the degradation where the Fe concentrations are lower when compared to the oldest fractions.

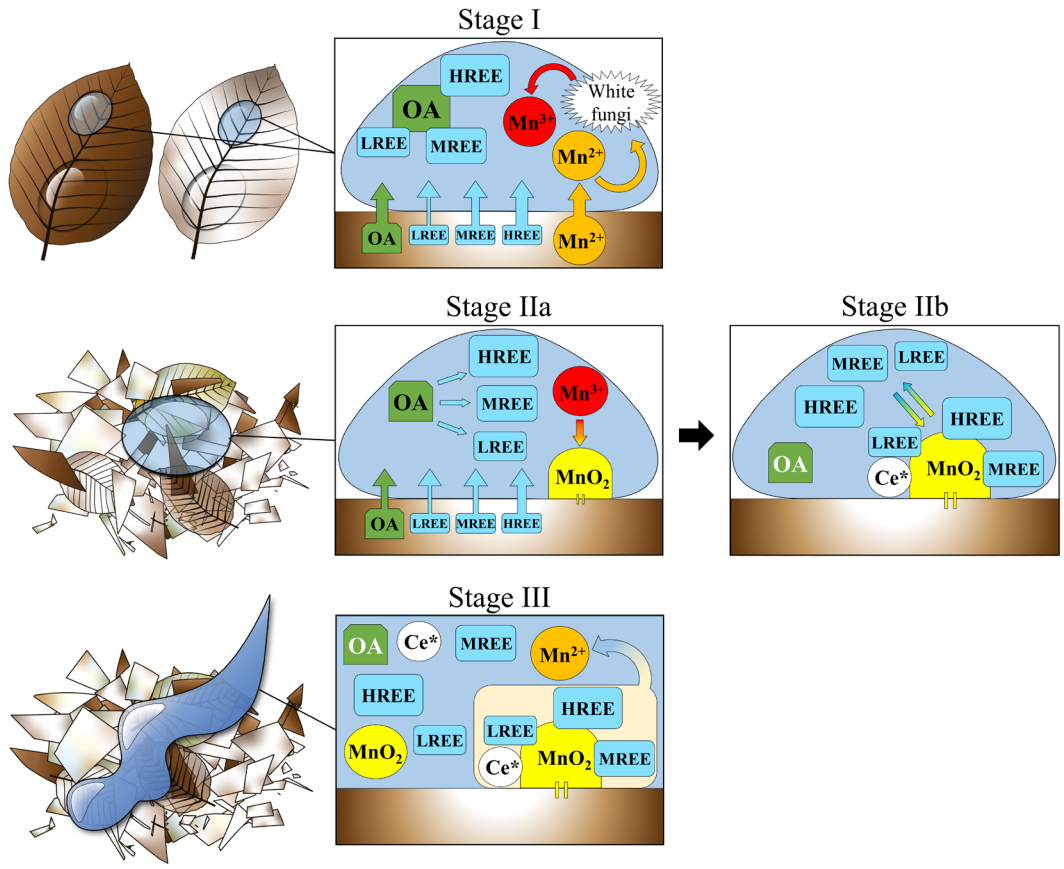

Figure 7.6: Conceptual model representing the main processes treated in this study occurring during the litter degradation.

Stage I Do OLn, Be OLn and Be OLv degradation

- Preferential release of HREEs and MREEs linked to their affinity for organic acids
- REEs complexation with organic acids and subsequent inhibition of Ce anomalies and TE
- Transformation of Mn^{2+} (coming from the litter) into Mn^{3+} operated by white fungi

Stage IIa Do OLv and Be OF degradation

- Preferential release of HREEs and MREEs linked to their affinity for organic acids
- REEs complexation with organic acids and subsequent inhibition of Ce anomalies and TE
- Accumulation and precipitation of Mn^{3+} under the form of Mn oxides
- Decrease in the OA/MnO_2 ratios (due to Increased concentration of MnO_2 and decreased release of organic acids), leads to the REEs-organic acids dissociation

Stage IIb Do OLv and Be OF degradation

- REEs released from the organic acids in **Stage IIa** are re-adsorbed onto the MnO_2 particles on the litter surface
- Scavenging of Ce and its subsequential enrichment on the Mn oxide surface

Stage III Do OLv and Be OF degradation

- Higher volume of water and higher turbulence lead to the dissolution and/or direct transportation of the Ce-enriched Mn oxides particles into solution, which inherits the enrichment in Ce and develops a TE (Be OF)

Therefore, it is precisely in those early stages of decay where one would expect a greater participation of siderophores in the geochemical behaviour of Ce. Kraemer *et al*. (2017) demonstrated that siderophores are able to scavenge Ce by oxidizing it to Ce (IV), forming stable complexes in solution and leading to the development of positive Ce anomalies. Anomalies that are not shown in the leachates of the younger litter fractions where one would expect them according to the iron-deficiency. However, the Ce enrichment occurs only in the leachates of the oldest litter fractions, suggesting that the process acting in these circumstances is timeframe-specific (during specific stages of the degradation) rather than being condition-specific (iron-deficiency). Other important aspects to consider are the much higher concentrations of manganese in the leachates when compared to iron and the different leaching yields that Fe shows between the two tree species (Table A7.3), while Ce anomaly instead shows the same dynamics. Fe oxides have been shown to potentially oxidize Ce(III) to Ce(IV) and scavenge this element from the water column leading to the development of Ce positive anomalies in the oxide fractions as reported by Bau and Koschinsky (2009). Nevertheless, the Mn/Fe ratios in the leachates of our litter samples ($33.6 \leq Mn/Fe \leq 277.4$) are much higher than the ones of the samples treated by the above-mentioned authors ($1.57 \leq Mn/Fe \leq 1.65$), suggesting that Mn might be a better candidate to act in the oxidative scavenging of Ce during the degradation of the litter rather than Fe.

7.4.3 Behaviour of Ca and Eu during litter degradation

Calcium leaching yields are close to or even lower than those of trivalent metals during the first stages of Douglas-fir leaf degradation (Do FL and Do OLn), while its release increases from the oldest litter layer (Do OLv). In European beech samples, the leaching of Ca is not as low as for Douglas-fir samples but is lower than the other divalent elements (Mn and Mg). Calcium is involved in many plant's mechanisms and, among these, the stabilization of the cell wall structure is of vital importance. Indeed, it is an essential component of the calcium pectate, an insoluble molecule that forms polymers in between the cell walls linking them together (Bateman and Basham, 1976; Proseus and Boyer, 2012). The fact that calcium pectate is insoluble and that is positioned in between the cell walls makes this molecule less accessible to microorganisms during the initial stages of the degradation, leading to a reduced release of Ca. The fragmentation of the leaves and the decay of the weakest tissues during the first stages of degradation would therefore facilitate the accessibility of these insoluble components to the biological degradation (Norman, 1929), thus contributing to a higher Ca release from the oldest litter fractions. However, the stabilization of cell walls

cannot explain the increase in Ca concentrations observed in the litter fractions. This latter, on the other hand, can be explained by the Ca-translocation mechanism occurring during the leaf's senescence described by Turpault *et al.* (2021). At high concentrations, Ca is a toxic element for trees and during the senescence is translocated from the other tree organs to the leaves, where it crystalizes under the form of insoluble Ca-bearing biominerals and is released to the litter material during the leaf fall as a form of anti-toxicity mechanism. Calcium accumulation during the leaf's senescence can also explain the development of the slight Eu enrichment found in the Do OLn fraction in comparison to the fresh leaves (Eu/Eu*=1.09 and 0.93 in Do OLn and Do FL respectively). The linkage between Ca and Eu in plants lies on the capability of Eu^{3+} to substitute Ca^{2+} in some physiological mechanisms due to their similar ionic radii. Stille *et al*. (2006) proposed that Eu positive anomalies in leaves can be related to its preferential uptake by plants. They argued that Eu^{3+} can follow the same Ca^{2+} fate in cells cytoplasm, in which Ca concentrations are controlled via oxalate crystals precipitation leading to the accumulation of Eu in leaves and the consequential development of a positive anomaly. In 2003, Gao *et al*. reported a preferential Eu accumulation in cell membranes and its capability to use calcium ion channels to enter inside cells and get absorbed by cytoplasmatic organelles. Ding *et al*. (2005) linked Eu enrichments in roots to the precipitation of Eu-enriched phosphate particles, while Brioschi *et al*. (2013) proposed that the origin of such anomalies in roots should be attributed to Ca-depleted soils where plants may suffer of Ca-deficiency and where Eu-substitution of Ca is responsible for the enrichments especially in soils characterised by high Eu/Ca ratios. In the case of the Weierbach soil, the Eu/Ca ratios in the first 60 cm of soil under the Douglas-fir stand ranged from 0.0005 to 0.0044 (Moragues-Quiroga *et al*., 2017) which, according to Brioschi *et al*. (2013), indicates a Ca depletion. Nonetheless, the slight enrichment in Eu is occurring in the Do OLn fraction and not in the fresh leaves where instead the Eu/Eu* is below 1. Then, it is our opinion that the Eu enrichment in the litter cannot be linked to the Ca-depleted soil as it does not occur during the leaf entire living period. In this study, the Eu enrichment in Do OLn indicates its involvement in Ca-dedicated biochemical pathways, which would lead to an anomalous accumulation of Eu in respect to the other REE in Douglas-fir litter. The fact the Eu/Eu* increases in Do OLn and not in Do FL, suggests that Eu is involved in the same process of Ca translocation that occurs during the leaves' senescence. Moreover, the positive Eu anomalies observed in the Do OLn and Do OLv leachates (Figs. 7.3c and 7.5a) suggest that at least part of the Eu is fractionated into slightly less degradation-resistant compounds - compared to the lignin where the other REEs are supposed to stay bound, or

into biogenic minerals, which are released from the cytoplasm after the cell wall breaks. The presence of these afore-mentioned compounds in the leachates and their subsequent digestion would deliver additional Eu content to the solution, leading to the development of positive anomalies in the leachates of Do OLv and Do OLn fractions. This would be in line with Gao *et al*. (2003), Turpault *et al* (2021) and partially with Stille *et al*. (2006). In fact, if a preferential absorption of Eu by trees had played a role in the development of a positive anomaly in the leaves, we would have observed an enrichment already in the Do FL, in which instead it does not occur.

Although, the reason for calcium behaving differently in the two tree species during the litter degradation cannot be explained with our experiment, it could be due to possible differences in the chemical and/or mechanical structures of the leaves or in the physiology of the tree species.

7.4.4 Rare earth elements as a proxy for litter degradation resistance?

Both tree species show a progressive decrease in the Y/Ho ratios, indicating that during the degradation of the litter material, Y decouples from Ho, as it is preferentially leached. This trend in the Y/Ho ratios is also accompanied by the enrichment in LREE proceeding towards decay in both species, as shown by the La_N/Yb_N ratios. These ratios can be thought of as proxies for classifying resistance to the litter degradation of the two tree species in the Weierbach forest. As illustrated in Figure 7.7, the smaller the slope of the regression line, the lower the resistance. In accordance with this, Douglas-fir samples appear to be less resistant than the European beech ones. This is in line with the higher yields of trivalent metals we observed in the leachates of Douglas-fir samples as they are bound to the most resistant tissues. It is interesting to note that the fresh leaves from both species have a close position in the graph, indicating a similar stage of degradation (none) which changes over time.

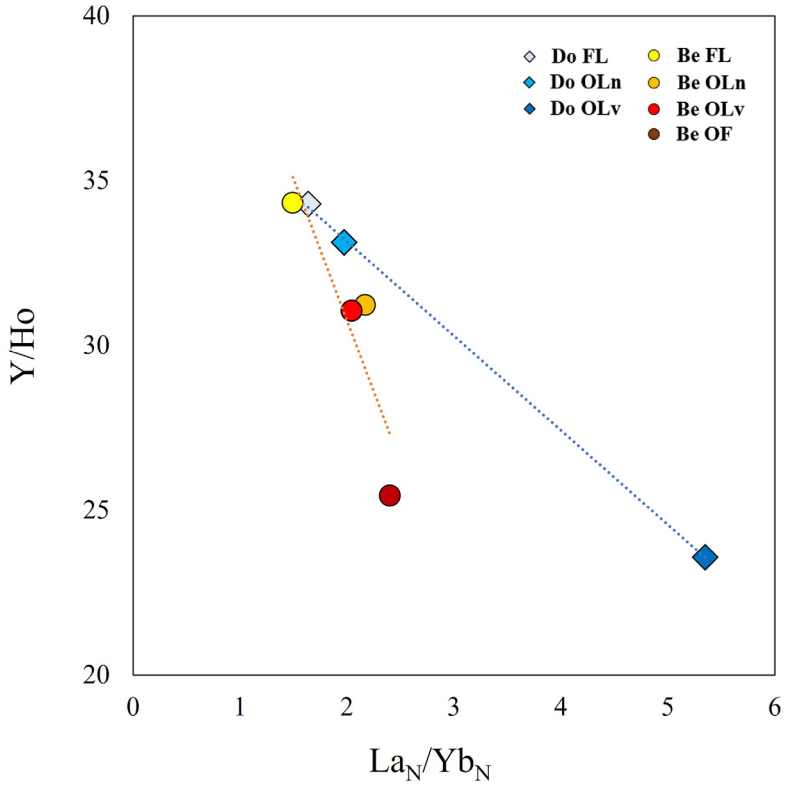

Figure 7.7: Y/Ho vs La_N/Tb_N ratios of fresh leaves and litter samples of Douglas-fir (blue scale) and European beech (red scale).

7.4.5 REEs in soil solutions

The differences in the average soil solution REEs patterns observed between the two experimental sites in the Weierbach catchment seem to be linked to the different REEs release occurring during the degradation of the litter at each plot. Indeed, from a depth close to the litter layers (soil solution at 20 cm depth) to the deepest soil layer (soil solution at 60 cm depth), the evolution of the HREEs enrichment, Ce anomaly and specific MREEs (Gd and/or Eu) enrichments in soil solutions (Fig. 7.4) could be discussed according to similarities with the litter leachates (Fig. 7.3 c-d). It may be expected that if any degrading litter compound can contribute to the soil solution REEs composition, it would be more easily observed close to the surface and would disappear progressively with depth, being diluted by the water-rock interaction processes and changing in redox conditions that control REEs in soils (Braun *et al.,* 1998; Laveuf and Cornu, 2009). Our results are in accordance with this expectation. For instance, particularities in the REEs patterns of these litter leachates

(especially for the last two stages of degradations for both species) seem to be mirrored by their respective soil solutions. Indeed, Eu and Gd enrichments, observed independently in both litter leachates (Do OLv and Be OF), were also found in the related soil solutions (1.08 ≤ Gd/Gd* ≤ 1.21 in Be SS and 1.06 ≤ Eu/Eu* ≤ 1.15 in Do SS). In both profiles, such anomalies are higher at 40 cm and decrease at 60 cm. This is in line with the leachate REEs patterns normalized by the respective bulk litter concentrations reported in Figure 7.5. Indeed, in the patterns of Be OLv and Be OF, Gd is the most enriched, while in patterns of Do OLn and Do OLv Eu leads the MREEs enrichment. This may indicate a preferential release of these two elements to the soil solutions during the natural leaching operated by rainfall and throughfall on Do OLn, Do OLv fractions in the Douglas-fir stand and of Be OLv, Be OF fractions in the beech stand. Moreover, REEs patterns of soil solutions from both profiles show Ce positive anomalies (Ce/Ce* = 1.14 in Do SS20 and Ce/Ce* = 1.39 in Be SS20) that are close to those in the leachates of the oldest litter fractions. The amplitude of these anomalies decreases with the increasing depth until they disappear at 60 cm. Here again, the natural leaching of the oldest litter material could lead to the desorption of REEs from the MnO_2 or the direct transport into solution of Mn oxide nano-particles enriched in Ce, finally leading to a positive Ce anomaly in soil solutions. However, due to its redox sensitive nature, Ce dynamics are not easily understandable in soil solutions in which, due to the oxidative conditions we would expect there to be a depletion (negative Ce/Ce*) linked to the precipitation of Ce^{4+} as cerianite and adsorption onto Fe-Mn oxy-hydroxides.

Other important features of leachate patterns that are mirrored in the soil solutions are the HREEs and MREEs enrichments for the Douglas-fir and European beech stands, respectively, when compared to LREEs. Indeed, average Douglas-fir soil solutions showed quite stable La_N/Yb_N ratios at all depths with values comprised between 0.50 (Do SS40) and 0.66 (Do SS60), which are in line with the La_N/Yb_N ratios of Douglas-fir litter leachates (0.10 ≤ La_N/Yb_N ≤ 0.82). Concerning the beech stand, La_N/Gd_N in average soil solutions shows values between 0.46 (Be SS20) and 0.57 (Be SS40), still in line with the values of beech litter leachates (0.43 ≤ La_N/Gd_N ≤ 0.51) obtained with our experiment. Similarities like these suggest a strong impact of the litter degradation on what is the REEs signature of soil solutions, especially at shallower depths, and the fact that the anomalies tend to disappear in the deepest solutions strengthen this assumption.

It must be said that the same environmental conditions to which the litter is generally exposed are not found in the laboratory. Conditions under which a greater degradation efficiency would be expected and that were avoided due to limitations present in the

laboratory (such as the limited exchange of gases with the atmosphere, limited light, greater volume of water per litter surface area, lower concentration of microorganisms). Additional *in-situ* studies regarding the REEs dynamics in the Weierbach catchment's soils are necessary to better understand and quantify the real contribution of litter degradation to the REEs composition of soil solutions in a forest ecosystem. Moreover, chromatographic analysis of the leachates and SEM analysis of litter surfaces could help, respectively, to elucidate what kind of REEs ligands are present in the different leachates and to observe the existence (or not) of MnO_2 particles deposited on the surface of the oldest litter fractions.

7.5 Conclusions

We focused our attention on the role of forest vegetation on REEs and major cations sequestration and release into and from leaf tissues during the litter degradation. As shown in our experiment and similarly for both tree species, major cations and nutrients like Na, Mg, K, and Mn are preferentially located in more labile tissues and are easily released during litter degradation, while Pb, Fe, Al and REEs tend to be accumulated in the most recalcitrant tissues. We conjecture that such a sequestration in degradation-resistant tissues is imputable to the binding with lignins as the most resistant compounds in leaves.

Our results clearly show that litter degradation plays an important role in the REEs dynamics in forest ecosystems. New findings related to REEs dynamics during litter degradation and the potential of REEs as complementary tracers for litter degradation processes were highlighted. The observation that the Ce anomaly and tetrad effect only occur in leachates of the oldest litter fractions can be linked to the accumulation of MnO_2 on the surface of the litter after the first years of degradation. In comparison to the major cations, REEs presented marked differences during the degradation of the litters of European beech and Douglas-fir. In this latter, Eu seems to be involved in the same Ca translocation pathway that occurs during the leaf senescence. Moreover, the evolution of the La_N/Yb_N and Y/Ho ratios could be used as a proxy to analyse the resistance to the degradation of the leaves and litter between these two tree species.

Finally, the type of tree cover and the degradation stage of the litter are important parameters to consider when studying the chemistry of REEs in forest soil waters. Similarities between the REEs patterns of fresh leaves and litter leachates and REEs patterns of soil solutions have been reported, possibly suggesting the importance of vegetation in determining the REEs signatures in soil solutions. When compared to the other elements in the series, HREEs are preferentially released from litter into solution due to the

stronger affinity they have with the organic acids produced during the leaves' degradation stages. This would also explain the unexpected positive Ce anomaly that can be observed in the shallower soil solutions of the Weierbach experimental catchment in Luxembourg.

CHAPTER 8

Synthesis

The aim of this PhD project was to study rare earth elements (REEs) dynamics and fractionation processes across the regolith-tree system to evaluate if it is possible to use them as complementary tracers to water stable isotopes in Eco-hydrological studies. This, in order to overcome the issues related to the only use of water stable isotopes for understanding water uptake dynamics in the regolith-plant system. To achieve these goal, two complementary studies were conducted.

8.1 Main findings

8.1.1 Identifying processes fractionating H and O isotopes in the regolith-three system

The first study, reported in Chapters 3 and 4, was based on identifying the processes fractionating H and O isotopes during water uptake and within trees. Three new *in-situ* vacuum extraction (*IS*VE) techniques for collecting tree sap were developed and compared to conventional methods based on cryogenic extraction (CE) of water from tree cores in order to uncover what processes are responsible of the biases often observed in isotopic data of eco-hydrological research in the regolith-plant system. This study revealed that tree physiology and biochemistry may play a key role on fractionating O and H stable isotopes within trees, leading to changes in the isotopic composition of the different tree water pools. This is reflected both in *IS*VE sap and in CE waters. As a result, xylem sap gets gradually enriched in heavy isotopes as it moves from the roots to the branches and CE waters present relatively lighter H and heavier O composition in comparison to the xylem sap. A combination of processes can contribute to modify the isotopic signature of the water in trees before and during the cryogenic extraction. Among these, were suggested: mixing of water with different ages; H-exchange reactions between water and organic molecules in tree biochemical pathways; contemporary extraction and subsequent analysis of biogenic volatile organic compounds (BVOCs) together with the water samples; water compartmentation within tree tissues.

Root water extracted with the *IS*VE method appears as the most reliable sample to identify the origin of the water absorbed by trees when using water stable isotopes. The O and H isotopic composition of the *IS*VE root sap resulted similar to those of soil solutions, suggesting their preferential uptake. This similarity with the source seems to be linked to the capability of the *IS*VE technique to extract water from the xylem conduits – of which composition falls onto the LMWL – and to the fact that water in roots did not encounter (or encounter to a lesser extent) biochemical isotopic fractionation, as this water was recently absorbed.

Besides from tree physiology and water extraction techniques, the use of combustion module for analysing CE waters was suggested to potentially bias the analytical results by impacting the isotopic values of the analysed samples. This may be linked to two factors: combustion of organic compounds extracted together with the water during the CE process due to the high temperatures and vacuum applied; addition of oxygen with unknown isotopic composition from an external source as comburent for the combustion. As a results of the combustion, additional molecules of water can be generated and analyzed together with the sample, contributing to its final isotopic composition.

8.1.2 REEs patterns and fractionation across the regolith-three system

The second study – discussed in Chapters 5, 6 and 7 – focused on investigating the patterns and dynamics of REEs across the different compartments of the regolith-tree system. Its aim was to gain insights into their fractionation during water uptake, transportation across trees and their subsequent release into the environment through leaf exudation and litter degradation.

Roots inherit REEs patterns similar to those of the soil solutions absorbed with a slight difference among REEs groups (light – LREE, medium – MREE, and heavy – HREE), which are taken up in the order LREEs>MREEs>HREEs. While LREEs and MREEs pattern shapes indeed are similar to those of the solutions showing an MREE enrichment and a positive Ce anomaly, HREEs appears depleted both in the root bulk and in the root sap. This seems to be linked to the preferential distribution of heavier REEs in the soil solutions due to the presence of dissolved organic molecules that may prevent HREEs to pass through the roots. The development of the positive Ce anomaly in the roots is likely due to oxidizing conditions at the rhizosphere level that are determined by the release of O from the roots as well as the presence of Fe oxides in the surrounding soil. In such oxidative environment, Ce(III) is oxidized to Ce(IV) precipitating in the roots and fractionating during the water

absorption. This leads to the development of a positive Ce anomaly in the bulk root composition and a negative Ce anomaly in the sap. Y and Gd are the most mobile elements in the water/root interface, suggesting reduced absorption by the roots' membranes in comparison to the other REEs.

By understanding the processes involved in the REEs fractionation during the water uptake and by comparing the REEs patterns of roots and root sap with those of the potential water sources, it was possible to assume the preferential absorption of the shallow soil solutions by *Fagus sylvatica* in spring and groundwater in summer (at the hillslope site).

Throughout its flow from the roots to the branches, sap exhibits an enrichment in HREEs. This observation aligns with the findings of previous studies (Censi *et al*., 2014; Grosjean *et al*., 2019; Yuan *et al*., 2017-2018), which reported a preferential translocation of these elements towards the upper parts of trees. Such selective relocation is attributed to the higher affinity that HREEs have towards the organic molecules present within the sap. In the same path, Gd and Y show slightly different behaviour. While Y preserves its enhanced mobility being enriched in the branch sap in the regards of root sap, Gd/Gd* remains stable across the tree. Therefore, the mobility of Y and Gd is enhanced for both at the interfaces between compartments (e.g. root/soil water interface) and behave coherently, while during the flow across the trees in the sap, Y appears as a more mobile element. Finally, due to the high similarity between the ionic radii of Eu^{3+} and Ca^{2+}, Eu may fractionate from the sap, during the flow to the branches, to replace Ca in some molecules involved in the stabilization of cell walls (e.g. Ca-pectate). As a result, sap gets depleted in Eu, while the other tree organs – especially tissues with high lignin content – become enriched and show positive Eu anomalies.

The REEs composition of the transpired water was compared to those of the rainfall, throughfall and atmospheric dust in order to investigate the impact of tree exudates on the REEs chemistry of incident waters, and to discern the plants-derived input from that of the atmospheric dust. Y showed up as the most mobile REEs in the system, being preferentially released from leaves and showing an enrichment in the REEs patterns of transpired water samples. Transpired waters as well as throughfall samples exhibited positive Eu anomalies, probably originated from the interaction of the solutions with atmospheric dust particles, which showed a marked Eu enrichment. The enhanced mobility of Gd at the interfaces could not be verified due to the Eu enrichment – that did not allow for its graphical observation, and to a lower data reliability.

REEs behaviour during the wet degradation of litter was studied by performing leaching experiments with ultrapure water on the forest litter, to monitor the release of REEs and other cations. Two tree species were chosen for this study, *Fagus sylvatica* and *Pseudotsuga menziesii*, in order to compare the chemical release during the degradation of litter of evergreen and deciduous species and their respective impacts on soil solution REEs chemistry. The study discusses the role of competitive interactions between lignins and organic ligands in REEs fractionation during the degradation of litter. Lignins serve as a chelating agent, capturing REEs and other potentially harmful metals like Al, Fe, and Pb. They trap these elements in the "dead" tissues, thereby preventing them from entering living cells. This process fractionates REEs, with LREEs and MREEs being preferentially trapped in the litter and HREEs being instead leached. The preferential release of HREEs is promoted by the presence of organic ligands in the solution, towards HREEs have stronger affinity than the other elements of the series. Over time, these combined processes lead to a continuous enrichment of LREEs – and a depletion of HREEs – in the litter bulk composition. The REEs composition of fresh leaves shows an enrichment of Y, which suggests that the increased mobility of this element guides its primary storage to the leaves. During litter degradation, Y exhibits higher mobility compared to other REEs, leading to its preferential release from the leaves during this process. As a result, Y is enriched in litter leachates and a depleted in the older litter fractions.

Biological activity, particularly of white fungi, may indirectly governs the behaviour of Ce during litter degradation. These organisms possess the ability to oxidize Mn^{2+} to Mn^{3+}, which accumulates on the litter surface and precipitates as MnO_2. In turn, MnO_2 becomes enriched in Ce through an oxidative scavenging process during the litter wet degradation. Ce-enriched MnO_2 nanoparticles are subsequently released into solution when in contact with incident waters, resulting in the development of positive Ce anomalies in leachates. These anomalies are then inherited by shallower soil solutions when the leaching waters permeate the soil. The different characteristics of the REEs patterns in the leachates of the two tree species were found to be mirrored in the respective soil solutions, suggesting a significant impact of litter degradation (and of specific tree cover) in what is the REEs composition of the soil waters.

In order to consolidate the key findings regarding the REEs study presented in this thesis, a conceptual model has been developed (Figure 8.1). This model comprehensively illustrates the observed fractionation and dynamics of REEs across various compartments

within the regolith-tree system, synthetizing the key processes documented in Chapters 5-7 concerning *Fagus sylvatica* trees.

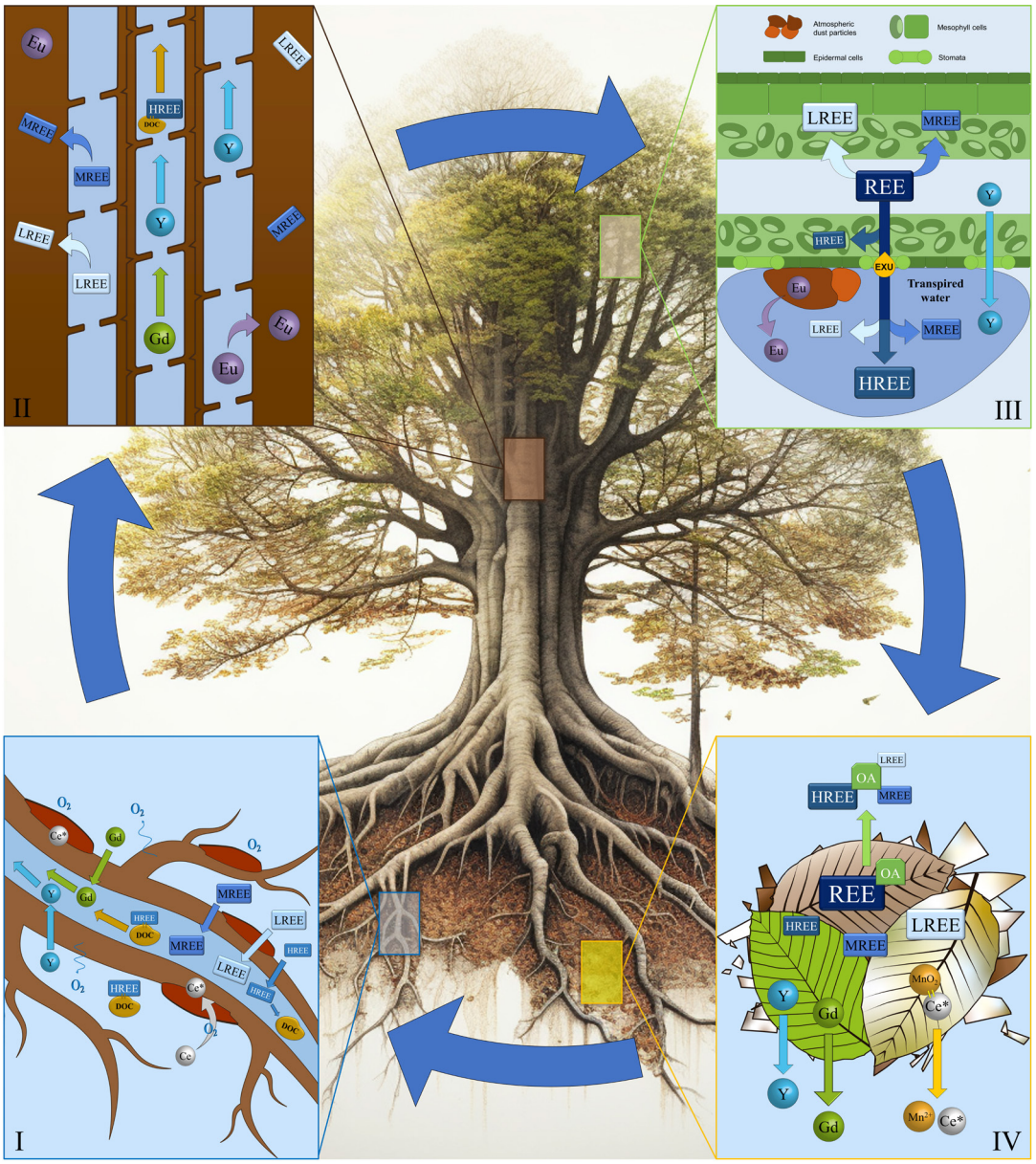

Figure 8.1: Conceptual model synthesizing the main of REEs fractionation processes within their biogeochemical cycle at tree scale.

The model divides the whole REEs cycle at tree scale into 4 main phases, highlighting the main processes treated in this thesis:

I. Root water uptake: at this stage, LREEs and MREEs are preferentially taken up by the roots, while HREEs tend to stay in the soil solutions bound to organic ligands. The oxidative environment created by the O released from roots, as well as the presence of FeO_2 plaques, makes Ce precipitating as Ce oxide in the roots, creating a depletion in the sap and an enrichment in the root tissues. Gd and Y can bypass the root's membranes, being able to move from the soil solution to the sap with less impediment in comparison to the other REEs. HREEs in the root sap tend to form complexes with organic molecules.

II. Root-to-branch transportation: in the root-branch flow path, LREEs and MREEs are distributed in the solid tree tissues, while HREEs, which are bound to the organic ligands in the sap, are preferentially kept in the sap and transported towards the upper part of the tree. Y and Gd are not fractionated in the tree tissues across the tree and tend to stay in the sap. Eu is also fractionated in lignified tissues, creating a depletion in the sap and an enrichment in the tree organs.

III. Leaves exudation: at this stage, a LREEs and MREEs distribution in the leaf tissues is observed. On the contrary, HREEs are preferentially released back to the environment with the exudates towards which they have higher affinity. Y appears enriched in the transpired water, due to its higher mobility in the regards of the other REEs. Atmospheric dust appears to contribute to the development of an Eu positive anomaly in the transpired water.

IV. Litter wet degradation: during this stage, REEs are released from the litter solid fraction into the environment in the order LREEs>MREEs>HREEs, due to the different affinities of these groups towards the organic acids present in the leaching solution. Gd and Y demonstrates higher mobility in the regards of the other REEs also at this stage, resulting in an enrichment in the leaching solutions and a consequential depletion in the litter bulk composition, overtime. Leaching solutions results enriched during the litter degradation process. Such an enrichment seems to be mediated by white fungi, and include the migration of Ce-enriched MnO_2 nanoparticles from the litter surface to the leaching solution. When these latter percolate through the soil, the characteristics of their REEs patterns are inherited by the shallower soil solutions. Finally, the cycle begins again.

8.2 Contribution to eco-hydrological studies

This work contributes in advancing the understanding of water stable isotopes fractionation in the regolith-plant system, as well as developing a multi-tracer and multidisciplinary approach to trace water flows in forested ecosystems. It aligns with other recent eco-hydrological and technical studies (Chen *et al.*, 2020; Barbeta *et al*., 2020 and 2022; Nehemy *et al.,* 2022; Wen *et al*., 2022), which attribute an increasingly important role to trees in modifying the isotopic composition of waters and highlights how the most common methods for tree water extraction and analysis can introduce biases in the isotopic analysis. This study, therefore, positions itself alongside those that challenge the more simplistic view adopted in past decades, which considered trees more as passive "pipes" in the regards of stable isotopes of O and H, in favour of a more intricate perspective that grants these organisms a fundamental role in modifying water isotopic signatures. The results presented in this work, indeed, demonstrate how trees are capable of modifying the isotopic signature of internal waters both directly through biochemical reactions and indirectly due to the different physical dynamics of isotopes of the same element during the flow through tree tissues. Additionally, it partly contributes to the resolution of the main issues related to cryogenic vacuum distillation by proposing alternative *in-situ* extraction methods. These latter not only proved to be more cost-effective compared to the more common technique, but also appear to be more accurate in identifying the water source absorbed by trees.

In addition to the advancement in water stable isotopes eco-hydrology, the use of multiple tracers reported in this study may improve the accuracy and precision of water source identification during tree water uptake. Different tracers have unique characteristics and behave differently in the environment. The principle behind combining multiple tracers, is the possibility to cross-validate the results and reduce the uncertainties associated with each individual tracer. This comprehensive approach may provide a more robust understanding of water uptake dynamics and may lead to more reliable results and forecasts. In this work, the first foundations have been laid for a multi-tracer/multidisciplinary method by coupling water stable isotopes and REEs for studying water dynamics in the regolith-plant system. While, a first approach with water stable isotopes, revealed the preferential absorption of surface waters by the root systems of *Fagus sylvatica* during the leaf-out period, the implementation of the study of the REEs dynamics at the water/root/sap interfaces, helped to confirm these findings. Moreover, while water stable isotopes demonstrated limitations of applicability during summer, when transpiration becomes more pronounced and isotopic modifications do not allow the recognition of the water uptaken (at

least from branches), the in-depth study of REEs dynamics at the soil/root interface and in the root-branch section enabled the potential recognition of the original water source, at least at the hillslope site. This multidisciplinary approach, although presenting a wide margin for improvement, can be used as an exemplary way to take the first steps toward the development of alternative and more comprehensive methods to address complex environmental issues when traditional methods have significant limitations of applicability.

8.3 Concluding remarks and future perspectives

The complexity of forest ecosystems makes it particularly difficult to use tracers for studying water resource dynamics, especially when biological entities such as trees are involved, as they are capable of significantly altering the isotopic and chemical signature of absorbed environmental waters. Understanding the processes involved in these modifications is therefore crucial for accurately reconstructing water pathways and identifying their origin more precisely. All this translates into the need to integrate eco-hydrology with other disciplines, such as plant biochemistry, to combine the study of various processes involving the different tracers with the quantitative and statistical approaches of hydrology. This work essentially seeks to introduce three fundamental innovations in the field of eco-hydrology: new methods for sampling tree sap; REEs as tracers of tree water uptake; and a multi-tracer and multidisciplinary approach that also considers the biochemical and physiological variables as a fundamental part of tracers' studies. From this perspective, this project is in line with other recent studies that have used a multidisciplinary and/or multi-tracer approaches for hydrological research (e.g., Antonelli *et al*., 2017; Pfister *et al*., 2017; Abbott *et al*., 2016; Florent *et al*., 2022; Barbeta *et al*., 2022), opening the doors to new avenues of research in the field of eco-hydrology. The biochemical interactions between water and organic molecules (Yakir and DeNiro, 1989; Yakir *et al*., 1990; Cormier *et al*., 2018) are complex processes that lead to modifications in the isotopic signature of the various water compartments in trees, making it difficult to recognize the original source. It is therefore crucial to consider these processes as a fundamental part of hydrological dynamics in forest ecosystems and integrate them into eco-hydrological models that utilize these tracers. While some of these processes are qualitatively known, the quantification of their impact on the isotopic signature of waters is still unclear. Further studies aimed at quantifying the impact of tree biochemical and physiological processes on the isotopic signature of waters are necessary. Similarly, further investigations regarding the species of BVOCs extracted through CE could provide important information on the quantity and quality of organic

species present in the various water compartments within the tree and their impact related to isotopic exchanges occurring in various biochemical pathways. Acquiring this information could prove critical for greater accuracy in tracing the origin of absorbed waters, potentially being implemented in existing models reducing their uncertainty. Additional experiments could be based on the use of ISVE techniques during the summer period, applying them to the roots of different tree species. This would allow for more precise information on the use of water resources by trees during drier periods, informing relevant authorities about the allocation of water resources, and about the most resilient tree species for potential reforestation projects in the context of a rapid climate change.

Regarding the use of REEs for recognizing absorbed water resources, developing experiments under controlled conditions (known water and soil composition) may help to accurately model which resources participate in the mixing that leads to the formation of the final composition of root sap (extracted from the primary root). An example could be represented by hydroponic experiments in which the roots are isolated into compartments at different depths and provided with waters of different REEs compositions. With knowledge of the various fractionation processes during uptake (Chapter 5), it would be virtually possible to combine a biological membrane model with a chemical mixing model to obtain information on the absorbed water sources, taking into account the REEs fractionation at the root/water source interface.

From and eco-hydrological perspective, Y showed interesting features. Among these, the higher mobility in comparison to the other REEs and the conservative concentration across the regolith-plant system (Fig. 8.2), highlight its potential as new tracer for understanding water uptake dynamics. While one would typically expect Y to be absorbed by root tissues, similarly to other trivalent metals like Fe, Al, and Ln^{+3}, Y appears instead to be preferentially transferred to the sap. Identifying water sources with contrasting Y concentrations may aid in recognizing the one being absorbed. For instance, as shown in Figure 8.2, Y concentration in the root sap falls between those of soil solutions and shallow groundwater. This may indicate that the root sap results from the mixing of these two sources, which is in partly in contrast with what we observed in Chapter 5, where the uptake of soil solutions was suggested by using the whole REEs spectrum. However, it's important to consider the occurrence of element remobilization within the tree (Chapter 5 and 7), which could lead to higher-than-expected Y concentrations in the root sap. Therefore, additional experiments using Y-labelled water are necessary to better understand Y dynamics within the tree and during water uptake.

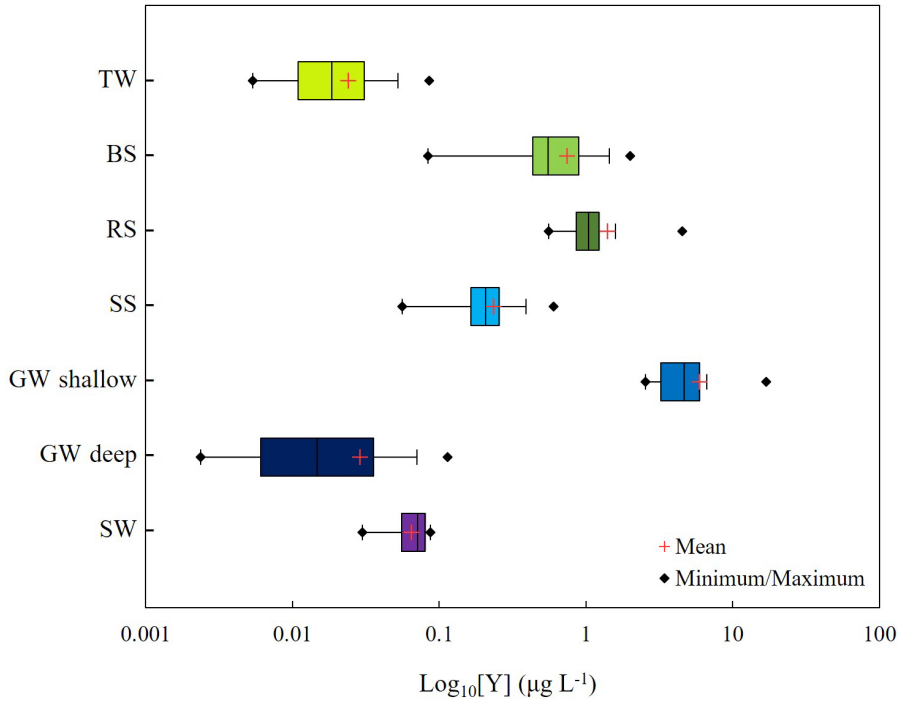

Figure 8.2: Evolution of Y concentrations across the regolith-tree system of this study, considering streamwater (SW), deep and shallow groundwaters (GW), soil solutions (SS), root sap (RS), branch sap (BS) and transpired water (TW).

Moreover, it would be valuable to combine the study of Y with other conservative tracers. For example, Hissler *et al*. (2023) introduced a novel approach using Pb isotopes to investigate tree water uptake dynamics. The authors showed distinct Pb isotopic signatures in water resources within the WEC regolith, enabling differentiation between soil solutions, shallow and deep groundwaters. Despite being preliminary findings, these tracers already show promise in distinguishing water pools, potentially opening up new avenues for ecohydrological and biogeochemical studies within the catchments' critical zone. It is therefore encouraged to utilize this study as a starting point for developing new analytical and experimental methods to comprehensively assess water dynamics throughout the entire vegetative period, both from qualitatively and quantitatively perspectives. However, the possibility for further studies in this field is vast and it is limited only by the imagination of scientists engaged in multidisciplinary research. It is crucial to promote and foster such research approaches, encouraging collaboration among researchers from diverse fields of study. This collaborative effort can offer a multitude of perspectives on the same scientific problem, enriching the exploration and refining the understanding of complex phenomena.

APPENDIX

Appendix to Chapter 3

Table A3.1: $\delta^{18}O$ and $\delta^{2}H$ values used for the study reported in Chapter 3.

Sample name	Sample type	Site	Date	$\delta^{18}O$	$\delta^{2}H$
P7 TS1	*I*SVE Bole sap	Plateau	31/03/2021	-8.43	-53.76
P7 TS2	*I*SVE Bole sap	Plateau	31/03/2021	-7.45	-48.02
P7 TS3	*I*SVE Bole sap	Plateau	31/03/2021	-8.92	-57.62
P9 TS1	*I*SVE Bole sap	Hillslope	31/03/2021	-7.81	-49.09
P9 TS2	*I*SVE Bole sap	Hillslope	31/03/2021	-8.39	-54.05
P9 TS3	*I*SVE Bole sap	Hillslope	31/03/2021	-7.33	-46.30
RP1 TS1	*I*SVE Bole sap	Riparian	31/03/2021	-7.99	-53.07
RP1 TS2	*I*SVE Bole sap	Riparian	31/03/2021	-7.59	-48.13
RP1 TS3	*I*SVE Bole sap	Riparian	31/03/2021	-7.24	-45.36
P7 PP1	Overpr. Branch sap	Plateau	06/07/2020	-6.52	-44.25
P7 PP4	Overpr. Branch sap	Plateau	06/07/2020	-6.45	-43.55
P7 PP2	Overpr. Branch sap	Plateau	06/07/2020	-6.90	-46.34
P7 PP3	Overpr. Branch sap	Plateau	06/07/2020	-7.10	-47.26
P9 PP1	Overpr. Branch sap	Hillslope	06/07/2020	-6.58	-44.71
P9 PP2	Overpr. Branch sap	Hillslope	06/07/2020	-6.90	-45.78
P9 PP3	Overpr. Branch sap	Hillslope	06/07/2020	-7.01	-46.88
P9 PP4	Overpr. Branch sap	Hillslope	06/07/2020	-7.01	-47.83
RP1 PP1	Overpr. Branch sap	Riparian	06/07/2020	-5.64	-39.53
RP1 PP3	Overpr. Branch sap	Riparian	06/07/2020	-7.33	-47.77
P7 PP1	Overpr. Branch sap	Plateau	10/08/2020	-5.93	-43.35
P7 PP2	Overpr. Branch sap	Plateau	10/08/2020	-6.67	-46.10
P7 PP3	Overpr. Branch sap	Plateau	10/08/2020	-7.52	-48.79
P9 PP1	Overpr. Branch sap	Hillslope	10/08/2020	-6.94	-47.68
P9 PP2	Overpr. Branch sap	Hillslope	10/08/2020	-6.81	-47.38
P9 PP3	Overpr. Branch sap	Hillslope	10/08/2020	-6.91	-47.81
RP1 PP1	Overpr. Branch sap	Riparian	10/08/2020	-6.76	-40.64
RP1 PP3	Overpr. Branch sap	Riparian	10/08/2020	-5.92	-42.24
P7 GW	P7 Groundwater	Plateau	27/03/2017	-8.33	-52.05
P7 GW	P7 Groundwater	Plateau	27/03/2017	-8.04	-52.19
P7 GW	P7 Groundwater	Plateau	30/03/2017	-8.24	-52.71

P7 GW	P7 Groundwater	Plateau	30/03/2017	-8.22	-52.18
P7 GW	P7 Groundwater	Plateau	04/04/2017	-8.25	-52.48
P7 GW	P7 Groundwater	Plateau	04/04/2017	-8.17	-52.17
P7 GW	P7 Groundwater	Plateau	11/04/2017	-8.2	-52.38
P7 GW	P7 Groundwater	Plateau	20/04/2017	-8.24	-52.33
P7 GW	P7 Groundwater	Plateau	04/05/2017	-8.23	-52.15
P7 GW	P7 Groundwater	Plateau	04/05/2017	-8.17	-53.08
P7 GW	P7 Groundwater	Plateau	16/05/2017	-8.17	-51.88
P7 GW	P7 Groundwater	Plateau	16/05/2017	-8.26	-52.65
RP GW	RP Groundwater	Riparian area	03/03/2020	-8.40	-53.99
P7 GW	P7 Groundwater	Plateau	09/03/2020	-8.69	-55.02
P7 GW	P7 Groundwater	Plateau	09/03/2020	-8.52	-55.32
P9 GW	P9 Groundwater	Hillslope	09/03/2020	-8.61	-54.72
P7 GW	P7 Groundwater	Plateau	31/03/2021	-8.82	-56.50
P7 GW	P7 Groundwater	Plateau	31/03/2021	-8.78	-56.09
P9 GW	P9 Groundwater	Hillslope	31/03/2021	-8.83	-56.10
RP GW	RP Groundwater	Riparian	31/03/2021	-8.70	-55.05
P7 BS1	*I*SVE Branch Sap	Plateau	23/03/2017	-5.29	-35.51
P7 BS1	*I*SVE Branch Sap	Plateau	27/03/2017	-5.58	-38.01
P7 BS1	*I*SVE Branch Sap	Plateau	30/03/2017	-5.52	-38.26
P7 BS1	*I*SVE Branch Sap	Plateau	04/04/2017	-5.48	-37.90
P7 BS1	*I*SVE Branch Sap	Plateau	11/04/2017	-5.30	-37.56
P7 BS1	*I*SVE Branch Sap	Plateau	20/04/2017	-4.82	-35.62
P7 BS1	*I*SVE Branch Sap	Plateau	28/04/2017	-4.58	-34.75
P7 BS1	*I*SVE Branch Sap	Plateau	04/05/2017	-4.86	-35.84
P7 BS1	*I*SVE Branch Sap	Plateau	16/05/2017	-5.38	-38.05
P7 BS1	*I*SVE Branch Sap	Plateau	09/03/2020	-5.71	-35.86
P7 BS2	*I*SVE Branch Sap	Plateau	09/03/2020	-5.62	-35.09
P7 BS3	*I*SVE Branch Sap	Plateau	09/03/2020	-5.93	-34.86
P7 BS4	*I*SVE Branch Sap	Plateau	09/03/2020	-5.55	-34.07
P9 BS1	*I*SVE Branch Sap	Hillslope	09/03/2020	-5.76	-34.51
P9 BS2	*I*SVE Branch Sap	Hillslope	09/03/2020	-5.99	-35.28
P9 BS3	*I*SVE Branch Sap	Hillslope	09/03/2020	-5.77	-35.11
RB1 BS1	*I*SVE Branch Sap	Riparian	09/03/2020	-5.78	-35.13
RP1 BS2	*I*SVE Branch Sap	Riparian	09/03/2020	-5.68	-32.77
RP3 BS1	*I*SVE Branch Sap	Riparian	09/03/2020	-5.65	-34.46
RP3 BS2	*I*SVE Branch Sap	Riparian	09/03/2020	-5.77	-35.64
RP3 BS3	*I*SVE Branch Sap	Riparian	09/03/2020	-5.76	-35.57
P7 BS1	*I*SVE Branch Sap	Plateau	31/03/2021	-0.86	-18.03
P7 BS2	*I*SVE Branch Sap	Plateau	31/03/2021	-4.13	-34.47
P7 BS3	*I*SVE Branch Sap	Plateau	31/03/2021	-3.58	-32.10

P9 BS1	*IS*VE Branch Sap	Hillslope	31/03/2021	-2.86	-28.03
P9 BS2	*IS*VE Branch Sap	Hillslope	31/03/2021	-4.15	-33.66
P9 BS3	*IS*VE Branch Sap	Hillslope	31/03/2021	-4.07	-34.80
RB1 BS1	*IS*VE Branch Sap	Riparian	31/03/2021	-2.10	-19.73
RP1 BS2	*IS*VE Branch Sap	Riparian	31/03/2021	-3.23	-28.25
RP1 BS3	*IS*VE Branch Sap	Riparian	31/03/2021	-4.05	-32.42
RP1 RS1	*IS*VE Root Sap	Riparian	23/03/2017	-7.04	-43.98
RP1 RS1	*IS*VE Root Sap	Riparian	27/03/2017	-7.79	-49.12
RP1 RS1	*IS*VE Root Sap	Riparian	30/03/2017	-7.65	-48.45
RP1 RS1	*IS*VE Root Sap	Riparian	04/04/2017	-7.54	-48.27
RP1 RS1	*IS*VE Root Sap	Riparian	11/04/2017	-7.52	-49.03
P7 RS1	*IS*VE Root Sap	Plateau	09/03/2020	-7.95	-50.09
P7 RS2	*IS*VE Root Sap	Plateau	09/03/2020	-7.51	-46.43
P7 RS3	*IS*VE Root Sap	Plateau	09/03/2020	-7.95	-49.76
P7 RS4	*IS*VE Root Sap	Plateau	09/03/2020	-8.21	-51.58
P9 RS1	*IS*VE Root Sap	Hillslope	09/03/2020	-7.55	-46.56
P9 RS2	*IS*VE Root Sap	Hillslope	09/03/2020	-7.52	-46.52
P9 RS3	*IS*VE Root Sap	Hillslope	09/03/2020	-7.81	-49.09
RP1 RS1	*IS*VE Root Sap	Riparian	09/03/2020	-8.14	-51.27
RP1 RS2	*IS*VE Root Sap	Riparian	09/03/2020	-8.15	-51.34
P7 RS1	*IS*VE Root Sap	Plateau	31/03/2021	-8.64	-56.90
P7 RS2	*IS*VE Root Sap	Plateau	31/03/2021	-9.12	-60.84
P7 RS3	*IS*VE Root Sap	Plateau	31/03/2021	-9.40	-62.23
P9 RS1	*IS*VE Root Sap	Hillslope	31/03/2021	-8.33	-53.52
P9 RS2	*IS*VE Root Sap	Hillslope	31/03/2021	-9.03	-58.81
P9 RS3	*IS*VE Root Sap	Hillslope	31/03/2021	-8.64	-55.58
RP1 RS1	*IS*VE Root Sap	Riparian	31/03/2021	-7.52	-48.89
RP1 RS2	*IS*VE Root Sap	Riparian	31/03/2021	-8.29	-54.44
RP1 RS3	*IS*VE Root Sap	Riparian	31/03/2021	-8.38	-54.77
P7 SS40-1	Soil Solution 40 cm	Plateau	31/03/2021	-9.72	-64.51
P7 SS40-2	Soil Solution 40 cm	Plateau	31/03/2021	-11.00	-74.71
P9 SS40	Soil Solution 40 cm	Hillslope	31/03/2021	-9.96	-68.35
P7 SS60-1	Soil Solution 60 cm	Plateau	31/03/2021	-9.89	-66.04
P7 SS60-2	Soil Solution 60 cm	Plateau	31/03/2021	-10.75	-72.30
P9 SS60	Soil Solution 60 cm	Hillslope	31/03/2021	-9.77	-65.59
P7 SS20	Soil Solution 20 cm	Plateau	27/03/2017	-9.33	-60.65
P7 SS20	Soil Solution 20 cm	Plateau	30/03/2017	-9.25	-60.35
P7 SS20	Soil Solution 20 cm	Plateau	04/04/2017	-9.29	-60.47
P7 SS20	Soil Solution 20 cm	Plateau	11/04/2017	-9.41	-60.46
P7 SS20	Soil Solution 20 cm	Plateau	20/04/2017	-9.43	-60.76
P7 SS20	Soil Solution 20 cm	Plateau	28/04/2017	-9.14	-59.5

P7 SS20	Soil Solution 20 cm	Plateau	04/05/2017	-9.1	-59.16
P7 SS20	Soil Solution 20 cm	Plateau	16/05/2017	-8.9	-57.7
RP1 SS20	Soil Solution 20 cm	Riparian	09/03/2020	-8.29	-53.46
RP2 SS20	Soil Solution 20 cm	Riparian	09/03/2020	-8.41	-53.59
RP3 SS20	Soil Solution 20 cm	Riparian	09/03/2020	-8.33	-53.23
P7 SS20	Soil Solution 20 cm	Plateau	09/03/2020	-8.81	-55.43
P9 SS20	Soil Solution 20 cm	Hillslope	09/03/2020	-8.92	-57.41
RP SS1	Soil Solution 20 cm	Riparian	31/03/2021	-8.68	-55.38
RP SS2	Soil Solution 20 cm	Riparian	31/03/2021	-8.80	-56.27
RP SS3	Soil Solution 20 cm	Riparian	31/03/2021	-8.74	-55.95
P7 SS20-1	Soil Solution 20 cm	Plateau	31/03/2021	-8.31	-53.23
P7 SS20-2	Soil Solution 20 cm	Plateau	31/03/2021	-9.43	-62.68
P9 SS20	Soil Solution 20 cm	Hillslope	31/03/2021	-8.44	-54.92
P7 SS40	Soil Solution 40 cm	Plateau	09/03/2020	-8.03	-49.57
P9 SS40	Soil Solution 40 cm	Hillslope	09/03/2020	-7.51	-47.76
P7 SS60	Soil Solution 60 cm	Plateau	27/03/2017	-8.19	-52.53
P7 SS60	Soil Solution 60 cm	Plateau	30/03/2017	-7.74	-49.53
P7 SS60	Soil Solution 60 cm	Plateau	04/04/2017	-7.4	-46.98
P7 SS60	Soil Solution 60 cm	Plateau	11/04/2017	-7.77	-50.32
P7 SS60	Soil Solution 60 cm	Plateau	09/03/2020	-8.33	-54.33
SW	Streamwater	Riparian	09/03/2020	-8.51	-54.02
SW	Streamwater	Riparian	31/03/2021	-8.67	-55.39

Appendix to Chapter 4

Table A4.1: $\delta^{18}O$ and $\delta^{2}H$ values of the samples treated in Chapter 4. CE = Cryogenic extraction; *IS*VE = in-situ vacuum extraction

Sample name	Sample type	Date	$\delta^{18}O$	$\delta^{2}H$
P7 TC1	CE Bole	09/03/2020	-5.88	-56.85
P7 TC2	CE Bole	09/03/2020	-5.49	-48.76
P7 TC3	CE Bole	09/03/2020	-5.94	-60.25
P9 TC1	CE Bole	09/03/2020	-5.29	-55.53
P9 TC2	CE Bole	09/03/2020	-5.66	-56.58
P9 TC3	CE Bole	09/03/2020	-5.60	-52.38
RP1 TC1	CE Bole	09/03/2020	-6.09	-59.28
RP1 TC2	CE Bole	09/03/2020	-7.37	-60.93
RP1 TC3	CE Bole	09/03/2020	-6.91	-59.24
RP2 TC1	CE Bole	09/03/2020	-6.93	-53.03
RP2 TC2	CE Bole	09/03/2020	-6.68	-54.36
RP3 TC1	CE Bole	09/03/2020	-4.47	-48.97
RP3 TC2	CE Bole	09/03/2020	-5.97	-53.87
RP3 TC3	CE Bole	09/03/2020	-4.66	-47.81
P7 RS1	*IS*VE Root sap	09/03/2020	-7.95	-50.09
P7 RS2	*IS*VE Root sap	09/03/2020	-7.51	-46.43
P7 RS3	*IS*VE Root sap	09/03/2020	-7.95	-49.76
P9 RS1	*IS*VE Root sap	09/03/2020	-7.55	-46.56
P9 RS2	*IS*VE Root sap	09/03/2020	-7.52	-46.52
P9 RS3	*IS*VE Root sap	09/03/2020	-7.81	-49.09
RP RS1	*IS*VE Root sap	09/03/2020	-8.14	-51.27
RP RS2	*IS*VE Root sap	09/03/2020	-8.15	-51.34
P7 TC1	CE Bole	31/03/2021	-6.89	-71.30
P7 TC2	CE Bole	31/03/2021	-3.04	-62.51
P7 TC3	CE Bole	31/03/2021	-6.62	-69.43
P9 TC1	CE Bole	31/03/2021	-6.08	-65.18
P9 TC2	CE Bole	31/03/2021	-5.56	-68.46

P9 TC3	CE Bole	31/03/2021	-3.20	-64.12
RP1 TC1	CE Bole	31/03/2021	-3.32	-57.72
RP1 TC2	CE Bole	31/03/2021	-4.43	-55.93
RP1 TC3	CE Bole	31/03/2021	-2.09	-61.65
P7 RC1	CE Root	31/03/2021	-3.15	-73.75
P7 RC2	CE Root	31/03/2021	-9.31	-76.91
P7 RC3	CE Root	31/03/2021	-8.95	-75.81
P7 TS1	CE Root	31/03/2021	-8.43	-53.76
P7 TS2	CE Root	31/03/2021	-7.45	-48.02
P7 TS3	CE Root	31/03/2021	-8.92	-57.62
P9 RC1	CE Root	31/03/2021	-9.63	-75.63
P9 RC2	CE Root	31/03/2021	-8.64	-72.48
P9 RC3	CE Root	31/03/2021	-8.14	-64.63
P9 TS1	CE Root	31/03/2021	-7.81	-49.09
P9 TS2	CE Root	31/03/2021	-8.39	-54.05
P9 TS3	CE Root	31/03/2021	-7.33	-46.30
RP RC1	CE Root	31/03/2021	-7.87	-71.99
RP RC2	CE Root	31/03/2021	-5.39	-63.24
RP RC3	CE Root	31/03/2021	-4.88	-66.86
RP TS1	CE Root	31/03/2021	-7.99	-53.07
RP TS2	CE Root	31/03/2021	-7.59	-48.13
RP TS3	CE Root	31/03/2021	-7.24	-45.36
P7 RS1	*IS*VE Root sap	31/03/2021	-8.64	-56.90
P7 RS2	*IS*VE Root sap	31/03/2021	-9.12	-60.84
P7 RS3	*IS*VE Root sap	31/03/2021	-9.40	-62.23
P9 RS1	*IS*VE Root sap	31/03/2021	-8.33	-53.52
P9 RS2	*IS*VE Root sap	31/03/2021	-9.03	-58.81
P9 RS3	*IS*VE Root sap	31/03/2021	-8.64	-55.58
RP RS1	*IS*VE Root sap	31/03/2021	-7.52	-48.89
RP RS2	*IS*VE Root sap	31/03/2021	-8.29	-54.44
RP RS3	*IS*VE Root sap	31/03/2021	-8.38	-54.77

Table A4.2: BVOCs δ^2H values used for the IsoSource mixing model in Chapter 4. Data from Liu *et al*. (2006), Nhu-Trang *et al*. (2006) and Chikaraishi and Naraoka (2003).

Species/Sample	Compound	δ^2H
Commercial oregano oil	Carvacrol	-211
Commercial oregano oil	Carvacrol	-210
Commercial oregano oil	Carvacrol	-210
Commercial oregano oil	Carvacrol	-208
Commercial oregano oil	Carvacrol	-204
Commercial savory oil	Carvacrol	-219
Commercial savory oil	Carvacrol	-218
Commercial savory oil	Carvacrol	-215
Commercial savory oil	Carvacrol	-212
Commercial savory oil	Carvacrol	-212
Commercial savory oil	Carvacrol	-167
Commercial thyme oil	Carvacrol	-226
Commercial thyme oil	Carvacrol	-231
Coridothymus capitatus L.	Carvacrol	-196
Coridothymus capitatus L.	Carvacrol	-193
Origanum compactum	Carvacrol	-212
Origanum compactum	Carvacrol	-210
Origanum heracleoticum L.	Carvacrol	-223
Origanum heracleoticum L.	Carvacrol	-220
Origanum heracleoticum L.	Carvacrol	-219
Origanum heracleoticum L.	Carvacrol	-218
Origanum heracleoticum L.	Carvacrol	-213
Origanum heracleoticum L.	Carvacrol	-212
Origanum heracleoticum L.	Carvacrol	-211
Origanum heracleoticum L.	Carvacrol	-210
Origanum heracleoticum L.	Carvacrol	-209
Origanum heracleoticum L.	Carvacrol	-208
Origanum heracleoticum L.	Carvacrol	-207
Origanum heracleoticum L.	Carvacrol	-204
Origanum heracleoticum L.	Carvacrol	-203
Satureja montana L.	Carvacrol	-229
Satureja montana L.	Carvacrol	-227
Satureja montana L.	Carvacrol	-226
Satureja montana L.	Carvacrol	-226
Satureja montana L.	Carvacrol	-226
Satureja montana L.	Carvacrol	-225
Satureja montana L.	Carvacrol	-225

Satureja montana L.	Carvacrol	-224
Satureja montana L.	Carvacrol	-223
Satureja montana L.	Carvacrol	-222
Satureja montana L.	Carvacrol	-224
Achnatherum splendens	n-alkanes	-173
Achnatherum splendens	n-alkanes	-182
Achnatherum splendens	n-alkanes	-180
Achnatherum splendens	n-alkanes	-178
Agropyron desertorum	n-alkanes	-168
Agropyron desertorum	n-alkanes	-185
Agropyron desertorum	n-alkanes	-184
Agropyron desertorum	n-alkanes	-179
Artemisia scoparia	n-alkanes	-140
Artemisia scoparia	n-alkanes	-142
Artemisia scoparia	n-alkanes	-133
Artemisia scoparia	n-alkanes	-138
Asparagus officinalis	n-alkanes	-131
Asparagus officinalis	n-alkanes	-164
Asparagus officinalis	n-alkanes	-154
Asparagus officinalis	n-alkanes	-149
Bothriochloa ischaemum	n-alkanes	-157
Bothriochloa ischaemum	n-alkanes	-173
Bothriochloa ischaemum	n-alkanes	-163
Bothriochloa ischaemum	n-alkanes	-152
Bothriochloa ischaemum	n-alkanes	-170
Bothriochloa ischaemum	n-alkanes	-157
Bothriochloa ischaemum	n-alkanes	-186
Bothriochloa ischaemum	n-alkanes	-188
Bothriochloa ischaemum	n-alkanes	-173
Bothriochloa ischaemum	n-alkanes	-165
Bothriochloa ischaemum	n-alkanes	-177
Bothriochloa ischaemum	n-alkanes	-164
Caragana stenophylla	n-alkanes	-133
Caragana stenophylla	n-alkanes	-153
Caragana stenophylla	n-alkanes	-143
Citibetica kom	n-alkanes	-145
Citibetica kom	n-alkanes	-165
Citibetica kom	n-alkanes	-164
Citibetica kom	n-alkanes	-158
Cleistogenes squarrosa	n-alkanes	-149
Cleistogenes squarrosa	n-alkanes	-176

Cleistogenes squarrosa	n-alkanes	-161
Cleistogenes squarrosa	n-alkanes	-178
Cleistogenes squarrosa	n-alkanes	-151
Cleistogenes squarrosa	n-alkanes	-174
Cleistogenes squarrosa	n-alkanes	-154
Cleistogenes squarrosa	n-alkanes	-176
Corispermum hyssopifolium	n-alkanes	-123
Corispermum hyssopifolium	n-alkanes	-116
Corispermum hyssopifolium	n-alkanes	-124
Corispermum hyssopifolium	n-alkanes	-121
Cryptomeria japonica	n-alkanes	-175
Cryptomeria japonica	n-alkanes	-178
Cryptomeria japonica	n-alkanes	-168
Cryptomeria japonica	n-alkanes	-153
Cryptomeria japonica	n-alkanes	-146
Cryptomeria japonica	n-alkanes	-144
Cryptomeria japonica	n-alkanes	-169
Cryptomeria japonica	n-alkanes	-165
Cryptomeria japonica	n-alkanes	-156
Cryptomeria japonica	n-alkanes	-141
Cryptomeria japonica	n-alkanes	-140
Cryptomeria japonica	n-alkanes	-141
Cryptomeria japonica	n-alkanes	-169
Cryptomeria japonica	n-alkanes	-163
Cryptomeria japonica	n-alkanes	-134
Cryptomeria japonica	n-alkanes	-136
Cryptomeria japonica	n-alkanes	-157
Cryptomeria japonica	n-alkanes	-180
Cryptomeria japonica	n-alkanes	-148
Cryptomeria japonica	n-alkanes	-143
Cryptomeria japonica	n-alkanes	-156
Cryptomeria japonica	n-alkanes	-159
Cryptomeria japonica	n-alkanes	-147
Cryptomeria japonica	n-alkanes	-141
Dracocephalum moldavica	n-alkanes	-140
Dracocephalum moldavica	n-alkanes	-167
Dracocephalum moldavica	n-alkanes	-183
Dracocephalum moldavica	n-alkanes	-163
Haloxylon ammodendron	n-alkanes	-152
Haloxylon ammodendron	n-alkanes	-113
Haloxylon ammodendron	n-alkanes	-140

Haloxylon ammodendron	n-alkanes	-114
Haloxylon ammodendron	n-alkanes	-145
Haloxylon ammodendron	n-alkanes	-129
Haloxylon ammodendron	n-alkanes	-145
Haloxylon ammodendron	n-alkanes	-119
Heteropappus less	n-alkanes	-185
Heteropappus less	n-alkanes	-186
Heteropappus less	n-alkanes	-206
Heteropappus less	n-alkanes	-192
Lespedeza davurica	n-alkanes	-133
Lespedeza davurica	n-alkanes	-136
Lespedeza davurica	n-alkanes	-131
Lespedeza davurica	n-alkanes	-133
Oxytropis aciphylla	n-alkanes	-142
Oxytropis aciphylla	n-alkanes	-148
Peganum harmala	n-alkanes	-158
Pennisetum Xaccidum	n-alkanes	-194
Pinus tabulaeformis	n-alkanes	-136
Pinus tabulaeformis	n-alkanes	-150
Salsola collina	n-alkanes	-128
Stipa bungeana	n-alkanes	-156
Stipa bungeana	n-alkanes	-171
Stipa glareosa	n-alkanes	-162
Stipa grandis	n-alkanes	-107
Stipagrandis	n-alkanes	-200
Sviciifolia hance	n-alkanes	-112
Cryptomeria japonica	n-Alkanoic acid	-159
Cryptomeria japonica	n-Alkanoic acid	-157
Cryptomeria japonica	n-Alkanoic acid	-129
Cryptomeria japonica	n-Alkanoic acid	-131
Cryptomeria japonica	n-Alkanoic acid	-145
Cryptomeria japonica	n-Alkanoic acid	-165
Cryptomeria japonica	n-Alkanoic acid	-144
Cryptomeria japonica	n-Alkanoic acid	-138
Cryptomeria japonica	n-Alkanoic acid	-153
Cryptomeria japonica	n-Alkanoic acid	-153
Cryptomeria japonica	n-Alkanoic acid	-133
Cryptomeria japonica	n-Alkanoic acid	-136
Commercial oregano oil	p-Cymene	-251
Commercial savory oil	p-Cymene	-263
Commercial savory oil	p-Cymene	-271

Commercial savory oil	p-Cymene	-262
Commercial savory oil	p-Cymene	-264
Commercial savory oil	p-Cymene	-247
Commercial thyme oil	p-Cymene	-293
Commercial thyme oil	p-Cymene	-292
Commercial thyme oil	p-Cymene	-282
Commercial thyme oil	p-Cymene	-268
Commercial thyme oil	p-Cymene	-272
Commercial thyme oil	p-Cymene	-266
Commercial thyme oil	p-Cymene	-247
Commercial thyme oil	p-Cymene	-280
Coridothymus capitatus L.	p-Cymene	-265
Origanum compactum	p-Cymene	-264
Origanum heracleoticum L.	p-Cymene	-283
Origanum heracleoticum L.	p-Cymene	-283
Origanum heracleoticum L.	p-Cymene	-276
Origanum heracleoticum L.	p-Cymene	-284
Origanum heracleoticum L.	p-Cymene	-274
Origanum heracleoticum L.	p-Cymene	-274
Origanum heracleoticum L.	p-Cymene	-269
Origanum heracleoticum L.	p-Cymene	-262
Origanum heracleoticum L.	p-Cymene	-269
Origanum heracleoticum L.	p-Cymene	-267
Origanum heracleoticum L.	p-Cymene	-261
Origanum heracleoticum L.	p-Cymene	-259
Origanum heracleoticum L.	p-Cymene	-259
Satureja montana L.	p-Cymene	-285
Satureja montana L.	p-Cymene	-289
Satureja montana L.	p-Cymene	-286
Satureja montana L.	p-Cymene	-283
Satureja montana L.	p-Cymene	-283
Satureja montana L.	p-Cymene	-283
Satureja montana L.	p-Cymene	-278
Satureja montana L.	p-Cymene	-282
Satureja montana L.	p-Cymene	-283
Satureja montana L.	p-Cymene	-280
Satureja montana L.	p-Cymene	-269
Thymus vulgaris L.	p-Cymene	-299
Thymus vulgaris L.	p-Cymene	-300
Thymus vulgaris L.	p-Cymene	-300
Thymus vulgaris L.	p-Cymene	-296

Thymus vulgaris L.	p-Cymene	-289
Thymus vulgaris L.	p-Cymene	-283
Thymus vulgaris L.	p-Cymene	-287
Thymus vulgaris L.	p-Cymene	-284
Thymus vulgaris L.	p-Cymene	-287
Thymus vulgaris L.	p-Cymene	-282
Thymus vulgaris L.	p-Cymene	-276
Thymus vulgaris L.	p-Cymene	-275
Thymus vulgaris L.	p-Cymene	-281
Thymus vulgaris L.	p-Cymene	-280
Thymus zygis L.	p-Cymene	-279
Thymus zygis L.	p-Cymene	-272
Thymus zygis L.	p-Cymene	-271
Thymus zygis L.	p-Cymene	-272
Thymus zygis L.	p-Cymene	-270
Commercial oregano oil	Thymol	-244
Commercial oregano oil	Thymol	-225
Commercial oregano oil	Thymol	-250
Commercial savory oil	Thymol	-224
Commercial savory oil	Thymol	-231
Commercial thyme oil	Thymol	-258
Commercial thyme oil	Thymol	-245
Commercial thyme oil	Thymol	-241
Commercial thyme oil	Thymol	-239
Commercial thyme oil	Thymol	-239
Commercial thyme oil	Thymol	-201
Commercial thyme oil	Thymol	-199
Commercial thyme oil	Thymol	-78
Commercial thyme oil	Thymol	-243
Commercial thyme oil	Thymol	-238
Coridothymus capitatus L.	Thymol	-231
Origanum compactum	Thymol	-235
Origanum compactum	Thymol	-244
Origanum heracleoticum L.	Thymol	-256
Origanum heracleoticum L.	Thymol	-263
Satureja montana L.	Thymol	-249
Satureja montana L.	Thymol	-247
Satureja montana L.	Thymol	-245
Satureja montana L.	Thymol	-246
Satureja montana L.	Thymol	-245
Satureja montana L.	Thymol	-243

Satureja montana L.	Thymol	-246
Satureja montana L.	Thymol	-244
Satureja montana L.	Thymol	-244
Thymus vulgaris L.	Thymol	-259
Thymus vulgaris L.	Thymol	-256
Thymus vulgaris L.	Thymol	-254
Thymus vulgaris L.	Thymol	-252
Thymus vulgaris L.	Thymol	-248
Thymus vulgaris L.	Thymol	-247
Thymus vulgaris L.	Thymol	-247
Thymus vulgaris L.	Thymol	-245
Thymus vulgaris L.	Thymol	-243
Thymus vulgaris L.	Thymol	-243
Thymus vulgaris L.	Thymol	-241
Thymus vulgaris L.	Thymol	-240
Thymus vulgaris L.	Thymol	-240
Thymus vulgaris L.	Thymol	-239
Thymus zygis L.	Thymol	-242
Thymus zygis L.	Thymol	-239
Thymus zygis L.	Thymol	-238
Thymus zygis L.	Thymol	-237
Thymus zygis L.	Thymol	-234
Commercial savory oil	y-Terpinene	-257
Commercial thyme oil	y-Terpinene	-267
Coridothymus capitatus L.	y-Terpinene	-252
Origanum heracleoticum L.	y-Terpinene	-275
Origanum heracleoticum L.	y-Terpinene	-248
Origanum heracleoticum L.	y-Terpinene	-274
Origanum heracleoticum L.	y-Terpinene	-264
Origanum heracleoticum L.	y-Terpinene	-262
Origanum heracleoticum L.	y-Terpinene	-252
Origanum heracleoticum L.	y-Terpinene	-223
Origanum heracleoticum L.	y-Terpinene	-241
Origanum heracleoticum L.	y-Terpinene	-223
Origanum heracleoticum L.	y-Terpinene	-217
Satureja montana L.	y-Terpinene	-273
Satureja montana L.	y-Terpinene	-283
Satureja montana L.	y-Terpinene	-273
Satureja montana L.	y-Terpinene	-277
Satureja montana L.	y-Terpinene	-275
Satureja montana L.	y-Terpinene	-271

Satureja montana L.	y-Terpinene	-268
Satureja montana L.	y-Terpinene	-269
Satureja montana L.	y-Terpinene	-271
Satureja montana L.	y-Terpinene	-256
Thymus vulgaris L.	y-Terpinene	-277
Thymus vulgaris L.	y-Terpinene	-270
Thymus vulgaris L.	y-Terpinene	-272
Thymus vulgaris L.	y-Terpinene	-285
Thymus vulgaris L.	y-Terpinene	-270
Thymus vulgaris L.	y-Terpinene	-265
Thymus vulgaris L.	y-Terpinene	-273
Thymus vulgaris L.	y-Terpinene	-277
Thymus vulgaris L.	y-Terpinene	-266
Thymus vulgaris L.	y-Terpinene	-251
Thymus zygis L.	y-Terpinene	-249
Thymus zygis L.	y-Terpinene	-248
Thymus zygis L.	y-Terpinene	-251

References for the values of biogenic volatile organic compounds (BVOCs) considered for the IsoSource mixing model adopted in Chapter 4:

Liu, W., Yang, H. & Li, L. Hydrogen isotopic compositions of n-alkanes from terrestrial plants correlate with their ecological life forms. Oecologia 150, 330–338 (2006). https://doi.org/10.1007/s00442-006-0494-0

Chikaraishi, Y., Naraoka, H. Compound-specific deltaD-delta13C analyses of n-alkanes extracted from terrestrial and aquatic plants. Phytochemistry. 2003 Jun;63(3):361-71. doi: 10.1016/s0031-9422(02)00749-5

Nhu-Trang, T. T., Casabianca, H., Grenier-Loustalot, M. F. Deuterium/hydrogen ratio analysis of thymol, carvacrol, γ-terpinene and p-cymene in thyme, savory and oregano essential oils by gas chromatography–pyrolysis–isotope ratio mass spectrometry, Journal of Chromatography A, Volume 1132, Issues 1–2, 2006, Pages 219-227, ISSN 0021-9673, https://doi.org/10.1016/j.chroma.2006.07.088

Appendix to Chapter 5

Table A5.1: REEs concentrations for all samples collected for the study in Chapter 5.

Sample name	Sample type	Site	Date	La	Ce	Pr	Nd	Sm	Eu	Gd	Tb	Dy	Y	Ho	Er	Tm	Yb	Lu
				µg/L	*µg/L*	*µg/L*	*µg/L*	*µg/L*	*µg/L*	*µg/L*	*µg/L*	*µg/L*	*µg/L*	*µg/L*	*µg/L*	*µg/L*	*µg/L*	*µg/L*
LoQ	-	-	-	0.001	0.001	0.001	0.005	0.005	0.001	0.005	0.001	0.005	0.001	0.005	0.001	0.005	0.001	0.005
GW1	Groundwater	Plateau	27/03/2017	0.969	0.669	0.423	2.119	0.564	0.156	0.911	0.138	0.836	6.643	0.175	0.489	0.061	0.340	0.054
GW1	Groundwater	Plateau	30/03/2017	0.836	0.584	0.368	1.888	0.502	0.136	0.792	0.121	0.719	5.717	0.151	0.423	0.053	0.299	0.047
GW1	Groundwater	Plateau	04/04/2017	0.572	0.436	0.277	1.435	0.399	0.108	0.613	0.089	0.531	4.111	0.111	0.317	0.040	0.233	0.039
GW1	Groundwater	Plateau	04/05/2017	0.428	0.416	0.260	1.411	0.425	0.108	0.579	0.081	0.475	3.352	0.099	0.292	0.038	0.236	0.040
GW5	Groundwater	Plateau	04/05/2017	0.014	0.013	0.006	0.033	0.009	0.003	0.013	0.002	0.012	0.111	<LoQ	0.008	<LoQ	0.006	<LoQ
GW1	Groundwater	Plateau	16/05/2017	0.379	0.408	0.243	1.364	0.411	0.108	0.552	0.076	0.443	2.936	0.093	0.272	0.035	0.219	0.038
GW1	Groundwater	Plateau	09/03/2020	2.493	1.683	1.076	5.099	1.402	0.375	2.300	0.355	2.095	16.872	0.448	1.238	0.151	0.830	0.130
GW3	Groundwater	Riparian	09/03/2020	0.002	0.001	<LoQ	<LoQ	<LoQ	<LoQ	<LoQ	<LoQ	<LoQ	<LoQ	<LoQ	0.001	<LoQ	0.002	<LoQ
GW5	Groundwater	Plateau	09/03/2020	0.006	0.006	0.002	0.005	<LoQ	<LoQ	<LoQ	<LoQ	<LoQ	0.033	<LoQ	0.002	<LoQ	0.002	<LoQ
GW9	Groundwater	Hillslope	09/03/2020	0.037	0.038	0.015	0.069	0.018	0.005	0.025	0.003	0.015	0.107	<LoQ	0.009	<LoQ	0.007	<LoQ
GW1	Groundwater	Plateau	06/05/2020	0.703	0.685	0.404	2.122	0.660	0.167	0.916	0.129	0.722	5.200	0.153	0.459	0.060	0.373	0.061
GW3	Groundwater	Riparian	06/05/2020	0.018	0.015	0.005	0.023	0.009	0.002	0.011	0.001	0.006	0.049	<LoQ	0.004	<LoQ	0.004	<LoQ
GW9	Groundwater	Hillslope	06/05/2020	0.020	0.019	0.008	0.035	0.010	0.002	0.013	0.002	0.009	0.070	<LoQ	0.005	<LoQ	0.005	<LoQ
GW1	Groundwater	Plateau	25/05/2020	0.364	0.469	0.236	1.237	0.369	0.095	0.505	0.070	0.397	2.540	0.083	0.242	0.032	0.202	0.032
GW3	Groundwater	Riparian	25/05/2020	0.005	0.006	0.002	<LoQ	<LoQ	<LoQ	<LoQ	<LoQ	<LoQ	0.014	<LoQ	0.001	<LoQ	0.001	<LoQ
GW9	Groundwater	Hillslope	25/05/2020	0.013	0.011	0.003	0.013	<LoQ	0.001	0.006	0.001	<LoQ	0.030	<LoQ	0.002	<LoQ	0.003	<LoQ
GW3	Groundwater	Riparian	15/06/2020	0.056	0.059	0.015	0.067	0.021	0.006	0.028	0.003	0.016	0.114	<LoQ	0.010	<LoQ	0.010	<LoQ
GW9	Groundwater	Hillslope	15/06/2020	0.003	0.004	0.001	0.005	<LoQ	0.001	<LoQ	0.000	<LoQ	0.007	<LoQ	0.001	<LoQ	0.001	<LoQ
GW3	Groundwater	Riparian	06/07/2020	0.014	0.014	0.004	0.018	0.005	0.002	0.008	0.001	0.006	0.039	<LoQ	0.004	<LoQ	0.004	<LoQ
GW9	Groundwater	Hillslope	06/07/2020	0.005	0.017	0.003	0.013	0.004	0.001	0.005	0.000	<LoQ	0.012	<LoQ	0.002	<LoQ	0.002	<LoQ
GW9	Groundwater	Hillslope	10/08/2020	0.005	0.007	0.002	0.010	0.002	0.001	<LoQ	0.000	<LoQ	0.015	<LoQ	0.002	<LoQ	0.002	<LoQ
GW5	Groundwater	Plateau	25/09/2020	0.004	0.010	0.001	<LoQ	<LoQ	<LoQ	<LoQ	<LoQ	<LoQ	0.015	<LoQ	0.001	<LoQ	0.001	<LoQ
P7 BS1	*I*SVE Branch sap	Plateau	23/03/2017	0.215	0.322	0.059	0.287	0.061	0.017	0.088	0.011	0.062	0.618	0.013	0.035	0.004	0.019	0.003
P7 BS1	*I*SVE Branch sap	Plateau	27/03/2017	0.180	0.242	0.042	0.199	0.041	0.011	0.060	0.008	0.041	0.395	0.008	0.022	0.003	0.012	0.002
P7 BS1	*I*SVE Branch sap	Plateau	30/03/2017	0.272	0.345	0.055	0.240	0.044	0.012	0.067	0.008	0.047	0.466	0.009	0.024	0.003	0.014	0.002
P7 BS1	*I*SVE Branch sap	Plateau	04/04/2017	0.311	0.381	0.062	0.269	0.053	0.014	0.072	0.008	0.047	0.480	0.010	0.025	0.003	0.016	0.002
P7 BS1	*I*SVE Branch sap	Plateau	11/04/2017	0.444	0.501	0.075	0.313	0.054	0.015	0.081	0.009	0.052	0.548	0.011	0.028	0.003	0.016	0.002
RP BS1	*I*SVE Branch sap	Riparian	11/04/2017	0.491	0.387	0.077	0.345	0.089	0.023	0.107	0.010	0.042	0.255	0.007	0.016	0.001	0.009	0.001
P7 BS1	*I*SVE Branch sap	Plateau	20/04/2017	0.647	0.693	0.103	0.429	0.078	0.020	0.102	0.013	0.063	0.656	0.013	0.033	0.004	0.017	0.003
RP BS1	*I*SVE Branch sap	Riparian	20/04/2017	0.788	0.606	0.114	0.483	0.118	0.030	0.154	0.014	0.060	0.376	0.010	0.025	0.002	0.012	0.002
P7 BS1	*I*SVE Branch sap	Plateau	28/04/2017	1.204	1.310	0.201	0.866	0.151	0.044	0.230	0.027	0.141	1.439	0.027	0.074	0.008	0.040	0.006
RP BS1	*I*SVE Branch sap	Riparian	28/04/2017	1.049	0.769	0.134	0.570	0.137	0.036	0.183	0.017	0.068	0.507	0.012	0.030	0.003	0.016	0.003
P7 BS1	*I*SVE Branch sap	Plateau	04/05/2017	0.615	0.666	0.109	0.463	0.094	0.023	0.124	0.015	0.081	0.755	0.015	0.038	0.004	0.020	0.004

RP BS1	*I*SVE Branch sap	Riparian	04/05/2017	0.644	0.462	0.078	0.318	0.074	0.019	0.100	0.010	0.046	0.327	0.008	0.018	0.002	0.009	0.001
P7 BS1	*I*SVE Branch sap	Plateau	16/05/2017	2.719	1.969	0.310	1.200	0.283	0.071	0.361	0.035	0.158	1.270	0.028	0.066	0.006	0.039	0.006
RP BS1	*I*SVE Branch sap	Riparian	16/05/2017	0.010	0.013	0.002	0.006	<LoQ	0.001	0.003	<LoQ	0.003	0.029	<LoQ	0.002	<LoQ	<LoQ	<LoQ
P7 BS1	*I*SVE Branch sap	Plateau	09/03/2020	0.689	1.089	0.176	0.832	0.174	0.049	0.275	0.033	0.182	1.998	0.037	0.099	0.010	0.047	0.006
P7 BS2	*I*SVE Branch sap	Plateau	09/03/2020	0.692	1.044	0.153	0.664	0.128	0.033	0.185	0.022	0.103	1.138	0.021	0.055	0.004	0.022	0.000
P7 BS3	*I*SVE Branch sap	Plateau	09/03/2020	0.647	1.047	0.200	0.974	0.193	0.051	0.299	0.034	0.178	1.878	0.036	0.094	0.009	0.045	0.006
P9 BS1	*I*SVE Branch sap	Hillslope	09/03/2020	0.233	0.378	0.118	0.656	0.200	0.050	0.249	0.033	0.178	1.278	0.034	0.094	0.010	0.048	0.005
P9 BS2	*I*SVE Branch sap	Hillslope	09/03/2020	0.580	0.864	0.260	1.230	0.254	0.060	0.308	0.029	0.114	0.798	0.019	0.043	0.004	0.019	0.002
P9 BS3	*I*SVE Branch sap	Hillslope	09/03/2020	0.434	0.752	0.150	0.729	0.146	0.037	0.194	0.022	0.111	0.889	0.021	0.052	0.006	0.026	0.001
RP1 BS1	*I*SVE Branch sap	Riparian	09/03/2020	0.359	0.644	0.073	0.371	0.089	0.025	0.120	0.013	0.059	0.434	0.011	0.025	0.002	0.011	0.000
RP1 BS2	*I*SVE Branch sap	Riparian	09/03/2020	0.589	0.676	0.098	0.424	0.088	0.028	0.143	0.015	0.072	0.641	0.013	0.030	0.003	0.012	0.002
RP1 BS3	*I*SVE Branch sap	Riparian	09/03/2020	0.303	0.365	0.086	0.447	0.096	0.026	0.152	0.015	0.059	0.476	0.012	0.024	0.002	0.010	<LoQ
RP3 BS1	*I*SVE Branch sap	Riparian	09/03/2020	0.148	0.229	0.024	0.102	0.026	0.011	0.029	0.003	0.012	0.084	0.003	0.007	0.000	0.003	<LoQ
RP3 BS2	*I*SVE Branch sap	Riparian	09/03/2020	0.459	0.748	0.116	0.558	0.129	0.040	0.174	0.017	0.069	0.553	0.014	0.029	0.003	0.016	0.000
RP3 BS3	*I*SVE Branch sap	Riparian	09/03/2020	0.120	0.269	0.044	0.251	0.074	0.021	0.106	0.011	0.042	0.332	0.008	0.018	0.002	0.009	0.001
P7 RS1	*I*SVE Root sap	Plateau	23/03/2017	0.749	0.847	0.141	0.611	0.117	0.032	0.153	0.019	0.101	1.007	0.021	0.052	0.006	0.028	0.004
P7 RS1	*I*SVE Root sap	Plateau	27/03/2017	0.407	0.439	0.069	0.279	0.058	0.017	0.088	0.012	0.060	0.557	0.012	0.032	0.003	0.017	0.002
P7 RS1	*I*SVE Root sap	Plateau	30/03/2017	0.946	0.965	0.143	0.606	0.115	0.035	0.167	0.022	0.117	1.105	0.023	0.058	0.006	0.031	0.005
P7 RS1	*I*SVE Root sap	Plateau	04/04/2017	0.932	0.918	0.141	0.599	0.113	0.038	0.175	0.021	0.115	1.102	0.023	0.061	0.006	0.031	0.005
P7 RS1	*I*SVE Root sap	Plateau	11/04/2017	1.023	1.013	0.125	0.503	0.084	0.028	0.117	0.014	0.077	0.821	0.016	0.041	0.004	0.019	0.003
P7 RS1	*I*SVE Root sap	Plateau	09/03/2020	0.805	0.872	0.126	0.552	0.095	0.033	0.157	0.018	0.094	1.074	0.020	0.052	0.005	0.023	0.003
P7 RS2	*I*SVE Root sap	Plateau	09/03/2020	0.650	0.911	0.138	0.640	0.123	0.036	0.192	0.024	0.139	1.593	0.029	0.076	0.007	0.036	0.005
P7 RS3	*I*SVE Root sap	Plateau	09/03/2020	0.894	0.947	0.136	0.575	0.100	0.031	0.144	0.016	0.081	0.872	0.016	0.041	0.004	0.019	0.002
P9 RS1	*I*SVE Root sap	Hillslope	09/03/2020	1.853	2.380	0.532	2.397	0.504	0.124	0.645	0.070	0.360	2.505	0.066	0.165	0.019	0.099	0.014
P9 RS2	*I*SVE Root sap	Hillslope	09/03/2020	1.286	1.283	0.239	0.956	0.182	0.049	0.222	0.022	0.100	0.863	0.018	0.042	0.004	0.019	0.002
P9 RS3	*I*SVE Root sap	Hillslope	09/03/2020	6.484	7.002	1.564	6.603	1.212	0.280	1.441	0.138	0.629	4.548	0.105	0.242	0.023	0.118	0.016
RP RS1	*I*SVE Root sap	Riparian	09/03/2020	0.786	1.108	0.132	0.606	0.147	0.042	0.202	0.023	0.110	0.841	0.020	0.043	0.004	0.023	0.001
P7 BS PP (mix)	Overp. Branch sap	Plateau	06/07/2020	0.059	0.086	0.021	0.127	0.024	0.006	0.044	0.006	0.027	0.217	0.007	0.016	0.001	0.006	<LoQ
P9 PP (mix)	Overp. Branch sap	Hillslope	06/07/2020	0.038	0.051	0.011	0.059	0.011	0.003	0.018	0.003	0.009	0.064	0.004	0.004	0.000	0.001	<LoQ
RP BS PP (mix)	Overp. Branch sap	Riparian	06/07/2020	0.063	0.116	0.020	0.101	0.035	0.006	0.032	0.004	0.019	0.102	0.005	0.010	0.001	0.007	<LoQ
P7 BS PP (mix)	Overp. Branch sap	Plateau	10/08/2020	0.030	0.048	0.007	0.238	0.008	0.000	0.012	0.002	0.005	0.049	0.002	0.004	0.000	0.001	<LoQ
P9 PP (mix)	Overp. Branch sap	Hillslope	10/08/2020	0.049	0.072	0.015	0.074	0.023	0.003	0.019	0.003	0.009	0.055	0.002	0.005	0.000	0.003	<LoQ
RP BS PP (mix)	Overp. Branch sap	Riparian	10/08/2020	0.072	0.083	0.014	0.075	0.018	0.005	0.031	0.004	0.013	0.091	0.003	0.006	0.000	0.004	<LoQ
P7 SS20	Soil Sol. 20 cm	Plateau	27/03/2017	0.226	0.690	0.071	0.302	0.070	0.015	0.070	0.010	0.056	0.301	0.010	0.030	0.004	0.028	0.004
P7 SS20	Soil Sol. 20 cm	Plateau	30/03/2017	0.195	0.655	0.062	0.257	0.059	0.014	0.063	0.008	0.046	0.252	0.008	0.025	0.003	0.025	0.003
P7 SS20	Soil Sol. 20 cm	Plateau	04/04/2017	0.190	0.635	0.058	0.246	0.054	0.013	0.057	0.008	0.045	0.254	0.009	0.024	0.003	0.025	0.004
P7 SS20	Soil Sol. 20 cm	Plateau	11/04/2017	0.183	0.636	0.055	0.241	0.055	0.013	0.058	0.008	0.043	0.241	0.008	0.023	0.003	0.022	0.003
P7 SS20	Soil Sol. 20 cm	Plateau	20/04/2017	0.169	0.618	0.053	0.228	0.052	0.013	0.054	0.008	0.043	0.237	0.008	0.023	0.003	0.022	0.004
P7 SS20	Soil Sol. 20 cm	Plateau	28/04/2017	0.150	0.526	0.047	0.198	0.046	0.011	0.045	0.006	0.037	0.207	0.007	0.020	0.003	0.020	0.003
P7 SS20	Soil Sol. 20 cm	Plateau	04/05/2017	0.143	0.499	0.045	0.187	0.040	0.010	0.046	0.006	0.035	0.197	0.007	0.020	0.003	0.018	0.003
P7 SS20	Soil Sol. 20 cm	Plateau	16/05/2017	0.152	0.523	0.047	0.202	0.045	0.011	0.046	0.006	0.037	0.207	0.007	0.020	0.003	0.020	0.003
P7 SS20	Soil Sol. 20 cm	Plateau	09/03/2020	0.118	0.428	0.038	0.165	0.036	0.009	0.038	0.006	0.032	0.192	0.006	0.019	0.003	0.019	<LoQ
P9 SS20	Soil Sol. 20 cm	Hillslope	09/03/2020	0.313	0.868	0.084	0.350	0.071	0.017	0.081	0.011	0.067	0.391	0.011	0.031	0.004	0.027	<LoQ
RP SS1	Soil Sol. 20 cm	Riparian	09/03/2020	0.175	0.309	0.039	0.160	0.034	0.007	0.037	0.005	0.031	0.210	0.006	0.018	0.002	0.017	<LoQ

RP SS2	Soil Sol. 20 cm	Riparian	09/03/2020	0.155	0.262	0.031	0.126	0.022	0.005	0.025	0.004	0.021	0.160	0.004	0.012	0.002	0.013	<LoQ
RP SS3	Soil Sol. 20 cm	Riparian	09/03/2020	0.187	0.334	0.045	0.195	0.050	0.011	0.052	0.007	0.038	0.256	0.008	0.024	0.003	0.024	<LoQ
P7 SS20	Soil Sol. 20 cm	Plateau	11/03/2020	0.117	0.436	0.042	0.157	0.034	0.009	0.028	0.006	0.032	0.175	0.006	0.016	0.003	0.020	<LoQ
P7 SS20	Soil Sol. 20 cm	Plateau	13/03/2020	0.117	0.436	0.042	0.157	0.034	0.009	0.028	0.006	0.032	0.175	0.006	0.016	0.003	0.020	<LoQ
P7 SS20	Soil Sol. 20 cm	Plateau	06/05/2020	0.298	0.947	0.094	0.415	0.098	0.023	0.100	0.015	0.082	0.464	0.014	0.043	0.006	0.042	<LoQ
P9 SS20	Soil Sol. 20 cm	Hillslope	06/05/2020	0.270	0.634	0.067	0.266	0.053	0.011	0.053	0.007	0.040	0.230	0.007	0.021	0.003	0.018	<LoQ
RP SS1	Soil Sol. 20 cm	Riparian	06/05/2020	0.076	0.136	0.017	0.067	0.015	0.004	0.017	0.002	0.013	0.081	0.003	0.008	0.001	0.008	<LoQ
RP SS2	Soil Sol. 20 cm	Riparian	06/05/2020	0.145	0.304	0.039	0.172	0.042	0.010	0.051	0.007	0.038	0.218	0.007	0.023	0.003	0.020	<LoQ
RP SS3	Soil Sol. 20 cm	Riparian	06/05/2020	0.107	0.224	0.033	0.158	0.040	0.011	0.052	0.006	0.035	0.180	0.006	0.019	0.003	0.018	<LoQ
P7 SS20	Soil Sol. 20 cm	Plateau	25/05/2020	0.119	0.413	0.039	0.165	0.041	0.009	0.043	0.006	0.034	0.203	0.006	0.019	0.003	0.020	<LoQ
P9 SS20	Soil Sol. 20 cm	Hillslope	25/05/2020	0.216	0.532	0.058	0.238	0.047	0.010	0.046	0.006	0.035	0.217	0.007	0.019	0.003	0.019	<LoQ
RP SS1	Soil Sol. 20 cm	Riparian	25/05/2020	0.034	0.071	0.010	0.046	0.012	0.003	0.014	0.002	0.011	0.058	0.002	0.007	<LoQ	0.005	<LoQ
RP SS2	Soil Sol. 20 cm	Riparian	25/05/2020	0.054	0.148	0.020	0.091	0.030	0.007	0.034	0.004	0.026	0.122	0.004	0.014	0.002	0.014	<LoQ
RP SS3	Soil Sol. 20 cm	Riparian	25/05/2020	0.053	0.129	0.021	0.112	0.036	0.008	0.042	0.005	0.027	0.137	0.005	0.014	0.002	0.015	<LoQ
RP SS1	Soil Sol. 20 cm	Riparian	15/06/2020	0.027	0.057	0.009	0.040	0.012	0.003	0.016	0.002	0.010	0.056	0.002	0.006	<LoQ	0.005	<LoQ
RP SS2	Soil Sol. 20 cm	Riparian	15/06/2020	0.024	0.066	0.009	0.043	0.014	0.004	0.017	0.002	0.013	0.060	0.002	0.008	<LoQ	0.008	<LoQ
RP SS3	Soil Sol. 20 cm	Riparian	15/06/2020	0.049	0.121	0.020	0.102	0.034	0.009	0.041	0.005	0.026	0.138	0.005	0.015	0.002	0.014	<LoQ
RP SS1	Soil Sol. 20 cm	Riparian	06/07/2020	0.076	0.166	0.026	0.124	0.042	0.010	0.049	0.006	0.032	0.171	0.006	0.017	0.002	0.013	<LoQ
RP SS2	Soil Sol. 20 cm	Riparian	06/07/2020	0.026	0.069	0.009	0.045	0.015	0.004	0.017	0.002	0.013	0.062	0.002	0.007	<LoQ	0.008	<LoQ
RP SS3	Soil Sol. 20 cm	Riparian	06/07/2020	0.058	0.149	0.025	0.136	0.041	0.010	0.049	0.006	0.034	0.168	0.006	0.017	0.002	0.016	<LoQ
RP SS1	Soil Sol. 20 cm	Riparian	10/08/2020	0.018	0.047	0.008	0.042	0.013	0.003	0.018	0.002	0.013	0.065	0.002	0.006	<LoQ	0.005	<LoQ
RP SS2	Soil Sol. 20 cm	Riparian	10/08/2020	0.024	0.067	0.009	0.043	0.013	0.004	0.016	0.002	0.012	0.058	0.002	0.007	<LoQ	0.007	<LoQ
RP SS3	Soil Sol. 20 cm	Riparian	10/08/2020	0.061	0.154	0.026	0.142	0.043	0.010	0.051	0.006	0.032	0.165	0.005	0.018	0.002	0.017	<LoQ
P7 SS40	Soil Sol. 40 cm	Plateau	09/03/2020	0.349	0.976	0.087	0.367	0.092	0.017	0.084	0.010	0.063	0.465	0.012	0.037	0.005	0.028	<LoQ
P9 SS40	Soil Sol. 40 cm	Hillslope	09/03/2020	0.612	1.102	0.115	0.474	0.089	0.019	0.096	0.013	0.076	0.599	0.015	0.048	0.006	0.039	<LoQ
P7 SS40	Soil Sol. 40 cm	Plateau	06/05/2020	0.313	0.897	0.083	0.349	0.074	0.016	0.080	0.011	0.062	0.434	0.012	0.037	0.005	0.030	<LoQ
P9 SS40	Soil Sol. 40 cm	Hillslope	06/05/2020	0.728	1.159	0.117	0.451	0.079	0.017	0.089	0.012	0.076	0.549	0.014	0.042	0.006	0.034	<LoQ
P7 SS40	Soil Sol. 40 cm	Plateau	25/05/2020	0.134	0.442	0.039	0.167	0.038	0.009	0.041	0.005	0.030	0.193	0.005	0.016	0.002	0.016	<LoQ
P9 SS40	Soil Sol. 40 cm	Hillslope	25/05/2020	0.078	0.164	0.021	0.092	0.020	0.005	0.024	0.003	0.025	0.208	0.006	0.020	0.003	0.019	<LoQ
P7 SS60	Soil Sol. 60 cm	Plateau	30/03/2017	0.369	0.742	0.054	0.214	0.033	0.008	0.046	0.008	0.040	0.296	0.009	0.020	0.003	0.017	0.002
P7 SS60	Soil Sol. 60 cm	Plateau	04/04/2017	0.296	0.598	0.035	0.124	0.017	0.006	0.031	0.005	0.031	0.233	0.005	0.014	0.002	0.010	0.001
P7 SS60	Soil Sol. 60 cm	Plateau	11/04/2017	0.409	0.836	0.062	0.235	0.044	0.012	0.072	0.010	0.063	0.418	0.011	0.028	0.003	0.017	0.003
P7 SS60	Soil Sol. 60 cm	Plateau	09/03/2020	0.326	0.775	0.062	0.258	0.050	0.014	0.069	0.011	0.059	0.418	0.011	0.029	0.003	0.020	<LoQ
P7 SS60	Soil Sol. 60 cm	Plateau	06/05/2020	0.304	0.702	0.058	0.238	0.045	0.012	0.064	0.009	0.056	0.409	0.010	0.027	0.003	0.020	<LoQ
SW	Streamwater	Riparian	09/03/2020	0.009	0.017	0.004	0.027	0.010	0.002	0.011	0.001	0.006	0.030	0.001	0.004	<LoQ	0.004	<LoQ
SW	Streamwater	Riparian	06/05/2020	0.019	0.033	0.011	0.056	0.021	0.006	0.024	0.003	0.016	0.064	0.003	0.008	<LoQ	0.007	<LoQ
SW	Streamwater	Riparian	25/05/2020	0.024	0.042	0.011	0.072	0.025	0.006	0.029	0.003	0.017	0.078	0.003	0.009	<LoQ	0.008	<LoQ
SW	Streamwater	Riparian	15/06/2020	0.026	0.049	0.014	0.077	0.029	0.008	0.033	0.004	0.020	0.087	0.004	0.010	0.001	0.010	<LoQ

Table A5.2: REEs concentrations in *Fagus sylvatica* compartments treated in Chapter 5.

Sample name	Sample type	La	Ce	Pr	Nd	Sm	Eu	Gd	Tb	Dy	Y	Ho	Er	Tm	Yb	Lu
		ng/g	*ng/g*	*ng/g*	*ng/g*	*ng/g*	*ng/g*	*ng/g*	*ng/g*	*ng/g*	*ng/g*	*ng/g*	*ng/g*	*ng/g*	*ng/g*	*ng/g*
Lux-H-2-BGB	Big branch wood	7.33	9.62	1.12	4.26	1.05	0.37	1.26	0.14	0.57	3.39	0.10	0.25	0.03	0.15	0.04
Lux-H-3-BGB	Big branch wood	4.66	7.10	0.70	2.79	0.66	0.36	0.83	0.09	0.51	2.71	0.07	0.20	0.02	0.12	0.03
Lux-H-1-BT	Bole wood	8.92	10.33	0.84	2.80	0.55	0.27	0.72	0.07	0.39	2.37	0.05	0.14	0.02	0.08	0.02
Lux-H-2-BT	Bole wood	3.39	3.66	0.50	1.87	0.51	0.24	0.59	0.05	0.26	1.53	0.05	0.11	0.01	0.08	0.02
Lux-H-3-BT	Bole wood	3.63	4.97	0.38	1.21	0.29	0.28	0.30	0.04	0.17	1.23	0.04	0.08	0.01	0.06	0.02
Lux-H-1-EGB	Big branch bark	92.35	136.37	18.54	68.78	13.62	4.08	13.72	1.78	8.08	52.62	1.46	4.05	0.46	2.52	0.45
Lux-H-2-EGB	Big branch bark	69.34	113.97	15.95	65.69	14.18	4.72	15.23	1.67	8.48	49.42	1.36	3.66	0.49	2.59	0.46
Lux-H-3-EGB	Big branch bark	80.24	141.04	17.22	67.30	14.57	4.34	14.28	1.78	9.00	53.81	1.63	4.54	0.55	3.21	0.49
Lux-H-1-EText	Bole external bark	63.85	118.96	14.44	54.90	11.01	3.76	10.70	1.46	8.04	45.16	1.75	4.27	0.62	3.88	0.68
Lux-H-2-EText	Bole external bark	131.14	308.30	38.14	147.55	30.27	7.45	27.88	3.92	22.67	126.90	4.32	11.71	1.49	10.26	1.40
Lux-H-3-EText	Bole external bark	66.88	140.48	17.56	68.95	12.61	4.46	13.52	1.86	9.79	55.01	1.76	4.44	0.57	3.94	0.56
Lux-H-1-ETint	Bole internal bark	48.56	45.48	5.74	22.20	3.99	3.09	5.44	0.48	2.41	18.58	0.40	1.13	0.11	0.61	0.17
Lux-H-2-ETint	Bole internal bark	20.70	23.19	3.88	16.55	3.50	2.39	5.03	0.54	2.19	12.56	0.33	0.69	0.09	0.36	0.11
Lux-H-3-ETint	Bole internal bark	19.84	22.34	3.38	13.73	4.07	3.28	4.50	0.50	2.07	10.19	0.33	0.54	0.06	0.31	0.12
Lux-H-1-PBtot	Smal branch total	87.65	143.37	16.14	61.16	10.82	2.78	10.78	1.42	7.44	46.51	1.38	3.70	0.45	2.89	0.40
Lux-H-2-PBtot	Smal branch total	68.45	114.05	13.92	53.99	11.31	2.89	11.02	1.40	6.71	41.30	1.29	3.49	0.47	2.49	0.45
Lux-H-3-PBtot	Smal branch total	55.64	91.49	10.42	40.40	8.38	2.30	7.79	1.07	5.49	32.43	1.08	2.84	0.34	2.06	0.38
Lux-H-3-R0-10	Roots 0-10 cm	339.69	879.47	79.13	290.28	61.89	12.89	51.76	7.84	44.97	194.64	7.36	20.80	2.35	18.71	3.23
Lux-H-1-R0-10	Roots 0-10 cm	639.09	1612.01	168.03	626.78	129.96	26.37	108.88	12.75	59.42	249.15	10.08	26.23	3.34	19.52	3.86
Lux-H-2-R0-10	Roots 0-10 cm	521.60	1445.29	121.13	465.27	98.51	22.48	88.67	11.63	68.16	298.44	12.30	28.93	3.79	23.50	3.78
Lux-H-1-R10-30	Roots 10-30 cm	2048.30	8102.05	675.18	2736.52	619.77	143.47	581.15	67.95	300.08	1207.48	52.31	123.88	17.06	110.04	15.91
Lux-H-2-R10-30	Roots 10-30 cm	897.38	2649.36	213.06	802.92	162.07	38.41	155.15	16.49	85.76	409.69	14.11	38.89	5.04	26.61	5.71
Lux-H-3-R10-30	Roots 10-30 cm	1997.45	5083.17	485.34	1864.53	345.74	85.15	367.24	42.80	193.30	951.40	31.44	75.13	10.64	56.58	9.28

Table A5.3: DOC concentrations for root and branch sap samples and soil solutions treated in Chapter 5.

Sample name	Sample type	Site	Date	DOC *mg/L*
P7 BS1	*I*SVE Branch sap	Plateau	23/03/2017	2417
P7 BS1	*I*SVE Branch sap	Plateau	27/03/2017	2277
P7 BS1	*I*SVE Branch sap	Plateau	30/03/2017	1763
P7 BS1	*I*SVE Branch sap	Plateau	04/04/2017	1480
P7 BS1	*I*SVE Branch sap	Plateau	11/04/2017	1314
RP BS1	*I*SVE Branch sap	Riparian	11/04/2017	1606
P7 BS1	*I*SVE Branch sap	Plateau	20/04/2017	1270
P7 BS1	*I*SVE Branch sap	Plateau	28/04/2017	279
P7 BS1	*I*SVE Branch sap	Plateau	04/05/2017	249
RP BS1	*I*SVE Branch sap	Riparian	04/05/2017	1209
RP BS1	*I*SVE Branch sap	Riparian	16/05/2017	638
P7 BS1	*I*SVE Branch sap	Plateau	09/03/2020	3543
P7 BS2	*I*SVE Branch sap	Plateau	09/03/2020	2338
P7 BS3	*I*SVE Branch sap	Plateau	09/03/2020	3983
P9 BS1	*I*SVE Branch sap	Hillslope	09/03/2020	2030
P9 BS2	*I*SVE Branch sap	Hillslope	09/03/2020	2924
P9 BS3	*I*SVE Branch sap	Hillslope	09/03/2020	2665
RP1 BS1	*I*SVE Branch sap	Riparian	09/03/2020	2814
RP1 BS2	*I*SVE Branch sap	Riparian	09/03/2020	1824
RP1 BS3	*I*SVE Branch sap	Riparian	09/03/2020	2711
RP3 BS1	*I*SVE Branch sap	Riparian	09/03/2020	1459
RP3 BS2	*I*SVE Branch sap	Riparian	09/03/2020	1977
RP3 BS3	*I*SVE Branch sap	Riparian	09/03/2020	2159
P7 RS1	*I*SVE Root sap	Plateau	09/03/2020	421

P7 RS2	*IS*VE Root sap	Plateau	09/03/2020	92
P7 RS3	*IS*VE Root sap	Plateau	09/03/2020	3141
P9 RS1	*IS*VE Root sap	Hillslope	09/03/2020	377
P9 RS2	*IS*VE Root sap	Hillslope	09/03/2020	466
P9 RS3	*IS*VE Root sap	Hillslope	09/03/2020	134
RP RS1	*IS*VE Root sap	Riparian	09/03/2020	211
P7 SS20	Soil Solution 20 cm	Plateau	09/03/2020	13
P9 SS20	Soil Solution 20 cm	Hillslope	09/03/2020	22
RP SS1	Soil Solution 20 cm	Riparian	09/03/2020	7
RP SS2	Soil Solution 20 cm	Riparian	09/03/2020	6
RP SS3	Soil Solution 20 cm	Riparian	09/03/2020	7
P7 SS40	Soil Solution 40 cm	Plateau	09/03/2020	10
P9 SS40	Soil Solution 40 cm	Hillslope	09/03/2020	7
P7 SS60	Soil Solution 60 cm	Plateau	09/03/2020	16

Appendix to Chapter 6

Table A6.1: REEs concentrations for all samples collected for the study in Chapter 6. In black the accepted values, in blue the values below the limit of quantification (LoQ), DL is the detection limit. Some values that fall below the LoQ are in black (accepted) as the samples were pre-concentrated during the digestion step and the analytical concentrations were above the LoQ before applying the pre-concentration factor.

Sample name	Sample type	Sample date	La *ng/L*	Ce *ng/L*	Pr *ng/L*	Nd *ng/L*	Sm *ng/L*	Eu *ng/L*	Gd *ng/L*	Tb *ng/L*	Dy *ng/L*	Y *ng/L*	Ho *ng/L*	Er *ng/L*	Tm *ng/L*	Yb *ng/L*	Lu *ng/L*
LoQ	-	-	1	1	1	5	5	1	5	1	5	1	5	1	5	1	5
P7 TW Blank	Blank	25/05/2020	<DL	<DL	<DL	<DL	<DL	<DL	<DL	<DL	<DL	<DL	<DL	<DL	<DL	<DL	<DL
P9 TW Blank	Blank	25/05/2020	<DL	<DL	<DL	<DL	<DL	<DL	<DL	<DL	<DL	<DL	<DL	<DL	<DL	<DL	<DL
RP TW Blank	Blank	25/05/2020	<DL	<DL	<DL	<DL	<DL	<DL	<DL	<DL	<DL	<DL	<DL	<DL	<DL	<DL	<DL
P7 TW Blank	Blank	15/06/2020	<DL	<DL	<DL	<DL	<DL	<DL	<DL	<DL	<DL	<DL	<DL	<DL	<DL	<DL	<DL
P9 TW Blank	Blank	15/06/2020	<DL	<DL	<DL	<DL	<DL	<DL	<DL	<DL	<DL	<DL	<DL	<DL	<DL	<DL	<DL
RP TW Blank	Blank	15/06/2020	<DL	<DL	<DL	<DL	<DL	<DL	<DL	<DL	<DL	<DL	<DL	<DL	<DL	<DL	<DL
RP TW Blank	Blank	15/06/2020	<DL	<DL	<DL	<DL	<DL	<DL	<DL	<DL	<DL	<DL	<DL	<DL	<DL	<DL	<DL
P7 TW Blank	Blank	06/07/2020	<DL	<DL	<DL	<DL	<DL	<DL	<DL	<DL	<DL	<DL	<DL	<DL	<DL	<DL	<DL
P9 TW Blank	Blank	06/07/2020	<DL	<DL	<DL	<DL	<DL	<DL	<DL	<DL	<DL	<DL	<DL	<DL	<DL	<DL	<DL
RP TW Blank	Blank	06/07/2020	<DL	<DL	<DL	<DL	<DL	<DL	<DL	<DL	<DL	<DL	<DL	<DL	<DL	<DL	<DL
P7 TW Blank	Blank	10/08/2020	<DL	<DL	<DL	<DL	<DL	<DL	<DL	<DL	<DL	<DL	<DL	<DL	<DL	<DL	<DL
P9 TW Blank	Blank	10/08/2020	<DL	<DL	<DL	<DL	<DL	<DL	<DL	<DL	<DL	<DL	<DL	<DL	<DL	<DL	<DL
RP TW Blank	Blank	10/08/2020	<DL	<DL	<DL	<DL	<DL	<DL	<DL	<DL	<DL	<DL	<DL	<DL	<DL	<DL	<DL
P7 TW Blank	Blank	25/09/2020	<DL	<DL	<DL	<DL	<DL	<DL	<DL	<DL	<DL	<DL	<DL	<DL	<DL	<DL	<DL
P9 TW Blank	Blank	25/09/2020	<DL	<DL	<DL	<DL	<DL	<DL	<DL	<DL	<DL	<DL	<DL	<DL	<DL	<DL	<DL
Rain	Rainfall	09/03/2020	1.26	2.83	0.52	<DL	1.49	0.03	0.13	<DL	0.50	0.71	0.07	0.18	<DL	0.44	0.31
Rain	Rainfall	20/05/2020	3.63	7.35	0.67	1.26	0.18	0.17	0.36	<DL	0.59	2.82	0.13	0.35	<DL	0.35	0.27
Rain	Rainfall	25/05/2020	5.31	10.09	1.41	4.26	0.19	0.48	1.46	0.04	1.30	7.77	0.33	1.15	<DL	1.07	0.35
Rain	Rainfall	10/06/2020	0.35	0.72	0.07	<DL	0.64	0.03	<DL	<DL	0.20	0.04	0.06	0.28	<DL	0.30	0.33
Rain	Rainfall	17/06/2020	0.96	2.06	0.31	0.04	1.21	0.01	0.22	<DL	0.51	0.88	0.11	0.29	<DL	0.40	0.39
Rain	Rainfall	30/06/2020	2.75	5.05	0.83	1.76	1.67	<DL	0.42	0.03	0.46	3.21	0.22	0.60	<DL	0.59	0.31

Rain	Rainfall	01/09/2020	2.51	4.20	0.65	0.20	1.31	0.17	0.09	-	0.40	1.79	0.21	0.28	<DL	0.44	0.27
P7 TH1	Throughfall	09/03/2020	7.27	13.05	1.70	6.86	0.47	0.16	1.91	0.22	0.48	4.03	<DL	0.34	0.12	0.09	<DL
P7 TH2	Throughfall	09/03/2020	8.97	18.64	2.04	8.65	1.52	0.10	2.30	0.25	0.86	5.93	0.09	0.55	0.06	0.35	<DL
P7 TH3	Throughfall	09/03/2020	15.76	30.35	3.13	11.66	2.12	0.25	2.58	0.29	1.62	9.47	0.29	0.57	0.13	0.64	<DL
P9 TH1	Throughfall	09/03/2020	2.47	4.36	0.77	1.67	0.41	<DL	0.98	0.06	<DL	0.54	<DL	0.04	0.01	<DL	<DL
P9 TH2	Throughfall	09/03/2020	12.17	22.06	2.50	8.85	1.65	0.04	2.25	0.23	0.60	4.06	<DL	0.38	0.02	0.43	<DL
P9 TH3	Throughfall	09/03/2020	7.56	14.02	2.19	9.72	0.71	0.43	2.43	0.40	1.07	6.60	<DL	0.81	0.07	0.30	<DL
RP TH1	Throughfall	09/03/2020	1.87	3.41	0.61	2.63	0.31	<DL	0.96	0.09	<DL	1.05	<DL	0.10	0.03	0.19	<DL
RP TH2	Throughfall	09/03/2020	1.14	1.58	0.29	1.31	<DL	<DL	0.74	0.08	<DL	0.06	<DL	0.08	0.03	<DL	<DL
RP TH3	Throughfall	09/03/2020	3.07	4.10	0.62	2.74	0.95	<DL	1.43	0.06	0.06	1.52	<DL	<DL	0.03	0.03	<DL
P9 TH1	Throughfall	06/05/2020	11.28	9.65	2.24	9.43	3.30	0.38	4.87	0.70	4.66	43.04	0.84	3.41	0.44	2.93	0.18
P9 TH2	Throughfall	06/05/2020	15.59	22.10	4.20	20.16	4.95	0.93	8.32	0.72	4.92	40.14	0.97	3.27	0.32	2.19	<DL
P9 TH3	Throughfall	06/05/2020	18.04	27.19	5.13	24.27	7.35	1.49	8.58	1.17	5.92	52.82	1.06	4.29	0.64	3.37	0.22
RP TH1	Throughfall	06/05/2020	13.20	21.30	3.13	15.11	4.92	0.70	4.64	0.54	2.74	28.18	0.55	2.21	0.20	1.23	<DL
RP TH2	Throughfall	06/05/2020	45.22	69.95	9.65	39.58	7.85	1.62	10.36	1.42	8.21	59.46	1.26	4.49	0.47	2.09	0.11
RP TH3	Throughfall	06/05/2020	14.38	23.43	4.21	18.28	3.60	0.77	5.65	0.74	3.28	25.87	0.51	1.89	0.20	1.55	<DL
P7 TH (mix)	Throughfall	20/05/2020	90.15	165.06	24.68	109.37	26.70	6.50	29.95	4.31	26.15	172.75	4.80	13.38	1.70	9.43	0.96
P7 TH (mix)	Throughfall	25/05/2020	55.83	104.18	14.15	63.50	14.92	2.81	13.41	2.05	12.50	79.56	2.57	6.78	1.08	6.44	0.57
P9 TH (mix)	Throughfall	25/05/2020	27.93	42.79	8.12	45.17	9.31	2.58	12.63	2.18	12.74	87.33	3.00	7.42	1.06	5.47	0.33
RP TH1	Throughfall	25/05/2020	6.86	7.06	0.90	4.99	0.96	0.26	1.74	<DL	1.41	16.18	0.25	1.19	<DL	0.89	<DL
RP TH2	Throughfall	25/05/2020	9.34	14.64	2.03	10.38	1.50	0.51	3.31	<DL	2.25	25.70	0.56	1.81	<DL	1.85	<DL
RP TH3	Throughfall	25/05/2020	11.55	16.39	2.37	13.43	2.18	0.68	3.34	<DL	2.98	28.01	0.63	2.09	<DL	1.26	<DL
P7 TH3	Throughfall	10/06/2020	38.41	73.90	10.41	42.29	8.92	2.25	10.04	0.74	5.77	42.11	1.28	3.18	0.26	2.60	<DL
P9 TH1	Throughfall	15/06/2020	9.08	17.64	1.88	12.13	1.10	0.41	2.12	<DL	1.58	8.13	0.24	0.74	<DL	0.14	<DL
P9 TH2	Throughfall	15/06/2020	13.81	26.17	2.95	17.63	2.40	0.81	3.43	<DL	2.60	15.21	0.42	1.73	<DL	0.44	<DL
P9 TH3	Throughfall	15/06/2020	8.83	12.49	2.01	9.86	1.58	0.20	2.09	<DL	1.72	16.96	<DL	1.02	<DL	0.60	<DL
RP TH1	Throughfall	15/06/2020	2.95	6.03	0.75	5.49	0.19	0.07	0.99	<DL	0.59	2.71	<DL	0.29	<DL	<DL	<DL
RP TH2	Throughfall	15/06/2020	8.40	19.28	2.28	11.36	2.68	0.41	3.08	<DL	1.45	11.06	0.27	0.68	<DL	0.46	<DL
RP TH3	Throughfall	15/06/2020	7.56	15.58	2.00	10.61	1.04	0.23	1.72	<DL	1.38	8.71	0.21	0.53	<DL	<DL	<DL
P7 TH1	Throughfall	17/06/2020	31.08	64.44	7.06	36.95	6.21	1.54	7.73	1.11	6.59	33.37	1.37	3.12	0.61	2.84	<DL
P7 TH2	Throughfall	17/06/2020	39.99	76.22	11.50	48.17	9.59	1.82	9.69	1.74	8.75	50.73	1.91	4.66	0.83	3.40	0.13
P7 TH3	Throughfall	17/06/2020	25.26	53.43	7.73	33.36	6.04	1.85	7.12	1.20	3.99	32.36	1.18	2.26	0.52	2.67	<DL

P7 TH1	Throughfall	24/06/2020	5.81	11.93	1.64	7.23	1.90	0.60	1.50	0.44	0.74	8.81	0.44	0.38	0.21	0.94	<DL
P7 TH2	Throughfall	24/06/2020	20.90	40.83	5.85	27.94	5.46	1.56	5.66	0.97	3.90	29.99	0.89	2.31	0.35	2.60	<DL
P7 TH3	Throughfall	24/06/2020	9.24	25.09	3.94	17.88	2.79	1.30	3.21	0.67	2.82	17.93	0.71	1.96	0.31	1.51	<DL
P7 TH (mix)	Throughfall	30/06/2020	34.00	60.84	8.00	33.12	6.88	1.64	6.73	1.11	5.94	31.85	1.21	3.19	0.54	2.30	0.10
P7 TH (mix)	Throughfall	06/07/2020	45.03	66.30	8.34	39.17	10.07	2.10	9.04	1.29	6.41	54.44	1.96	4.21	0.78	4.34	0.08
P9 TH1	Throughfall	06/07/2020	15.50	18.39	2.92	13.47	3.22	0.92	2.26	0.41	1.60	21.55	0.51	1.36	0.36	1.61	<DL
P9 TH2	Throughfall	06/07/2020	21.51	28.36	4.08	19.16	4.45	1.01	3.16	0.91	2.84	32.17	0.51	2.08	0.34	2.04	<DL
P9 TH3	Throughfall	06/07/2020	19.35	26.52	3.90	15.82	3.27	0.94	2.75	0.55	1.76	22.49	0.52	1.02	0.28	1.30	<DL
RP TH1	Throughfall	06/07/2020	10.32	17.11	3.07	14.10	4.66	1.09	2.83	0.76	2.93	25.38	0.68	1.77	0.41	1.57	<DL
RP TH2	Throughfall	06/07/2020	17.90	31.14	5.45	21.40	5.57	1.72	5.19	0.91	3.24	33.72	0.94	2.49	0.51	2.35	<DL
RP TH3	Throughfall	06/07/2020	13.14	27.37	4.75	16.41	4.77	1.76	4.44	0.96	3.76	29.23	0.88	2.16	0.36	2.47	<DL
P7 TH (mix)	Throughfall	04/08/2020	138.34	271.42	37.80	170.07	34.38	8.47	35.18	5.67	33.50	193.60	6.64	20.73	2.87	16.78	1.89
P9 TH (mix)	Throughfall	10/08/2020	33.25	60.77	8.86	45.47	10.08	2.12	9.51	1.45	8.10	58.08	1.84	5.86	0.68	4.22	0.32
RP TH1	Throughfall	10/08/2020	20.50	40.74	5.70	25.98	5.55	1.37	6.05	0.89	4.60	31.17	1.04	3.16	0.38	2.36	0.16
RP TH2	Throughfall	10/08/2020	61.97	126.44	17.31	80.82	15.92	4.44	20.21	2.99	16.35	110.51	3.74	8.24	1.48	7.09	0.31
RP TH3	Throughfall	10/08/2020	27.63	60.56	8.31	35.12	6.94	1.73	8.22	1.21	6.48	39.16	1.26	3.45	0.47	2.92	0.37
P7 TH1	Throughfall	01/09/2020	40.37	80.74	11.26	51.20	9.52	1.67	10.70	1.54	7.60	44.33	1.76	4.72	0.94	4.55	0.02
P9 TH (mix)	Throughfall	25/09/2020	126.25	252.85	38.31	158.99	28.59	9.36	32.89	5.13	28.12	180.45	6.59	15.71	2.74	18.00	2.22
P7 TW1	Transp. water	25/05/2020	7.13	9.27	1.68	6.50	0.87	0.27	2.10	<DL	1.77	16.41	0.30	1.27	<DL	0.38	<DL
P7 TW2	Transp. water	25/05/2020	5.74	8.32	0.88	5.85	1.37	0.30	1.42	<DL	0.38	7.14	0.16	0.63	<DL	<DL	<DL
P7 TW3	Transp. water	25/05/2020	4.52	4.41	0.71	3.22	0.47	0.05	1.46	<DL	0.24	10.95	<DL	0.49	<DL	<DL	<DL
P7 TW4	Transp. water	25/05/2020	4.74	5.48	0.55	2.96	0.18	0.16	1.33	<DL	0.91	10.35	<DL	0.66	<DL	<DL	<DL
P9 TW1	Transp. water	25/05/2020	17.84	50.24	5.78	25.24	6.10	1.00	4.69	<DL	2.52	18.24	0.43	1.44	<DL	1.20	<DL
P9 TW2	Transp. water	25/05/2020	9.63	14.02	2.28	10.26	1.92	0.46	3.29	<DL	1.86	17.11	0.32	1.16	<DL	0.11	<DL
P9 TW3	Transp. water	25/05/2020	10.57	15.00	2.31	10.45	0.67	0.53	2.18	<DL	1.85	18.38	0.31	1.16	<DL	0.28	<DL
RP1 TW1	Transp. water	25/05/2020	4.46	9.72	1.02	3.66	0.39	0.15	1.29	<DL	0.55	2.58	0.03	0.34	<DL	<DL	<DL
RP1 TW2	Transp. water	25/05/2020	2.42	4.44	0.38	2.16	0.01	0.27	0.59	<DL	0.05	1.43	0.00	0.34	<DL	<DL	<DL
RP1 TW3	Transp. water	25/05/2020	3.01	3.77	0.45	2.56	0.03	0.12	0.81	<DL	0.30	6.87	0.09	0.49	<DL	<DL	<DL
RP3 TW1	Transp. water	25/05/2020	11.76	16.47	3.19	14.29	4.48	0.97	5.47	<DL	4.08	34.80	0.77	2.71	<DL	1.16	<DL
RP3 TW2	Transp. water	25/05/2020	3.45	6.35	0.92	3.23	0.76	0.29	1.80	<DL	1.14	5.35	0.10	0.71	<DL	0.26	<DL
RP3 TW3	Transp. water	25/05/2020	2.93	3.51	0.39	2.28	0.17	0.16	1.69	<DL	1.38	13.04	0.38	2.61	0.14	2.78	<DL
P7 TW1	Transp. water	15/06/2020	19.61	31.02	4.35	23.98	3.66	0.92	5.27	0.94	2.74	34.93	1.45	5.28	0.69	5.05	0.41

P7 TW2	Transp. water	15/06/2020	8.25	8.17	1.36	5.47	1.00	0.28	1.39	0.28	1.78	12.19	0.40	0.87	0.13	0.63	<DL
P7 TW3	Transp. water	15/06/2020	11.04	8.82	1.96	8.49	3.46	0.88	1.96	0.54	1.95	36.82	0.87	1.92	0.72	4.29	0.12
P7 TW4	Transp. water	15/06/2020	5.83	4.56	0.87	3.25	1.20	0.48	1.55	0.39	0.74	20.39	0.51	1.68	0.48	3.25	0.01
P9 TW1	Transp. water	15/06/2020	8.82	13.54	2.17	7.99	2.00	0.43	2.32	0.51	1.39	15.03	0.65	1.86	0.49	2.93	<DL
P9 TW2	Transp. water	15/06/2020	10.18	15.65	2.75	11.42	1.61	1.01	2.81	0.52	2.86	20.22	0.63	2.58	0.60	4.05	0.16
P9 TW3	Transp. water	15/06/2020	6.24	7.33	1.33	6.83	<DL	<DL	1.61	0.39	2.38	15.35	0.57	1.66	0.39	3.97	<DL
P9 TW4	Transp. water	15/06/2020	3.86	3.96	0.67	2.90	1.00	0.27	0.24	0.29	0.12	6.40	0.17	0.25	0.17	0.63	<DL
RP1 TW1	Transp. water	15/06/2020	8.85	12.35	1.91	12.93	3.47	1.04	1.54	0.59	2.09	21.14	0.67	2.07	0.48	2.39	<DL
RP1 TW2	Transp. water	15/06/2020	5.65	6.63	1.04	6.52	2.21	0.82	1.65	0.41	2.26	20.49	0.94	3.37	0.93	4.50	0.08
RP1 TW3	Transp. water	15/06/2020	5.56	7.41	1.26	4.36	1.41	0.61	1.55	0.31	1.08	12.05	0.53	1.82	0.46	2.20	0.01
RP3 TW1	Transp. water	15/06/2020	19.68	9.74	1.86	9.52	2.44	0.69	2.41	0.74	2.72	30.71	1.14	4.48	0.84	4.73	0.42
RP3 TW2	Transp. water	15/06/2020	8.40	5.27	1.27	5.29	1.46	0.39	1.94	0.45	2.07	21.96	0.62	1.95	0.42	2.11	0.08
RP3 TW3	Transp. water	15/06/2020	50.56	16.20	3.24	16.14	3.48	0.98	4.35	0.74	4.62	40.60	1.06	3.15	0.46	2.90	0.18
P7 TW1	Transp. water	06/07/2020	5.55	7.13	1.21	5.32	1.11	0.34	1.67	0.28	1.41	12.01	0.48	1.28	0.28	1.47	0.18
P7 TW2	Transp. water	06/07/2020	7.11	8.60	1.03	5.38	1.13	0.20	1.09	0.22	1.37	8.38	0.33	0.92	0.20	1.24	0.05
P7 TW3	Transp. water	06/07/2020	21.33	15.68	3.15	14.26	3.29	1.13	4.30	0.80	3.32	61.89	1.45	4.05	0.58	3.36	0.03
P7 TW4	Transp. water	06/07/2020	23.80	17.78	4.16	18.73	5.15	1.54	6.02	1.22	5.68	85.77	1.56	6.72	1.03	6.64	0.75
P9 TW1	Transp. water	06/07/2020	5.71	6.41	0.89	5.02	1.24	0.09	1.05	0.23	1.20	10.86	0.34	1.24	0.30	2.53	0.30
P9 TW2	Transp. water	06/07/2020	7.22	11.00	1.51	6.85	1.59	0.37	1.53	0.31	1.35	9.84	0.34	1.15	0.24	1.53	0.04
P9 TW3	Transp. water	06/07/2020	18.19	17.06	3.15	13.91	3.71	1.27	4.84	0.80	3.53	38.02	0.96	2.48	0.55	3.29	0.08
P9 TW4	Transp. water	06/07/2020	2.44	3.17	0.46	1.27	0.07	0.34	0.87	0.25	0.39	6.43	0.20	0.07	0.15	0.86	<DL
RP1 TW1	Transp. water	06/07/2020	18.21	14.97	4.40	22.10	6.37	1.07	5.19	1.22	7.08	42.91	1.54	4.45	0.78	4.76	0.10
RP1 TW2	Transp. water	06/07/2020	2.98	3.10	0.41	2.22	0.26	<DL	0.60	0.14	0.42	3.73	0.19	0.36	0.08	0.34	<DL
RP1 TW3	Transp. water	06/07/2020	4.49	4.68	0.70	3.83	0.64	0.14	0.78	0.15	0.20	5.41	0.19	0.37	0.06	0.31	<DL
RP3 TW1	Transp. water	06/07/2020	18.93	19.81	4.58	28.52	7.28	1.51	6.57	1.43	6.37	44.25	1.53	3.88	0.78	3.75	0.08
RP3 TW2	Transp. water	06/07/2020	16.30	13.87	2.38	10.76	2.02	1.28	2.44	0.61	2.71	30.20	0.53	1.78	0.26	2.43	<DL
RP3 TW3	Transp. water	06/07/2020	17.62	20.55	5.38	28.11	6.76	1.85	10.04	1.39	8.06	62.55	2.06	5.47	0.62	3.76	0.28
P7 TW3	Transp. water	10/08/2020	8.97	10.17	1.69	7.05	1.15	0.13	2.60	0.31	0.42	21.16	0.66	1.64	0.30	1.06	<DL
P7 TW4	Transp. water	10/08/2020	13.97	21.65	3.50	15.02	2.63	0.99	3.32	0.81	2.55	27.66	0.84	2.03	0.33	1.55	<DL
P9 TW3	Transp. water	10/08/2020	13.84	19.54	2.88	15.38	1.91	0.37	3.51	0.62	2.44	23.21	0.75	1.53	0.29	1.63	<DL
P9 TW4	Transp. water	10/08/2020	2.19	4.46	0.28	2.81	<DL	<DL	0.89	0.26	0.01	5.81	0.30	0.58	0.08	0.28	<DL
RP1 TW2	Transp. water	10/08/2020	32.80	56.19	9.00	45.57	10.92	2.77	10.57	2.06	12.02	76.43	2.11	6.48	0.92	4.84	0.36

RP3 TW3	Transp. water	10/08/2020	9.33	16.87	2.53	11.47	2.80	0.48	3.63	0.50	1.43	16.16	0.70	1.74	0.21	1.20	<DL
P7 TW1	Transp. water	25/09/2020	30.10	52.00	7.26	34.74	10.34	1.71	6.50	1.22	6.12	52.49	1.57	3.67	0.62	3.28	<DL
P7 TW3	Transp. water	25/09/2020	16.84	32.17	4.32	24.33	3.98	0.99	5.19	0.96	4.28	26.58	1.34	2.48	0.33	2.33	<DL
P7 TW4	Transp. water	25/09/2020	9.58	17.41	2.68	14.19	2.17	0.72	2.01	0.55	1.84	18.53	0.63	1.87	0.35	1.47	<DL
P9 TW3	Transp. water	25/09/2020	21.89	37.47	5.49	22.33	5.09	0.73	6.30	0.85	2.32	30.34	1.14	2.82	0.48	2.36	<DL
P9 TW4	Transp. water	25/09/2020	9.97	15.11	1.86	9.62	1.01	0.25	2.09	0.40	1.01	15.72	0.58	1.84	0.27	0.70	<DL

Table A6.2: REEs concentrations (in ng g^{-1} in WEC atmospheric dust collected for this study.

Sample name	La	Ce	Pr	Nd	Sm	Eu	Gd	Tb	Dy	Y	Ho	Er	Tm	Yb	Lu
	ng/g	*ng/g*	*ng/g*	*ng/g*	*ng/g*	*ng/g*	*ng/g*	*ng/g*	*ng/g*	*ng/g*	*ng/g*	*ng/g*	*ng/g*	*ng/g*	*ng/g*
atm. dust	15025	29799	3396	13006	2400	531	2079	298	1866	9200	355	1110	154	1080	162

Appendix to Chapter 7

Table A7.1: Limits of quantification and blank values for the ICP-MS analysis of Rare Earth Elements and associated major and trace elements.

Sample	La	Ce	Pr	Nd	Sm	Eu	Gd	Tb	Dy	Y	Ho	Er	Tm	Yb	Lu	Na	K	Mg	Ca	Mn	Pb	Al	Fe
Unit	*ng/L*	*ng/L*	*ng/L*	*ng/L*	*ng/L*	*ng/L*	*ng/L*	*ng/L*	*ng/L*	*ng/L*	*ng/L*	*ng/L*	*ng/L*	*ng/L*	*ng/L*	*µg/L*	*µg/L*	*µg/L*	*µg/L*	*µg/L*	*ng/L*	*µg/L*	*µg/L*
LoQ	1	1	1	5	5	1	5	1	5	1	5	1	5	1	5	25	25	25	25	0.1	25	4	0.5
Min. blank-1	<LoQ	<LoQ	<LoQ	<LoQ	<LoQ	<LoQ	<LoQ	<LoQ	<LoQ	<LoQ	<LoQ	<LoQ	<LoQ	<LoQ	<LoQ	<LoQ	<LoQ	<LoQ	<LoQ	6.3	<LoQ	25.6	<LoQ
Min. blank-2	<LoQ	<LoQ	<LoQ	<LoQ	<LoQ	<LoQ	<LoQ	<LoQ	<LoQ	<LoQ	<LoQ	<LoQ	<LoQ	<LoQ	<LoQ	<LoQ	<LoQ	<LoQ	<LoQ	2.5	<LoQ	<LoQ	<LoQ
Min. blank-3	<LoQ	<LoQ	<LoQ	<LoQ	<LoQ	<LoQ	<LoQ	<LoQ	<LoQ	<LoQ	<LoQ	<LoQ	<LoQ	<LoQ	<LoQ	<LoQ	<LoQ	<LoQ	<LoQ	<LoQ	<LoQ	<LoQ	<LoQ
Min. blank-4	<LoQ	<LoQ	<LoQ	<LoQ	<LoQ	<LoQ	<LoQ	<LoQ	<LoQ	<LoQ	<LoQ	<LoQ	<LoQ	<LoQ	<LoQ	<LoQ	<LoQ	<LoQ	<LoQ	<LoQ	<LoQ	102	<LoQ
An. blank-1	<LoQ	<LoQ	<LoQ	<LoQ	<LoQ	<LoQ	<LoQ	<LoQ	<LoQ	<LoQ	<LoQ	<LoQ	<LoQ	<LoQ	<LoQ	<LoQ	<LoQ	<LoQ	<LoQ	5.2	<LoQ	<LoQ	<LoQ
An. blank-2	<LoQ	<LoQ	<LoQ	<LoQ	<LoQ	<LoQ	<LoQ	<LoQ	<LoQ	<LoQ	<LoQ	<LoQ	<LoQ	<LoQ	<LoQ	<LoQ	<LoQ	<LoQ	<LoQ	<LoQ	<LoQ	<LoQ	<LoQ
Leach. blank	<LoQ	<LoQ	<LoQ	<LoQ	<LoQ	<LoQ	<LoQ	<LoQ	<LoQ	<LoQ	<LoQ	<LoQ	<LoQ	<LoQ	<LoQ	<LoQ	<LoQ	<LoQ	<LoQ	<LoQ	<LoQ	<LoQ	<LoQ

Table A7.2: REEs concentrations in the atmospheric dust of the Weierbach experimental catchment (in µg g-1); and REEs and associated major and trace elements concentrations in the different bulk fractions of litter and fresh leaves of European beech (Be) and Douglas-fir (Do).

Sample	La	Ce	Pr	Nd	Sm	Eu	Gd	Tb	Dy	Y	Ho	Er	Tm	Yb	Lu	Na	K	Mg	Ca	Mn	Pb	Al	Fe
Unit	*ng/g*	*ng/g*	*ng/g*	*ng/g*	*ng/g*	*ng/g*	*ng/g*	*ng/g*	*ng/g*	*ng/g*	*ng/g*	*ng/g*	*ng/g*	*ng/g*	*ng/g*	*µg/g*	*µg/g*	*µg/g*	*µg/g*	*µg/g*	*µg/g*	*µg/g*	*µg/g*
Do FL	154.64	261.18	30.35	119.07	23.46	5.28	22.58	3.36	19.19	121.27	3.54	9.86	1.13	6.79	0.97	313	4321	1057	4886	3489	0.8	323	203
Do OLn	109.17	182	20.3	75.88	13.92	3.59	13.79	2.02	10.44	67.86	2.05	5.41	0.67	3.98	<LoQ	235	2371	965	6075	4027	0.6	265	160
Do OLv	5314.5	10991	1312.1	4866.2	808.8	140.2	480.8	52	223.8	840.74	35.7	90.13	11.5	71.42	10	126	2851	1546	3954	2540	7.2	7275	4657
Be FL	50.09	81.41	10.46	39.95	7.94	1.73	8.21	1.18	6.17	42.79	1.25	3.33	0.4	2.41	<LoQ	133	6266	1155	2968	1683	0.2	62.9	92.1
Be OLn	252.96	450.04	54.22	203.73	38.04	7.26	30.09	4.11	22.13	121.72	3.9	10.91	1.38	8.37	1.2	50.6	813	705	5440	2621	1.6	341	307
Be OLv	388.26	691.73	83.49	319.17	59.11	11.93	50.57	6.66	35.42	196.27	6.32	17.36	2.2	13.64	1.92	48.2	1109	770	6452	3077	2.6	489	448
Be OF	3718.8	7101	856.12	3172.8	562.1	100.8	378.9	47.7	254.5	1187.4	46.7	127.8	17.3	111.4	15.6	158	2652	1441	6264	3475	12.2	6928	4287
atm. dust	15025	29799	3396	13006	2400	531	2079	298	1866	9200	355	1110	154	1080	162	-	-	-	-	-	-	-	-

Table A7.3: REE (in ng L-1) and associated major and trace element (in ug L-1) concentrations, DOC concentration (in mg L-1) and pH in leachates of fresh leaves and litter leachates of European beech (Be) and Douglas-fir (Do).

Sample	La	Ce	Pr	Nd	Sm	Eu	Gd	Tb	Dy	Y	Ho	Er	Tm	Yb	Lu	Na	K	Mg	Ca	Mn	Pb	Al	Fe	pH	DOC
Unit	*ng/L*	*ng/L*	*ng/L*	*ng/L*	*ng/L*	*ng/L*	*ng/L*	*ng/L*	*ng/L*	*ng/L*	*ng/L*	*ng/L*	*ng/L*	*ng/L*	*ng/L*	*µg/L*	*µg/L*	*µg/L*	*µg/L*	*µg/L*	*µg/L*	*µg/L*	*µg/L*		*mg/L*
Do FL	61	211	35	215	62	13	71	10	72	397	16	45	6	42	<LoQ	9713	142814	13395	9386	30959	4.33	1676	661	4.70	1687
Do OLn	83	243	38	206	49	15	53	9	62	453	14	47	8	60	<LoQ	11521	123642	38892	20455	111300	10.40	2787	534	4.05	2937
Do OLv	395	975	102	405	98	31	102	14	83	465	17	44	<LoQ	35	<LoQ	4908	55078	24326	65004	70099	10.71	1547	417	5.02	1039
Be FL	19	29	5	20	<LoQ	<LoQ	<LoQ	<LoQ	<LoQ	<LoQ	<LoQ	4	<LoQ	<LoQ	<LoQ	1259	153391	8095	9731	9046	1.48	<LoQ	33	5.04	873
Be OLn	140	304	41	157	42	9	38	<LoQ	29	<LoQ	6	16	<LoQ	11	<LoQ	1871	41881	10062	27753	21443	4.02	263	94	5.97	591
Be OLv	469	988	134	563	135	30	140	18	96	703	19	54	6	35	<LoQ	1849	56863	17599	65166	54594	19.66	597	261	4.61	1468
Be OF	323	1064	90	375	72	18	104	10	57	381	13	33	0	25	<LoQ	2354	33082	8556	27722	20871	12.51	664	621	4.89	791

Table A7.4: REE average concentrations in the soil solutions collected under European beech (Be) and Douglas-fir (Do) at 20, 40 and 60 cm depth (in ng L-1) in the soil of the Weierbach experimental catchment.

Sample	La	Ce	Pr	Nd	Sm	Eu	Gd	Tb	Dy	Ho	Er	Tm	Yb	Lu
Unit	*ng/L*	*ng/L*	*ng/L*	*ng/L*	*ng/L*	*ng/L*	*ng/L*	*ng/L*	*ng/L*	*ng/L*	*ng/L*	*ng/L*	*ng/L*	*ng/L*
Do SS20	144	365	40	162	37	9	38	5	30	6	18	3	19	<LoQ
Do SS40	145	395	41	163	38	11	39	6	33	7	20	3	21	<LoQ
Do SS60	429	1012	111	459	103	28	104	13	78	16	48	7	47	7
Be SS20	271	881	83	345	82	19	82	11	64	13	36	5	35	<LoQ
Be SS40	1142	2943	301	1242	248	59	278	34	190	39	107	14	86	13
Be SS60	264	467	70	298	62	15	74	10	54	11	29	4	22	<LoQ

BIBLIOGRAPHY

Abbott, B. W., Baranov, V., Mendoza-Lera, C., Nikolakopoulou, M., Harjung, A., Kolbe, T., Balasubramanian, M. N., Vaessen, T. N., Ciocca, F., Campeau, A., Wallin, M. B., Romeijn, P., Antonelli, M., Gonçalves, J., Datry, T., Laverman, A. M., De Dreuzy, J.-R., Hannah, D. M., Krause, S., … Pinay, G. (2016). Using multi-tracer inference to move beyond single-catchment ecohydrology. Earth-Science Reviews, 160, 19–42. https://doi.org/10.1016/j.earscirev.2016.06.014

Adeleke, R., Nwangburuka, C. and Oboirien, B.: Origins, roles and fate of organic acids in soils: A review, South African J. Bot., 108, 393–406, doi:10.1016/j.sajb.2016.09.002, 2017.

Adomako, D., Gibrilla, A., Maloszewski, P., Ganyaglo, S. Y., & Rai, S. P. (2015). Tracing stable isotopes (δ^2H and $\delta^{18}O$) from meteoric water to groundwater in the Densu River basin of Ghana. Environmental Monitoring and Assessment, 187(5), 264.https://doi.org/10.1007/s10661-015-4498-2

Albery, W. J., & Knowles, J. R. (1977). Efficiency and Evolution of Enzyme Catalysis. Angewandte Chemie International Edition in English, 16(5), 285–293. https://doi.org/10.1002/anie.197702851

Albers, D., Migge, S., Schaefer, M. and Scheu, S.: Decomposition of beech leaves (Fagus sylvatica) and spruce needles (Picea abies) in pure and mixed stands of beech and spruce, Soil Biol. Biochem., 36(1), 155–164, doi:10.1016/j.soilbio.2003.09.002, 2004.

Alejandro, S., Höller, S., Meier, B. and Peiter, E.: Manganese in Plants: From Acquisition to Subcellular Allocation, Front. Plant Sci., 11(March), 1–23, doi:10.3389/fpls.2020.00300, 2020.

Alibo, D.S., Nozaki, Y. Rare earth elements in seawater: particle association, shale-normalization, and Ce oxidation, Geochimica et Cosmochimica Acta, Volume 63, Issues 3–4, 1999, Pages 363-372, ISSN 0016-7037, https://doi.org/10.1016/S0016-7037(98)00279-8

Allen, S. T., & Kirchner, J. W. (2022). Potential effects of cryogenic extraction biases on plant water source partitioning inferred from xylem-water isotope ratios. Hydrological Processes, 36(2). https://doi.org/10.1002/hyp.14483

Amann, B. T., Mulqueen, P. and Horrocks, W. D. W.: A continuous spectrophotometric assay for the activation of plant NAD kinase by calmodulin, calcium(II), and europium(III) ions, J. Biochem. Biophys. Methods, 25(4), 207–217, doi:10.1016/0165-022X(92)90015-3, 1992.

Améglio, T., Bodet, C., Lacointe, A., Cochard, H. (2002). Winter embolism, mechanisms of xylem hydraulic conductivity recovery and springtime growth patterns in walnut and peach trees. Tree Physiol. 2002 Dec;22(17):1211-20. https://doi.org/10.1093/treephys/22.17.1211

Antonelli, M., Wetzel, C.E., Ector, L., Teuling, A.J., Pfister, L. (2017). On the potential for terrestrial diatom communities and diatom indices to identify anthropic disturbance in soils. Ecological Indicators, 75, 73-81. https://doi.org/10.1016/j.ecolind.2016.12.003

Aubert, D., Stille, P., Probst, A., Gauthier-lafaye, F., Pourcelot, L., & Del nero, M. (2002). Characterization and migration of atmospheric REE in soils and surface waters. Geochimica et Cosmochimica Acta, 66(19), 3339–3350. https://doi.org/10.1016/S0016-7037(02)00913-4

Augusti, A., Betson, T. R., & Schleucher, J. (2006). Hydrogen exchange during cellulose synthesis distinguishes climatic and biochemical isotope fractionations in tree rings. New Phytologist, 172(3), 490–499. https://doi.org/10.1111/j.1469-8137.2006.01843.x

Austin, A. T. and Ballaré, C. L.: Dual role of lignin in plant litter decomposition in terrestrial ecosystems, Proc. Natl. Acad. Sci. U. S. A., 107(10), 4618–4622, doi:10.1073/pnas.0909396107, 2010.

Ayenew, T., Fikre, S., Wisotzky, F., Demlie, M., & Wohnlich, S. (2009). Hierarchical cluster analysis of hydrochemical data as a tool for assessing the evolution and dynamics of groundwater across the Ethiopian rift. International Journal of Physical Sciences, 4, 76-90

Barbecot, F., Guillon, S., Pili, E., Larocque, M., Gibert-Brunet, E., Hélie, J., Noret, A., Plain, C., Schneider, V., Mattei, A. and Meyzonnat, G. (2018). Using Water Stable Isotopes in

the Unsaturated Zone to Quantify Recharge in Two Contrasted Infiltration Regimes. Vadose Zone Journal, 17: 1-13 170170.

Barbeta, A., Burlett, R., Martín-Gómez, P., Fréjaville, B., Devert, N., Wingate, L., Domec, J., & Ogée, J. (2022). Evidence for distinct isotopic compositions of sap and tissue water in tree stems: Consequences for plant water source identification. New Phytologist, 233(3), 1121–1132. https://doi.org/10.1111/nph.17857

Barbeta, A., Gimeno, T. E., Clavé, L., Fréjaville, B., Jones, S. P., Delvigne, C., Wingate, L., & Ogée, J. (2020). An explanation for the isotopic offset between soil and stem water in a temperate tree species. New Phytologist, 227(3), 766–779. https://doi.org/10.1111/nph.16564

Barbeta, A., Jones, S. P., Clavé, L., Wingate, L., Gimeno, T. E., Fréjaville, B., Wohl, S., & Ogée, J. (2019). Unexplained hydrogen isotope offsets complicate the identification and quantification of tree water sources in a riparian forest. Hydrology and Earth System Sciences, 23(4), 2129–2146. https://doi.org/10.5194/hess-23-2129-2019

Barnes, C. J., & Allison, G. B. (1988). Tracing of water movement in the unsaturated zone using stable isotopes of hydrogen and oxygen. Journal of Hydrology, 100(1), 143–176. https://doi.org/10.1016/0022-1694(88)90184-9

Basov, A., Fedulova, L., Vasilevskaya, E., & Dzhimak, S. (2019). Possible Mechanisms of Biological Effects Observed in Living Systems during 2H/1H Isotope Fractionation and Deuterium Interactions with Other Biogenic Isotopes. Molecules, 24(22), 4101. https://doi.org/10.3390/molecules24224101

Bau, M. (1991). Rare-earth element mobility during hydrothermal and metamorphic fluid-rock interaction and the significance of the oxidation state of europium. Chemical Geology, 93(3–4), 219–230. https://doi.org/10.1016/0009-2541(91)90115-8

Bau, M. (1996). Controls on the fractionation of isovalent trace elements in magmatic and aqueous systems: Evidence from Y/Ho, Zr/Hf, and lanthanide tetrad effect. Contributions to Mineralogy and Petrology, 123(3), 323–333. https://doi.org/10.1007/s004100050159

Bau, M. Scavenging of dissolved yttrium and rare earths by precipitating iron oxihydroxed: experimental evidence for Ce oxidation, Y-Ho fractionation, and lanthanide tetrad effect. Geochim. Cosmochim. Acta 1999, 63, 67–77.

Bau, M. (1999). Scavenging of dissolved yttrium and rare earths by precipitating iron oxyhydroxide: Experimental evidence for Ce oxidation, Y-Ho fractionation, and lanthanide tetrad effect. Geochimica et Cosmochimica Acta, 63(1), 67–77. https://doi.org/10.1016/S0016-7037(99)00014-9

Bau, M., & Dulski, P. (1996). Distribution of yttrium and rare-earth elements in the Penge and Kuruman iron-formations, Transvaal Supergroup, South Africa. Precambrian Research, 79(1–2), 37–55. https://doi.org/10.1016/0301-9268(95)00087-9

Bau, M., & Koschinsky, A. (2009). Oxidative scavenging of cerium on hydrous Fe oxide: Evidence from the distribution of rare earth elements and yttrium between Fe oxides and Mn oxides in hydrogenetic ferromanganese crusts. GEOCHEMICAL JOURNAL, 43(1), 37–47. https://doi.org/10.2343/geochemj.1.0005

Bateman, D. F. and Basham, H. G.: Degradation of Plant Cell Walls and Membranes by Microbial Enzymes, Physiol. Plant Pathol., 316–355, doi:10.1007/978-3-642-66279-9_13, 1976.

Beyer, M., & Dubbert, M. (2019). X Water Worlds and how to investigate them: A review and future perspective on <i>in situ</i> measurements of water stable isotopes in soils and plants [Preprint]. Ecohydrology/Instruments and observation techniques. https://doi.org/10.5194/hess-2019-600

Bienfait, H.: Prevention of stress in iron metabolism of plants, Acta Bot. Neerl., 38(2), 105–129, doi:/10.1111/j.1438-8677.1989.tb02035.x, 1989

Bonanno, E., Blöschl, G., & Klaus, J. (2021). Flow directions of stream-groundwater exchange in a headwater catchment during the hydrologic year. Hydrological Processes, 35(8). https://doi.org/10.1002/hyp.14310

Boyer, J. S., Leaf Water Potentials Measured with a Pressure Chamber, Plant Physiology, Volume 42, Issue 1, January 1967, Pages 133–137, https://doi.org/10.1104/pp.42.1.133

Braun, J. J., Viers, J., Dupré, B., Polve, M., Ndam, J. and Muller, J. P.: Solid/liquid REE fractionation in the lateritic system of Goyoum, East Cameroon: The implication for the present dynamics of the soil covers of the humid tropical regions, Geochim. Cosmochim. Acta, 62(2), 273–299, doi:10.1016/S0016-7037(97)00344-X, 1998

Bréda, N., Huc, R., Granier, A., & Dreyer, E. (2006). Temperate forest trees and stands under severe drought: a review of ecophysiological responses, adaptation processes and

long-term consequences. Annals of Forest Science, 63(6), 625–644. https://doi.org/10.1051/forest:2006042

Brinkmann, N., Eugster, W., Buchmann, N., & Kahmen, A. (2019). Species-specific differences in water uptake depth of mature temperate trees vary with water availability in the soil. Plant Biology , 21(1), 71–81. https://doi.org/10.1111/plb.12907

Brioschi, L., Steinmann, M., Lucot, E., Pierret, M. C., Stille, P., Prunier, J., & Badot, P. M. (2013). Transfer of rare earth elements (REE) from natural soil to plant systems: Implications for the environmental availability of anthropogenic REE. Plant and Soil, 366(1–2), 143–163. https://doi.org/10.1007/s11104-012-1407-0

Brooks R., Barnard, H. R., Coulombe, R., & McDonnell, J. J. (2010). Ecohydrologic separation of water between trees and streams in a Mediterranean climate. Nature Geoscience, 3(2), 100–104. https://doi.org/10.1038/ngeo722

Brun, C. B., Åström, M. E., Peltola, P. and Johansson, M. B.: Trends in major and trace elements in decomposing needle litters during a long-term experiment in Swedish forests, Plant Soil, 306(1–2), 199–210, doi:10.1007/s11104-008-9572-x, 2008

Burda, K., Strzałka, K., & Schmid, G. H. (1995). Europium- and Dysprosium-Ions as Probes for the Study of Calcium Binding Sites in Photosystem II. Zeitschrift Für Naturforschung C, 50(3–4), 220–230. https://doi.org/10.1515/znc-1995-3-410

Burgess, S. S. O., Adams, M. A., Turner, N. C., & Ward, B. (2000). Characterisation of hydrogen isotope profiles in an agroforestry system: implications for tracing water sources of trees. Agricultural Water Management, 45(3), 229–241. https://doi.org/10.1016/S0378-3774(00)00105-0

Byrne, R. H., & Li, B. (1995). Comparative complexation behavior of the rare earths. Geochimica et Cosmochimica Acta, 59(22), 4575–4589. https://doi.org/10.1016/0016-7037(95)00303-7

Cai, L., Chen, Xi, Huang, R., Smettem, K. Runoff change induced by vegetation recovery and climate change over carbonate and non-carbonate areas in the karst region of South-west China, Journal of Hydrology, Volume 604, 2022, 127231, ISSN 0022-1694, https://doi.org/10.1016/j.jhydrol.2021.127231.

Carlier, C., Wirth, S.B., Cochand, F., Hunkeler, D., Brunner, P. Geology controls streamflow dynamics. J. Hydrol., 566 (2018), pp. 756-769, 10.1016/j.jhydrol.2018.08.069

Carrión-Mero, P., Montalván-Burbano, N., Herrera-Franco, G., Domínguez-Granda, L., Bravo-Montero, L., Morante-Carballo, F. Research Trends in Groundwater and Stable Isotopes. Water 2022, 14, 3173. https://doi.org/10.3390/w14193173

Censi, P., Cangemi, M., Brusca, L., Madonia, P., Saiano, F., Zuddas, P. The behavior of rare-earth elements, Zr and Hf during biologically-mediated deposition of silica-stromatolites and carbonate-rich microbial mats, Gondwana Research, Volume 27, Issue 1, 2015, Pages 209-215, ISSN 1342-937X, https://doi.org/10.1016/j.gr.2013.09.014

Censi, P., Saiano, F., Pisciotta, A., & Tuzzolino, N. (2014). Geochemical behaviour of rare earths in Vitis vinifera grafted onto different rootstocks and growing on several soils. Science of The Total Environment, 473–474, 597–608. https://doi.org/10.1016/j.scitotenv.2013.12.073

Chadwick, O. A., Derry, L. A., Vitousek, P. M., Huebert, B. J. and Hedin, L. O.: Changing sources of nutrients during four million years of ecosystem development, Nature, 397(6719), 491–497, doi:10.1038/17276, 1999.

Chang, C., Li, F., Liu, C., Gao, J., Tong, H., & Chen, M. (2016). Fractionation characteristics of rare earth elements (REEs) linked with secondary Fe, Mn, and Al minerals in soils. Acta Geochimica, 35(4), 329–339. https://doi.org/10.1007/s11631-016-0119-1

Cheesman, A. W., & Cernusak, L. A. (2017). Infidelity in the outback: climate signal recorded in Δ18O of leaf but not branch cellulose of eucalypts across an Australian aridity gradient. Tree Physiology, 37(5), 554–564. https://doi.org/10.1093/treephys/tpw121

Chen, Y., Helliker, B. R., Tang, X., Li, F., Zhou, Y., & Song, X. (2020). Stem water cryogenic extraction biases estimation in deuterium isotope composition of plant source water. Proceedings of the National Academy of Sciences, 117(52), 33345–33350. https://doi.org/10.1073/pnas.2014422117

Cheng, J., Ding, C., Li, X., Zhang, T., & Wang, X. (2015). Rare Earth Element Transfer from Soil to Navel Orange Pulp (Citrus sinensis Osbeck cv. Newhall) and the Effects on Internal Fruit Quality. PLOS ONE, 10(3), e0120618. https://doi.org/10.1371/journal.pone.0120618

Chorover, J., R. Kretzschmar, F. Garcia-Pichel, and D. L. Sparks. 2007. Soil biogeochemical processes in the critical zone. Elements 3, 321-326.

Cidu, R., Buscaroli, A., Biddau, R., Da Pelo, S., Zannoni, D., Vianello, G., Dinelli, E., Vittori Antisari, L. and Carbone, S.: Dynamics of rare earth elements in water–soil systems: The case study of the Pineta San Vitale (Ravenna, Italy), Geoderma, 193–194, 52–67, doi:10.1016/j.geoderma.2012.10.009, 2013

Clark, I. D., & Fritz, P. (1997). Environmental isotopes in hydrogeology. CRC press.

Cloutier, V., R. Lefebvre, R. Therrien, and M. M. Savard (2008). “Multivariate statistical analysis of geochemical data as indicative of the hydrogeochemical evolution of groundwater in a sedimentary rock aquifer system”. Journal of Hydrology 353.3-4, 294–313. doi: 10.1016/j.jhydrol.2008.02.015

Cochard, H., Lemoine, D., Améglio, T., Granier, A. (2001). Mechanisms of xylem recovery from winter embolism in Fagus sylvatica. Tree Physiol. Jan;21(1):27-33. https://doi.org/10.1093/treephys/21.1.27

Cogulet, A., Blanchet, P. and Landry, V.: Wood degradation under UV irradiation: A lignin characterization, J. Photochem. Photobiol. B Biol., 158, 184–191, doi:10.1016/j.jphotobiol.2016.02.030, 2016

Coppin, F., Berger, G., Bauer, A., Castet, S., & Loubet, M. (2002). Sorption of lanthanides on smectite and kaolinite. Chemical Geology, 182(1), 57–68. https://doi.org/10.1016/S0009-2541(01)00283-2

Cormier, M.-A., Werner, R. A., Sauer, P. E., Gröcke, D. R., Leuenberger, M. C., Wieloch, T., Schleucher, J., & Kahmen, A. (2018). 2 H-fractionations during the biosynthesis of carbohydrates and lipids imprint a metabolic signal on the δ 2 H values of plant organic compounds. New Phytologist, 218(2), 479–491. https://doi.org/10.1111/nph.15016

Costa Filho, R. N., Alencar, G., Skagerstam, B.-S., & Andrade, J. S. (2013). Morse potential derived from first principles. EPL, 101(1), 10009. https://doi.org/10.1209/0295-5075/101/10009

Constabel, C.P., Barbehenn, R. (2008). Defensive Roles of Polyphenol Oxidase in Plants. In: Schaller, A. (eds) Induced Plant Resistance to Herbivory. Springer, Dordrecht. https://doi.org/10.1007/978-1-4020-8182-8_12

Craig, H, Isotopic Variations in Meteoric Waters, 1961, Science, 1702-1703, 133, 3465, doi:10.1126/science.133.3465.1702

Cui, Y.-Q., Ma, J.-Y., Feng, Q., Sun, J.-H., & Sun, W. (2017). Water sources and water-use efficiency of desert plants in different habitats in Dunhuang, NW China. Ecological Research, 32(2), 243–258. https://doi.org/10.1007/s11284-017-1433-8

Davis, J. C. and R. J. Sampson (1986). Statistics and data analysis in geology. Vol. 646. Wiley New York.

Davranche, M., Pourret, O., Gruau, G., Dia, A., Jin, D. and Gaertner, D.: Competitive binding of REE to humic acid and manganese oxide: Impact of reaction kinetics on development of cerium anomaly and REE adsorption, Chem. Geol., 247(1–2), 154–170, doi:10.1016/j.chemgeo.2007.10.010, 2008.

Davranche, M., Pourret, O., Gruau, G., Dia, A. and Le Coz-Bouhnik, M.: Adsorption of REE(III)-humate complexes onto MnO2: Experimental evidence for cerium anomaly and lanthanide tetrad effect suppression, Geochim. Cosmochim. Acta, 69(20), 4825–4835, doi:10.1016/j.gca.2005.06.005, 2005.

Dawson, T. E. (1993). Hydraulic lift and water use by plants: implications for water balance, performance and plant-plant interactions. Oecologia, 95(4), 565–574. https://doi.org/10.1007/BF00317442

Dawson, T. E., & Ehleringer, J. R. (1991). Streamside trees that do not use stream water. Nature, 350(6316), 335–337. https://doi.org/10.1038/350335a0

Dawson, T. E., & Ehleringer, J. R. (1993). Isotopic enrichment of water in the 'woody' tissues of plants: Implications for plant water source, water uptake, and other studies which use the stable isotopic composition of cellulose. Geochimica et Cosmochimica Acta, 57(14), 3487–3492. https://doi.org/10.1016/0016-7037(93)90554-A

DeNiro, D. Y. A. M. (1990). Oxygen and Hydrogen Isotope Fractionation during Cellulose Metabolism in Lemna gibba L. Plant Physiology, (93), 325–332. https://doi.org/10.1104/pp.93.1.325

Deniro, M. J., & Epstein, S. (1981). Influence of diet on the distribution of nitrogen isotopes in animals. Geochimica et Cosmochimica Acta, 45(3), 341–351. https://doi.org/10.1016/0016-7037(81)90244-1

Dia, A., Gruau, G., Olivié-Lauquet, G., Riou, C., Molénat, J. and Curmi, P.: The distribution of rare earth elements in groundwaters: Assessing the role of source-rock composition,

redox changes and colloidal particles, Geochim. Cosmochim. Acta, 64(24), 4131–4151, doi:10.1016/S0016-7037(00)00494-4, 2000.

Ding, S., Liang, T., Yan, J., Zhang, Z., Huang, Z., & Xie, Y. (2007). Fractionations of rare earth elements in plants and their conceptive model. Science in China Series C: Life Sciences, 50(1), 47–55. https://doi.org/10.1007/s11427-007-2040-7

Ding, S., Liang, T., Zhang, C., Yan, J., & Zhang, Z. (2005). Accumulation and fractionation of rare earth elements (REEs) in wheat: Controlled by phosphate precipitation, cell wall absorption and solution complexation. Journal of Experimental Botany, 56(420), 2765–2775. https://doi.org/10.1093/jxb/eri270

Ding, S., Liang, T., ChaoSheng Zhang, ZeChun Huang, YaNing Xie, and, & TongBin Chen. (2006). Fractionation Mechanisms of Rare Earth Elements (REEs) in Hydroponic Wheat: An Application for Metal Accumulation by Plants. Environmental Science & Technology, 40(8), 2686–2691. https://doi.org/10.1021/es052091b

Douinot, A., Iffly, J. F., Tailliez, C., Meisch, C., and Pfister, L. (2022): Flood patterns in a catchment with mixed bedrock geology and a hilly landscape: identification of flashy runoff contributions during storm events, Hydrol. Earth Syst. Sci., 26, 5185–5206, https://doi.org/10.5194/hess-26-5185-2022

Dudareva, N., Negre, F., Nagegowda, D. A., & Orlova, I. (2006). Plant Volatiles: Recent Advances and Future Perspectives. Critical Reviews in Plant Sciences, 25(5), 417–440. https://doi.org/10.1080/07352680600899973

Duvert, C., Canham, C. A., Barbeta, A., Alvarez Cortes, D., Chandler, L., Harford, A. J., Leggett, A., Setterfield, S. A., Humphrey, C. L., & Hutley, L. B. (2022). Deuterium depletion in xylem water and soil isotopic effects complicate the assessment of riparian tree water sources in the seasonal tropics. Ecohydrology, 15(6). https://doi.org/10.1002/eco.2383

Effah, E., Holopainen, J. K., & McCormick, A. C. (2019). Potential roles of volatile organic compounds in plant competition. Perspectives in Plant Ecology, Evolution and Systematics, 38, 58–63. https://doi.org/10.1016/j.ppees.2019.04.003

Ehleringer, J. R., Barnette, J. E., Jameel, Y., Tipple, B. J., & Bowen, G. J. (2016). Urban water - a new frontier in isotope hydrology. Isotopes in Environmental and Health Studies, 52(4-5), 477–486. https://doi.org/10.1080/10256016.2016.1171217

Ehleringer, J. R., & Dawson, T. E. (1992). Water uptake by plants: perspectives from stable isotope composition. Plant, Cell & Environment, 15(9), 1073–1082. https://doi.org/10.1111/j.1365-3040.1992.tb01657.x

El-ramady, H. R.: Ecotoxicology of rare earth elements: Ecotoxicology of rare earth elements within soil and plant environments, .” KG: VDM Verlag Dr. Muller Aktiengsellsellshaft & Co; 2010.

Estep, M. F., & Hoering, T. C. (1980). Biogeochemistry of the stable hydrogen isotopes. Geochimica et Cosmochimica Acta, 44(8), 1197–1206. https://doi.org/10.1016/0016-7037(80)90073-3

Evaristo, J., McDonnell, J. J., Scholl, M. A., Bruijnzeel, L. A., & Chun, K. P. (2016). Insights into plant water uptake from xylem-water isotope measurements in two tropical catchments with contrasting moisture conditions: Ecohydrological Separation in Less Seasonal Humid Tropics. Hydrological Processes, 30(18), 3210–3227. https://doi.org/10.1002/hyp.10841

Everitt, B. and T. Hothorn (2011). An Introduction to Applied Multivariate Analysis with R - 4 Multidimensional Scaling, 61–74.

Evert, R.F. (2006). Esau's Plant Anatomy: Meristems, Cells, and Tissues of the Plant Body: Their Structure, Function, and Development, 3rd Edition.

Fabiani, G., Schoppach, R., Penna, D., & Klaus, J. (2022). Transpiration patterns and water use strategies of beech and oak trees along a hillslope. Ecohydrology, 15(2). https://doi.org/10.1002/eco.2382

Fang, J., & Lechowicz, M. J. (2006). Climatic limits for the present distribution of beech (Fagus L.) species in the world. Journal of Biogeography, 33(10), 1804–1819. https://doi.org/10.1111/j.1365-2699.2006.01533.x

FAO. The State of the World’s Forests (2022)

Farrington, P., Turner, J. V., & Gailitis, V. (1996). Tracing water uptake by jarrah (Eucalyptus marginata) trees using natural abundances of deuterium. Trees, 11(1), 9–15. https://doi.org/10.1007/PL00009654

Florent, P., Cauchie, H.-M., & Ogorzaly, L. (2022). A Virological Perspective on the Use of Bacteriophages as Hydrological Tracers. Water, 14(24), 3991. https://doi.org/10.3390/w14243991

Franceschi, V. R., Krokene, P., Christiansen, E., & Krekling, T. (2005). Anatomical and chemical defenses of conifer bark against bark beetles and other pests. The New Phytologist, 167(2), 353–375. https://doi.org/10.1111/j.1469-8137.2005.01436.x

Friedman Jr. H. G., Choppin, G. R. and Feuerbacher, D. G. Journal of Chemical Education 1964 41 (7), 354. DOI: 10.1021/ed041p354

Fujino, M., Sakakibara, K., Tsujimura, M., Suzuki, K. Influence of alpine vegetation on water storage and discharge functions in an alpine headwater of Northern Japan Alps, Journal of Hydrology X, Volume 18, 2023, 100146, ISSN 2589-9155, https://doi.org/10.1016/j.hydroa.2022.100146

Galewsky, J., Steen-Larsen, H. C., Field, R. D., Worden, J., Risi, C., and Schneider, M. (2016), Stable isotopes in atmospheric water vapor and applications to the hydrologic cycle, Rev. Geophys., 54, 809– 865, doi:10.1002/2015RG000512

Galloway, A. F., Knox, P., & Krause, K. (2020). Sticky mucilages and exudates of plants: Putative microenvironmental design elements with biotechnological value. New Phytologist, 225(4), 1461–1469. https://doi.org/10.1111/nph.16144

Gao, Y., Zeng, F., Yi, A., Ping, S., & Jing, L. (2003). Research of the Entry of Rare Earth Elements Eu^{3+} and La^{3+} into Plant Cell. Biological Trace Element Research, 91(3), 253–265. https://doi.org/10.1385/BTER:91:3:253

Gascuel-Odoux, C., & Mérot, P. (1986). Variabilité spatiale du transfert de l'eau dans le sol: Utilisation du traçage et analyse géostatistique. Journal of Hydrology, 89(1), 93–107. https://doi.org/10.1016/0022-1694(86)90145-9

Gat, J. R. (2010). Stable isotope hydrology: Deuterium and oxygen-18 in the water cycle (2nd ed.). Springer Science & Business Media.

Gautam, M. K., Lee, K. S., Berg, B., Song, B. Y. and Yeon, J. Y.: Trends of major, minor and rare earth elements in decomposing litter in a cool temperate ecosystem, South Korea, Chemosphere, 222, 214–226, doi:10.1016/j.chemosphere.2019.01.114, 2019.

Glaser, B., Klaus, J., Frei, S., Frentress, J., Pfister, L., Hopp, L., 2016. On the value of surface saturated area dynamics mapped with thermal infrared imagery for modeling the hillslope-riparian-stream continuum. Water Resour. Res., DOI: 10.1002/2015WR018414

Gómez, L., Contreras, A., Bolonio, D., Quintana, J., Oñate-Sánchez, L. and Merino, I.: Phytoremediation with trees, Adv. Bot. Res., 89, 281-321, 2019.

Gourdol, L., Clément, R., Juilleret, J., Pfister, L., & Hissler, C. (2021). Exploring the regolith with electrical resistivity tomography in large-scale surveys: Electrode spacing-related issues and possibility. Hydrology and Earth System Sciences, 25(4), 1785–1812. https://doi.org/10.5194/hess-25-1785-2021

Grantham, H.S., Duncan, A., Evans, T.D. et al. Anthropogenic modification of forests means only 40% of remaining forests have high ecosystem integrity. Nat Commun 11, 5978 (2020). https://doi.org/10.1038/s41467-020-19493-3

Graus, M., Schnitzler J.P., Hansel, A., Cojocariu, C., Rennenberg, H., Wisthaler, A., Kreuzwieser, J. Transient Release of Oxygenated Volatile Organic Compounds during Light-Dark Transitions in Grey Poplar Leaves, Plant Physiology, Volume 135, Issue 4, August 2004, Pages 1967–1975, https://doi.org/10.1104/pp.104.043240

Grobety, B., Giere, R., Dietze, V., & Stille, P. (2010). Airborne Particles in the Urban Environment. Elements, 6(4), 229–234. https://doi.org/10.2113/gselements.6.4.229

Gröning M., Lutz H.O., Roller-Lutz Z., Kralik M., Gourcy L., Pöltenstein L., "A simple rain collector preventing water re-evaporation dedicated for δ18O and δ2H analysis of cumulative precipitation samples",Journal of Hydrology, Volumes 448–449, Pages 195-200, 2012, https://doi.org/10.1016/j.jhydrol.2012.04.041.

Grosjean, N., Le Jean, M., Berthelot, C. et al. Accumulation and fractionation of rare earth elements are conserved traits in the Phytolacca genus. Sci Rep 9, 18458 (2019). https://doi.org/10.1038/s41598-019-54238-3

Guenther, A., Hewitt, C. N., Erickson, D., Fall, R., Geron, C., Graedel, T., Harley, P., Klinger, L., Lerdau, M., Mckay, W. A., Pierce, T., Scholes, B., Steinbrecher, R., Tallamraju, R., Taylor, J., & Zimmerman, P. (1995). A global model of natural volatile organic compound emissions. Journal of Geophysical Research, 100(D5), 8873. https://doi.org/10.1029/94JD02950

Güler, C. and G. D. Thyne (2004). “Hydrologic and geologic factors controlling surface and groundwater chemistry in Indian Wells-Owens Valley area, southeastern California, USA”. Journal of Hydrology 285.1-4, 177–198. doi: 10.1016/j.jhydrol.2003.08.019.

Güler, C., G. D. Thyne, J. E. McCray, and K. A. Turner (2002). “Evaluation of graphical and multivariate statistical methods for classification of water chemistry data”. Hydrogeology Journal 10.4, 455–474. doi: 10.1007/s10040-002-0196-6

Guo, L. B. and Sims, R. E. H.: Litter decomposition and nutrient release via litter decomposition in New Zealand eucalypt short rotation forests, Agric. Ecosyst. Environ., 75(1–2), 133–140, doi:10.1016/S0167-8809(99)00069-9, 1999.

Gwenzi, W., Mangori, L., Danha, C., Chaukura, N., Dunjana, N. and Sanganyado, E.: Sources, behaviour, and environmental and human health risks of high-technology rare earth elements as emerging contaminants, Sci. Total Environ., 636, 299–313, doi:10.1016/j.scitotenv.2018.04.235, 2018.

Harkins, W. D. (1917). The evolution of the elements and the stability of complex atoms. i. a new periodic system which shows a relation between the abundance of the elements and the structure of the nuclei of atoms. Journal of the American Chemical Society, 39(5), 856–879. https://doi.org/10.1021/ja02250a002

Harris, K. R., & Woolf, L. A. (1980). Pressure and temperature dependence of the self diffusion coefficient of water and oxygen-18 water. Journal of the Chemical Society, London. Faraday Transactions 1, 76(0), 377–385. https://doi.org/10.1039/F19807600377

Hannigan, R. E., & Sholkovitz, E. R. (2001). The development of middle rare earth element enrichments in freshwaters: Weathering of phosphate minerals. Chemical Geology, 175(3–4), 495–508. https://doi.org/10.1016/S0009-2541(00)00355-7

Hartigan, J. A. (1975). Clustering algorithms. John Wiley & Sons, Inc. Pearson, K. (1901). “Principal components analysis”. The London, Edinburgh, and Dublin. Philosophical Magazine and Journal of Science 6.2, 559

Hastie, T. e. a. (2009). “Springer Series in Statistics The Elements of Statistical Learning”. The Mathematical Intelligencer 27.2, 83–85

Heidari, H., Warziniack, T., Brown, T.C., Arabi, M. Impacts of Climate Change on Hydroclimatic Conditions of U.S. National Forests and Grasslands. Forests 2021, 12, 139. https://doi.org/10.3390/f12020139

Hermoso de Mendoza, I., Boucher, E., Gennaretti, F., Lavergne, A., Field, R., and Andreu-Hayles, L.: A new snow module improves predictions of the isotope-enabled MAIDENiso forest growth model, Geosci. Model Dev., 15, 1931–1952, https://doi.org/10.5194/gmd-15-1931-2022, 2022

Hill, S. A., Waterhouse, J. S., Field, E. M., Switsur, V. R., & Ap Rees, T. (1995). Rapid recycling of triose phosphates in oak stem tissue. Plant, Cell & Environment, 18(8), 931–936. https://doi.org/10.1111/j.1365-3040.1995.tb00603.x

Hissler, C., Stille, P., Guignard, C., Iffly, J. F., Pfister, L. Rare Earth Elements as Hydrological Tracers of Anthropogenic and Critical Zone Contributions: A Case Study at the Alzette River Basin Scale. Procedia Earth and Planetary Science, Volume 10, 2014, Pages 349-352, ISSN 1878-5220, https://doi.org/10.1016/j.proeps.2014.08.036

Hissler, C., Stille, P., Juilleret, J., Iffly, J. F., Perrone, T., & Morvan, G. (2015). Elucidating the formation of terra fuscas using Sr–Nd–Pb isotopes and rare earth elements. Applied Geochemistry, 54, 85–99. https://doi.org/10.1016/j.apgeochem.2015.01.011

Hissler, C., Martínez-Carreras, N., Barnich, F., Gourdol, L., Iffly, J. F., Juilleret, J., Klaus, J., & Pfister, L. (2021). The Weierbach experimental catchment in Luxembourg: A decade of critical zone monitoring in a temperate forest - from hydrological investigations to ecohydrological perspectives. Hydrological Processes, 35(5). https://doi.org/10.1002/hyp.14140

Hissler, C., Hostache, R., Iffly, J.F., Pfister, L., Stille, P.: Anthropogenic rare earth element fluxes into floodplains: coupling between geochemical monitoring and hydrodynamic-sediment transport modelling. C. R. Geoscience 347 294–303, doi: 10.1016/j.crte.2015.01.003, 2015a.

Hissler, C., Stille, P. Iffly, J.F., Guignard, C., Chabaux, F., Pfister, L.: Origin and Dynamics of Rare Earth Elements during flood events in contaminated river basins: Sr-Nd-Pb evidence. Environ. Sci. Technol., 50(9), 4624-4631. doi:10.1021/acs.est.5b03660, 2016.

Hoek van Dijke, A. J., Mallick, K., Teuling, A. J., Schlerf, M., Machwitz, M., Hassler, S. K., Blume, T., and Herold, M. (2019). Does the Normalized Difference Vegetation Index

explain spatial and temporal variability in sap velocity in temperate forest ecosystems? Hydrol. Earth Syst. Sci., 23, 2077–2091. https://doi.org/10.5194/hess-23-2077-2019

Holbrook N.M. (1995) Stem water Storage. In Plant Stems: Physiology and Functional Morphology (ed. B.L. Gartner), pp. 151–174. Academic Press, San Diego.

Houhou, J., Lartiges, B. S., France-Lanord, C., Guilmette, C., Poix, S., & Mustin, C. (2010). Isotopic tracing of clear water sources in an urban sewer: A combined water and dissolved sulfate stable isotope approach. Water Research, 44(1), 256–266. https://doi.org/10.1016/j.watres.2009.09.024

Houston Durrant, T., de Rigo, D., & Caudullo, G. (2016). Fagus sylvatica in Europe: distribution, habitat, usage and threats. In S.-M.-A. J. C. G. De Rigo D. Mauri A. Houston Durrant T. (Ed.), European Atlas of Forest Tree Species (pp. 94–95). L-2995 Luxembourg, Luxembourg.: Publications Office of the European Union. https://data.europa.eu/doi/10.2760/776635

Hu, Y., Liu, Z., Zhao, M., Zeng, Q., Zeng, C., Chen, B., Chen, C., He, H., Cai, X., Ou, Y., & Chen, J. (2018). Using deuterium excess, precipitation and runoff data to determine evaporation and transpiration: A case study from the Shawan Test Site, Puding, Guizhou, China. Geochimica et Cosmochimica Acta, 242, 21–33. https://doi.org/10.1016/j.gca.2018.08.049

Imadi, S. R., Waseem, S., Kazi, A. G., Azooz, M. M. and Ahmad, P.: Aluminum Toxicity in Plants: An Overview, Plant Met. Interact. Emerg. Remediat. Tech., 1–20, doi:10.1016/B978-0-12-803158-2.00001-1, 2016.

Jabiol, B., Zanella, A., Ponge, J. F., Sartori, G., Englisch, M., van Delft, B., de Waal, R. and Le Bayon, R. C.: A proposal for including humus forms in the World Reference Base for Soil Resources (WRB-FAO), Geoderma, 192(1), 286–294, doi:10.1016/j.geoderma.2012.08.002, 2013.

Jandl, R., Spathelf, P., Bolte, A. et al. Forest adaptation to climate change—is non-management an option? Annals of Forest Science 76, 48 (2019). https://doi.org/10.1007/s13595-019-0827-x

Jasechko, S., Sharp, Z. D., Gibson, J. J., Birks, S. J., Yi, Y., & Fawcett, P. J. (2013). Terrestrial water fluxes dominated by transpiration. Nature, 496(7445), 347–350. https://doi.org/10.1038/nature11983

Jin, L., Ma, L., Dere, A., White, T., Mathur, R. and Brantley, S. L.: REE mobility and fractionation during shale weathering along a climate gradient, Chem. Geol., 466, 352–379, doi:10.1016/j.chemgeo.2017.06.024, 2017.

Joshi, S. K., Rai, S. P., Sinha, R., Gupta, S., Densmore, A. L., Rawat, Y. S., & Shekhar, S. (2018). Tracing groundwater recharge sources in the northwestern Indian alluvial aquifer using water isotopes (δ18O, δ2H and 3H). Journal of Hydrology, 559, 835–847. https://doi.org/10.1016/j.jhydrol.2018.02.056

Jouzel, J., & Souchez, R. (1982). Melting–Refreezing at the Glacier Sole and the Isotopic Composition of the Ice. Journal of Glaciology, 28(98), 35-42. doi:10.3189/S0022143000011771

Juilleret, J., Dondeyne, S., Vancampenhout, K., Deckers, J., & Hissler, C. (2016). Mind the gap: A classification system for integrating the subsolum into soil surveys. Geoderma, 264, 332–339. https://doi.org/10.1016/j.geoderma.2015.08.031

Juranic, N.: Nephelauxetic Effect in Paramagnetic Shielding of Transition-Metal Nuclei in Octahedral d6 Complexes, J. Am. Chem. Soc., 111(21), 8326, doi:10.1021/ja00203a074, 1989.

Kagawa, A., Battipaglia, G. (2022). Post-photosynthetic Carbon, Oxygen and Hydrogen Isotope Signal Transfer to Tree Rings – How Timing of Cell Formations and Turnover of Stored Carbohydrates Affect Intra-annual Isotope Variations. In: Siegwolf, R.T.W., Brooks, J.R., Roden, J., Saurer, M. (eds) Stable Isotopes in Tree Rings. Tree Physiology, 8. Springer, Cham. https://doi.org/10.1007/978-3-030-92698-4_15

Kagi, H., Dohmoto, Y., Takano, S., & Masuda, A. (1993). Tetrad effect in lanthanide partitioning between calcium sulfate crystal and its saturated solution. Chemical Geology, 107(1–2), 71–82. https://doi.org/10.1016/0009-2541(93)90102-O

Karandashev, K., Xu, Z.-H., Meuwly, M., Vaníček, J., & Richardson, J. O. (2017). Kinetic isotope effects and how to describe them. Structural Dynamics (Melville, N.Y.), 4(6), 061501. https://doi.org/10.1063/1.4996339

Keiluweit, M., Nico, P., Harmon, M. E., Mao, J., Pett-Ridge, J. and Kleber, M.: Long-term litter decomposition controlled by manganese redox cycling, Proc. Natl. Acad. Sci. U. S. A., 112(38), E5253–E5260, doi:10.1073/pnas.1508945112, 2015.

Kendall, C., & McDonnell, J. J. (1998). Isotope Tracers in Catchment Hydrology. Elsevier Science. https://books.google.lu/books?id=kiLo1U0cmIIC

Khan, N., Seshadri, B., Bolan, N., Saint, C. P., Kirkham, M. B., Chowdhury, S., Yamaguchi, N., Lee, D. Y., Li, G., Kunhikrishnan, A., Qi, F., Karunanithi, R., Qiu, R., Zhu, Y.-G., & Syu, C. H. (2016). Root Iron Plaque on Wetland Plants as a Dynamic Pool of Nutrients and Contaminants. In Advances in Agronomy (Vol. 138, pp. 1–96). Elsevier. https://doi.org/10.1016/bs.agron.2016.04.002

Kovaříková, M., Tomášková, I., & Soudek, P. (2019). Rare earth elements in plants. Biologia plantarum, 63, Article 20-32. https://doi.org/10.32615/bp.2019.003

Krishna, M. P. and Mohan, M.: Litter decomposition in forest ecosystems: a review, Energy, Ecol. Environ., 2(4), 236–249, doi:10.1007/s40974-017-0064-9, 2017.

Krokene, P. (2015). Chapter 5 – Conifer Defense and Resistance to Bark Beetles. Editor(s): Vega, F. E., Hofstetter R. W. Bark Beetles, Academic Press, 2015, 177-207. https://doi.org/10.1016/B978-0-12-417156-5.00005-8

Kuglerova, L., Jansson, R., Ågren, A., Laudon, H., Malm-Renöfält, B. (2014) Groundwater discharge creates hotspots of riparian plant species richness in a boreal forest stream network. Ecology, 95(3): 715-725 http://dx.doi.org/10.1890/13-0363.1

Labeeuw, L., Martone, P. T., Boucher, Y. and Case, R. J.: Ancient origin of the biosynthesis of lignin precursors, Biol. Direct, 10(1), 1–21, doi:10.1186/s13062-015-0052-y, 2015.

Lachassaghe, P., Lafforgue, M. Forest and the Water Cycle: Quantity, Quality, Management. Cambridge Scholars Publishing. ISBN 978-1-4438-8825-7

Landwehr, J. M., & Coplen, T. B. (2004). Isotopes in Environmental Studies. Line-Conditioned Excess: A New Method for Characterizing Stable Hydrogen and Oxygen Isotope Ratios in Hydrologic Systems. Presented at the Isotopes in Environmental Studies Aquatic Forum 2004, Monaco.

Lang, P. F., & Smith, B. C. (2003). Ionization Energies of Atoms and Atomic Ions. Journal of Chemical Education, 80(8), 938. https://doi.org/10.1021/ed080p938

Larter, M., Brodribb, T. J., Pfautsch, S., Burlett, R., Cochard, H., & Delzon, S. (2015). Extreme Aridity Pushes Trees to Their Physical Limits. Plant Physiology, 168(3), 804–807. https://doi.org/10.1104/pp.15.00223

Laveuf, C., & Cornu, S. (2009). A review on the potentiality of Rare Earth Elements to trace pedogenetic processes. Geoderma, 154(1–2), 1–12. https://doi.org/10.1016/j.geoderma.2009.10.002

Lehmann, M. M., Goldsmith, G. R., Schmid, L., Gessler, A., Saurer, M., & Siegwolf, R. T. W. (2018). The effect of ^{18} O-labelled water vapour on the oxygen isotope ratio of water and assimilates in plants at high humidity. New Phytologist, 217(1), 105–116. https://doi.org/10.1111/nph.14788

Leisola, M., Pastinen, O. and Axe, D. D.: Lignin--Designed Randomness, BIO-Complexity., 2012(3), 1–11, doi:10.5048/bio-c.2012.3, 2012.

Lequy, É., Conil, S. and Turpault, M. P.: Impacts of Aeolian dust deposition on European forest sustainability: A review, For. Ecol. Manage., 267, 240–252, doi:10.1016/j.foreco.2011.12.005, 2012.

Levan, M. A., & Riha, S. J. (1986). The precipitation of black oxide coatings on flooded conifer roots of low internal porosity. Plant and Soil, 95(1), 33–42. https://doi.org/10.1007/BF02378850

Levia, D. F., Hudson, S. A., Llorens, P., & Nanko, K. (2017). Throughfall drop size distributions: A review and prospectus for future research. WIREs Water, 4(4). https://doi.org/10.1002/wat2.1225

Lewis, B. D., & Spalding, E. P. (1998). Nonselective Block by La 3+ of Arabidopsis Ion Channels Involved in Signal Transduction. Journal of Membrane Biology, 162(1), 81–90. https://doi.org/10.1007/s002329900344

Li, X., Chen, Z., Chen, Z. and Zhang, Y.: A human health risk assessment of rare earth elements in soil and vegetables from a mining area in Fujian Province, Southeast China, Chemosphere, 93(6), 1240–1246, doi:10.1016/j.chemosphere.2013.06.085, 2013.

Liang, T., Ding, S., Wenchong, S., Zhongyi, C., Zhang, C. and Li, H.: A review of fractionations of rare earth elements in plants, J. Rare Earths, 26(1), 7–15, doi:10.1016/S1002-0721(08)60027-7, 2008.

Liang, T., Zhang, S., Wang, L., Kung, H. Te, Wang, Y., Hu, A. and Ding, S.: Environmental biogeochemical behaviors of rare earth elements in soil-plant systems, Environ. Geochem. Health, 27(4), 301–311, doi:10.1007/s10653-004-5734-9, 2005.

Lindner, M., Fitzgerald, J. B., Zimmermann, N. E., Reyer, C., Delzon, S., van der Maaten, E., … Hanewinkel, M. (2014). Climate change and European forests: what do we know, what are the uncertainties, and what are the implications for forest management? Journal of Environmental Management, 146, 69–83. https://doi.org/10.1016/j.jenvman.2014.07.030

Lintunen, A., Preisler, Y., Oz, I., Yakir, D., Vesala, T., & Hölttä, T. (2021). Bark Transpiration Rates Can Reach Needle Transpiration Rates Under Dry Conditions in a Semi-arid Forest. Frontiers in Plant Science, 12, 790684. https://doi.org/10.3389/fpls.2021.790684

Liu, Y., & Yamanaka, T. (2012). Tracing groundwater recharge sources in a mountain–plain transitional area using stable isotopes and hydrochemistry. Journal of Hydrology, 464-465, 116–126. https://doi.org/10.1016/j.jhydrol.2012.06.053

Liu, C., Liu, W.-S., Huot, H., Guo, M.-N., Zhu, S.-C., Zheng, H.-X., Morel, J. L., Tang, Y.-T., & Qiu, R.-L. (2022). Biogeochemical cycles of nutrients, rare earth elements (REEs) and Al in soil-plant system in ion-adsorption REE mine tailings remediated with amendment and ramie (Boehmeria nivea L.). Science of The Total Environment, 809, 152075. https://doi.org/10.1016/j.scitotenv.2021.152075

Liu, C., Liu, W.-S., van der Ent, A., Morel, J. L., Zheng, H.-X., Wang, G.-B., Tang, Y.-T., & Qiu, R.-L. (2021). Simultaneous hyperaccumulation of rare earth elements, manganese and aluminum in Phytolacca americana in response to soil properties. Chemosphere, 282, 131096. https://doi.org/10.1016/j.chemosphere.2021.131096

López-Días, V., Barnich, F., Schoppach, R. Multi-bed trap for water isotope analyses, LU502099. Luxembourg Institute of Science and Technology (LIST), Luxembourg (LU). PCT filled May 2023 (International application number PCT/EP2023/063346)

Luo, Y., & Sternberg, L. (1991). Deuterium heterogeneity in starch and cellulose nitrate of cam and C3 plants. Phytochemistry, 30(4), 1095–1098. https://doi.org/10.1016/S0031-9422(00)95179-3

Ma, L., Jin, L. and Brantley, S. L.: How mineralogy and slope aspect affect REE release and fractionation during shale weathering in the Susquehanna/Shale Hills Critical Zone Observatory, Chem. Geol., 290(1–2), 31–49, doi:10.1016/j.chemgeo.2011.08.013, 2011.

Maathuis, F. J. M.: Sodium in plants: Perception, signalling, and regulation of sodium fluxes, J. Exp. Bot., 65(3), 849–858, doi:10.1093/jxb/ert326, 2014.

Marsac, R., Davranche, M., Gruau, G., & Dia, A. (2010). Metal loading effect on rare earth element binding to humic acid: Experimental and modelling evidence. Geochimica et Cosmochimica Acta, 74(6), 1749–1761. https://doi.org/10.1016/j.gca.2009.12.006

Martin, L. A., Vignati, D. A. L., & Hissler, C. (2021). Contrasting distribution of REE and yttrium among particulate, colloidal and dissolved fractions during low and high flows in peri-urban and agricultural river systems. Science of The Total Environment, 790, 148207. https://doi.org/10.1016/j.scitotenv.2021.148207

Martín-Gómez, P., Serrano, L., & Ferrio, J. P. (2017). Short-term dynamics of evaporative enrichment of xylem water in woody stems: implications for ecohydrology. Tree Physiology, 37(4), 511–522. https://doi.org/10.1093/treephys/tpw115

Martinez Del Castillo, E., Zang, C. S., Buras, A., Hacket-Pain, A., Esper, J., Serrano-Notivoli, R., … de Luis, M. (2022). Climate-change-driven growth decline of European beech forests. Communications Biology, 5(1), 163. https://doi.org/10.1038/s42003-022-03107-3

Martínez-Carreras, N., Hissler, C., Gourdol, L., Klaus, J., Juilleret, J., Iffly, J. F., & Pfister, L. (2016). Storage controls on the generation of double peak hydrographs in a forested headwater catchment. Journal of Hydrology, 543, 255–269. https://doi.org/10.1016/j.jhydrol.2016.10.004

Martínez-Carreras, N., Ogorzaly, L., Walczak, C., Merlin, C., Montargès-Pelletier, E., Gantzer, C., Iffly, J.-F., Cauchie, H.-M., Hissler, C. F-Specific RNA Bacteriophage Transport in Stream Water: Hydro-Meteorological Controls and Association with Suspended Solids. Water 2021, 13, 2250. https://doi.org/10.3390/w13162250

Mason Earles, J., Sperling, O., Silva, L. C. R., McElrone, A. J., Brodersen, C. R., North, M. P., & Zwieniecki, M. A. (2016). Bark water uptake promotes localized hydraulic recovery in coastal redwood crown: Localized hydraulic recovery via bark water uptake. Plant, Cell & Environment, 39(2), 320–328. https://doi.org/10.1111/pce.12612

Matheny, A. M., Bohrer, G., Garrity, S. R., Morin, T. H., Howard, C. J., & Vogel, C. S. (2015). Observations of stem water storage in trees of opposing hydraulic strategies. Ecosphere, 6(9), art165. https://doi.org/10.1890/ES15-00170.1

McCully, M. E. (1999). ROOTS IN SOIL: Unearthing the Complexities of Roots and Their Rhizospheres. Annual Review of Plant Physiology and Plant Molecular Biology, 50(1), 695–718. https://doi.org/10.1146/annurev.arplant.50.1.695

McElrone, A. J., Choat, B., Gambetta, G. A. & Brodersen, C. R. (2013) Water Uptake and Transport in Vascular Plants. Nature Education Knowledge 4(5):6

McGuire, K. and McDonnell, J. (2007). Stable Isotope Tracers in Watershed Hydrology. In Stable Isotopes in Ecology and Environmental Science (eds R. Michener and K. Lajtha). https://doi.org/10.1002/9780470691854.ch11

McLennan, S. M. (1994). Rare earth element geochemistry and the “tetrad” effect. Geochimica et Cosmochimica Acta, 58(9), 2025–2033. https://doi.org/10.1016/0016-7037(94)90282-8

Meinzer, F. C., Brooks, J. R., Domec, J.-C., Gartner, B. L., Warren, J. M., Woodruff, D. R., Bible, K., & Shaw, D. C. (2006). Dynamics of water transport and storage in conifers studied with deuterium and heat tracing techniques. Plant, Cell and Environment, 29(1), 105–114. https://doi.org/10.1111/j.1365-3040.2005.01404.x

Melloul, A. and M. Collin (1992). “The ’principal components’ statistical method as a complementary approach to geochemical methods in water quality factor identification; application to the Coastal Plain aquifer of Israel”. Journal of Hydrology 140.1-4, 49–73. doi: 10.1016/0022-1694(92)90234-M

Moll, H., Sachs, S. & Geipel, G.: Plant cell (Brassica napus) response to europium(III) and uranium(VI) exposure. Environ Sci. Pollut. Res. 27, 32048–32061, dot:10.1007/s11356-020-09525-2, 2020.

Möller, P., & Bau, M. (1993). Rare-earth patterns with positive cerium anomaly in alkaline waters from Lake Van, Turkey. Earth and Planetary Science Letters, 117(3–4), 671–676. https://doi.org/10.1016/0012-821X(93)90110-U

Möller, P., Dulski, P., & De Lucia, M. (2021). REY Patterns and Their Natural Anomalies in Waters and Brines: The Correlation of Gd and Y Anomalies. Hydrology, 8(3), 116. https://doi.org/10.3390/hydrology8030116

Möller, P. (2002). The distribution of rare earth elements and yttrium in water-rock interactions: field observations and experiments. In: Stober, I., Bucher, K. (eds) Water-

Rock Interaction. Water Science and Technology Library, vol 40. Springer, Dordrecht. https://doi.org/10.1007/978-94-010-0438-1_4

Montemagno, A., Hissler, C., Bense, V., Teuling, A. J., Ziebel, J., & Pfister, L. (2022). Dynamics of rare earth elements and associated major and trace elements during Douglas-fir (Pseudotsuga menziesii) and European beech (Fagus sylvatica L.) litter degradation. Biogeosciences, 19(13), 3111–3129. https://doi.org/10.5194/bg-19-3111-2022

Mook, W. G., & Mook, W. G. (2005). Introduction to Isotope Hydrology: Stable and Radioactive Isotopes of Hydrogen, Oxygen and Carbon. Taylor & Francis Group.

Moragues-Quiroga, C., Juilleret, J., Gourdol, L., Pelt, E., Perrone, T., Aubert, A., Morvan, G., Chabaux, F., Legout, A., Stille, P., & Hissler, C. (2017). Genesis and evolution of regoliths: Evidence from trace and major elements and Sr-Nd-Pb-U isotopes. CATENA, 149, 185–198. https://doi.org/10.1016/j.catena.2016.09.015

Morris, L.A. Nutrient cycling, Encyclopedia of Forest Sciences, 3, 1227–1235, ISBN 0-12-145160-7.

Muir, K. S., & Coplen, T. B. (1981). Tracing Ground-water Movement By Using the Stable Isotopes Of Oxygen and Hydrogen, Upper Penitencia Creek Alluvial Fan, Santa Clara Valley, California. Santa Clara Valley Water District. https://pubs.usgs.gov/wsp/2075/report.pdf

Munns, R., Passioura, J.B. (1984) Hydraulic Resistance of Plants. III. Effects of NaCl in Barley and Lupin. Functional Plant Biology 11, 351-359. https://doi.org/10.1071/PP9840351

Nakada, R., Shibuya, T., Suzuki, K. and Takahashi, Y.: Europium anomaly variation under low-temperature water-rock interaction: A new thermometer, Geochemistry Int., 55(9), 822–832, doi:10.1134/S001670291709004X, 2017.

Nehemy, M. F., Benettin, P., Allen, S. T., Steppe, K., Rinaldo, A., Lehmann, M. M., & McDonnell, J. J. (2022). Phloem water isotopically different to xylem water: Potential causes and implications for ecohydrological tracing. Ecohydrology, 15(3). https://doi.org/10.1002/eco.2417

Nikolic, M. and Pavlovic, J.: Plant Responses to Iron Deficiency and Toxicity and Iron Use Efficiency in Plants, Plant Micronutrient Use Efficiency, 55-69, doi:10.1016/B978-0-12-812104-7.00004-6, 2018.

Norman, A. G.: The Biological Decomposition of Pectin, Ann. Bot., 43(170), 233–243, doi:10.1111/j.1469-8137.1941.tb07026.x, 1929.

Olivarez, A. M., & Owen, R. M. (1991). The europium anomaly of seawater: Implications for fluvial versus hydrothermal REE inputs to the oceans. Chemical Geology, 92(4), 317–328. https://doi.org/10.1016/0009-2541(91)90076-4

Ouellette, R. J., & David Rawn, J. (2018). Introduction to Organic Reaction Mechanisms. Organic Chemistry: Structure, Mechanism, and Synthesis (Second Edition), 51-86, Academic Press. https://doi.org/10.1016/B978-0-12-812838-1.50003-7

Orlowski, N., Breuer, L., and McDonnell, J. J. (2016) Critical issues with cryogenic extraction of soil water for stable isotope analysis. Ecohydrol., 9: 1– 5. doi: 10.1002/eco.1722

Pacyna, J.M., Atmospheric Deposition, Encyclopedia of Ecology, 275-285, doi:10.1016/B978-008045405-4.00258-5, 2008.

Pagano, G., Aliberti, F., Guida, M., Oral, R., Siciliano, A., Trifuoggi, M. and Tommasi, F.: Rare earth elements in human and animal health: State of art and research priorities, Environ. Res., 142, 215–220, doi:10.1016/j.envres.2015.06.039, 2015.

Page, V. and Feller, U.: Heavy Metals in Crop Plants: Transport and Redistribution Processes on the Whole Plant Level, Agronomy, 5(3), 447–463, doi:10.3390/agronomy5030447, 2015.

Park S. Nobel (2009) ,Physicochemical and Environmental Plant Physiology (Fourth Edition), Academic Press, ISBN 9780123741431. https://doi.org/10.1016/B978-0-12-374143-1.00018-1

Patten, A. M., Vassão D. G., Wolcott, M. P., Davin, L. B., Lewis, N. G. (2010). Trees: A Remarkable Biochemical Bounty, Editor(s): Hung-Wen (Ben) Liu, Lew Mander, Comprehensive Natural Products II, Elsevier, 2010, Pages 1173-1296, ISBN 9780080453828, https://doi.org/10.1016/B978-008045382-8.00083-6

Penna, D., Stenni, B., Šanda, M., Wrede, S., Bogaard, T. A., Michelini, M., Fischer, B. M. C., Gobbi, A., Mantese, N., Zuecco, G., Borga, M., Bonazza, M., Sobotková, M., Čejková,

B., and Wassenaar, L. I.: Technical Note: Evaluation of between-sample memory effects in the analysis of δ2H and δ18O of water samples measured by laser spectroscopes, Hydrol. Earth Syst. Sci., 16, 3925–3933, https://doi.org/10.5194/hess-16-3925-2012, 2012

Penna, D., Hopp, L., Scandellari, F., Allen, S. T., Benettin, P., Beyer, M., Geris, J., Klaus, J., Marshall, J. D., Schwendenmann, L., Volkmann, T. H. M., von Freyberg, J., Amin, A., Ceperley, N., Engel, M., Frentress, J., Giambastiani, Y., McDonnell, J. J., Zuecco, G., … Kirchner, J. W. (2018). Ideas and perspectives: Tracing terrestrial ecosystem water fluxes using hydrogen and oxygen stable isotopes – challenges and opportunities from an interdisciplinary perspective. Biogeosciences, 15(21), 6399–6415. https://doi.org/10.5194/bg-15-6399-2018

Peñuelas, J., Llusià, J. The Complexity of Factors Driving Volatile Organic Compound Emissions by Plants. Biologia Plantarum 44, 481–487 (2001). https://doi.org/10.1023/A:1013797129428

Pfister, L, Martínez-Carreras, N, Hissler, C, et al. Bedrock geology controls on catchment storage, mixing, and release: A comparative analysis of 16 nested catchments. Hydrological Processes. 2017; 31: 1828– 1845. https://doi.org/10.1002/hyp.11134

Pfister, L., Wetzel, C.E., Klaus, J., Martínez-Carreras, N., Antonelli, M., Teuling, A.J. and McDonnell, J.J. (2017), Terrestrial diatoms as tracers in catchment hydrology: a review. WIREs Water, 4: e1241. https://doi.org/10.1002/wat2.1241

Pourrut, B., Shahid, M., Dumat, C., Winterton, P. and Pinelli, E.: Lead Uptake, Toxicity, and Detoxification in Plants, Rev. Environ. Contam. Toxicol., 213, 113–136, doi:10.1007/978-1-4419-9860-6_4, 2011.

Pourret, O., & Davranche, M. (2013). Rare earth element sorption onto hydrous manganese oxide: A modeling study. Journal of Colloid and Interface Science, 395, 18–23. https://doi.org/10.1016/j.jcis.2012.11.054

Pourret, O., Davranche, M., Gruau, G., & Dia, A. (2007). Rare earth elements complexation with humic acid. Chemical Geology, 243(1–2), 128–141. https://doi.org/10.1016/j.chemgeo.2007.05.018

Proseus, T. E., & Boyer, J. S. (2012). Pectate chemistry links cell expansion to wall deposition in Chara corallina. Plant Signaling & Behavior, 7(11), 1490–1492. https://doi.org/10.4161/psb.21777

Quinn, K.A.; Byrne, R.H.; Schijf, J. Comparative scavenging of yttrium and the rare earth elements in seawater: competitive influences of solution and surface chemistry. Aquat. Chem. 2004, 100, 59–80.

Raffa, K. F., Aukema, B. H., Bentz, B. J., Carroll, A. L., Hicke J. A., Turner, M. G., Romme, W.H. (2013). Cross-scale Drivers of Natural Disturbances Prone to Anthropogenic Amplification: The Dynamics of Bark Beetle Eruptions, BioScience, Volume 58, Issue 6, June 2008, Pages 501–517, https://doi.org/10.1641/B580607

Rahman, M. M., Tsukamoto, J., Rahman, M. M., Yoneyama, A. and Mostafa, K. M.: Lignin and its effects on litter decomposition in forest ecosystems, Chem. Ecol., 29(6), 540–553, doi:10.1080/02757540.2013.790380, 2013.

Rambeck, W. A., & Bassham, J. A. (1973). Tritium incorporation and retention in photosynthesizing algae. Biochimica et Biophysica Acta (BBA) - General Subjects, 304(3), 725–735. https://doi.org/10.1016/0304-4165(73)90219-5

Ramos, S. J., Dinali, G. S., Oliveira, C., Martins, G. C., Moreira, C. G., Siqueira, J. O. and Guilherme, L. R. G.: Rare Earth Elements in the Soil Environment, Curr. Pollut. Reports, 2(1), 28–50, doi:10.1007/s40726-016-0026-4, 2016.

Regulski, F. J., Jr, & Peterson, J. L. (1982). Portable device for the extraction of xylem sap from trees. Plant Disease, 66(1), 53–54.

Reimann, C., P. Filzmoser, R. Garrett, and R. Dutter (2011). Statistical data analysis explained: applied environmental statistics with R. John Wiley & Sons.

Reynolds, R., Neff, J., Reheis, M. and Lamothe, P.: Atmospheric dust in modern soil on aeolian sandstone, Colorado Plateau (USA): Variation with landscape position and contribution to potential plant nutrients, Geoderma, 130(1–2), 108–123, doi:10.1016/j.geoderma.2005.01.012, 2006.

Rieder, S. V., & Rose, I. A. (1959). The Mechanism of the Triosephosphate Isomerase Reaction. Journal of Biological Chemistry, 234(5), 1007–1010. https://doi.org/10.1016/S0021-9258(18)98120-2

Rim, K. T., Koo, K. H. and Park, J. S.: Toxicological evaluations of rare earths and their health impacts to workers: A literature review, Saf. Health Work, 4(1), 12–26, doi:10.5491/SHAW.2013.4.1.12, 2013.

Rizvi, A.R., Baig, S., Barrow, E., Kumar, C. (2015). Synergies between Climate Mitigation and Adaptation in Forest Landscape Restoration. Gland, Switzerland: IUCN

Rodriguez, N. B., McGuire, K. J., & Klaus, J. (2018). Time-varying storage–water age relationships in a catchment with a Mediterranean climate. Water Resources Research, 54(6), 3988–4008. https://doi.org/10.1029/2017wr021964

Rout, G., Samantaray, S., Das, P., Aluminium toxicity in plants : a review, Agronomie, 21(1), 3–21,

doi:10.1051/agro:2001105, 2001.

Rundel, P. W., Ehleringer, J. R., & Nagy, K. A. (Eds.). (1989). Stable Isotopes in Ecological Research (Vol. 68). Springer New York. https://doi.org/10.1007/978-1-4612-3498-2

Saatz, J., Vetterlein, D., Mattusch, J., Otto, M., & Daus, B. (2015). The influence of gadolinium and yttrium on biomass production and nutrient balance of maize plants. Environmental Pollution, 204, 32–38. https://doi.org/10.1016/j.envpol.2015.03.052

Samuel, D., & Silver, B. L. (1965). Oxygen Isotope Exchange Reactions of Organic Compounds. In V. Gold (Ed.), Advances in Physical Organic Chemistry (Vol. 3, pp. 123–186). Academic Press. https://doi.org/10.1016/S0065-3160(08)60300-7

Sardans, J. and Peñuelas, J.: Potassium Control of Plant Functions: Ecological and Agricultural Implications, Plants, 10(2), 419, doi:10.3390/plants10020419, 2021.

Scaini, A., Audebert, M., Hissler, C., Fenicia, F., Gourdol, L., Pfister, L., & Beven, K. J. (2017). Velocity and celerity dynamics at plot scale inferred from artificial tracing experiments and time-lapse ERT. Journal of Hydrology, 546, 28–43. https://doi.org/10.1016/j.jhydrol.2016.12.035

Savvides, A., van Ieperen, W., Dieleman, J. A., & Marcelis, L. F. M. (2013). Meristem temperature substantially deviates from air temperature even in moderate environments: is the magnitude of this deviation species-specific? Plant, Cell & Environment, 36(11), 1950–1960. https://doi.org/10.1111/pce.12101

Schijf, J. and Zoll, A. M.: When dissolved is not truly dissolved-The importance of colloids in studies of metal sorption on organic matter, J. Colloid Interface Sci., 361(1), 137–147, doi:10.1016/j.jcis.2011.05.029, 2011.

Schlesinger, W. H., & Jasechko, S. (2014). Transpiration in the global water cycle. Agricultural and Forest Meteorology, 189-190, 115–117. https://doi.org/10.1016/j.agrformet.2014.01.011

Schulz, K.J., DeYoung, J.H., Jr., Seal, R.R., II, and Bradley, D.C., eds., 2017, Critical mineral resources of the United States—Economic and environmental geology and prospects for future supply: U.S. Geological Survey Professional Paper 1802, 797 p., http://doi.org/10.3133/pp1802.

Shan, X., Wang, H., Zhang, S., Zhou, H., Zheng, Y., Yu, H. and Wen, B.: Accumulation and uptake of light rare earth elements in a hyperaccumulator Dicropteris dichotoma, Plant Sci., 165(6), 1343–1353, doi:10.1016/s0168-9452(03)00361-3, 2003.

Shannon, R. D. (1976). Revised effective ionic radii and systematic studies of interatomic distances in halides and chalcogenides. Acta Cryst. A32, 751–767.

Sharma, P. and Dubey, R. S.: Lead toxicity in plants, Braz. J. Plant Physiol., 17(1), doi:10.1590/S1677-04202005000100004, 2005.

Shaul, O.: Magnesium transport and function in plants: The tip of the iceberg, BioMetals, 15(3), 309–323, doi:10.1023/A:1016091118585, 2002.

Shtangeeva, I., & Ayrault, S. (2007). Effects of Eu and Ca on yield and mineral nutrition of wheat (Triticum aestivum) seedlings. Environmental and Experimental Botany.

Silva, P. S., Campos, J. E. G., Cunha, L. S., & Mancini, L. H. (2018). Relationships of stable isotopes, water-rock interaction and salinization in fractured aquifers, Petrolina region, Pernambuco State, Brazil. *REM - International Engineering Journal*, *71*(1), 19–25. https://doi.org/10.1590/0370-44672016710178

Singh, S., Tripathi, D. K., Singh, S., Sharma, S., Dubey, N. K., Chauhan, D. K. and Vaculík, M.: Toxicity of aluminium on various levels of plant cells and organism: A review, Environ. Exp. Bot., 137, 177–193, doi:10.1016/j.envexpbot.2017.01.005, 2017.

Smith, B.N. and Ziegler, H. (1990), Isotopic Fractionation of Hydrogen in Plants. Botanica Acta, 103: 335-342. https://doi.org/10.1111/j.1438-8677.1990.tb00171.x

Smith, R. M., & Martell, A. E. (1989). Critical Stability Constants. Springer US. https://doi.org/10.1007/978-1-4615-6764-6

Sohel, Md. S. I., Grau, A. V., McDonnell, J. J., & Herbohn, J. (2021). Tropical forest water source patterns revealed by stable isotopes: A preliminary analysis of 46 neighboring species. Forest Ecology and Management, 494, 119355. https://doi.org/10.1016/j.foreco.2021.119355

Sonke, J. E. and Salters, V. J. M.: Lanthanide-humic substances complexation. I. Experimental evidence for a lanthanide contraction effect, Geochim. Cosmochim. Acta, 70(6), 1495–1506, doi:10.1016/j.gca.2005.11.017, 2006.

Song, L., Zhu, J., Li, M., & Yu, Z. (2014). Water utilization of Pinus sylvestris var. Mongolica in a sparse wood grassland in the semiarid sandy region of Northeast China. Trees, 28(4), 971–982. https://doi.org/10.1007/s00468-014-1010-5

Staaf, H. (1980). Release of plant nutrients from decomposing leaf litter in a South Swedish beech forest, Ecography (Cop.), 3(2), 129–136, doi:10.1111/j.1600-0587.1980.tb00719.x, 1980.

Steinmann, M., Stille, P. (1997). Rare earth element behavior and Pb, Sr, Nd isotope systematics in a heavy metal contaminated soil, Applied Geochemistry, Volume 12, Issue 5, 1997, Pages 607-623, ISSN 0883-2927, https://doi.org/10.1016/S0883-2927(97)00017-6.

Sternberg, L. D. S. L., Deniro, M. J., & Savidge, R. A. (1986). Oxygen Isotope Exchange between Metabolites and Water during Biochemical Reactions Leading to Cellulose Synthesis 1. Plant Physiology, 82(2), 423–427. https://doi.org/10.1104/pp.82.2.423

Sternberg, L. D. S. L. (2009). Oxygen stable isotope ratios of tree-ring cellulose: the next phase of understanding. The New Phytologist, 181(3), 553–562. https://doi.org/10.1111/j.1469-8137.2008.02661.x

Stille, P., Pierret, M.-C., Steinmann, M., Chabaux, F., Boutin, R., Aubert, D., Pourcelot, L., & Morvan, G. (2009). Impact of atmospheric deposition, biogeochemical cycling and water–mineral interaction on REE fractionation in acidic surface soils and soil water (the

Strengbach case). Chemical Geology, 264(1–4), 173–186. https://doi.org/10.1016/j.chemgeo.2009.03.005

Stille, P., Steinmann, M., Pierret, M.-C., Gauthier-Lafaye, F., Chabaux, F., Viville, D., Pourcelot, L., Matera, V., Aouad, G., & Aubert, D. (2006). The impact of vegetation on REE fractionation in stream waters of a small forested catchment (the Strengbach case). Geochimica et Cosmochimica Acta, 70(13), 3217–3230. https://doi.org/10.1016/j.gca.2006.04.028

Suda, A., & Makino, T. (2016). Functional effects of manganese and iron oxides on the dynamics of trace elements in soils with a special focus on arsenic and cadmium: A review. Geoderma, 270, 68–75. https://doi.org/10.1016/j.geoderma.2015.12.017

Suzuki, Y., Yokoi, S., Katoh, M., Minato, M. and Takizawa, N.: Stability constants of Rare Earth complexes with some organic ligands, Rare Earths Mod. Sci. Technol., (1), 121–126, doi:10.1007/978-1-4613-3054-7, 1980.

Tagliavini, M., Tonon, G., Scandellari, F., Quiñones, A., Palmieri, S., Menarbin, G., Gioacchini, P. and Masia, A.: Nutrient recycling during the decomposition of apple leaves (Malus domestica) and mowed grasses in an orchard, Agric. Ecosyst. Environ., 118(1–4), 191–200, doi:10.1016/j.agee.2006.05.018, 2007.

Takahashi, Y., Châtellier, X., Hattori, K. H., Kato, K. and Fortin, D.: Adsorption of rare earth elements onto bacterial cell walls and its implication for REE sorption onto natural microbial mats, Chem. Geol., 219(1–4), 53–67, doi:10.1016/j.chemgeo.2005.02.009, 2005.

Takahashi, Y., Yamamoto, M., Yamamoto, Y. and Tanaka, K.: EXAFS study on the cause of enrichment of heavy REEs on bacterial cell surfaces, Geochim. Cosmochim. Acta, 74(19), 5443–5462, doi:10.1016/j.gca.2010.07.001, 2010.

Talbot, J. M., Yelle, D. J., Nowick, J. and Treseder, K. K.: Litter decay rates are determined by lignin chemistry, Biogeochemistry, 108(1–3), 279–295, doi:10.1007/s10533-011-9599-6, 2012.

Tang, J. and Johannesson, K. H.: Ligand extraction of rare earth elements from aquifer sediments: Implications for rare earth element complexation with organic matter in natural waters, Geochim. Cosmochim. Acta, 74(23), 6690–6705, doi:10.1016/j.gca.2010.08.028, 2010.

Taylor S. R. and McLennan S. M. (2009) Planetary Crusts: Their Composition and Evolution. Cambridge University Press, Cambridge. 378 pp.

Tchougréèff, A. and Drownkowski, R.: Nephelauxetic Effect Revisited, Int. J. Quantum Chem., 109(11), 2606–2621, doi:10.1002/qua.21989, 2009.

Tetzlaff, D., Buttle, J., Carey, S. K., Kohn, M. J., Laudon, H., McNamara, J. P., Smith, A., Sprenger, M., & Soulsby, C. (2021). Stable isotopes of water reveal differences in plant – soil water relationships across northern environments. Hydrological Processes, 35(1). https://doi.org/10.1002/hyp.14023

Terakado, Y., & Masuda, A. (1988). The coprecipitation of rare-earth elements with calcite and aragonite. Chemical Geology, 69(1–2), 103–110. https://doi.org/10.1016/0009-2541(88)90162-3

Thyne, G., C. G¨uler, and E. Poeter (2004). “Sequential analysis of hydrochemical data for watershed characterization”. Ground Water 42.5, 711–723. doi: 10.1111/j.1745-6584.2004.tb02725.x

Tian, H. E., Gao, Y. S., Li, F. M., & Zeng, F. (2003). Effects of Europium Ions (Eu^{3+}) on the Distribution and Related Biological Activities of Elements in Lathyrus sativus L. Roots. Biological Trace Element Research, 93(1–3), 257–270. https://doi.org/10.1385/BTER:93:1-3:257

Tommasi, F., Thomas, P. J., Pagano, G., Perono, G. A., Oral, R., Lyons, D. M., Toscanesi, M. and Trifuoggi, M.: Review of Rare Earth Elements as Fertilizers and Feed Additives: A Knowledge Gap Analysis, Arch. Environ. Contam. Toxicol., 81, 531-540, doi:10.1007/s00244-020-00773-4, 2021.

Toyama K, Terakado Y (2019) Estimation of the practical partitiom coefficients of rare earth elements between limestone and seawater: discussion and application. Geochem J 53:139–150.

Turpault, M. P., Kirchen, G., Calvaruso, C., Redon, P. O. and Dincher, M.: Exchanges of major elements in a deciduous forest canopy, Biogeochemistry, 152(1), 51–71, doi:10.1007/s10533-020-00732-0, 2021.

Tyler, G.: Rare earth elements in soil and plant systems - A review, Plant Soil, 267, 191–206, doi:10.1007/s11104-005-4888-2, 2004.

Tyree, M.T., Jarvis, P.G. (1982). Water in Tissues and Cells. In: Lange, O.L., Nobel, P.S., Osmond, C.B., Ziegler, H. (eds) Physiological Plant Ecology II. Encyclopedia of Plant Physiology, vol 12 / B. Springer, Berlin, Heidelberg. https://doi.org/10.1007/978-3-642-68150-9_3

Urey, H. C., Faegri, K., & Heuss, J. (1947). Oxygen isotope exchange between carbon dioxide and water. Journal of Chemical Physics, 15(7), 337-338.

Vázquez-Ortega, A., Zapata-Ríos, X., Rasmussen, C., McIntosh, J., Brooks, P. D., Perdrial, J., Amistadi, M. K., Chorover, J., Schaap, M., Harpold, A. and Pelletier, J. D.: Rare earth elements as reactive tracers of biogeochemical weathering in forested rhyolitic terrain, Chem. Geol., 391, 19–32, doi:10.1016/j.chemgeo.2014.10.016, 2015.

Vázquez-Ortega, A., Huckle, D., Perdrial, J., Amistadi, M. K., Durcik, M., Rasmussen, C., McIntosh, J. and Chorover, J.: Solid-phase redistribution of rare earth elements in hillslope pedons subjected to different hydrologic fluxes, Chem. Geol., 426, 1–18, doi:10.1016/j.chemgeo.2016.01.001, 2016.

Wang, X.-F., & Yakir, D. (2000). Using stable isotopes of water in evapotranspiration studies. Hydrological Processes, 14(8), 1407–1421. https://doi.org/10.1002/1099-1085(20000615)14:8<1407::aid-hyp992>3.0.co;2-k

Wang, X., & Liu, D. (2017). Integration of cerium chemical forms and subcellular distribution to understand cerium tolerance mechanism in the rice seedlings. Environmental Science and Pollution Research, 24(19), 16336–16343. https://doi.org/10.1007/s11356-017-9274-0

Wassenaar, L. I., & Terzer-Wassmuth, S. (2018). Stable isotopes in hydrologic research. In Handbook of environmental chemistry (pp. 1-36). Springer.

Wassenaar, L. I., Hendry, M. J., & Harrington, R. (2018). Stable isotopes in hydrology and water management. CRC Press.

Ward, J. H. (1963). “Hierarchical Grouping to Optimize an Objective Function”. Journal of the American Statistical Association 58.301, 236. doi: 10.2307/2282967

Weng, J. K. and Chapple, C.: The origin and evolution of lignin biosynthesis, New Phytol., 187(2), 273–285, doi:10.1111/j.1469-8137.2010.03327.x, 2010.

Wenming, D., Xiangke, W., Xiaoyan, B., Aixia, W., Jingzhou, D. and Tao, Z.: Comparative study on sorption/desorption of radioeuropium on alumina, bentonite and red earth: Effects of pH, ionic strength, fulvic acid, and iron oxides in red earth, Appl. Radiat. Isot., 54(4), 603–610, doi:10.1016/S0969-8043(00)00311-0, 2001.

West, J. B. (2019). Isotope tracers in environmental and earth sciences. John Wiley & Sons.

Wen, M., He, D., Li, M., Ren, R., Jin, J., & Si, B. (2022). Causes and factors of cryogenic extraction biases on isotopes of xylem water. Water Resources Research, 58, e2022WR032182. https://doi.org/10.1029/2022WR032182

White, J. W. C., Cook, E. R., Lawrence, J. R., & Wallace S., B. (1985). The DH ratios of sap in trees: Implications for water sources and tree ring DH ratios. Geochimica et Cosmochimica Acta, 49(1), 237–246.

Wilcox, W. M., Solo-Gabriele, H. M., & Sternberg, L. O. (2004). Use of stable isotopes to quantify flows between the Everglades and urban areas in Miami-Dade County Florida. Journal of Hydrology, 293(1), 1–19. https://doi.org/10.1016/j.jhydrol.2003.12.041

Wilm, H. G., Thornthwaite, C. W., Colman, E. A., Cummings, N. W., Croft, A. R., Gisborne, H. T., … Taylor, C. A. (1944). Report of the committee on transpiration and evaporation, 1943–44. Transactions, 25(5), 683. https://doi.org/10.1029/tr025i005p00683

Winter, T., S. Mallory, T. Allen, and D. Rosenberry (2000). “The use of principal component analysis for interpreting ground water hydrographs”. Groundwater 38.2, 234–246

Woolhouse, H. W.: Toxicity and Tolerance in the Responses of Plants to Metals, Physiol. Plant Ecol. III, 245–300, doi:10.1007/978-3-642-68153-0_8, 1983.

Xu, B., & Yu, S. (2013). Root iron plaque formation and characteristics under N2 flushing and its effects on translocation of Zn and Cd in paddy rice seedlings (Oryza sativa). Annals of Botany, 111(6), 1189–1195. https://doi.org/10.1093/aob/mct072

Yakir, D. (1992a). Variations in the natural abundance of oxygen-18 and deuterium in plant carbohydrates. Plant, Cell & Environment, 15(9), 1005–1020. https://doi.org/10.1111/j.1365-3040.1992.tb01652.x

Yakir, D. (1992b). Water Compartmentation in Plant Tissue: Isotopic Evidence. Water and Life, 205–222. Springer Berlin Heidelberg. https://doi.org/10.1007/978-3-642-76682-4_13

Yakir, D., & DeNiro, M. J. (1990). Oxygen and hydrogen isotope fractionation during cellulose metabolism in Lemna gibba L. Plant Physiology, 93(1), 325-332. https://doi.org/10.1104/pp.93.1.325

Yakir, D., DeNiro, M. J., & Rundel, P. W. (1989). Isotopic inhomogeneity of leaf water: Evidence and implications for the use of isotopic signals transduced by plants. Geochimica et Cosmochimica Acta, 53(10), 2769–2773. https://doi.org/10.1016/0016-7037(89)90147-6

Yan, L., Riaz, M., & Jiang, C. (2020). Exogenous application of proline alleviates B-deficiency-induced injury while aggravates aluminum toxicity in trifoliate orange seedlings. Scientia Horticulturae, 268, 109372. https://doi.org/10.1016/j.scienta.2020.109372

Yeghicheyan, D., Aubert, D., Bouhnik-Le Coz, M., Chmeleff, J., Delpoux, S., Djouraev, I., Granier, G., Lacan, F., Piro, J.-L., Rousseau, T., Cloquet, C., Marquet, A., Menniti, C., Pradoux, C., Freydier, R., Viera da Silva-Filho, E., Suchorski, K., 2019. A new Interlaboratory characterisation of silicon, rare earth elements and twenty-two other trace element concentrations in the natural river water certified reference material SLRS-6 (NRC-CNRC). Geostand. Geoanal. Res. 43 (3), 475–496. https://doi.org/ 10.1111/ggr.12268.

Yuan, M., Guo, M.-N., Liu, W.-S., Liu, C., van der Ent, A., Morel, J. L., Huot, H., Zhao, W.-Y., Wei, X.-G., Qiu, R.-L., & Tang, Y.-T. (2017). The accumulation and fractionation of Rare Earth Elements in hydroponically grown Phytolacca americana L. Plant and Soil, 421(1–2), 67–82. https://doi.org/10.1007/s11104-017-3426-3

Yuan, M., Liu, C., Liu, W.-S., Guo, M.-N., Morel, J. L., Huot, H., Yu, H.-J., Tang, Y.-T., & Qiu, R.-L. (2018). Accumulation and fractionation of rare earth elements (REEs) in the naturally grown Phytolacca americana L. in southern China. International Journal of Phytoremediation, 20(5), 415–423. https://doi.org/10.1080/15226514.2017.1365336

Zaharescu, D. G., Burghelea, C. I., Dontsova, K., Presler, J. K., Maier, R. M., Huxman, T., Domanik, K. J., Hunt, E. A., Amistadi, M. K., Gaddis, E. E., Palacios-Menendez, M. A., Vaquera-Ibarra, M. O. and Chorover, J.: Ecosystem Composition Controls the Fate of Rare Earth Elements during Incipient Soil Genesis, Sci. Rep., 7(February), 1–15, doi:10.1038/srep43208, 2017.

Zeng, F., Tian, H. E., Wang, Z., An, Y., Gao, F., Zhang, L., Li, F., & Shan, L. (2003). Effect of Rare Earth Element Europium on Amaranthin Synthesis in Amarathus caudatus Seedlings. Biological Trace Element Research, 93(1–3), 271–282. https://doi.org/10.1385/BTER:93:1-3:271

Zhang, Z.Y., Wang, Y.Q., Li, F.L. et al. Distribution characteristics of rare earth elements in plants from a rare earth ore area. Journal of Radioanalytical and Nuclear Chemistry 252, 461–465 (2002). https://doi.org/10.1023/A:1015834232718

Zhao, L., Wang, L., Cernusak, L. A., Liu, X., Xiao, H., Zhou, M., & Zhang, S. (2016). Significant Difference in Hydrogen Isotope Composition Between Xylem and Tissue Water in Populus Euphratica. Plant, Cell & Environment, 39(8), 1848–1857. https://doi.org/10.1111/pce.12753

Zhao, Y., & Wang, L. (2018). Plant Water Use Strategy in Response to Spatial and Temporal Variation in Precipitation Patterns in China: A Stable Isotope Analysis. Forests, 9(3), 123. https://doi.org/10.3390/f9030123

Zhenggui, W., Ming, Y., Xun, Z., Fashui, H., Bing, L., Ye, T., Guiwen, Z., & Chunhua, Y. (2001). Rare earth elements in naturally grown fern Dicranopteris linearis in relation to their variation in soils in South-Jiangxi region (Southern China). Environmental Pollution, 114(3), 345–355. https://doi.org/10.1016/S0269-7491(00)00240-2

Zhou, S., Zhou, K., Wang, J. et al. Application of cluster analysis to geochemical compositional data for identifying ore-related geochemical anomalies. Front. Earth Sci. 12, 491–505 (2018). https://doi.org/10.1007/s11707-017-0682-8

Zhu, J., Chu, H., Xie, Z. et al. Effects of lanthanum on nitrification and ammonification in three Chinese soils. Nutrient Cycling in Agroecosystems 63, 309–314 (2002). https://doi.org/10.1023/A:1021163101692

Zhu, Z., Liu, C. Q., Wang, Z. L., Liu, X. and Li, J.: Rare earth elements concentrations and speciation in rainwater from Guiyang, an acid rain impacted zone of Southwest China, Chem. Geol., 442, 23–34, doi:10.1016/j.chemgeo.2016.08.038, 2016.

Ziegler, H. (1989). Hydrogen Isotope Fractionation in Plant Tissues. Stable Isotopes in Ecological Research, 105–123. Springer New York. https://doi.org/10.1007/978-1-4612-3498-2_8

SUMMARY

The basis for this thesis lies in the research questions being addressed, which serve two main objectives. Firstly, it seeks to advance tree water extraction methodologies and the interpretation of water stable isotopes data in eco-hydrology. Secondly, it aims to investigate the use of rare earth elements (REEs) as new eco-hydrological tracers by studying their behaviour within the regolith-tree system. This work potentially leads to an improved understanding of water dynamics in the transpiration pathway, giving insights regarding the water source(s) absorbed by trees and its distribution across tree tissues.

In Chapter 3, the primary emphasis is placed on understanding the effects of physical and biochemical processes on the O-H stable isotopes composition of water along the soil-branch flow path in *Fagus sylvatica* trees. This work introduces new *in-situ* vacuum extraction (*IS*VE) methods for sampling tree water, purposefully tailored to explore the interaction between isotope chemistry and tree physiology, which plays a pivotal role in determining the isotopic characteristics of various tree water reservoirs, with a particular focus on xylem water. The outcomes highlight the potential impact of tree biochemical pathways, as well as physical processes within the tree tissues, on the water stable isotopes signature of tree waters.

Chapter 4 focuses on the comparison of *IS*VE methods for tree water extraction, with the conventional cryogenic extraction (CE) approach commonly employed in eco-hydrological research. This chapter critically evaluates the strengths and limitations of these techniques and introduces new insights on how to interpret the isotopic composition of tree waters. The findings shown in this Chapter emphasize the importance of selecting appropriate extraction methods for accurately examining plant-water interactions in eco-hydrological research.

Chapter 5 focuses on investigating the potential use of REEs as tracers for water flows within the regolith-plant continuum. The research involved analysing the fractionation of REEs at the root level and along the xylem sap flow pathway. REEs showed fractionation processes occurring during the water uptake, as well as in the root-branch flow path. Potential processes involved in such fractionation are highlighted in this study.

Chapter 6 explores the impact of *Fagus sylvatica* exudates on the REEs composition of throughfall, which is the solution resulting from precipitation passing through the canopy of vegetation and reaching the ground surface. Special attention is given to the REEs composition of precipitation, throughfall, and transpired water, along with the potential influence of atmospheric dust on the resulting REEs patterns in these solutions. The findings reported in this Chapter highlight the importance of tree exudates in modifying the REEs chemistry of precipitation.

Chapter 7 focuses on the release of REEs and major elements back into the environment during wet degradation of litter. This study reports on laboratory leaching experiments which allow to identify the mechanisms involved in the fractionation of REEs between solid litter matter and leaching solution. Additionally, the potential impact of litter degradation on soil solutions REEs composition is assessed. The findings reported in this Chapter suggest that the tree species, as well as the degradation stage of the litter are important factors to consider when studying the chemistry of REEs in forest soil waters.

Chapter 8 provides a summary and discussion of the outcomes presented in Chapters 3 to 7, while additionally exploring potential directions for future research. In this thesis, as a result of a multidisciplinary approach and the development of new techniques for eco-hydrological studies, new perspectives on water stable isotopes and REEs dynamics in the regolith-tree system were explored. In particular, this involved introducing three key innovations in the eco-hydrology domain: new methods for sampling tree sap, the use of REEs as tracers for tree water uptake, and the adoption of a multi-tracer and multidisciplinary approach that considers biochemical and physiological variables for tracing water in forest ecosystems. This work improved our understanding of water stable isotopes and REEs dynamics within trees, paving the way for future multidisciplinary research focusing on the implementation of biochemical and physical processes in models of eco-hydrological fluxes.

ACKNOWLEDGEMENTS

This is the most challenging part of the thesis. I don't know where to begin since there are so many things I would like to write but I can imagine how tired you are already of reading this thesis, dear reader. The days of this long journey have been tough, sometimes lived in solitude forced by the pandemic, sometimes accompanied by the impostor syndrome. But today, as I write these words, I cannot think of nothing else but the beautiful memories that this adventure has left me with. These memories are tied to the people who have embarked with me on this journey, with whom I have shared many moments, enriching me and helping me grow.

I would like to express my heartfelt gratitude to Christophe Hissler, Victor Bense, Laurent Pfister and Ryan Teuling for granting me the opportunity to be part of their (our!) amazing research groups. Without you, this incredible experience would not have been possible. An additional thank you to the tireless Christophe Hissler, Victor Bense, and Ryan Teuling for guiding me on this adventure, showing unwavering interest in my ideas and aiding in my personal development throughout the past 5 years. Thank you for allowing me the freedom to express my creativity and for helping me develop my critical thinking and my love for science. I am particularly impressed by Christophe. As my daily supervisor, he made it to the the end with a PhD student like me. I hope to cultivate as much patience as you possess! Thank you to Laurent Pfister for demonstrating how a true leader should be: a knowledgeable scientist, a good listener and an empathetic human being. Thanks to all the colleagues from the LIST Catchment and Eco-hydrology group, Laurent Gourdol, Jean-François Iffly, Veneranda López Días, François Barnich, Loic Leonard, Núria Martínez-Carreras, Jérôme Juilleret, Stanislaus Schymanski, Oliver O' Nagy and Johanna Ziebel, who contributed in various ways to make this work possible and enjoyable, from analysis, sampling and filtrations, to scientific discussions, training, laughter and coffees.

A thank you to my dear colleagues PhD and Postdoc from room A008 (and subsequent modifications), Loic Martin, Giacomo Petrucci, Enrico Bonanno, Ginevra Fabiani, Marta Antonelli, Barbara Glaser, Nicolaus van Zweel, Nicolas Rodriguez, and all the PhDs from the Doctoral Training Unit and from the "Doctoral Fooding Unit" (personal achievement that I am very proud of), for making my days pleasant and teaching me the beauty of diversity.

A special thank you goes to my friends Enrico Bonanno and Ginevra Fabiani, who have always encouraged me throughout the most challenging times and taught me to never give up.

Thank you also to all the colleagues from the Hydrology and Quantitative Water Management Group at WUR, with whom I couldn't spend much time due to the pandemic and sampling campaigns. I hope to have the opportunity to get to know you better in the years to come!

Thanks to my former University professor Paolo Censi. Thanks for introducing me to the mysterious and fascinating world of geochemistry and for being a good mentor and an invaluable friend.

A thank you to my parents. Without your help, support, and sacrifices, I would never have been able to embark on such an amazing journey.

Thank you to my girlfriend Vanessa Mortillaro. Thank you for encouraging me to apply for this position. Thank you for your patience (a lot of it!), kindness, and support you have given me all these years. Without your encouragement and belief in me, the words in this document would never have been written.

Infine vorrei spendere le ultime righe per ringraziare la donna alla quale devo tutto, la donna eccezionale che era mia madre Anna Elisa (Annalisa) Algaria. Grazie per aver sempre creduto in me anche quando nessun altro lo avrebbe fatto. Grazie per avermi guidato, consigliato e supportato nei momenti più difficili della mia vita. Questo traguardo lo dedico a te, Mamma. Ovunque tu possa trovarti, spero che tu sia orgogliosa di me, anche solo la metà di quanto io lo sono di te.

LIST OF PUBLICATIONS

Peer-reviewed journals publications

Montemagno, A., Hissler, C., Bense, V., Teuling, A. J., Ziebel, J., & Pfister, L. (2022). Dynamics of rare earth elements and associated major and trace elements during Douglas-fir (*Pseudotsuga menziesii*) and European beech (*Fagus sylvatica L.*) litter degradation. *Biogeosciences*, 19(13), 3111–3129. https://doi.org/10.5194/bg-19-3111-2022

Montemagno, A., Keim, R.F., López-Días, V., Bense, V., Teuling, A.J., Hissler, C. Progressive enrichment in ^{18}O and ^{2}H in xylem water along sap flow paths in Fagus sylvatica trees. Ecohydrology. – *accepted for publication*

Montemagno, A. *et al*., Comparative analysis of cryogenic extraction and in-situ vacuum extraction methods for determining water stable isotopes composition of tree waters. – *in preparation*

Montemagno, A. *et al*.: Lanthanides and Yttrium (REY) dynamics during root absorption and transportation to the shoots of Fagus sylvatica trees in temperate forests: potential implication for eco-hydrological studies – *In preparation*

Other scientific publications

(2019). “Role of vegetation on Rare Earth Elements mobilization in the regolith below forest ecosystems” – Goldschmidt

(2021a). “Selective release and sequestration of elements operated by litter during degradation” – Goldschmidt

(2021b). “Inferring direct water exchange in the regolith-tree flow path by using $\delta^{2}H$ and $\delta^{18}O$” – OZCAR-TERENO conference

(2022a). “Sap extraction from trees: new avenues for H and O stable isotopes ecohydrology” – EGU General Assembly

(2022b). “Gradual ^{18}O and ^{2}H enrichment in xylem water in the pathway from roots to branches in *Fagus sylvatica L.*: potential impacts in ecohydrology. 3rd place as best oral presentation – ERB conference

Netherlands Research School for the
Socio-Economic and Natural Sciences of the Environment

D I P L O M A

for specialised PhD training

The Netherlands research school for the
Socio-Economic and Natural Sciences of the Environment
(SENSE) declares that

Alessandro Montemagno

born on the 2nd of May 1987 in Palermo, Italy

has successfully fulfilled all requirements of the
educational PhD programme of SENSE.

Wageningen, 6 November 2023

Chair of the SENSE board

Prof. dr. Martin Wassen

The SENSE Director

Prof. Philipp Pattberg

The SENSE Research School has been accredited by the Royal Netherlands Academy of Arts and Sciences (KNAW)

KONINKLIJKE NEDERLANDSE
AKADEMIE VAN WETENSCHAPPEN

The SENSE Research School declares that **Alessandro Montemagno** has successfully fulfilled all requirements of the educational PhD programme of SENSE with a work load of 30.2 EC, including the following activities:

SENSE PhD Courses

- Environmental research in context (2018)
- Research in context activity: 'Incorporation of fundamental rare earth elements geochemistry information in the relevant English and Italian Wikipedia pages' 2020)

Other PhD and Advanced MSc Courses

- Toolkit to successfully manage your research outputs, University of Luxembourg (2019)
- Introduction to R for Statistical Analysis, PE&RC - SENSE (2019)
- Basic statistics, PE&RC - WIMEK (2019)
- Programming for Everybody (Getting Started with Python), University of Michigan (2020)
- Project and Time Management, Wageningen Graduate Schools (2021)
- Career Orientation. Wageningen Graduate Schools (2021)
- Ecotoxicology: Risk Assessment, Postgraduate Education in Toxicology (2021)
- Research Data Management. Wageningen Graduate Schools and WUR Library (2021)

Oral and Poster Presentations

- Oral presentation - *Litter double standards: REE and nutrients release and sequestration operated by litter*. Workshop: Plant-Soil Interaction discussion (PSI), 16 February 2021, Wageningen, The Netherlands
- Oral presentation - *Selective release and sequestration of elements operated by litter during degradation.* European Association of Geochemistry - Geochemical Society, 04-09 July 2021, Barcelona, Spain
- Oral presentation - *Sap extraction from trees: New avenues for H and O stable isotopes ecohydrology*. EGU General Assembly, 23-27 May 2022, Vienna, Austria
- Poster presentation - *Role of vegetation on Rare Earth Elements mobilization in the regolith below forest ecosystems* (2019). European Association of Geochemistry and Geochemical Society, 18-23 August 2019, Barcelona, Spain
- Poster presentation - *Inferring direct water exchange in the regolith-tree flow path by using $\delta^{2}H$ and $\delta^{18}O$*. OZCAR and TERENO research networks – Strasbourg, 04-08 October 2021, Strasbourg, France

SENSE coordinator PhD education

Dr. ir. Peter Vermeulen

The presented research was carried out at the Luxembourg Institute of Science and Technology in association with the Hydrology and Quantitative Water Management Group of Wageningen University and Research.

This research received funding from the Luxembourg National Research Fund (FNR) within the framework of the 'Hydro-CSI' Doctoral Training Unit coordinated by Prof. Laurent Pfister under grant agreement No. PRIDE15/10623093/HYDRO-CSI.

Financial support from Wageningen University for several PhD courses and for printing this thesis is gratefully acknowledged.

Cover design by Alessandro Montemagno, periodic table design by www.sciencenotes.org


13 Al Aluminium 26.982
32 Ge Germanium 72.631
33 As Arsenic 74.922
31 Ga Gallium 69.723
51 Sb Antimony 121.760
30 Zn Zinc 65.38
50 Sn Tin 118.711
49 In Indium 114.818
82 Pb Lead 207.2
81 Tl Thallium 204.383
29 Cu Copper 63.546
28 Ni Nickel 58.693
48 Cd Cadmium 112.414
27 Co Cobalt 58.933
47 Ag Silver 107.868
80 Hg Mercury 200.592
114 Fl Flerovium [289]
113 Nh Nihonium [286]
46 Pd Palladium 106.42
79 Au Gold 196.967
45 Rh Rhodium 102.906
78 Pt Platinum 195.085
112 Cn Copernicium [285]
77 Ir Iridium 192.217
111 Rg Roentgenium [280]
67 Ho Holmium 164.930
76 Os Osmium 190.23
110 Ds Darmstadtium [281]
66 Dy Dysprosium 162.500
109 Mt Meitnerium [278]
65 Tb Terbium 158.925
98 Cf Californium 251.080
108 Hs Hassium [269]
64 Gd Gadolinium 157.25
97 Bk Berkelium 247.070
63 Eu Europium 151.964
96 Cm Curium 247.070
62 Sm Samarium 150.36
95 Am Americium 243.061
61 Pm Promethium 144.913
94 Pu Plutonium 244.064
93 Np Neptunium 237.048
92 U Uranium 238.029